UNIVERSITÀ DEGLI STUDI DI MILANO

DOTTORATO DI RICERCA IN SCIENZE DELLA TERRA
Ciclo XXXIV

DIPARTIMENTO DI SCIENZE DELLA TERRA

Ph.D. Thesis

STUDY OF THE PALEONTOLOGICAL RECORD OF THE BESANO FORMATION (MIDDLE TRIASSIC) AT "SASSO CALDO", VARESE, UNESCO WHL MONTE SAN GIORGIO

geo 01

GABRIELE BINDELLINI
Matr. N. R12303

Tutor:
Prof. MARCO BALINI

Cotutor:
Dr. CRISTIANO DAL SASSO

Coordinator of the Doctoral Program:
Prof.ssa MARIA IOLE SPALLA

Academic year 2020/2021

Index

Abstract

The Besano Formation consists of an alternation of laminated dolomitic banks and bituminous shales, and sparse cineritic tuffs that are dated as Late Anisian–Early Ladinian. It is one of the richest fossil-bearing formations from the Monte San Giorgio area; on the Italian side of Monte San Giorgio, the Sasso Caldo site is the one from which the greatest part of the Besano collection housed at the Museo di Storia Naturale di Milano is from. This Ph.D. thesis aims to the study of the Besano Formation macrofauna, through biochronostratigraphic zonation of the Sasso Caldo Site, revision of the large ichthyosaur *Besanosaurus leptorhynchus*), and study of the most important specimens, chosen for their preservation and rarity, but also to test the hypothesis of variations in the influence of open sea on the Besano basin.

All the available ammonoids and bivalves from the Sasso Caldo site (Besano Formation), housed in the collections of the Museo di Storia Naturale di Milano, were examined and determined. The systematic study led to the recognition of 15 ammonoid taxa belonging to 10 genera, and five species belonging to the bivalve genus *Daonella*. The study of bed-by-bed collected specimens allowed the biochronostratigraphic classification of the Sasso Caldo section and the time-calibration of invertebrate and vertebrate bioevents. Results evidence that at Sasso Caldo site crops out almost the entire middle to upper Besano Formation. corresponding the *Nevadites secedensis* ammonoid zone. The trend of distribution of specimens reflects the establishment of an intraplatform basin with discontinuous open-marine influence in the middle Besano Formation, while the upper Besano Formation corresponds to a shallower subtidal restricted platform environment.

Among the terrestrial taxa recovered at Sasso Caldo from the upper Besano Formation, a remarkably well-preserved fossil scorpion (BES SC 1973) is described in this thesis. This finding corroborates the hypothesized existence of a near shoreline during the deposition of the upper Besano Formation. BES SC 1973 is assigned to a new taxon gen. et sp. nov., included in the family Protobuthidae. This finding represents the first arachnid recorded from the Besano Formation, and the second genus attributed to the family Protobuthidae. This specimen is also the first reported Italian Mesozoic fossil scorpion.

Regarding vertebrates, MSNM V927 and 928, a portion of the axial skeleton of a large diapsid, is attributed to *Helveticosaurus zollingeri*, a rare diapsid known only from the Besano Formation. This animal was recovered in association with the ammonoid *Ticinites*, at the base of the *N. secedensis* Zone, in coincidence with the establishment of the intraplatform basin of the middle Besano Formation. This specimen is the first record of skeletal remains and the second specimen assigned to the taxon in Italy. In this work the niche occupied by this animal in the Middle Triassic coastal ecosystems and its swimming style are also revised and discussed.

MSNM V926, and SMNS 50010, respectively a portion of ribcage and an isolated partial forefin of a large ichthyosaur, were attributed to *Cymbospondylus buchseri*. MSNM V926 represents the first specimen attributed to this taxon and recovered on the Italian side of Monte San Giorgio.

A great part of this thesis is dedicated to the revision of *Besanosaurus leptorhynchus*. The specimens studied and attributed to *Besanosaurus leptorhynchus* preserve a remarkably complete cranial and postcranial anatomy so that this taxon can be now accounted among the best-understood Middle Triassic ichthyosaur taxa. The revision of the skull morphology of this taxon clarified long-standing controversies regarding its cranial anatomy and the taxonomy of shastasaurids from Monte San Giorgio. The six specimens here described represent a potential ontogenetic series composed of an embryo (inside the maternal cavity of BES SC 999), likely two subadults, and four adults. They can be ordered by increasing size as follows: embryonic material of BES SC 999, PIMUZ T 4376, PIMUZ T 1895, BES SC 999, BES SC 1016, GPIT 1793/1, PIMUZ T 4847. Also, *Besanosaurus* resulted the largest Middle Triassic ichthyosaur taxon of the Western Tethys to date, since

a full adult size is confidently estimated to be almost 8 m in PIMUZ T 4847. *Besanosaurus* is characterized by a long, slender, and gracile snout, representing an ecological specialization never seen before the Anisian in a large-sized diapsid. The study of the postcranial anatomy of *Besanosaurus leptorhynchus* is based on four specimens: PIMUZ T 4376, PIMUZ T 1895, BES SC 999, PIMUZ T 4847. The results suggest that this taxon possesses a peculiar bauplan, which in its proportions fits in between *Cymbospondylus* and the shastasaur-grade ichthyosaurs. Swimming capabilities of *Besanosaurus leptorhynchus* were tested and compared with *Cymbospondylus* and *Mixosaurus*. Among the ichthyosaurs from the Besano-Monte San Giorgio fauna (*Cymbopondylus,* mixosaurids, and *Besanosaurus*), different hunting strategies, demonstrated by different morphologies and dimensions of the rostra, as well as different body proportions and swimming styles, should have led to niche partitioning.

The key phylogenetic position occupied by *Besanosausurus leptorhynchus* in the ichthyosaurian phylogeny was investigated: the analysis shows that this taxon represents the basalmost member of shastasaur-grade ichthyosaurs, recovered to be a paraphyletic group.

Eventually is addressed a study of the embryonic material preserved in BES SC 999. We deem the material in the body cavity of BES SC 999 unambiguously embryonic and attributable to *Besanosaurus leptorhynchus.* Here the embryonic material is described in detail and qualitatively compared with the maternal specimen and to other known ichthyosaur prenatal specimens.

Chapter 1
Introduction to the thesis

1.1 Introduction and aims of the work

The Middle Triassic sedimentary succession of Monte San Giorgio (UNESCO WHL) consists of four different formations deposited on a carbonate platform along the western margin of the Neo-Tethys (Furrer, 1995; Röhl, et al. 2001; Etter, 2002; Stockar, et al. 2012). Above the Anisian San Salvatore Dolomite lies the 5- to 16-meters-thick Besano Formation that comprise the Anisian/Ladinian boundary and from which the greatest part of the well-known vertebrate fauna of Monte San Giorgio has been recovered (e.g., Bürgin et al., 1989; Furrer, 2003). The Besano Formation (also known as "Grenzbitumenzone") consists of an alternation of variably laminated dolomitic banks and bituminous shales, and sparse cineritic tuffs that are dated as Late Anisian–Early Ladinian (Brack & Rieber, 1986, 1993; Mundil et al., 1996; Brack et al., 2005; Wotzlaw et al., 2017). The Besano Formation is one of the richest fossil-bearing formations from the Monte San Giorgio area (e.g., Rieppel, 2019); on the Italian side of Monte San Giorgio, among the major fossiliferous localities, the Sasso Caldo site is the one which the greatest part of the Besano collection housed at the Museo di Storia Naturale di Milano (MSNM) comes from (e.g., Dal Sasso, 2004; Nosotti et al., 2008).

This Ph.D. thesis aims to fulfill two major goals: (1) the production and publication of a stratigraphic log matched by a bio-chronostratigraphy of the Sasso Caldo site, based on the study of the ammonoid and bivalve (*Daonella*) fauna; (2) a detailed and multi-level study of the holotype of *Besanosaurus leptorhynchus* (Reptilia: Ichthyosauria), BES SC 999, housed at the MSNM and unearthed in 1993 at the Sasso Caldo site. Previously, this taxon was known only from this single specimen, which is one of the most complete and well-preserved ichthyosaurs from the Besano Formation (Dal Sasso & Pinna, 1996). This work will therefore include results long-awaited by specialists: the first stratigraphic study of the site will be presented, including a bed-by-bed correlation to the known existing localities where the Besano Formation crops out (both in Switzerland and Italy); the taxon *Besanosaurus leptorhynchus* will be revised, with a complete osteological study, clarification of its phylogenetic position among Ichthyosauria, and assumptions on its functional anatomy, feeding ecology and autoecology, will be compared to other diapsid taxa of the Besano basin. The study of this taxon with a strong symbolic value, and of the Sasso Caldo site stratigraphy as well, represent new important contributions to the long history and tradition of research regarding the study of the Besano Formation, and of the Monte San Giorgio paleontological and geological heritage.

To revaluate the value of the paleontological record of the Italian sites where the Besano Formation crops out, few new specimens, chosen for their preservation, importance, and rarity, will be described and discussed in this thesis as well. Namely these include: the description of a remarkably well-preserved fossil scorpion (Arachnida: Scorpiones) from Sasso Caldo site and that likely represents a new genus and a new species; the description of a ribcage portion belonging to *Helveticosaurus zollingeri* (Reptilia: Diapsida), recovered at Piodelle-Selva Bella site, and that represents the first skeletal specimen of the taxon from Italy; the description of a ribcage portion belonging to *Cymbospondylus buchseri* (Reptilia: Ichthyosauria), recovered at Piodelle-Selva Bella site, and that represents the first report of the taxon from the Italian outcrops of the Besano Formation.

1.2 Monte San Giorgio

In 2003 the Monte San Giorgio Swiss side, located in southern Ticino, and in 2010 the Italian area of the same compound, in the north-east of Varese province, have been included in the UNESCO World Heritage List. The criterion for the inclusion in the UNESCO World Heritage List (whc.unesco.org) reads as follows: "Monte San Giorgio is the single best known record of marine life in the Triassic period, and records important remains of life on land as well. The site has produced diverse and numerous fossils, many of which show exceptional completeness and detailed preservation. The long history of study of the site, and the disciplined management of the resource have created a well-documented and cataloged body of specimens of exceptional quality, and are the basis for a rich associated geological literature. As a result, Monte San Giorgio provides the principal point of reference, relevant to future discoveries of marine Triassic remains throughout the world." The Monte San Giorgio area is in fact famous around the world for the rare invertebrate fossil fauna, the exceptionally well-preserved fossil fishes, and marine reptiles (e.g., Rieber 1973; Kuhn-Schnyder, 1974; Bürgin et al., 1989; Etter, 2002; Beardmore & Furrer, 2015).

With its inclusion in the UNESCO World Heritage List, the site has been recognized as one-of-a-kind "fossillagerstätte". This has been made possible thanks to the work of several generations of paleontologists, students, other professionals, and countless amateurs. The first finds were reported by Curioni in 1847, and since then, the site never stopped to gift us with spectacular specimens from the Middle Triassic. Most of the collected material comes from Swiss and Italian palaeontological excavations and mining, conducted between the end of the 19th and the first half of the 20th centuries by the University of Zurich and the Natural History Museum of Milan. In more recent times important dig campaign have been led also by the Museo Cantonale di Lugano and the University of Milan. Fossils have been collected from different horizons whose ages span from the Late Anisian to the Late Ladinian: the succession of several vertebrate fossils-rich levels from the Middle Triassic is dated back as ~237 to 243 million years ago. At least 21000 specimens, plants, and animals, invertebrate and vertebrate, of various dimensions, many of them with a perfect preservation and articulated skeletons, have been gathered thanks to the hard work of all those people who collaborated with the abovementioned institutions. Many specimens have been carefully prepared and then studied and published; many other fossils are still undergoing preparation and waiting their turn to be presented to the world. The best specimens are exposed in public museums, geographically distributed among Zurich, Milan, the Varese province, and the Canton Ticino in Switzerland. In the scientific publications the presence of more than 200 different animal and plant species were reported: 30 reptiles, 80 fishes, 100 invertebrates, 5 plants, and some exceptionally well-preserved insects and other arthropods. Not only the beauty of the specimens but also the richness of the fossil horizons and their proven inexhaustibility make the Monte San Giorgio a treasure chest that has definitely something still hidden inside that waits to be discovered.

1.2.1 Geographical introduction

Monte San Giorgio is located in the southern part of the Canton of Ticino, in Switzerland, next to the Italian border with the Varese Province, Lombardy (Italy) (Fig. 1.1). The mount reaches 1097 m a.s.l. and is surrounded by two branches of the Lake Lugano (271 m a.s.l.). Monte San Giorgio is part of a small mountain compound that includes Prasacco, a small mount in Switzerland, Monte Pravello (1015 m a.s.l.), crossed by the Italian/Switzerland border, Monte Orsa (998 m a.s.l.), Monte Casolo (625 m a.s.l.) and Monte Grumello (684 m a.s.l.) in the Italian territory. The UNESCO Monte San Giorgio world heritage area (the buffer zone

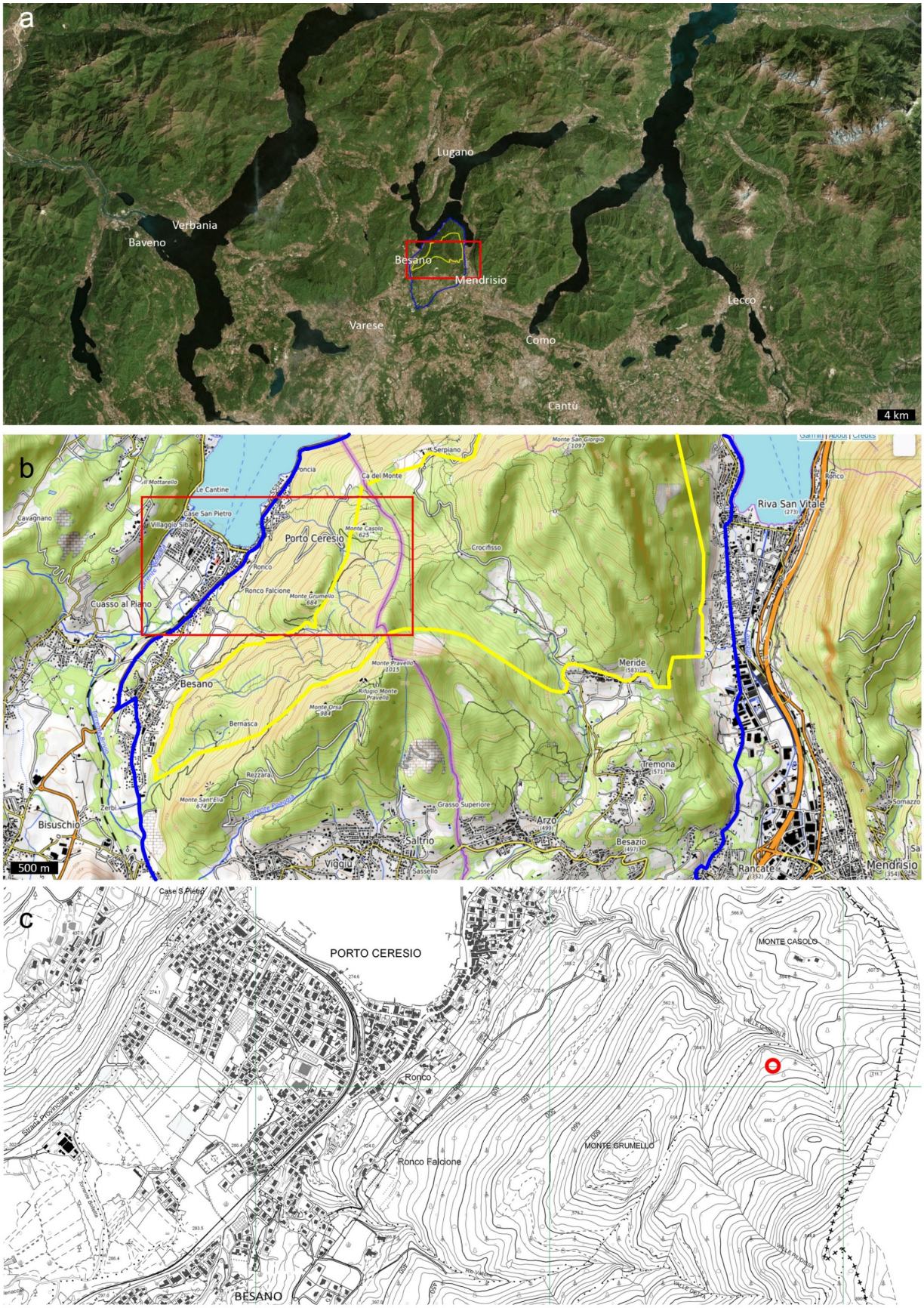

Fig. 1.1 – a) Geographical setting of Monte San Giorgio; b) enlargement of the area in the red rectangle of subfigure a; c) enlargement of the of the area in the red rectangle in subfigure b; red dot represents the Sasso Caldo site. UNESCO World Heritage property protected area (i.e., core zone) of Monte San Giorgio bordered in yellow; safeguarding area (i.e., buffer zone), for the Monte San Giorgio core zone, bordered in blue; pink line in subfigure b shows the Italian/Swiss boundary.

of the core protected as World Heritage property Fig. 1.1) includes this mountain compound and therefore is located partly in Switzerland and partly in Italy. The whole area gets the name from the highest mountain, Monte San Giorgio, located in Swiss territory. Geologically, it is constituted mostly by Mesozoic formations, including some levels bearing a great number of well-preserved fossils. In Monte San Giorgio, the richest and best preserved Middle Triassic fauna comes from the Besano Formation and the Meride Limestone. The Besano Formation outcrops extend from the municipality of Besano to the top of Monte San Giorgio, in southwest-northeast direction, and from the top of the mount to the south of Riva San Vitale municipality, in northeast-southwest direction. Sasso Caldo and Piodelle Selva-Bella mines, the site from which the studied material is from, respectively are located at the following coordinates: 45°54'03.5"N 8°55'11"E and 45°53'36.5"N 8°54'30.5"E.

1.2.2 Geological overview

The geology of the Monte San Giorgio compound is a key to the interpretation of the history of the Southern Alps, from the Carboniferous to the Late Jurassic, spanning for more than 150 million years (Fig. 1.2 and 1.3). The Monte San Giorgio Fossil lagerstätte belongs to the western termination of the Southern Alps. During the Middle Triassic, the South-Alpine domain was located at a northern intertropical latitude of about 15-18° (Muttoni et al. 2004) and was also strongly influenced by monsoonal circulation (Preto et al. 2010).

The South dipping omocline stratigraphic succession of Monte San Giorgio, on the Italian side of the mount, crops out against the slope (Fig. 1.2). The oldest rocks are found on the shores of the Lake Lugano, outcropping between Brusino Arsizio and Porto Ceresio, where they represent the Insubric crystalline basement, constituted by metamorphosized gneiss. The crystalline bedrock is overlain by several hundred-meters-thick volcanic rock succession of the Lower Permian, dated back to approximately 280 million years ago. Reaching Serpiano from Brusino Arsizio, the first outcropping lithology is a degraded andesite, commonly called "porfirite", whereas approaching the top of Monte San Giorgio a riolite, called "quarzifer porfid", crops out.

The first Triassic formation overlaying the Permian volcanoclastic rocks is the **Servino Formation**, dated back to the Olenekian. The formation is in erosional contact with the underlying Permian rocks and is constituted by arenaceous and conglomeratic deposits, which witness a transgressive phase. Overlaying the Servino Fm, the **Bellano Formation**, dated back to the Early Anisian (Sommaruga et al., 1997), consists of fluvio-deltaic deposits. These deposits unconformably overly the Lower Triassic transitional clastic deposits of the Servino.

Following the deposition of these continental deposits, the Late Anisian sediments witness a progressive transgression of a shallow epicontinental sea from the east towards the west (Fig. 1.4). In this sea, the Monte San Giorgio basin occupied a small area and resulted in a peculiar sedimentary succession including temporarily dysoxic to anoxic bottom water conditions (e.g., Bernasconi, 1994; Röhl et al. 2001; Etter 2002; Stockar 2010; Stockar et al. 2013). The progressive transgression and the setting of carbonate platform growth are witnessed by the **San Salvatore Dolomite**, which outcrops above the Bellano Formation (Zorn, 1971). This dolostone represents the remains of a carbonate platform, deposited in shallow marine waters, in subtropical climatic conditions. During the latest Anisian and the Ladinian, to the north and east, this shallow-water sedimentation continued with the Middle and Upper San Salvatore Dolomite (Zorn, 1971; Stockar, 2010), whereas in the Monte San Giorgio area the appearance of an intraplatform basin resulted in the deposition of the **Besano Formation** ("Grenzbitumenzone": Frauenfelder, 1916) followed above by the San Giorgio Formation and the Meride Limestone. The Besano Formation is 5 to16 m thick and spans from bed n°3 to bed n°186 of the "Punkt 902" Mirigioli section. It includes, in its upper portion (from bed n° 133–187), the Anisian/Ladinian boundary (Brack & Rieber, 1993; Brack et al., 2005). The formation is constituted by

an alternation of thin black shale layers and thicker variably laminated dolostones. It was deposited in a marine setting with an estimated depth of 30-130 m, located on a carbonate platform at the north-western rim of the Tethys Ocean, at about 20° north latitude (Bernasconi, 1991, 1994; Röhl et al., 2001; Furrer, 1995, 2003; Furrer & Vandelli, 2014). The water column has been hypothesized to be clearly stratified into oxygenated surface waters and disoxic to anoxic bottom waters. The strata deposited are characterized by organic-carbon rich layers, with well-preserved macro-lamination, testifying very quiet hydrodynamic conditions and a lack of post-depositional bioturbation. Most of the beautiful vertebrate fossils from Monte San Giorgio, whose importance has been widely appreciated worldwide, come from this formation. According to Röhl et al. (2001), the Besano formation can be subdivided into three portions: lower, middle, and upper Besano Formation; these respectively are hypothesized to have been deposited in a shallow restricted platform environment, a deeper intraplatform basin, and then again a shallower restricted platform environment. A great abundance of pelagic marine vertebrates is typical of the middle Besano Formation, which for this reason, and because of the facies recovered in this section of the formation, has been inferred to have had repeated open-marine influences (Röhl et al., 2001).

The Besano Formation grades upwards into the **San Giorgio Dolomite,** which is 60 meters thick. The base of the San Giorgio Dolomite is defined at layer 187 of the standard profile at the Mirigioli locality ("Punkt 902" site; Rieber 1973; Bernasconi 1994), where the Besano Formation was excavated bed by bed between 1950 and 1968 (Kuhn-Schnyder 1974). Above the San Giorgio Dolomite, crops out the Meride Limestone, which dates back to the Ladinian and is 400-600 m thick. The Besano Formation, the San Giorgio Dolomite, and the Meride Limestone were deposited in the same basin. The San Giorgio Dolomite and the Meride Limestone are coeval with the upper San Salvatore Dolomite East to Monte San Giorgio.

The **lower Meride Limestone** is 90-150 m thick and is made up of layers with variable thickness, interrupted by some levels of laminated limestone, rich in organic substance (though black shales are rare), or by yellowish tufaceous bentonite. The lower Meride Limestone is delimited above by a "Dolomitband" (Frauenfelder, 1916) that reaches 30 m in thickness. Above this, is located the upper portion of Meride Limestone, which consists of alternating limestone and marl layers, with an increasing content of clay towards the summit, deposited in an environment influenced by strong seasonal

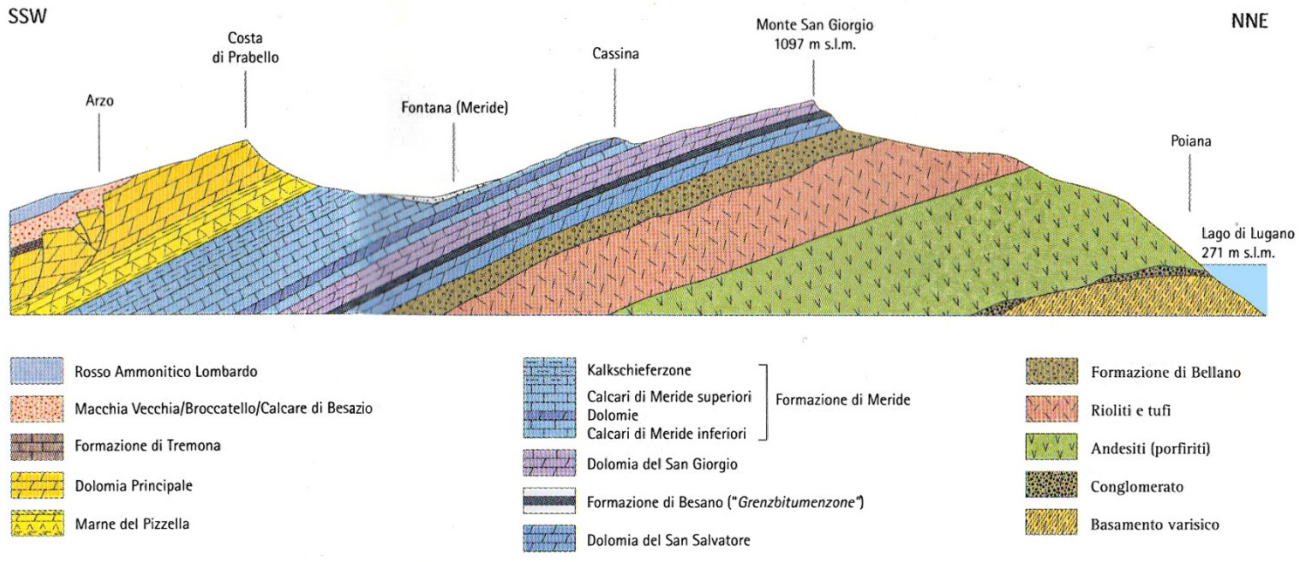

Fig. 1.2 - Simplified geological profile of Monte San Giorgio. Commissione scientifica del Monte San Giorgio (2014).

variations of sea level and salinity, and by a very close emerged area (Stockar & Renesto, 2011). The upper part of the lower Meride Limestone contains three fossiliferous horizons: **Cava inferiore**, **Cava superiore,** and **Cassina horizon**. Each of them has produced different associations of vertebrates and consists of finely laminated limestone with intercalated volcanic ash levels (Stockar et al., 2012). These horizons are respectively dated back to 241.02 ± 0.13, 241.07 ± 0.13 and 240.63 ± 0.13 MA (Stockar et al., 2012). Overall, about 180 meters of carbonate rock (Dolomia di San Giorgio and the inferior portion of the Meride Limestone) separate the Besano Formation from the Cava Inferiore horizon.

At the base of the **upper Meride Limestone**, just above the "Dolomitband", a fossiliferous layer, the "**Sceltrich level**", has recently been identified. The type locality is in Val Sceltrich, located on the SW side of Monte San Giorgio. Its investigation started in 2010 (Saller, 2016) when it was discovered by the researchers of the Museo Cantonale di Storia Naturale di Lugano. This layer, consisting of dark laminated limestone, rich in organic matter, is a few decimeters thick. The horizon, and the specimens found in it, are currently under study. The upper Meride Limestone includes the **Kalkschieferzone,** which has a thickness of 120 meters. The Kalkschieferzone consists of thin laminated layers of marl and clay and preserves a peculiar fauna of fish, reptiles, and arthropods (e.g., Krzeminski & Lombardo, 2001; Lombardo 2002; Lombardo & Tintori, 2004; Tintori & Lombardo, 2007). It records the last evolutionary stage of the lagoonal basin before the Carnian regression, progressively buried by an increasing contribution of siliciclastic material (Furrer, 1995).

In the Upper Triassic, during the Carnian, starting approximately 230 million years ago, the marine regression resulted in the establishment of extremely shallow marine areas and large flat continental areas. The **Pizzella Marl** deposited in this context and resulted in the deposition of marls of different colors (grey, dark grey, brown, red, and greenish), with an overall thickness that ranges from 0 to 20 m. These marls are sometimes intercalated with decimetric carbonates or salt strata. This regressive phase is again followed by a transgression that results in the deposition of the **Dolomia Principale** during the Norian, about 225 million years ago. This represents a large area of shallow water carbonate deposition with lagoons that extended along the entire Southern Alps, and that in Monte San Giorgio resulted in the deposition of a 400-600 m thick succession. The Rhaetic **Tremona Formation** represents the last formation of the Triassic carbonate sequence outcropping at Monte San Giorgio; this consists of fossil-rich limestones, partly dolomitized.

During the Early Jurassic (Hettangian), intense extensional tectonic activities lead to the breakup of the previously deposited Upper Triassic succession and a general deepening of the Lombardy basins occurred. However, the area of Monte San Giorgio, as well as of Arzo, was characterized by the presence of the submarine Arbostora threshold, rising adjacent to the deeper basin of Monte Generoso on the East and Monte Nudo on the West (Winterer & Bosellini, 1981; Furrer, 2003; Michetti et al., 2013). On the edge of the Arbostora threshold fracture zones appeared, characterized by broad and deep grooves. These were filled with breccias and fossil-rich muds: the variegated breccia formation is today referred to as **Macchia Vecchia**, whereas the fossil-rich limestones are named **Broccatello** (Wiedenmayer, 1963). While these formations were depositing, the deeper Monte Generoso Basin was filled by silica-rich limestones, which today form the **Moltrasio Limestone** (Bernoulli, 1964). On the other hand, similarly in the Monte Nudo Basin, the **Saltrio Formation** was deposited (Kälin & Tammann, 1977). The two basins had a very different depth, estimated to be 3000 m in the Monte Generoso basin and 1500 m in the Monte Nudo Basin (Furrer, 2003). Later, during the Pleinsbachian-Toarcian, the Arbostora threshold started to sink. In the Arzo and Besazio area, the **Besazio limestone** was deposited, characterized by the presence of several crinoids and ammonites, followed above by the limestones and marls of the **Rosso Ammonitico Lombardo**. At the same time, in the Clivio and Saltrio areas, the **Saltrio Formations** were deposited. Middle and Upper Jurassic units are also preserved in the area of

Besazio-Ligornetto-Clivio of Monte San Giorgio. These are characterized by the presence of radiolarites, marls, and limestones, which belong to the group of the Selcifero Lombardo. These rocks represent a 1000-2000 m deep basin as well as the last preserved formations outcropping in the Monte San Giorgio area. The formations deposited above the Selcifero Lombardo are preserved in the succession of the Gole della Breggia, southern-est to Monte San Giorgio, which spans from the Sinemurian to Upper Cretaceous.

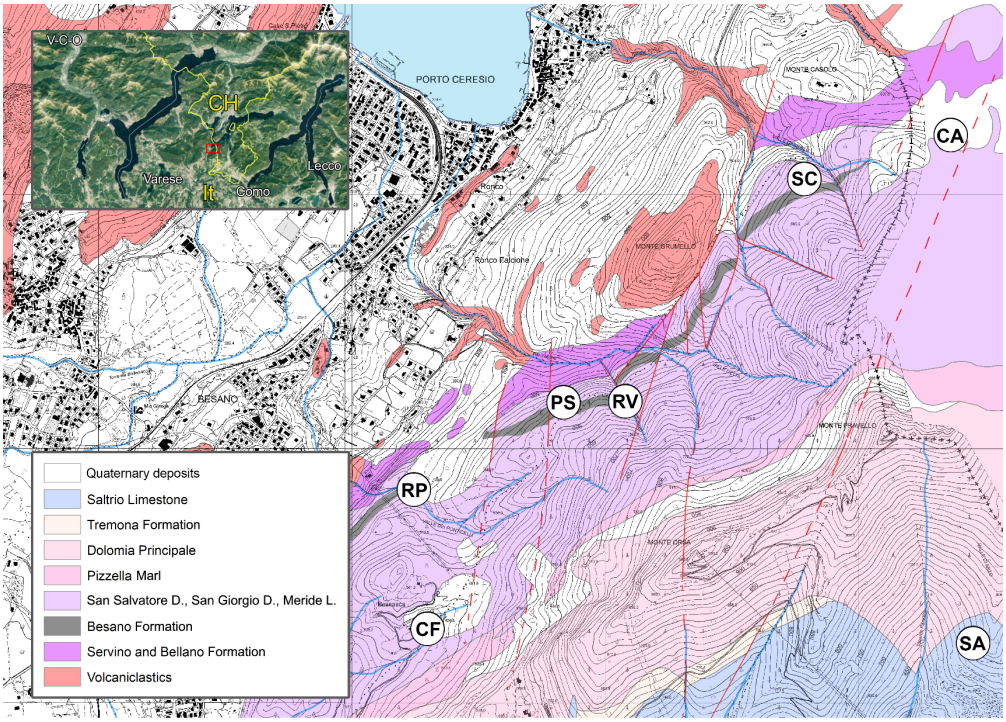

Fig. 1.3 - Schematic geological map of the Italian side of Monte San Giorgio, including the major paleontological sites. Abbreviations: RP, Rio Ponticelli; RV, Rio Vallone; PS, Miniera Piodelle - Selva Bella; SC, Sasso Caldo quarry; CA, Crocifisso-Acqua ferruginosa; CF, Ca' del Frate; SA, Saltrio, Salnova quarry.

The following figure (Fig. 1.4; Furrer, 1995: fig. 10) summarizes the evolution of the Monte San Giorgio basin during the Middle Triassic. The Late Anisian transgression of the Tethys Ocean in the Lombardy basin is testified by the presence of the lower Salvatore Dolomite, overlying the continental facies of the Bellano Formation. This dolomite is constituted by shallow water carbonate sediments, characterized by the presence of bioclast of dasycladacean algae, gastropods, and bivalves. The lower Salvatore Dolomite is followed by the Besano Formation, characterized by the deposition of finely laminated organic-rich dolomites and black shales. Density stratification in the water column, with anoxic bottom water below a pycnocline (Furrer, 1995), absence of bioturbation and very minor or no bottom water currents have facilitated the accumulation and preservation of countless fossils, among which several vertebrates perfectly preserved can be numbered, including large reptiles. The highest diversity in vertebrates (marine and terrestrial reptiles, as well as fishes) is recorded in the middle Besano Formation; this is characterized by the presence of a pelagic fauna, both in the composition of vertebrates (especially ichthyosaurs) and invertebrates, testifying the presence of a clear connection with the open sea during the deposition of this portion of the Formation (Röhl et al., 2001). On the other hand, during the deposition of the upper Besano Formation, this basin was progressively separated from the open sea by growing carbonate platforms and eventually developed into a lagoonal environment (Furrer, 1995; Furrer, 2003; Röhl, 2001). In contrast to the middle Besano Formation, where among marine reptiles Ichthyosaurs were dominant, these shallow waters were populated by sauropterygians and protorosaurs. Moreover, the presence of several terrestrial taxa, including vertebrates and plants, testify the presence of close landmasses. The Besano Formation is overlayed by the lower Meride Limestone, characterized by an alternation of micritic limestones and marls. Its typical invertebrate fauna is constituted by few ammonoids,

pelagic bivalves and radiolarians; vertebrates are represented by small to medium sauropterygians, protorosaurs, and fishes. The basin where the lower Meride Limestone deposited was hypothesized to be deeper than the underlying upper Besano Formation and the overlying upper portion of the Meride Limestone, recording in fact the deposition of fine-grained carbonate mud and clay below the normal wave base. The uppermost portion of the Meride Limestone (the Kalkschieferzone) is characterized by a lower diversity fauna, with common fossils of terrestrial plants; the presence of an increased input of siliciclastic detritus from the landmass, widespread barite, and gypsum crystals suggest that this portion of the Meride Limestone deposited in a wide shallow restricted lagoon. During the latest Ladinian and the earliest Carnian the input of fine siliciclastic material increased, reaching its maximum during the deposition of the Pizzella Marls (or Raibl Beds); during this phase, local deposition of evaporites in a sabkha environment is also observed (Furrer, 1995).

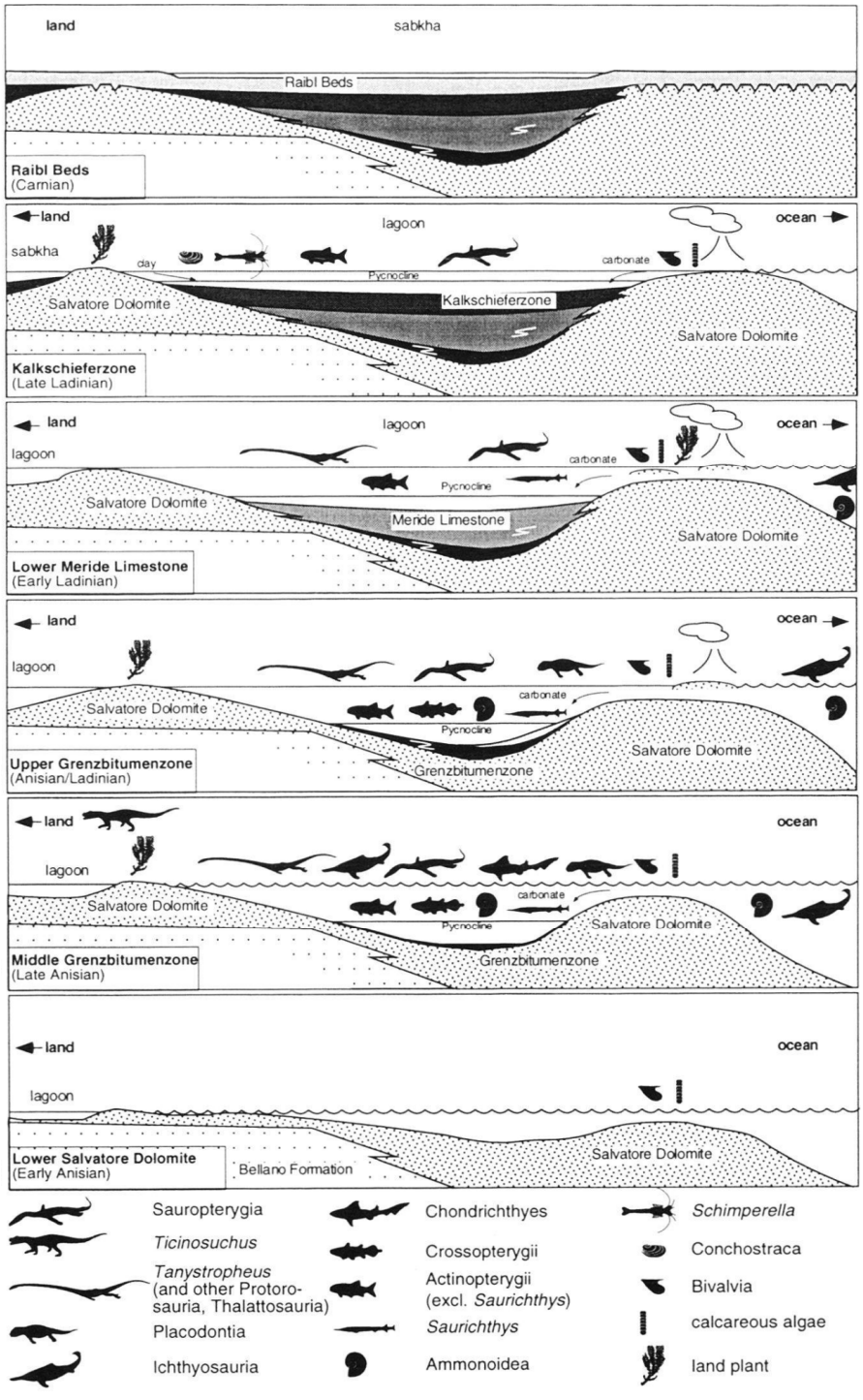

Fig. 1.4 - Simplified sketches of the environmental evolution of the Monte San Giorgio region, from Anisian to Carnian time. Not to scale. After Furrer, 1995.

1.2.3 Paleogeography of the area

At the beginning of the Permian and during the Early Triassic the Neo-Tethys started opening in between Gondwana and the Cimmerian blocks (Fig. 1.5), as the consequence of the migrations of the latter from southern paleolatitudes to subequatorial paleolatitudes (Kent & Muttoni, 2019). In this context, Monte San Giorgio and the wider Southern Alps region were located at the western end of the Tethys. The Middle Triassic is characterized by an extensive development of carbonate platforms worldwide, both in the Western Tethyan realm and in the Eastern Peri-Tethys basins (e.g., Gaetani et al., 2000; Szulc, 2000; Götz & Montenari, 2017). In these basins, the sedimentary successions testify an ongoing long transgressive phase characterizing the end of Permian and the beginning of Triassic, and recording the major recovery phase of marine biota after the Permian-Triassic extinction event (e.g., Chen & Benton, 2012).

During the Middle Triassic, the northern Peri-Tethys Basin (the Germanic Basin) was closed from the north but open unto the Tethys by tectonically controlled depressions (gates) (e.g., Szulc, 2000). South to the Germanic Basin, the western portion of the Southern Alps, during the Late Anisian and Ladinian, was characterized by the presence of several intra-platform basins (Berra et al., 2010). The basinal deposits of Monte San Giorgio can be considered an example of these (Fig. 1.6; Meister et al., 2013).

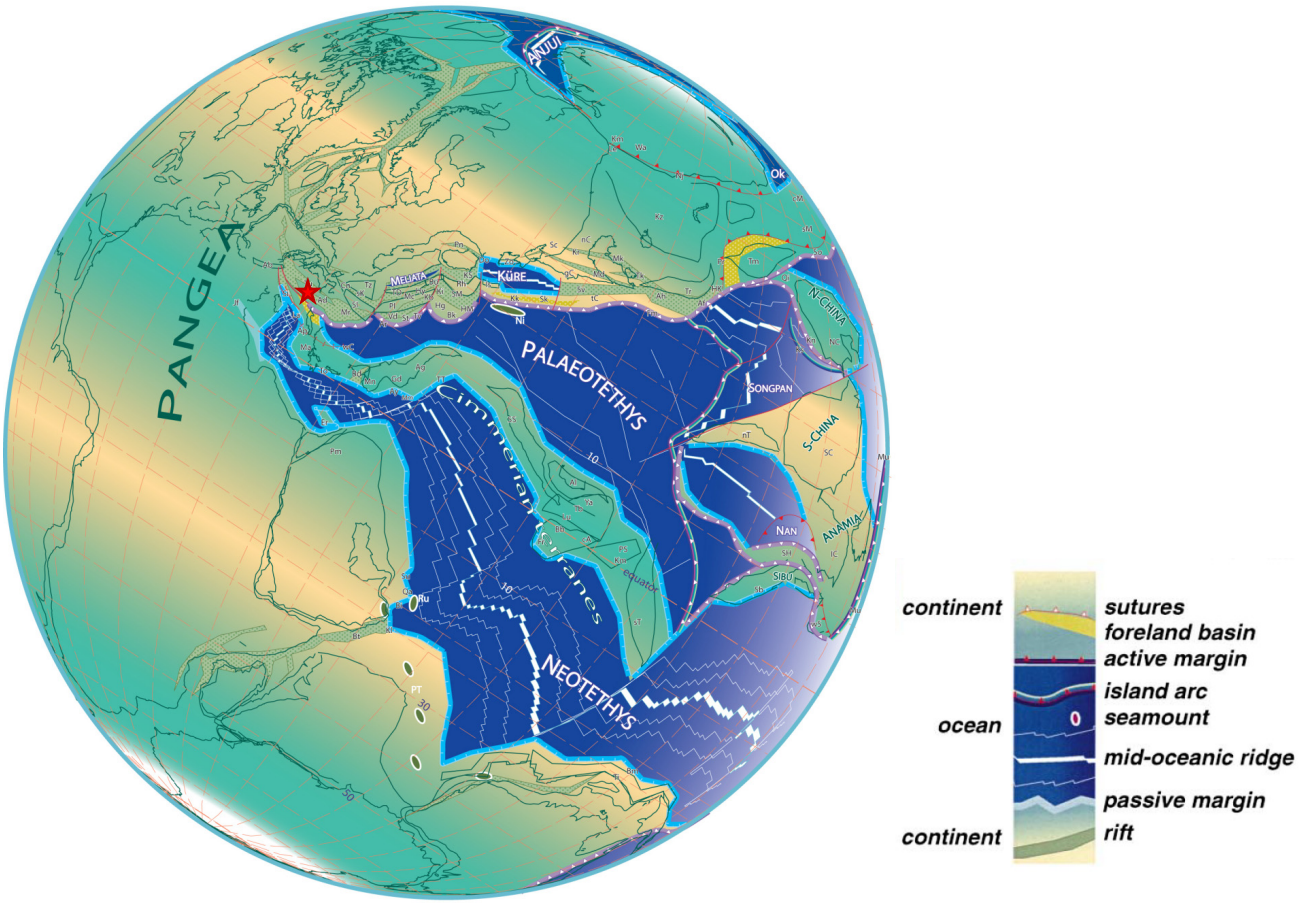

Fig. 1.5 - Paleogeographic reconstruction of the Earth ~240 Ma (Anisian). The globe is centered on the eastern Tethys Ocean. In this phase the Paleo-Tethys subduction is in its final stage. The red star shows the location of Monte San Giorgio. Modified from Stampfli & Borel (2004).

The presence of terrestrial fauna and flora recovered in the Besano Formation deposits (e.g., Krebs, 1965; Pinna & Arduini, 1978; Röhl et al., 2001; Scheyer et al., 2017), as well as in the lower Buchenstein Formation (Renesto et al, 2020), suggests the existence of a continental area to the South and an archipelago of small islands not far from each other (Fig. 1.6). In fact, Renesto et al. (2020) suggested that small-sized terrestrial reptiles could have spread from the mainland to islands, clinging to drifting vegetation, as it can happen in modern days.

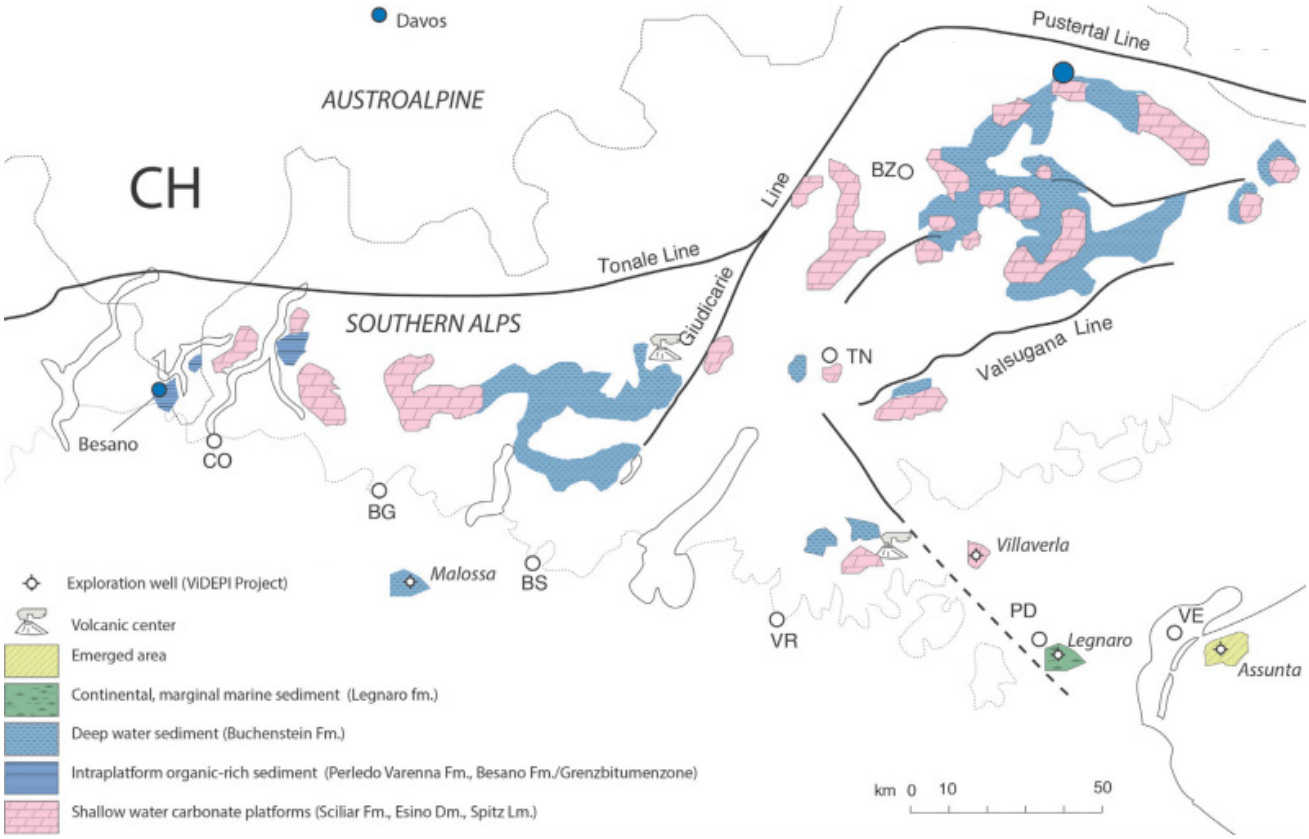

Fig. 1.6 - Paleogeographic reconstruction of the Southern Alps during the latest Anisian. Modified from Renesto et al. (2020).

1.3 Overview of the Besano Formation macrofauna from "Sasso Caldo"

A large collection of macrofossils unearthed at the Sasso Caldo site is housed in the Museo di Storia Naturale di Milano, as a result of more than 25 years of excavations carried out in the site by the paleontologists of the MSNM, under special permit of the Ministero per i Beni Culturali. During the excavations a total of almost 2000 specimens were recovered and now preserved in the museum collections. During the excavation carried out by the MSNM between 1985 and 2003, the sedimentary succession was divided into several "strata". Usually each "stratum" includes a couplet of layers, typically a (lower) dolomitic and an (upper) bituminous layer. The "strata" have been numbered in reversed stratigraphic order from top to bottom. From the analysis of the faunal composition of the Besano Formation at Sasso Caldo, (Fig. 1.7 and Fig. 1.8), including vertebrates and invertebrates, it appears that in the middle Besano Formation (below "stratum" 55 of Sasso Caldo, equivalent to bed 132 of P. 902; see chapter 2) a fauna strongly influenced by the connection with the open sea is present, whereas in the upper Besano Formation (above "stratum" 54) the faunal composition testifies a transition

to a shallower platform environment. This is consistent with what has been reported by Röhl et al. (2001), who hypothesized the presence of an intraplatform basin with a discontinuous open-marine influence during the deposition of the middle Besano Formation, and a shallower subtidal restricted platform environment during the deposition of the upper Besano Formation.
Namely, in the middle Besano Formation a rich and diverse ichthyosaurian fauna is recovered (at least three genera in between strata 87—61: *Besanosaurus, Cymbospondylus,* and *Mixosaurus*); Osteichthyes are abundant and represented by larger specimens than in the upper Besano Formation; Chondrichthyes are represented only by the genus *Acrodus;* sauropterygians are almost absent; ooids and *Daonella* are abundant whereas gastropods are very rare. A new interesting datum is the range of Thylacocephala: 62 specimens of thylacocephalan crustaceans range from st. 70 to st. 61 of the Sasso Caldo quarry; they all belong to the ornamented carapace group of *Microcaris-Atropicaris* (Teruzzi pers. com. 2019). Their supposed benthic way of life would seemingly be in contrast with anoxic or dysoxic conditions at the sea bottom (Affer & Teruzzi, 1999).
In the upper part of the Besano Formation at Sasso Caldo (above "stratum" 54, equivalent to bed 133 of P. 902), the fossil fauna is poorer than in the middle Besano Formation. Ammonoids are almost absent as specimens of *Daonella,* whereas gastropods are more frequent. Ichthyosaurs and Chondrichthyes are absent too, whereas Sauropterygia are present with the genera *Nothosaurus* and *Serpianosaurus*. One very well-preserved specimen of *Macrocnemus* (a terrestrial protorosaur) is also present at "stratum" 36. Such faunal composition testifies the environmental transition from a not so deep intraplatform basin, in the middle Besano Formation, to a shallow subtidal carbonate platform environment, in the upper Besano Formation.

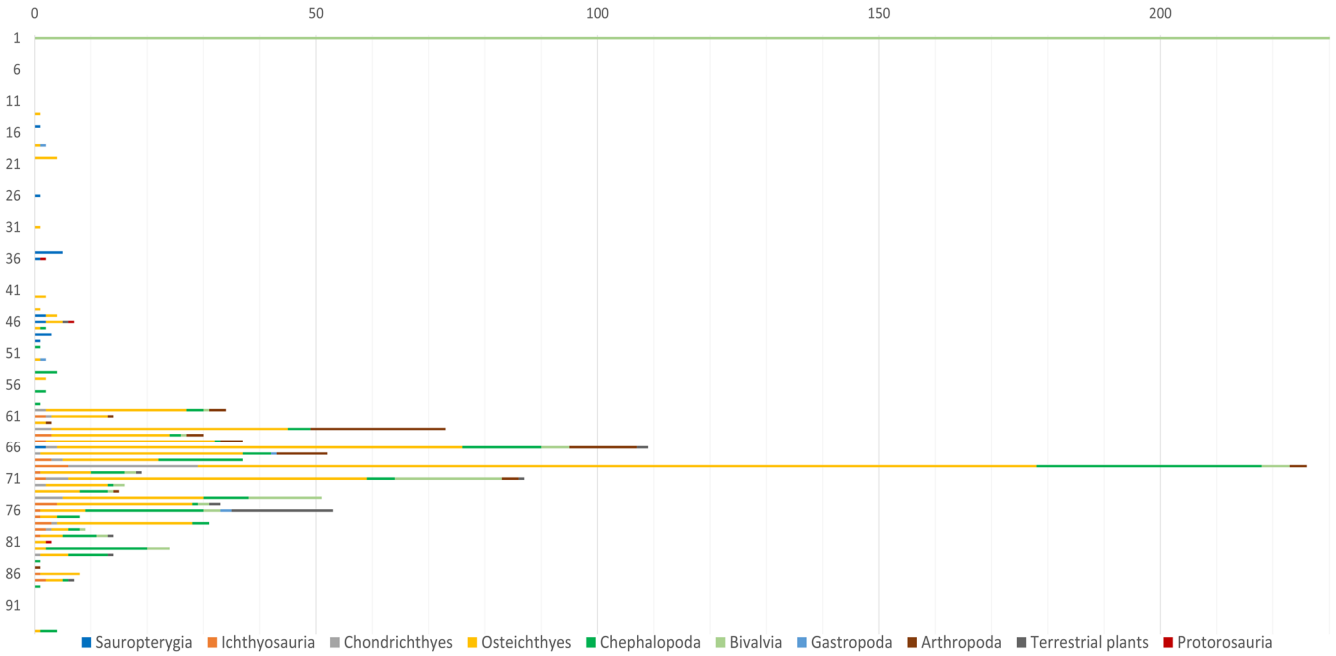

Fig. 1.7 - Number of specimens from the Sasso Caldo quarry, divided in taxonomic groups (x axis) and presented in stratigraphic order (y axis).

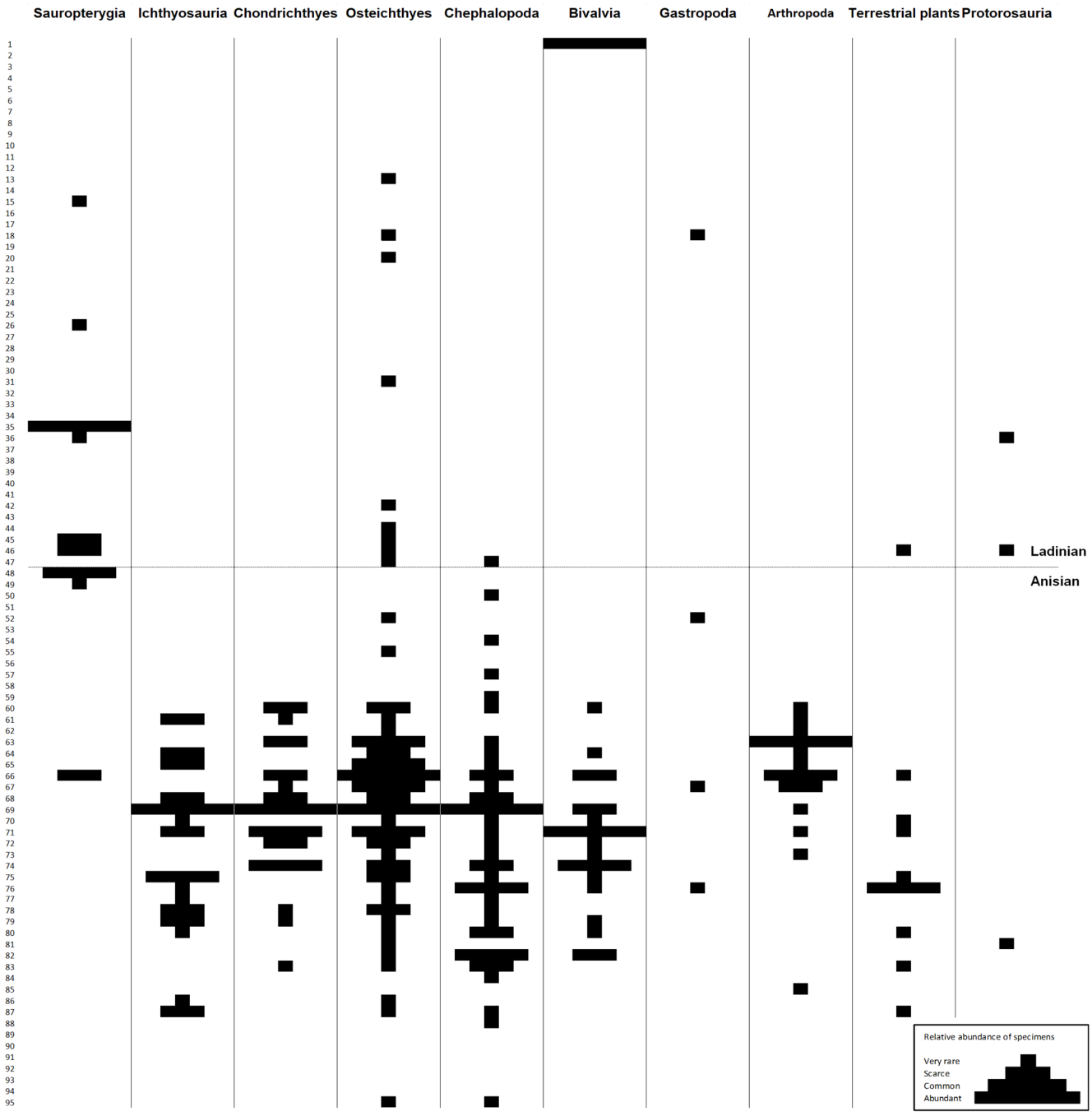

Fig. 1.8 - Macrofossil distribution within the Middle Triassic Besano Formation from Monte San Giorgio, noticed during bed-by-bed excavation at the Sasso Caldo quarry, carried out by the MSNM.

1.4 A brief introduction to the material studied

1.4.1 Invertebrates

During the excavations carried out by the Museo di Storia Naturale di Milano, between 1985 and 2003, 65 specimens of *Daonella* and 220 ammonoids have been collected at the Sasso Caldo quarry, Besano Formation. For most of these specimens, the exact stratigraphic position was recorded. The specimens were studied following a stratophenetic method (Gingerich, 1979). For this work, 83 ammonoids were classified at least at generic level and 44 at specific level, in addition to 59 specimens

of *Daonella* at a specific level. Ammonoids mostly occur within the dolomite levels, but occasionally some specimens were collected from the upper and lower boundary of the bituminous shales. The specimens are often represented only by a flattened internal or external mold, although hollow phragmocones, partly filled by calcite or more rarely pyrite geodes, are not uncommon. The shell is almost never preserved, with the exception of some rare cases. The study of these specimens in chapter 2 will allow a bed-by-bed correlation of the Sasso Caldo section with the known existing localities where the Besano Formation outcrops.

Remains of arthropods are rare, however a remarkably well-preserved scorpion (BES SC 1973) was recovered from the upper part of the Sasso Caldo outcrop: the specimen is complete and composed of a small main slab and its counterpart. A preliminary study (Viaretti et al., 2019) evidenced that this specimen consists of a fossil scorpion carcass. The fossil was examined through stereomicroscopy under natural and UV light, and through SEM. The preservation is exceptional: structures such as trichobothria and median eyes are clearly visible. Results are presented in chapter 3.

1.4.2 Vertebrates

The holotype of *Besanosaurus leptorhynchus* (BES SC 999) is one of the most fascinating fossil specimens from Italy (e.g., Dal Sasso, 2004). Its finding in the Besano Formation of the Sasso Caldo site is dated back to 1993. The specimen measures more than five meters from the tip of the rostrum to the last caudal vertebra. The skeleton is complete, but highly compressed, and lies in a ventrodorsal position with the paired elements symmetrically flattened along the left and right side of the body; this specimen also preserves embryonic material in the thoracic region, as well as soft tissue remains.

The study of *Besanosaurus leptorhynchus*, not only involved the redescription of the holotype, but also the analysis of 5 more specimens referable to the same taxon: these are PIMUZ T4376, 1895, and 4847 from the Paleontological collections of the Zurich University; GPIT 1793/1 from the Paleontological Collection of the Tübingen University, described by Maisch & Matzke (1997) as the holotype of *Mikadocephalus gracilirostris*; and one additional specimen from the MSNM collections (BES SC 1016). All of these specimens come from the Besano Formation.

In this thesis the specimen MSNM V926, attributed to *Cymbospondylus buchseri*, is also described. This consists of three complete vertebrae and, at least, 10 incomplete ribs. The vertebrae are complete and semi-articulated, exposed in right lateral view, and visible on the surface of the slab; these show clear rib articulations (diapophysis). The longest rib is 41,5 cm long. This fossil was collected in the 1950s from the waste material of the Piodelle-Selva Bella mines, near Besano (Varese). Along with the description of this specimen, an isolated fin housed at the Stuttgart Museum für Naturkunde (SMNS 50010) is also presented and attributed to the same taxon; this specimen was recovered at Punkt 902/Mirigioli dig site, on the Swiss side of Monte San Giorgio.

Lastly, a specimen referred to *Helveticosaurus zollingeri*, representing the first skeletal remains of this taxon from Italy, is described. The two slabs belonging to the specimen (MSNM V927 and 928) were collected in 1952 from the waste material of the Piodelle-Selva Bella mines, near Besano (Varese), and deposited in the collections of the MSNM: in the main slab and its counterpart, 9 vertebrae and 9 ribs, as well as the distal end of the left scapula, are recognizable; the second slab contains a portion of the posterodorsal rib cage. In chapter 4 is also redescribed a well-preserved isolated tooth (ST166120, housed at the Museo Scientifico-Naturalistico “Antonio Stoppani”) attributed to *Helveticosaurus* (Renesto & Pieroni 2013), the only known specimen belonging to this taxon before this work.

1.5 Rationale

The chapters composing this thesis are intended as standing alone publications. These are in preparation, submitted, or published. The following table summarizes the content of this work and the role that the student had in the preparation of the manuscripts. The role will be specified using the following acronyms: correspondent author (CA), writing manuscript (WM), figure preparation (FP), member of the collaboration team (MCT). Chapters will be presented in systematic order, depending on the fossil specimens described in each of them.

Chapter number	List of authors	Short title	Role
2	Balini, Bindellini, Teruzzi, Dal Sasso	Biochronostratigrapy of the Besano Formation at Sasso Caldo	MCT, WM, FP
3	Viaretti, Bindellini, Dal Sasso	A new Mesozoic scorpion from the Besano Formation	MCT, WM, FP
4	Bindellini, Dal Sasso	First skeletal remains of *Helveticosaurus* from Italy	CA, WM, FP
5	Bindellini, Dal Sasso	New cymbospondylid material from the Besano Formation	CA, WM, FP
6	Bindellini Wolniewicz, Miedema, Scheyer, Dal Sasso	Cranial anatomy of *Besanosaurus leptorhynchus*	CA, WM, FP
7	Bindellini, Wolniewicz, Miedema, Dal Sasso, Scheyer	Postcranial anatomy of Besanosaurus leptorhynchus	CA, WM, FP
8	Miedema, Bindellini, Wolniewicz, Maxwell, Dal Sasso	Late-stage embryonic material in the holotype of Besanosaurus leptorhynchus	MCT, WM, FP

In order to complete the three years' work, the student faced various phases in this order:

1- Study of the stratigraphic sections of the Besano Formation cropping out in Italy, with a special focus on the Sasso Caldo section.
2- Study of the invertebrates collection from the Sasso Caldo section, housed in the Museo di Storia Naturale di Milano.
3- Integrated biochronostratigraphic study of the Sasso Caldo section and writing of chapter 2.
4- Study of the vertebrates material housed in the Museo di Storia Naturale di Milano and recovered from the Italian outcrops of the Besano Formations
5- Collection visits around Europe (Zurich, Stuttgart, Tubing, Holzmaden, Venegono, Padova Uppsala) in order to observe or study relevant specimens of marine reptiles for comparison or publication.
6- Writing of chapters 6, 7, and 8, which namely include a complete and detailed revision of the known material attributed to *Besanosaurus leptorhynchus*.
7- Study and description of the most important specimens coming from the Italian outcrops of the Besano Formation and housed in the Museo di Storia Naturale di Milano, followed by the writing of chapters 3, 4, and 5.

1.6 References

Affer D. & Teruzzi G. 1999. Thylacocephalan crustaceans from the Besano Formation, Middle Triassic, N. Italy. *Rivista del Museo Civico di Scienze Naturali "E. Caffi",* 20, 5-8.

Beardmore S.R., Furrer, H. 2016. Taphonomic analysis of *Saurichthys* from two stratigraphic horizons in the Middle Triassic of Monte San Giorgio, Switzerland. *Swiss Journal of Geosciences*, 109: 1-16.

Bernasconi S.M. 1991. Geochemical and microbial controls on dolomite formation and organic matter production/preservation in anoxic environments a case study from the Middle Triassic Grenzbitumenzone, Southern Alps (Ticino, Switzerland). D. Phil. thesis, Swiss Federal Institute of Technology Zürich, Switzerland, 196 pp.

Bernasconi S.M. 1994. Geochemical and microbial controls on dolomite formation in anoxic environments: A case study from the Middle Triassic (Ticino, Switzerland). *Contributions to Sedimentology*, 19:1-109.

Bernoulli, D. 1964. Zur Geologie des Monte Generoso:(Lombardische Alpen); ein Beitrag z. Kenntnis der südalpinen Sedimente, Ph.d. thesis, Diss. Basel: Stämpfli & Cie.

Brack P, Rieber H. 1986. Stratigraphy and ammonoids of the lower Buchenstein Beds of the Brescian Prealps and Giudicarie and their significance for the Anisian/Ladinian Boundary. *Eclogae Geologicae Helvetiae*, 79:181-225.

Brack P, Rieber H, 1993. Towards a better definition of the Anisian/Ladinian boundary: New biostratigraphic data and correlations of boundary sections from the Southern Alps. *Eclogae Geologicae Helvetiae*, 86:415-527.

Brack P, Rieber H, Nicora A, Mundil R. 2005. The Global boundary Stratotype Section and Point (GSSP) of the Ladinian Stage (Middle Triassic) at Bagolino (Southern Alps, Northern Italy) and its implications for the Triassic time scale. *Episodes*, 28:233-244.

Bürgin T., Rieppel O., Sander P.M., Tschanz, K. 1989. The fossils of Monte San Giorgio. *Scientific American*, 260: 74-81.

Chen Z.Q., Benton M.J. 2012. The timing and pattern of biotic recovery following the end-Permian mass extinction. *Nature Geoscience*, 5: 375-383.

Dal Sasso C. 2004. Dinosaurs of Italy. Indiana University Press, Bloomington and Indianapolis, 216 pp.

Dal Sasso C, Pinna G. 1996. *Besanosaurus leptorhynchus* n. gen. n. sp., a new shastasaurid ichthyosaur from the Middle Triassic of Besano (Lombardy, N. Italy). *Paleontologia Lombarda*, Nuova serie, 4:3-23.

Etter W. 2002. Monte San Giorgio: Remarkable Triassic marine vertebrates. In: Bottjer DJ, Etter W, Hagadorn JW, Tang CM eds. *Exceptional fossil preservation. A unique view on the evolution of marine life*. New York: Columbia University Press, 220-242.

Frauenfelder A. 1916. Beiträge zur Geologie der Tessiner Kalkalpen. *Eclogae Geologicae Helvetiae*, 14: 247-367.

Furrer H. 1995. The Kalkschieferzone (Upper Meride Limestone; Ladinian) near Meride (Canton Ticino, Southern Switzerland) and the evolution of a Middle Triassic intraplatform basin. *Eclogae Geologicae Helvetiae*, 88:827-852.

Furrer H. 2003. Der Monte San Giorgio im Südtessin-vom Berg der Saurier zur Fossil-Lagerstätte internationaler Bedeutung. *Neujahrsblatt der Naturforschenden Gesellschaft in Zurich*, 206:64.

Gaetani M., Lozowski V., Szulc J., Arche A., Calvet F., López-Gómez J., Hirsch, F. 2000. Early Ladinian (238–235 Ma). In: Dercourt J., Gaetani M., Vrielynck B., Barrier E., Biju-Duval B., Brunet M.F., Cadet J.P., Crasquin S., Sandulescu M. (Eds.), Atlas Peri-Tethys, Paleogeographical Maps. CCGM/CGMW, Paris (Map 5).

Gingerich P.D. (1979). The stratophenetic approach to phylogeny reconstruction in vertebrate paleontology. In: Cracraft, J. & Eldredge, N. (Eds.): Phylogenetic analysis and paleontology, 41-77; New York, (Columbia University Press).

Götz, A.E., Montenari, M. 2017. A Facies-Independent Trans-European Anisian–Ladinian Marker Horizon? Significance and Impact for Sequence Stratigraphy and Intra-Tethyan Correlation. *Stratigraphy & Timescales*, 2: 391-409.

Muttoni G., Kent D.V. 2019. Adria as promontory of Africa and its conceptual role in the Tethys Twist and Pangea B to Pangea A Transformation in the Permian. *Rivista Italiana di Paleontologia e Stratigrafia*, 125: 249-269.

Krebs B. 1965. *Ticinosuchus ferox* nov. gen. nov. sp. *Schweizerische Paläontologische Abhandlungen,* 81:1–140.

Kuhn-Schnyder E. 1974. *Die triasfauna der tessiner Kalkalpen*. Naturforschenden Gesellschaft in Zürich, Zürich, 119 pp.

Meister P., Mckenzie J.A., Bernasconi S.M., Brack, P. 2013. Dolomite formation in the shallow seas of the Alpine Triassic. *Sedimentology*, 60: 270-291.

Mundil R, Brack P, Meier M, Rieber H, Oberli F. 1996. High resolution U-Pb dating of Middle Triassic volcaniclastics: Time-scale calibration and verification of tuning parameters for carbonate sedimentation. *Earth and Planetary Science Letters*, 141:137-151.

Muttoni G., Nicora A., Brack P., Kent D.V. 2004. Integrated Anisian/Ladinian boundary chronology. *Palaeogeography, Palaeoclimatology, Palaeoecology*, 208: 85-102.

Nosotti S., Teruzzi G., Teruzzi G. 2008. I rettili di Besano-Monte San Giorgio. *Natura*.

Pinna G. & Arduini P. 1978. Un nuovo esemplare di Besano in Lombardia. *Natura*, 69: 73-80

Preto, N., Kustatscher, E., & Wignall, P. B. 2010. Triassic climates—state of the art and perspectives. *Palaeogeography, Palaeoclimatology, Palaeoecology*, 290:1-10.

Renesto S. & Pieroni V. 2013 - Middle Triassic vertebrate remains from Rasa Village (Varese, Northern Italy). In: Tanner L.H., Spielmann J.A. & Lucas S.G. (eds.) - The Triassic System: New Developments in Stratigraphy and Paleontology, Bulletin 61: 485-488. New Mexico Museum of Natural History and Science, New Mexico.

Renesto S, Kustatscher E, Gianolla P. 2020. A putative juvenile specimen of *Eusaurosphargis dalsassoi* from the Anisian (Middle Triassic) of Piz Da Peres (Dolomites, Northern Italy). *Rivista Italiana di Paleontologia e Stratigrafia*, 126: 249-259.

Rieber H. 1973. Die Triasfauna der Tessiner Kalkalpen, XXII. Cephalopoden aus der Grenzbitumenzone (Mittlere Trias) des Monte San Giorgio (Kanton Tessin, Schweiz). *Schweizerische Paläontologische Abhandlungen*, 93:1-96.

Röhl H., Schmid-Röhl A., Furrer H., Frimmel A., Oschmann W., Schwark L. 2001. Microfacies, geochemistry and palaeoecology of the Middle Triassic Grenzbitumenzone from Monte San Giorgio (Canton Ticino, Switzerland). *Geologia Insubrica*, 6:1–13.

Saller, F. 2016. Anatomia, paleobiologia e filogenesi di *Macrocnemus bassanii* Nopcsa 1930 (Reptilia, Protorosauria). Ph.D. thesis. Università di Bologna.

Sommaruga A, Hochuli P, Mosar J. 1997. The Middle Triassic (Anisian) conglomerates from Capo San Martino, South of Lugano-Paradiso (Southern Alps, Switzerland). *Geologia Insubrica*, 2:1–14.

Scheyer T.M., Neenan J.M., Bodogan T., Furrer H., Obrist C., & Plamondon M. 2017. A new, exceptionally preserved juvenile specimen of *Eusaurosphargis dalsassoi* (Diapsida) and implications for Mesozoic marine diapsid phylogeny. *Scientific Reports*, 7: 1-22.

Stockar R. 2010. Facies, depositional environment, and palaeoecology of the Middle Triassic Cassina beds (Meride Limestone, Monte San Giorgio, Switzerland). *Swiss Journal of Geosciences*, 103: 101–119.

Stockar R., & Renesto S. 2011. Co-occurrence of *Neusticosaurus edwardsii* and *N. peyeri* (Reptilia) in the lower Meride limestone (Middle Triassic, Monte San Giorgio). *Swiss Journal of Geosciences*, 104: 167-178

Stockar R, Baumgartner PO, Condon D. 2012. Integrated Ladinian bio-chronostratigraphy and geochronology of Monte San Giorgio (Southern Alps, Switzerland). *Swiss Journal of Geosciences*, 105:85-108.

Stockar R., Adatte T., Baumgartner P.O., Foellmi K.B. 2013. Palaeoenvironmental significance of organic facies and stable isotope signatures: the Ladinian San Giorgio Dolomite and Meride Limestone of Monte San Giorgio (Switzerland, WHL UNESCO). *Sedimentology*, 60: 239–269

Szulc J. 2000. Middle Triassic evolution of the northern Peri-Tethys area as influenced by early opening of the Tethys Ocean. In *Annales Societatis Geologorum Poloniae*, 70: 1-48.

Viaretti M., Bindellini G., Dal Sasso C. 2019. An exceptionally well-preserved scorpion from the Besano Formation (Monte San Giorgio, Middle Triassic, Southern Alps): preliminary study. *Fossilia*, 2020: 53-55.

Winterer E.L., Bosellini, A. 1981. Subsidence and sedimentation on Jurassic passive continental margin, Southern Alps, Italy. *AAPG bulletin*, 65: 394-421.

Wotzlaw JF, Brack P, Storck JC. 2017. High-resolution stratigraphy and zircon U–Pb geochronology of the Middle Triassic Buchenstein Formation (Dolomites, northern Italy): precession-forcing of hemipelagic carbonate sedimentation and calibration of the Anisian–Ladinian boundary interval. *Journal of the Geological Society*, 175:71-85.

Zorn H. 1971. Paläontologische, stratigraphische und sedimentologische Untersuchungen des Salvatoredolomits (Mitteltrias) der Tessiner Kalkalpen: unter besonderer Berücksichtigung der Mikrofazies, Diagenese und Taxionomie der Lamellibranchiata. *Schweizerische Paläontologische Abhandlungen,* 91:1–90.

Chapter 2
Middle Triassic ammonoid and *Daonella* integrated biochronostratigraphy of the Besano Formation at "Sasso Caldo" section (Italy), Monte San Giorgio UNESCO WHL

*Draft of a manuscript to be submittted to the Rivista Italiana di Paleontologia e Stratigrafia.
Marco Balini[1], Gabriele Bindellini[1], Giorgio Teruzzi[2], Cristiano Dal Sasso[2]
[1] Dipartimento di Scienze della Terra "Ardito Desio", Università degli Studi di Milano, Milano, Italy.
[2] Sezione di Paleontologia, Museo di Storia Naturale di Milano, Milano, Italy.

2.1 Abstract

With this contribution, we show the results of the ammonoid and *Daonella* zonation of the Besano Formation (Anisian/Ladinian boundary) at "Sasso Caldo" (SC) quarry section on the Italian side of Monte San Giorgio (NW Lombardy). The Besano Fm is the most fossiliferous unit of the Middle Triassic succession of the Monte San Giorgio site (UNESCO WHL), which has provided one of the best preserved records of marine life in the Triassic period.
During the excavations led by the Natural History Museum of Milan (MSNM) at SC (from 1985 to 2003, directed by G. Teruzzi) almost 2000 specimens, including plant remains, vertebrates, and invertebrates, were collected. The collection stored at the MSNM includes 65 specimens of *Daonella* and more than 200 ammonoids. These fossils, whose stratigraphic importance has been proven in the past years (i.e., Rieber, 1969, 1973), have never been studied since now.
The biochronostratigraphic study of the Sasso Caldo succession allowed a precise correlation with the known Swiss fossil localities of Monte San Giorgio where the Besano Formation outcrops. Relatively good specimens range from bed 61 to bed 140. The genus *Repossia* ranges from bed 69 to bed 74; *Stoppaniceras* is present from bed 76 to bed 87, but also a single specimen of *S. variabilis* has been found at st. 61; *Nevadites* ranges from bed 96 to bed 108; *Serpianites* ranges from bed 100 to bed 116. In regard to the bivalve *Daonella*, *D. vaceki* is present from bed 65 to bed 70; *D. airaghii* occurs in bed 74; *D. pseudomoussoni* ranges from bed 74 to bed 82; *D. fascicostata* ranges from bed 84 to bed 108; *D. luganensis* occurs in bed 104. All of these taxa document the *Nevadites secedensis* Zone. Eventually we point out that, whereas the ranges of the *Daonella* species match perfectly with the already published Swiss material, the ranges of ammonoid genera slightly differ from the ranges reported in the Swiss localities.

2.2 Introduction

The Besano Formation (=Grenzbitumenzone; Late Anisian-Early Ladinian) is one of the most important Triassic marine fossil-bearing units in the world. This formation is documented in a small area in the surroundings of Monte San Giorgio, between Varese (Italy) and Lake Lugano (Switzerland) and is extremely rich in invertebrates and in well preserved vertebrates, which were discovered in the middle of the 19th century. The importance of the Besano Formation is not only in its peculiar paleontological record, but it has a wider value, because the sedimentary succession overlying it includes further six fossil-bearing intervals, each one so rich in fossils to be considered as a Fossil-lagerstatte. This extraordinary Middle Triassic fossil record of the Monte San Giorgio area has no equivalent in the World, and its outstanding value has been acknowledged by the selection in the UNESCO World Heritage List (https://whc.unesco.org/en/list/1090/; Felber et al., 2004; Furrer, 2004) on the Switzerland side in 2003, extended in 2010 to the Italian side.

The most attractive and historically important fossils from the Besano Formation are the marine reptiles and fishes, usually preserved in bituminous shales interbedeed between dolomite beds. Study of these fossils in the 19th and the early 20th centuries unraveled a crucial and at that time unexpected evolutionary development of some groups of reptiles, that after colonization of the continental environments in the Permian, in the Triassic left the subaerial environments to come back to marine environments (e.g., Dal Sasso & Pinna, 1996; Brinkmann, 1997; Maish & Matzke, 1998; Nosotti et al., 2008; Renesto et al., 2020; Bindellini et al., 2021).

The invertebrates are mostly documented in the dolomite beds, occasionally occurring in the bituminous shales. They are not as well preserved as the vertebrates, and this might be the reason why the literature on invertebrates is way less abundant than the one on vertebrates. Ammonoids were mentioned by Bassani (1886), Frauenfelder (1916) and Senn (1924), but systematic descriptions were provided by Mojsisovics (1882), Airaghi (1911, 1912), Rieber (1973, 1974). Two coleoidea were described by Rieber (1970, 1974), who also provided a detailed systematic study of the bivalve *Daonella* (Rieber, 1968; Rieber, 1969). Gastropods were reported by Bassani (1886), Furrer & Vandelli (2014) and Lopez-Arbarello et al. (2016) and Rieber (1973), but the only comprehensive systematic description has been recently published by Pieroni & Furrer (2020). Conodonts were described by Müller (1964) and Rieber (1980).

Most of the recent literature on invertebrates from the Besano Formation is based on bed-by-bed collections from localities sampled in the Swiss side of the UNESCO site. In this contribution we present the first study of bed-by-bed collected ammonoids and *Daonella* from a locality on the Italian side of the UNESCO site. The specimens were collected at Sasso Caldo, near Besano, during excavations led by the Museo di Storia Naturale di Milano (MSNM; field director G. Teruzzi) from 1985 to 2003.

2.3 Geological and stratigraphic setting

Sasso Caldo is one of the fossil localities of the Besano Formation in Italy (Fig. 2.1). It is located on the north-western slope of Monte Pravello, about 2 km NE of Besano, very close to the border with Switzerland. The locality might be reached by forest roads from Porto Ceresio or from Besano.
Monte Pravello and Monte San Giorgio ridge geologically consists of a south dipping, Lower to Upper Triassic sedimentary succession unconformably overlying Permian volcaniclastics (Fig. 2.2). The Olenekian to ?Early Anisian was characterized by siliciclastic sedimentation of the Servino and Bellano

Formation. The overlying San Salvatore Formation documents the establishment of a Carbonate platform environment during the Anisian. In the area west and north of Monte Pravello-Monte San Giorgio the shallow water carbonate sedimentation (San Salvatore Formation) persisted until the end of Ladinian (e.g., Zorn, 1971; Bernasconi 1991), while in the area of Monte Pravello-Monte San Giorgio an intraplatform basin was established. The sedimentary succession deposited in this setting consists of Besano Formation, Meride Limestone, and Kalkschieferzone (Fig. 2.2).

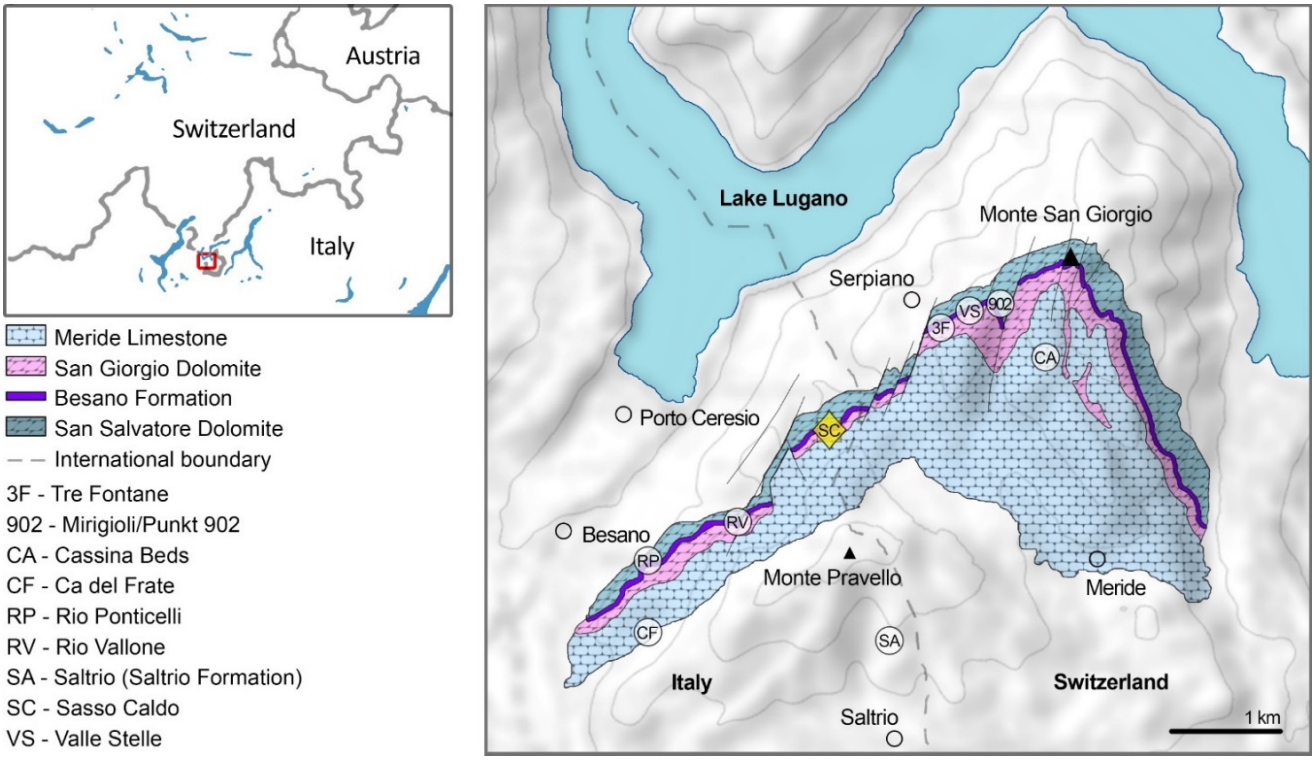

Fig. 2.1 - Relevant fossil sites in the Monte San Giorgio area. Map of the Monte San Giorgio area showing the Middle Triassic carbonate succession, the major paleontological quarries in the area (white circles), and the Sasso Caldo site (yellow rhombus).

The Besano Formation (Late Anisian-Early Ladinian) consists of a monotonous alternation of dolomite beds and bituminous shales, for a thickness of about 15-17 m. This unit is almost exactly equivalent to the Grenzbitumenzone, a local lithostratigraphic name used for several decades in Switzerland, but that is now synonymized with Besano Formation (Bernoulli et al. 2018). The most complete and best studied stratigraphic section of the Besano Formation is Punkt 902/Mirigioli in Switzerland, a historical site where the Palaeontologische Museum of Zurich and Basel University carried out extensive paleontological excavation from 1950 to 1968. The available knowledge on this site was summarized by Röhl et al. (2001), who divided the Grenzbitumenzone (=Besano Formation) in three parts: lower and upper part were deposited in a shallow restricted carbonate platform environment, while the middle part was deposited in a deeper intraplatform basin with frequent disoxic bottom conditions (e.g., Bernasconi, 1991). The first one is characterized by a great abundance of pelagic marine vertebrates, as well as pelagic invertebrates, and therefore likely strongly influenced by a connection with the open sea; On the other hand the upper Besano Formation is characterized by the presence of sauropterygians and terrestrial fauna and flora, and was likely close to a land mass.

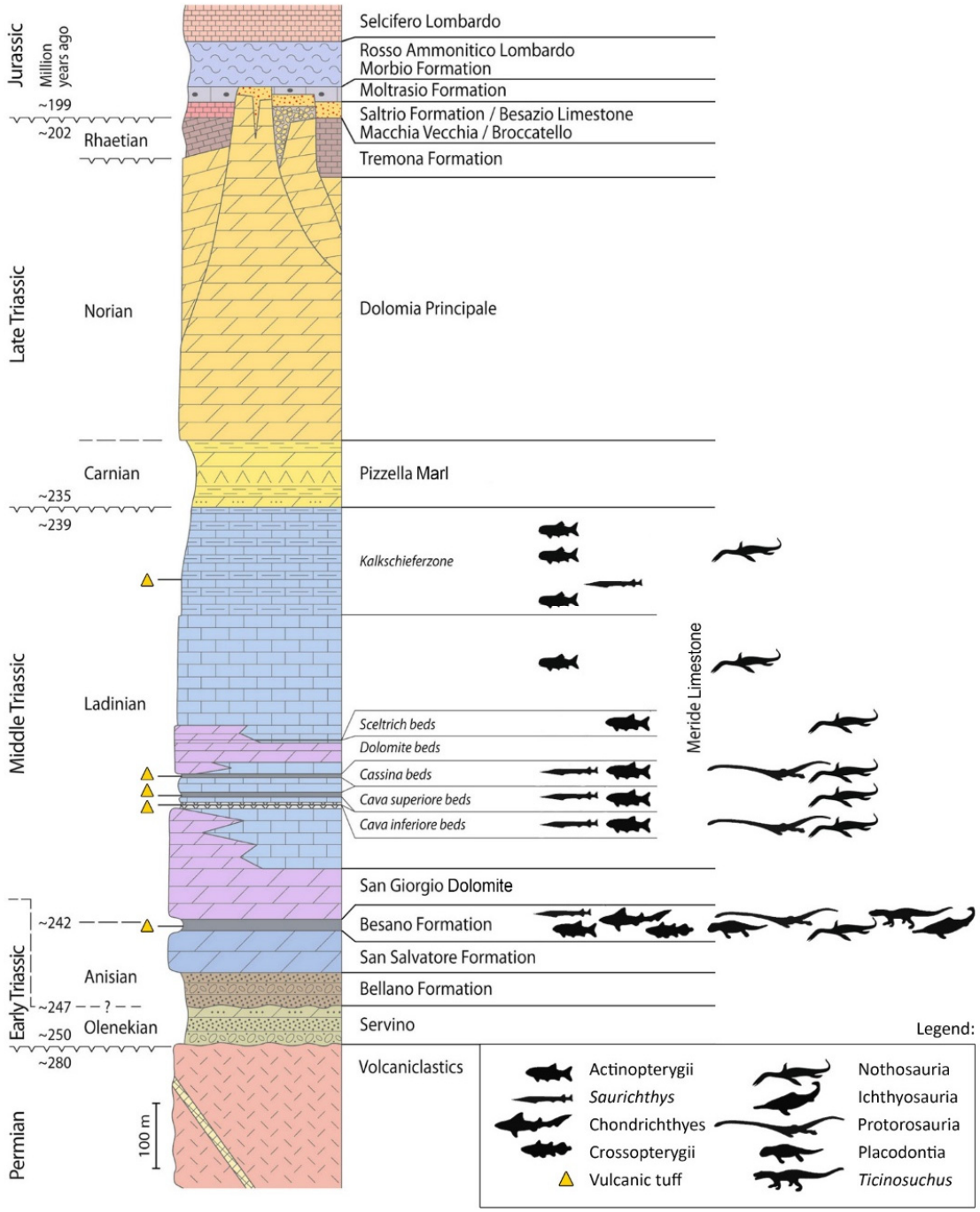

Fig. 2.2 - Sedimentary succession of the Monte San Giorgio area. Monte San Giorgio Scientific Commission (2014), modified.

2.3.1 The Sasso Caldo section

The site of paleontological excavation was identified after a survey of the area, and surface collecting. The excavation started in 1985 and field works were concluded in 2003. Sampling was carried out from top to bottom, and numbering was given following the reverse stratigraphic order (e.g., numbering increases from younger to older beds). Every number was given to a dolomite and overlying bituminous shale couplet, and such a couplet was defined as "stratum" (e.g., Dal Sasso & Pinna, 1996; Nosotti & Rieppel, 2003; Nosotti, 2007; Renesto et al., 2020; Teruzzi pers. com., 2019). The numbering of "strata" was reported on the outcrop by small metal plates (Fig. 2.3), that have endured for many years. The preservation

of this information was crucial, because the stratigraphic log of the section (Fig. 2.4) has been measured and described in 2018-19, many years after the end of the excavation in Sasso Caldo quarry. For completeness, simplicity and accuracy, thanks to the chronostratigraphic study perfomed for this research, the "strata" were converted using the bed numbers reported for Punkt 902 section (Fig. 2.4). This latter section is used as a reference since is it includes the whole section of the Besano Formation, it is well known and largely studied (e.g., Rieber, 1968; 1969; 1973; Bernasconi 1991; Brack et al., 2005). The Sasso Caldo section covers about 10 m of the Besano Formation and the very lower part of the overlying San Giorgio Dolomite (Fig. 2.3). The general lithology fully conforms with the typical lithology of the Besano Formation, with monotonous alternation of dolomites beds and bituminous shale interbeds with D/BS thickness ratio of 6.8. Six tuff layers are documented: four (Tc, bed 71, Td, and Te), up to 4 cm thick, in the lower part of the section, and two very thin layers in the upper part (bed 148 and bed 160). Tuff layers from the Besano Formation are well known are well known as stratigraphic markers (Brack & Rieber, 1986, 1993).

Fig. 2.3 - The Sasso Caldo section, Besano Formation, cropping out about 2 km NW of Besano (Va). The picture was taken in 2019 and documents the condition of the quarry after more than 15 years of inactivity. White small metal plates numbering the "strata" are still visible.

2.4 Materials and methods

2.4.1 Materials

The collection stored at the MSNM includes 65 specimens of *Daonella* and 220 ammonoids. We classified 83 ammonoids at least at generic level and 44 at specific level, in addition to 59 specimens of *Daonella* classified at specific level. The preservation of ammonoids depends on the nature of the embedding matrix. Ammonoids mostly occur within the dolomite beds, but occasionally some specimens were collected from the upper and lower boundary of the bituminous shales. The specimens from shaly interbeds are usually notably flattened (see also Rieber, 1973:fig. 3), while those from dolomite beds are less flattened. The specimens from dolomites exhibit features indicating rapid burial without infilling of the phragomocone, sediment compaction followed by dissolution of the test. As result, these Ammonoidea are usually preserved as slightly flattened internal molds of the body chamber and external mold of the entire shell. Hollow phragmocones, partly filled by calcite or more rarely pyrite geodes, are not uncommon.

2.4.2 Methods

The bedding of the Besano Formation at Sasso Caldo closely matches the bedding at Puntk 902 (see Bernasconi, 1991; Röhl et al. 2005), the most complete section in the Besano Formation. This tight fitting allowed us to convert the original field numbering of "strata" at Sasso Caldo, in reverse stratigraphic order, into an ascending numbering calibrated with the bedding at Punkt 902. The stratimetric calibration was further cross-checked with tuff layers and biochronostratigraphic correlations (see chapter 2.6)

The exact stratigraphic position of most of the ammonoids and *Daonella* was recorded during field works, then the collection was studied following a stratophenetic method (Gingerich, 1979). A crucial reference for this study has been the outstanding papers by Rieber (1969, 1973) on the daonellid and cephalopod fauna of the Besano Formation (Grenzbitumenzone *sensu* Rieber, 1973) from Punkt 902.

Specimens were inspected through a visual analysis. The morphological features were studied by using a Leica MZ9-5 stereomicroscope equipped with a plan 1.0x lens, 10/20x oculars, and a 0.63 to 6.0 zoom. Following Rieber (1973), well-preserved hollow specimens were cast with silicone rubber and the molds so obtained used to study the morphology of the ammonoid.

The photos for the plates presented at the end of this chapter were taken by using the Ammonium chloride withening technique (Teichert, 1948).

2.5 Results

All the available ammonoids and bivalves from the Sasso Caldo site (Besano Formation), housed in the collections of the Museo di Storia Naturale di Milano, were examined and determined. The systematic study led to the recognition of 15 ammonoid taxa belonging to 10 genera, and five species belonging to the bivalve genus *Daonella*.

2.5.1 Ammonoids

Ten genera belonging to Ammonoidea were recognized. These include *Repossia*, *Stoppaniceras*, *Nevadites*, *Serpianites*, *Lecanites*, *Longobardites*, *Celtites*, *Gymnites*, *Monophyllites*, and *Flexoptychites* (Fig. 2.4). These taxa have already been reported from Punkt 902, Besano Formation by Rieber (1973) and Brack &

Rieber (1986, 1993). *Serpianites* and *Repossia* are typical components of the ammonoid fauna of the Besano Formation (Rieber, 1973) together with *Stoppaniceras*. *Serpianites* has never been reported outside the Monte San Giorgio area, while *Repossia* occasionally has been reported outside Monte San Giorgio. The genus has been reported from Parina Valley (Sestini Fantini, 1996), Dolomites (De Zanche et al.,1995), and Balaton area (Vörös, 2018). All other genera exhibit a much wider paleobiogeographic and paleoecologic distribution (Fig. 2.4).

The genus *Repossia* is represented only by one species: *R. acutenodosa* (Pl. 1: Fig.3-6). This ammonoid ranges from bed 69 to 74. 12 specimens belong to this genus, of which eight were determined as *R. acutenodosa*.

The genus *Stoppaniceras* (Pl. 2) is present from bed 61 to bed 87, as reported by Rieber (1973) for Punkt 902 section; 19 specimens belong to this genus. This genus is represented by three species: a single specimen of *S. variabilis* has been found at bed 61; *S. artinii* (Pl. 2: Fig.1, 2, 4), is present from bed 76 to bed 82 with 14 specimens; a single specimen from bed 82 has been assigned to *S.* sp. indet. b (*sensu* Rieber, 1973; Pl. 2: Fig. Fig. 4). A single specimen of *S. variabilis* (Pl. 2: Fig. 5) is recovered in bed 61 and marks the lowermost preserved bed of the Besano Formation at Sasso Caldo.

The genus *Lecanites* ranges from bed 65 to bed 74; *L. misanii* (Pl. 1: Fig. 1, 2) occurs only in bed 76 and is represented by several specimens. The genus *Celtites*, represented by four specimens, is found from bed 82 to bed 100; this genus appears and disappears later than what was reported for Punkt 902 section, where it ranges from bed 81 to bed 87 (Rieber, 1973).

Nevadites (Pl. 3) ranges from bed 96 to bed 108; 22 specimens were assigned to this genus. *N. dealessandrii* (Pl. 3: Fig. 4-7) occurs only in bed 98 and 9 specimens were attributed to this taxon; two specimens were determined as *N.* cf. *ambrosionii* (Pl. 3: Fig. 1) and this species only occurs in bed 108. The range of *Nevadites* seems to appear and disappear a little earlier than what was reported by Rieber (1973) for Punkt 902 section, where this genus ranges from bed 98 to bed 112.

The genus *Serpianites* (Pl. 4) ranges from bed 100 to bed 116 with 13 specimens; the group *S. airaghii-serpianensis* occurs in bed 100; one specimen attributed to *S. serpianensis* (Pl. 4: Fig. 6) is found at bed 102; three specimens of *S. zinae* (Pl. 4: Fig. 3-5) were found in bed 104 and one specimen in bed 116. The presence of *S. zinae* in bed 104 is remarkable: in the Punkt 902 section it occurs only in bed 112, ~60 cm above to where is found at Sasso Caldo. The F.O. (first occurence) of the genus *Serpianites* is lower by one bed and the L.O. is higher (three dolomite levels above) than what has been described for the Punkt 902 section.

Long ranges taxa (*Longobardites*, *Gymnites*, *Monophyllites*, and *Flexoptychites*; Pl. 5 and Pl. 6) are found from bed 65 to bed 138. Undetermined ammonoids are found up until bed 145, close to the Anisian/Ladinian boundary. No specimens referable to *Chieseiceras chiesense* were found.

Following Brack et al. (2005) all of the above-mentioned taxa occur in the *N. secedensis* Zone, whereas the upper limit of the *R. reitzi* Zone should be placed below bed 61, from where *S. variabilis* was recovered. The upper limit of the Besano Formation with the San Giorgio Dolomite is gradational.

2.5.2 *Daonella*

Six species of the bivalve *Daonella* were recognized: *D. vaceki*, *D. pseudomoussoni*, *D. airaghii*, *D. fascicostata*, *D. luganensis*, *D. golana*. They were already known to occur in the Besano Formation (Rieber, 1968. 1969), and at Sasso Caldo range from bed 65 to bed 108 (Fig. 2.4).

Daonella vaceki (Pl. 7: Fig. 4-6) is present from bed 65 to bed 70; specimens of this species are usually found in large groups. *D. airaghii* (Pl. 7: 1-3) occurs only in bed 74, but is represented by several specimens. *D. pseudomoussoni* (Pl. 8) ranges from bed 74 to bed 82; five specimens were attributed to this species. *D. fascicostata* (Pl. 9) ranges from bed 84 to bed 108; 49 specimens were attributed to this species. *D. luganensis* occurs only in bed 104 with two specimens. All of these taxa document the *N. secedensis* Zone. A hiatus is

found also at Sasso Caldo at bed 73. A similar hiatus is reported by Rieber (1969) at bed 70. On the whole, the ranges of the genus *Daonella* closely match the ranges described for this bivalve in the P.902 section.

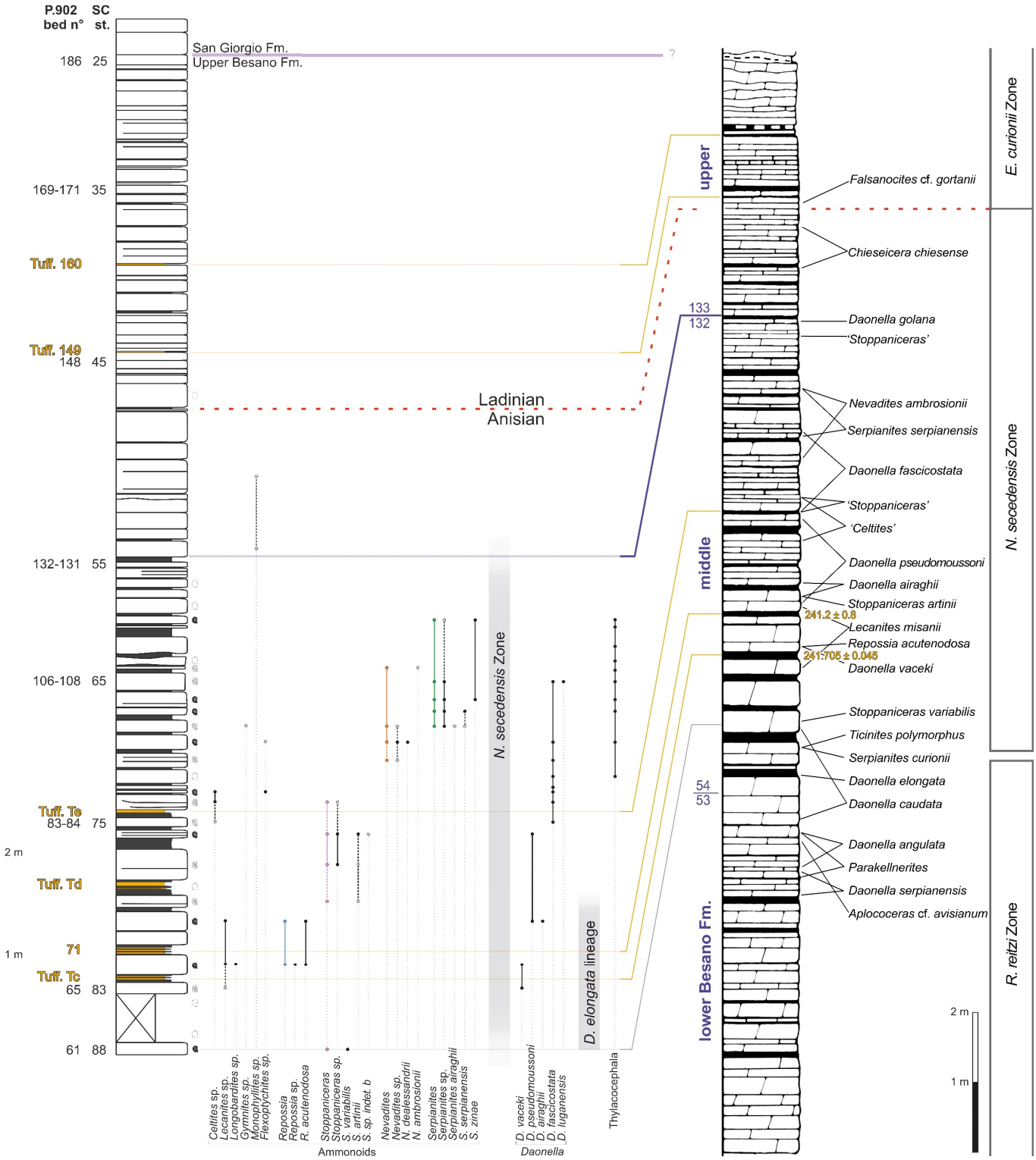

Fig. 2.4 – On the left, range chart of the section of the Besano Formation that crops out at Sasso Caldo site, including the ranges of ammonoids, the bivalve *Daonella*, and thylacocephalan crustaceans (see also Affer & Teruzzi, 1999). On the right, the stratigraphic log of the Besano Formation that crops out at Punkt 902 (modified from Brack et al., 2005) used as a reference to calibrate the bed cropping out at Sasso Caldo. Numerical age of Tc tuff. is from Wotzlaw et al. (2018); numerical age of bed 71 is from Mundil et al. (1996).

2.6 Integrated biochronostratigraphy

2.6.1 Zonation

Most of the ammonoid and *Daonella* species identified at Sasso Caldo are short ranging, whose stratigraphic distribution has been calibrated in the past years during the huge work that led to the definition of the GSSP of the Ladinian stage at Bagolino section (Southern Alps, eastern Lombardy; Brack et al., 2005).
Nevadites, which occurs from bed 96 to 108, is the marker of the *Nevadites secedensis* chronozone (Brack & Rieber, 1993), the uppermost zone of the Upper Anisian. The index species of this zone does not occur in the Besano Formation, neither at Sasso Caldo nor at Punkt 902, but the taxonomic assignment to *Nevadites* of the species *Balatonites ambrosionii* Airaghi, 1912 and of *B. de alessandri* Airaghi 1912 is now well established (i.e., Mietto & Manfrin ,1995; Pieroni, 2011).
The lower boundary of the *N. secedensis* Zone, marked by the F.O. of *Ticinites polymorphus* (see the definition by Brack & Rieber, 1993) cannot be identified at Sasso Caldo, because *T. polymorphus* has not been found in the collection from this site. This boundary is probably located just below the lowermost bed of Sasso Caldo section, because of the occurrence in the lowermost part of the section of *Stoppaniceras* (from bed 61 upward) and of *Daonella vaceki*, (beds 65-70). *Stoppaniceras* first occur at the base of the *N. secedensis* Zone (Brack & Rieber, 1993, fig 13), and *D vaceki*, recorded just above *Stoppaniceras*, occurs in the lower part of the zone (bed 69 of Punkt 902: see Brack et al. 2005, fig. 6b).
The available collection does not include taxa of the uppermost part of the *Nevadites secedensis* Zone, such as *Chieseiceras* Brack & Rieber, 1986, therefore it is not possible to locate at Sasso Caldo this part of the zone and the Anisian/Ladinian boundary, at least on the basis of fossils.
The *Nevadites secedensis* Zone is for sure documented up to bed 116, because of the occurrence of *Serpianites* (beds 100-116), a short ranging genus that is typical of the upper middle part of the *N. secedensis* Zone (see Brack & Rieber, 1993, fig. 13). *Monophyllites* that occurs in beds 133-140, is a long ranging taxon, whose range is Anisian-Upper Ladinian (e.g. Tozer, 1981), therefore is useless for biochronostratigraphic analysis.

2.6.2 Correlation

Most of the ammonoid and *Daonella* species identified at Sasso Caldo also occur in the Besano Formation at Punkt 902 section (Rieber, 1993; Brack & Rieber, 1993; Brack et al. 2005), thus making the correlation between the two sections very easy.
Taking into account that the collections made by Rieber from Punkt 902 were much larger than the collection from Sasso Caldo, the correlation shown in Fig. 2.4 is notably consistent. The most interesting point is that the biochronostratigraphy validates the bed-by-bed correlation of the two sections based on the thickness of the beds and the position of the tuff layers.
The ammonoid and *Daonella* correlations further support the identification of the middle-upper part of the Middle Triassic Besano Formation (Röhl et al. 2001) at Sasso Caldo (beds 61-131). The proposed environment of this portion of the Besano Formation is a rather deep intraplatform basin with open marine connections, and this is supported by the occurrence of open marine taxa such as *Stoppaniceras*, *Nevadites*, and *Daonella*.

2.7 Conclusions

The study of ammonoids and pelagic bivalve *Daonella* from the collections made during the excavation at Sasso Caldo quarry from 1985 to 2003 might be summarized as follows:

- All the available ammonoids and bivalves from the Sasso Caldo site (Besano Formation), housed in the collections of the Museo di Storia Naturale di Milano, were examined and determined. This allowed a precise characterization of the Besano Formation section cropping out at Sasso Caldo.

- Ammonoid and *Daonella* integrated biochronostratigraphy allowed a high-resolution correlation of the Sasso Caldo section with the Punkt 902 section (Rieber, 1969, 1973; Brack et al., 2005): a precise bed-by-bed correlation of the section to the exposed section at Punkt 902 has been carried out.

- Ammonoids genera recovered at Sasso Caldo are *Repossia*, *Stoppaniceras*, *Nevadites*, *Serpianites*, *Lecanites*, *Longobardites*, *Celtites*, *Gymnites*, *Monophyllites*, and *Flexoptychites*. *Daonella* is represented by the species *D. vaceki*, *D. pseudomoussoni*, *D. airaghii*, *D. fascicostata*, and *D. luganensis*. These taxa occur and testify the *N. secedensis* Zone.

- Based on the ammonoid and *Daonella* integrated biochronostratigraphy, at Sasso Caldo crops out a section of the Besano Formation that goes from bed 61 to bed 186. This includes almost the entire middle Besano Formation and the entire upper Besano Formation. The uppermost 25 beds at Sasso Caldo are referred to the San Giorgio Dolomite.

- Here is confirmed the subdivision proposed by Röhl et al. (2001) of the Besano Formation. It can be subdivided into three portions: lower, middle, and upper. The latter two crop out at Sasso Caldo. The middle Besano Formation was deposited in an intraplatform basin: a great abundance of pelagic marine vertebrates, as well as pelagic invertebrates, is typical of the middle Besano Formation, therefore likely strongly influenced by a connection with the open sea. The upper Besano Formation was deposited in a shallower restricted platform environment, characterized by the presence of sauropterygians and terrestrial fauna and flora, suggesting the existence of a continental area in close proximity.

- The precise correlation with P.902 allows to unify the documentation on the fossil record of the Italian and the Swiss outcrops of the Besano Formation. Moreover, this result gives a complete and integrated perspective of the Besano basin fossil fauna and environment during the Middle Triassic, for both the Italian and Swiss sides of Monte San Giorgio.

2.8 References

Affer, D. & Teruzzi, G. (1999) - Thylacocephalan crustaceans from the Besano Formation, Middle Triassic, N. Italy. *Rivista del Museo civico di Scienze Naturali "E. Caffi",* 20: 5-8.

Airaghi, C. (1911) - Ammoniti degli scisti bituminosi di Besano in Lombardia. *Bollettino della Società Geologica Italiana*, 30: 1048–1050.

Airaghi, C. (1912) - I molluschi degli scisti bituminosi di Besano in Lombardia. *Atti della Società italiana di scienze naturali*, 51: 1–30

Bassani, F. (1886) - Sui fossili e sull'età degli schisti bituminosi triassici di Besano in Lombardia. *Atti della Società italiana di scienze naturali*, 29: 15–72

Bernasconi, S. M. (1991) - Geochemical and Microbial Controls on Dolomite Formation in-Anoxic Environments. *Contrib. Sedimentology*, 19: 1-109.

Bernoulli D., Ambrosi C., Scapozza C., Castelletti C. & Wiedenmayer F. (2018) - Il Foglio geologico 1373 Mendrisio con parte del Foglio geologico 1374 Como, scala 1:25'000 Atlante geologico della Svizzera 1: 25 000, Note esplicative. In: Dall'Agnolo, Stephan, (ed.) Ufficio federale di topografia, CH- 3084 Wabern, Wabern. ISBN 978-3-302-40077-8.

Bindellini G., Wolniewicz A.S., Miedema F., Scheyer T.M., & Dal Sasso C. (2021) - Cranial anatomy of *Besanosaurus leptorhynchus* Dal Sasso & Pinna, 1996 (Reptilia: Ichthyosauria) from the Middle Triassic Besano Formation of Monte San Giorgio, Italy/Switzerland: taxonomic and palaeobiological implications. *PeerJ*, 9: e11179.

Brack, P., & Rieber, H. (1993) - Towards a better definition of the Anisian/Ladinian boundary: New biostratigraphic data and correlations of boundary sections from the Southern Alps. *Eclogae Geologicae Helvetiae*, 86: 415-527.

Brack, P., Rieber, H., Nicora, A., & Mundil, R. (2005) - The global boundary stratotype section and point (GSSP) of the Ladinian Stage (Middle Triassic) at Bagolino (Southern Alps, Northern Italy) and its implications for the Triassic time scale. *Episodes-Newsmagazine of the International Union of Geological Sciences*, 28: 233-244.

Brinkmann W. (1997) - Die Ichthyosaurier (Reptilia) aus der Mitteltrias des Monte San Giorgio (Tessin, Schweiz) und von Besano (Lombardei, Italien) – der aktuelle Forschungsstand. *Vierteljarsschrift der Naturforschenden Gesellschaft in Zürich*, 142: 69–78.

Dal Sasso, C., & Pinna, G. (1996) - *Besanosaurus leptorhynchus* n. gen. n. sp., a new shastasaurid ichthyosaur from the Middle Triassic of Besano (Lombardy, N. Italy). *Paleontologia Lombarda*, 4: 1-23.

De Zanche V., Gianolla P., Manfrin S., Mietto P. & Roghi G. (1995) - A Middle Triassic Back-stepping Carbonate Platform in the Dolomites (Italy): Sequence Stratigraphy and Biochronostratigraphy. *Memorie di Scienze Geologiche*, 47: 135-155.

Fantini Sestini N. (1996) - The Ladinian ammonoids from the Calcare di Esino of Val Parina (Bergamasc Alps, Northern Italy). Pt. 2. *Rivista Italiana di Paleontologia e Stratigrafia*, 102: 211-226.

Felber, M., Furrer, H., & Tintori, A. (2004) - The Triassic of Monte San Giorgio in the World Heritage List of UNESCO: An opportunity for science, the local people and tourism. *Eclogae Geologicae Helvetiae*, *97*: 1-2.

Frauenfelder, A. (1916) - Beiträge zur Geologie der Tessiner Kalkalpen. Ecl. geol. helv., 14: 247-367.

Frauenfelder, A. (1916) - Beiträge zur Geologie der Tessiner Kalkalpen. *Eclogae Geologicae Helvetiae*, 14: 247-367.

Furrer, H. (1995) - The Kalkschieferzone (Upper Meride Limestone; Ladinian) near Meride (Canton Ticino, Southern Switzerland) and the evolution of a Middle Triassic intraplatform basin. *Eclogae Geologicae Helvetiae*, 88: 827-852.

Furrer, H. (2003) - Der Monte San Giorgio im Südtessin—Vom Berg der Saurier zur Fossil-Lagerstätte internationaler Bedeutung. Neujahrsblatt der Naturforschenden Gesellschaft Zürich, 206: 1–64.

Furrer, H. & Vandelli, A. (2014) - Guide to the museum of fossils from Monte San Giorgio Meride (p. 128). Meride: Fondazione del Monte San Giorgio. ISBN: 978-88-940067-2-8.

Gingerich P.D. (1979) - The stratophenetic approach to phylogeny reconstruction in vertebrate paleontology. In: Cracraft, J. & Eldredge, N. (Eds.): Phylogenetic analysis and paleontology, 41-77; New York, (Columbia University Press).

López-Arbarello A., Bürgin T., Furrer H. & Stockar R. (2016) - New holostean fshes (Actinopterygii: Neopterygii) from the Middle Triassic of the Monte San Giorgio (Canton Ticino, Switzerland). PeerJ, 4, e2234. https://doi. org/10.7717/peerj.2234.

Maisch M.W. & Matzke A.T. (1998) - Observations on Triassic ichthyosaurs. Part II: A new ichthyosaur with palatal teeth from Monte San Giorgio. N*eues Jahrbuch für Geologie und Paläontologie-Monatshefte*, 1998: 26-41.

Mietto P. & Manfrin S. (1995) - A high resolution Middle Triassic ammonoid standard scale in the Tethys Realm. A preliminary report. *Bulletin de la Societé Geologique de France*, 166: 539-563.

Müller W. (1964) - Conodonten aus der mittleren Trias der Tessiner Kalkalpen. *Eclogae Geologicae Helvetiae*, 57: 747-753.

Mundil R., Brack P., Meier M., Rieber H. & Oberli F. (1996) - High resolution U-Pb dating of Middle Triassic volcaniclastics: Time-scale calibration and verification of tuning parameters for carbonate sedimentation. *Earth and Planetary Science Letters*, 141: 137-151.

Nosotti S. (2007) - *Tanystropheus longobardicus* (Reptilia, Protorosauria): re-interpretations of the anatomy based on new specimens from the Middle Triassic of Besano (Lombardy, Northern Italy): *Memorie della Societa Italiana di Scienze Naturali e del Museo Civico di Storia Naturale di Milano*, 35.

Nosotti S. & Rieppel O. (2003) - *Eusaurosphargis dalsassoi* n. gen. n. sp., a new, unusual diapsid reptile from the Middle Triassic of Besano (Lombardy, N Italy). *Memorie della Società Italiana di Scienze Naturali e del Museo Civico di Storia Naturale di Milano*, 31: 1-33.

Nosotti S., Teruzzi G., Teruzzi G. (2008) - I rettili di Besano-Monte San Giorgio. *Natura*.

Pieroni V. (2011) - La Rasa di Varese e i suoi fossili. Editore: Pietro Macchione. Varese.

Pieroni V., & Furrer H. (2020) - Middle Triassic gastropods from the Besano Formation of Monte San Giorgio, Switzerland. *Swiss Journal of Palaeontology*, 139: 1-9.

Renesto S., Dal Sasso C., Fogliazza F. & Ragni C. (2020) - New findings reveal that the Middle Triassic ichthyosaur *Mixosaurus cornalianus* is the oldest amniote with a dorsal fin. *Acta Paleontologica Polonica*, 65: 511-522.

Rieber H. (1968) - Die Artengruppe der *Daonella elongata* Mojs. aus der Grenzbitumenzone der mittleren Trias des Monte San Giorgio (Kt. Tessin, Schweiz). *Paläontologische Zeitschrift*, 42: 33-61.

Rieber H. (1969) - Daonellen aus der Grenzbitumenzone der mittleren Trias des Monte San Giorgio (Kt. Tessin, Schweiz). *Eclogae Geologicae Helvetiae*, 62: 657–683.

Rieber H. (1973) - Die Triasfauna der Tessiner Kalkalpen. Cephalopoden aus der Grenzbitumenzone (Mittlere Trias) des Monte San Giorgio (Kt. Tessin, Switzerland). *Schweiz. Palaeontol. Abh*., 93: 1-96.

Rieber H. (1974). *Breviconoteuthis breviconus REIS*, ein Phragmoteuthide aus der Mittleren Trias des Monte San Giorgio, Kanton Tessin, Schweiz. *Mitteilungen aus dem Paläontologischen Institut der Universität Zürich*, 93.

Rieber H. (1970). *Phragmoteuthis*? *ticinensis* n. sp., ein Coleoidea-Rest aus der Grenzbitumenzone (Mittlere Trias) des Monte San Giorgio (Kt. Tessin, Schweiz). *Paläontologische Zeitschrift*, 44: 32-40.

Rieber H. (1974). *Breviconoteuthis breviconus REIS, ein Phragmoteuthide aus der Mittleren Trias des Monte San Giorgio, Kanton Tessin, Schweiz*. Paläontologisches Institut.

Rieber H. (1980) - Ein Conodonten-cluster aus der Grenzbitumenzone (Mittlere Trias) cles Monte San Giorgio (Kt. Tessin/ Schweiz): *Naturhistorisches Museum in Wien, Annalen*, 83: 265-274.

Rieber H.P. (2000) - Monte San Giorgio und Besano, mittlere Trias, Schweiz und Italien. In: Meischner D. (eds) Europäische Fossillagerstätten. Springer, Berlin, Heidelberg. https://doi.org/10.1007/978-3-642-57198-5_12

Röhl H.J., Schmid-Röhl A., Furrer H., Frimmel A., Oschmann W. & Schwark L. (2001) - Microfacies, geochemistry and palaeoecology of the Middle Triassic Grenzbitumenzone from Monte San Giorgio (Canton Ticino, Switzerland). *Geologia Insubrica*, 6: 1-13.

Senn A. (1924) - *Beiträge zur Geologie des Alpensüdrandes zwischen Mendrisio und Varese*. Eclogae Geologicae Helvetiae, 18(4): 550-632.

Teichert C. (1948) - A simple device for coating fossils with Ammonium Chloride. *Journal of Paleontology*, 22: 102–104.

Tozer E.T. (1981) - Triassic Ammonoidea: Classification, Evolution and Relationship, with Permian and Jurassic Forms. In House M.R. & Senior J.R. (Eds.) - The Ammonoidea. The Syst. Assoc. sp. vol. 18: 65-100, Academic Press, London, New York.

Vörös A. (2018) - The Upper Anisian ammnoids of the Balaton Highland (Middle Triassic, Hungary). *Geologica Hungarica, Series Palaeontologica*, 60: 1-240.

Wotzlaw J.F., Brack P. & Storck, J.C. (2018) - High-resolution stratigraphy and zircon U–Pb geochronology of the Middle Triassic Buchenstein Formation (Dolomites, northern Italy): precession-forcing of hemipelagic carbonate sedimentation and calibration of the Anisian–Ladinian boundary interval. *Journal of the Geological Society*, 175: 71-85.

Zorn H. (1971) - Paläontologische, stratigraphische und sedimentologische Untersuchungen des Salvatoredolomits (Mitteltrias) der Tessiner Kalkalpen. *Schwiz. Palaont. Abh*., 91, 1-90.Rieber H. 1969. Daonellen aus der Grenzbitumenzone der mittleren Trias des Monte San Giorgio (Kt. Tessin, Switzerland). *Eclogae geol. Helv*., 62: 657-683.

2.9 Plates

2.9.1 Ammonoids

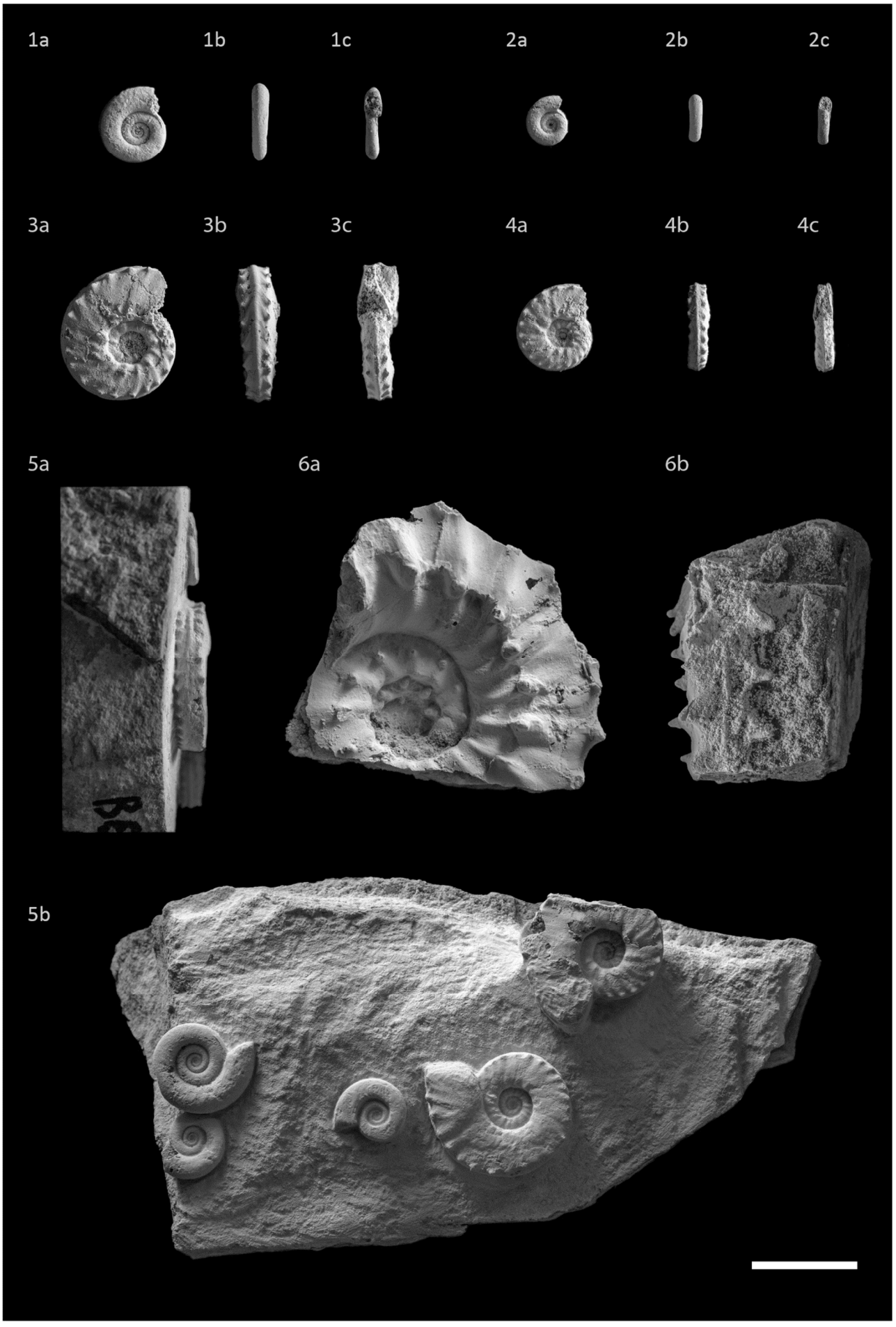
1a
1b
1c
2a
2b
2c
3a
3b
3c
4a
4b
4c
5a
6a
6b
5b

Plate 1

Fig. 1 - *Lecanites misanii*, BES SC 1751a, bed 69-70: 1a) lateral view; 1b) ventral view; 1c) oral view.
Fig. 2 - *Lecanites misanii*, BES SC 1751b, bed 69-70: 2a) lateral view; 2b) ventral view; 2c) oral view.
Fig. 3 - *Repossia acutenodosa*, BES SC 1752a, bed 69-70: 3a) lateral view; 3b) ventral view; 3c) oral view.
Fig. 4 - *Repossia acutenodosa*, BES SC 1752b, bed 69-70: 4a) lateral views; 3b) ventral view; 3c) oral view.
Fig. 5 - BES SC 1763, bed 69-70: 6a) *Repossia acutenodosa* in ventral view; 6b) *Lecanites misanii* on the left (3) and *Repossia acutenodosa* on the right (2) in lateral view.
Fig. 6 - *Repossia acutenodosa*, BES SC 1764, bed 69-70: 5a) lateral view; 5b) ventral view.
Scale bar equals 2 cm.

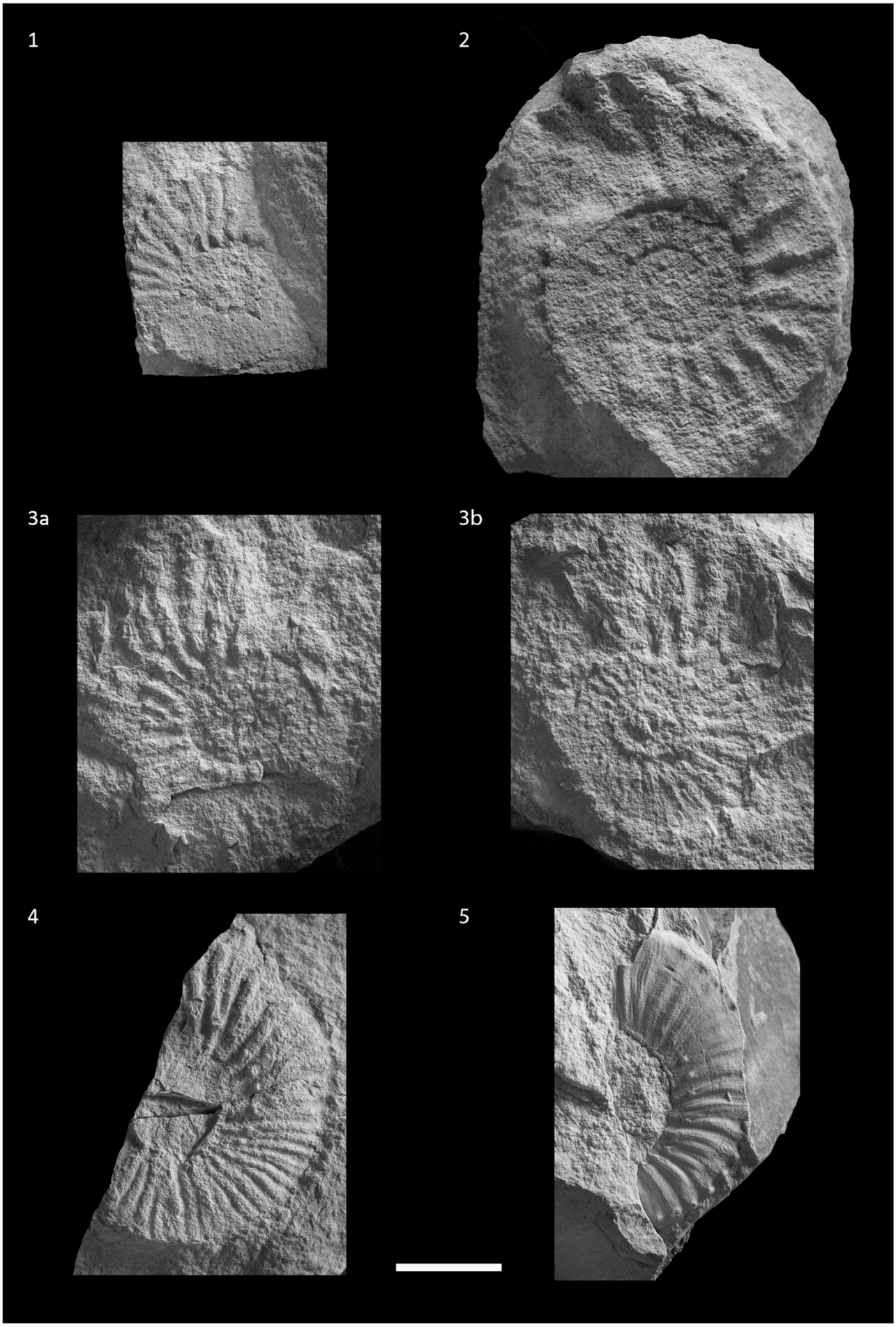
1
2
3a
3b
4
5

Plate 2

Fig. 1 - *Stoppaniceras artinii*, BES SC 1197 in lateral view, bed 82.

Fig. 2 - *Stoppaniceras artinii*, BES SC 1283 in lateral view, bed 82.

Fig. 3 -*Stoppaniceras* sp. (cfr. *S.* indet b, Rieber 1973), BES SC 1385, bed 82: 3a) actual specimen; 3b) counterprint).

Fig. 4 - *Stoppaniceras* cfr. *artinii*, BES SC 1275 in lateral view, bed 73.

Fig. 5 - *Stoppaniceras variabilis*, BES SC 1913 in lateral view, bed 61.

Scale bar equals 2 cm.

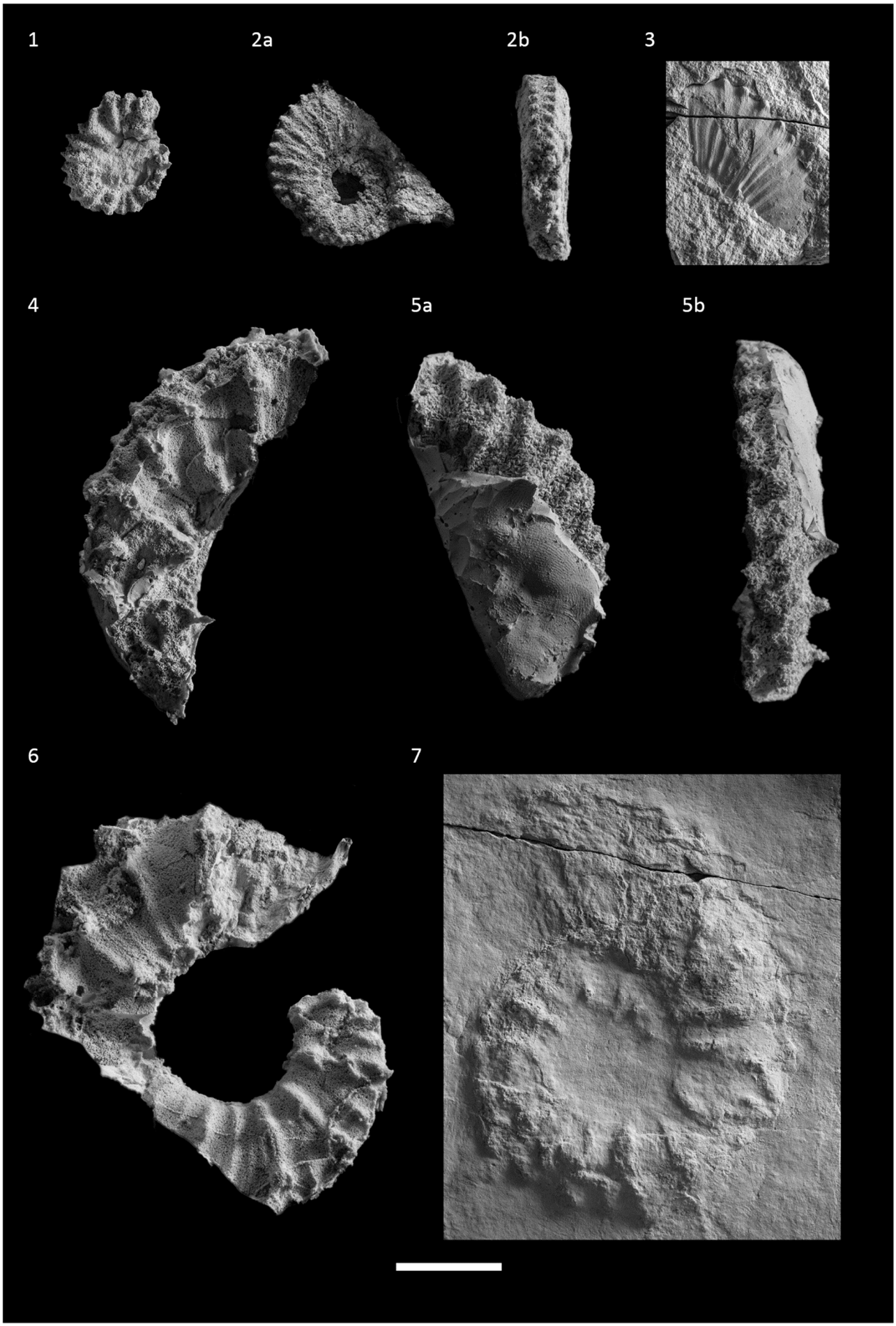
1
2a
2b
3
4
5a
5b
6
7

Plate 3

Fig. 1 - *Nevadites* cf. *ambrosionii*, BES SC 1331, bed 108.

Fig. 2 - *Nevadites* sp., BES SC 954 in lateral view, bed 98: 2a) lateral view; 2b) ventral view.

Fig. 3 - cf. *Nevadites*, BES SC 1972 in lateral view, bed 100.

Fig. 4 - *Nevadites dealessandrii*, BES SC 1229 in lateral view, bed 98.

Fig. 5 - *Nevadites dealessandrii*, BES SC 1476 in lateral view, bed 98: 5a) lateral view; 5b) ventral view.

Fig. 6 - *Nevadites dealessandrii*, BES SC 943 in lateral view, bed 98.

Fig. 7 - *Nevadites dealessandrii*, BES SC 1255 in lateral view, bed 98.

Scale bar equals 2 cm.

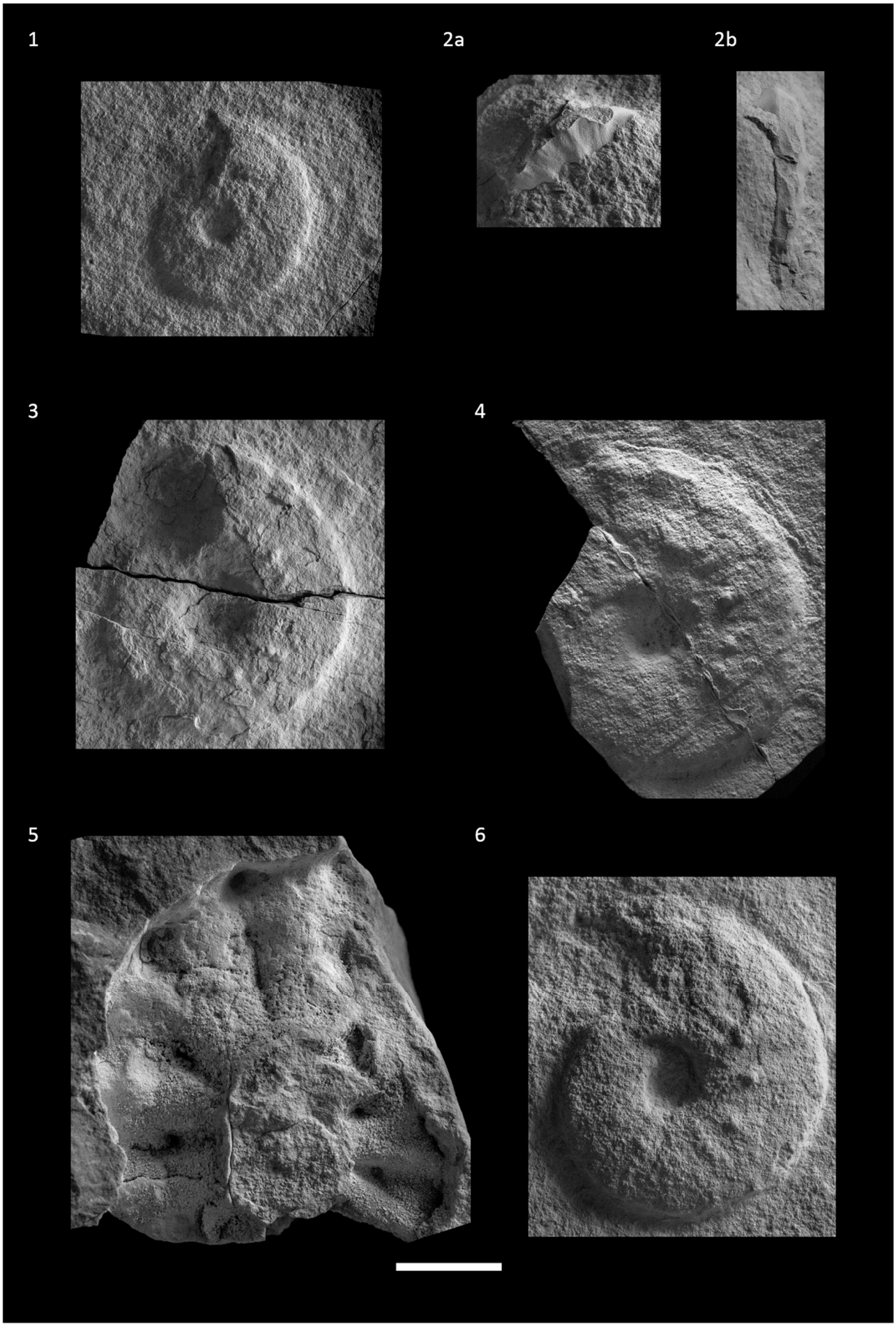
1
2a
2b
3
4
5
6

Plate 4

Fig. 1 - *Serpianites* sp., BES SC 400 in lateral view, bed 104.
Fig. 2 - *Serpianites* gr. *airaghii-serpianensis*, BES SC 709, bed 100: 2a) lateral view; 2b) ventral view.
Fig. 3 - *Serpianites zinae*, BES SC 476 in lateral view, bed 116.
Fig. 4 - *Serpianites zinae*, BES SC 405 in lateral view, bed 104.
Fig. 5 - *Serpianites zinae*, BES SC 365 in lateral view, bed 104.
Fig. 6 - *Serpianites serpianensis*, BES SC 1950 in lateral view, bed 104.
Scale bar equals 2 cm.

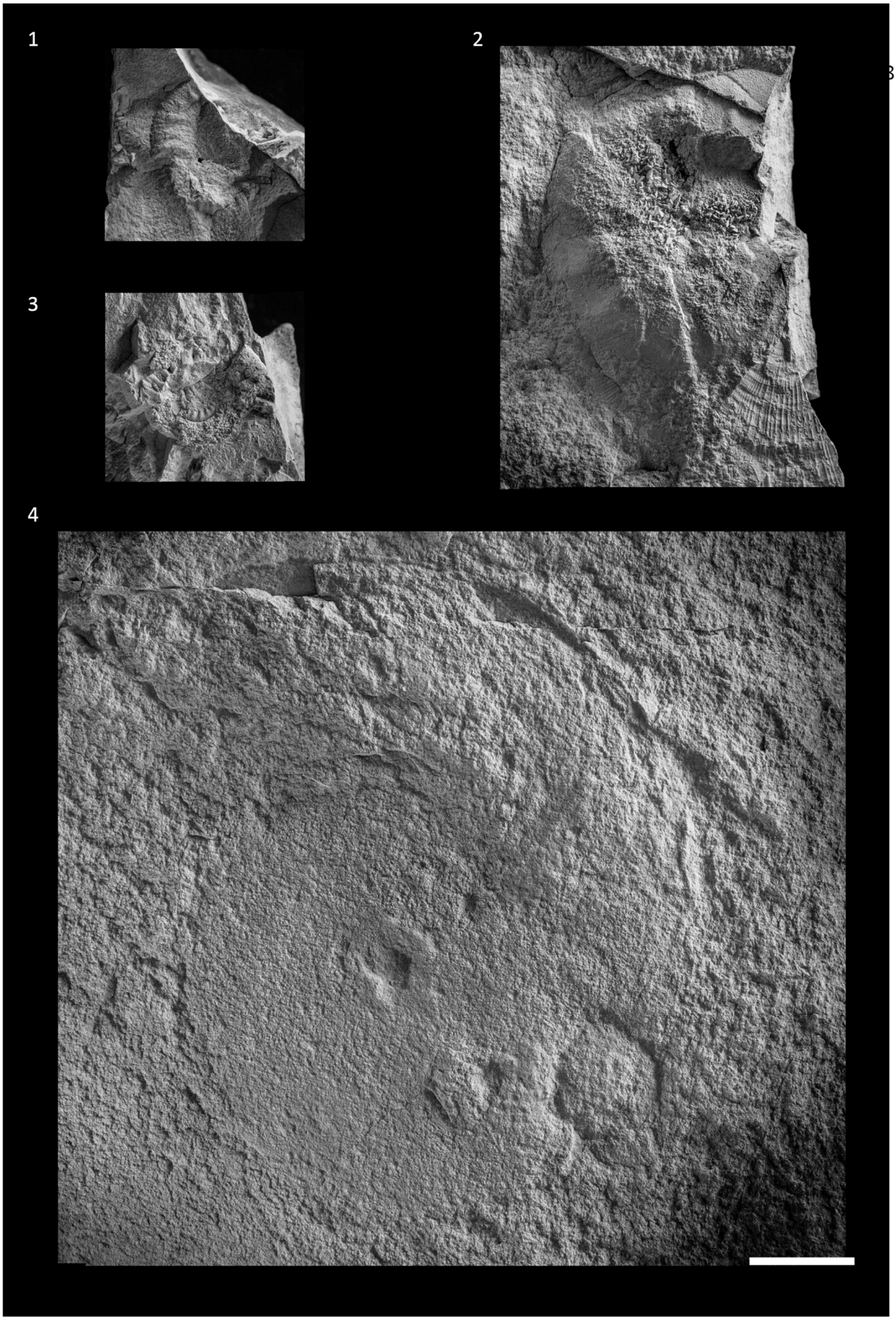
1
2
3
4

Plate 5

Fig. 1, 3 - *Celtites* sp.: 1) BES SC 1726 in lateral view, bed 90; 3) BES SC 1209 in lateral view, bed 86-88.
Fig. 2 - *Longobardites* sp., BES SC 1662 in lateral view, bed 69-70.
Fig. 4 - *Flexoptychites* sp., BES SC 1061 in lateral view, bed 69-70.
Scale bar equals 2 cm.


1
2
3

Plate 6
Fig. 1, 2 - indet.: 1) BES SC 730 in lateral view, bed 133-134; 2) BES SC 291 in lateral view, bed 133-134.
Fig. 3 - cf. *Monophyllites*, BES SC 1916 in lateral view, bed 133-134.
Scale bar equals 2 cm.

2.9.2 *Daonella*

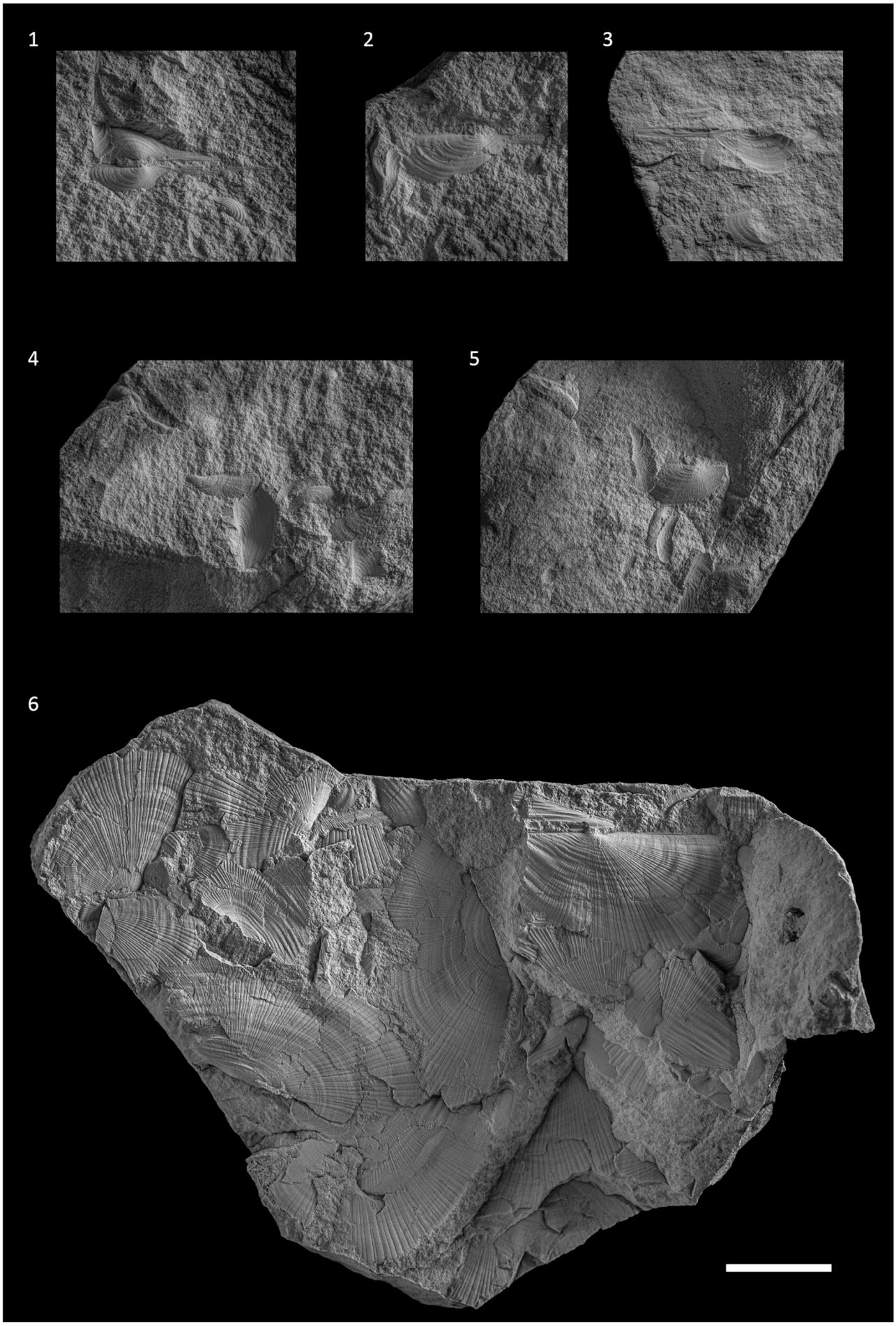
1
2
3
4
5
6

Plate 7

Fig. 1 - *Daonella airaghii*, BES SC 1648a, bed 74.
Fig. 2 - *Daonella airaghii*, BES SC 1648b, bed 74.
Fig. 3 - *Daonella airaghii*, BES SC 1648c, bed 74.
Fig. 4 - *Daonella* cf. *vaceki*, BES SC 1735, bed 69-70.
Fig. 5 - *Daonella* cf. *vaceki*, BES SC 1738, bed 69-70.
Fig. 6 - *Daonella vaceki*, BES SC 1682, bed 69-70.
Scale bar equals 2 cm.

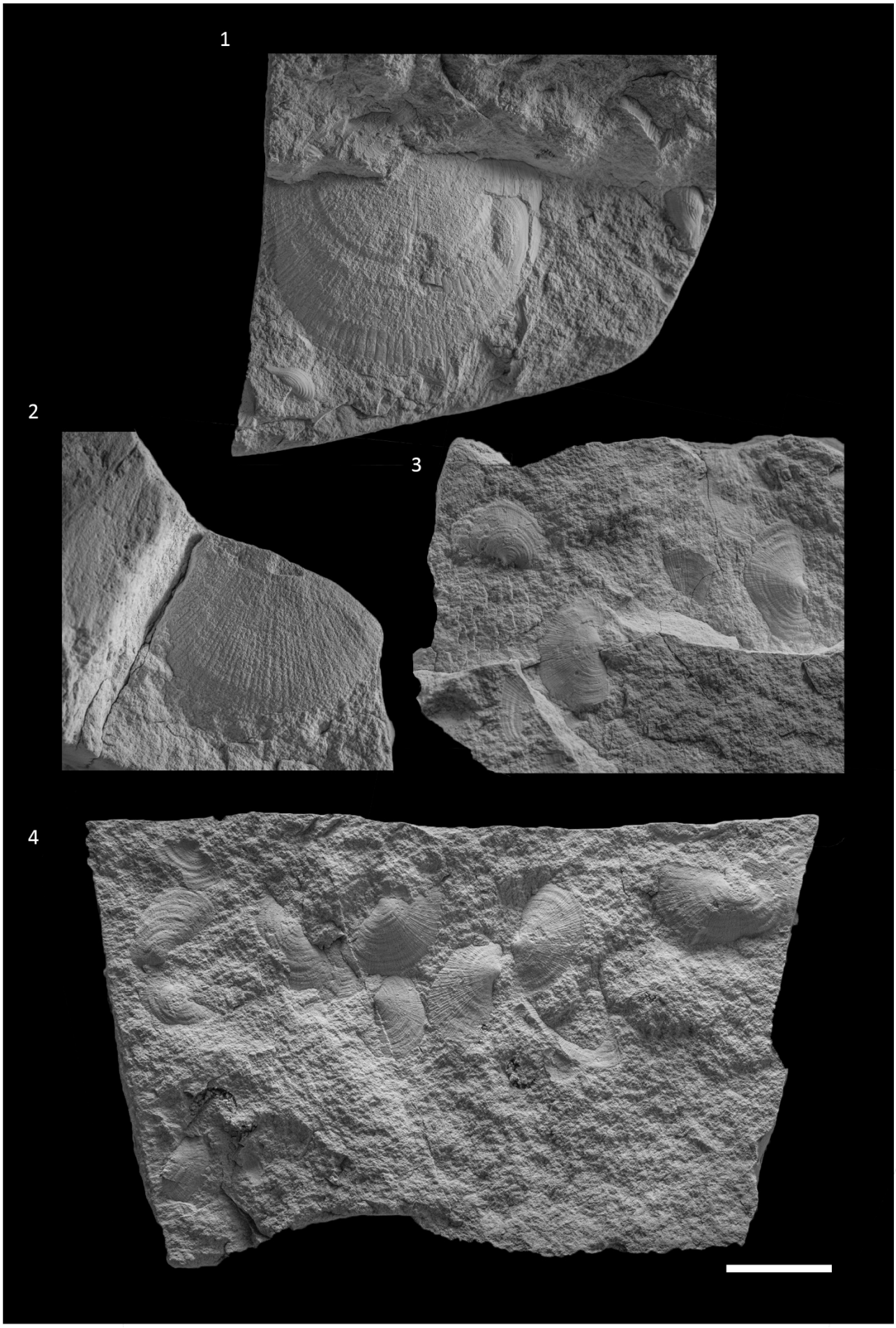
1
2
3
4

Plate 8

Fig. 1 - *Daonella pseudomoussoni* associated with *D. airaghii*, BES SC 1649, bed 74.
Fig. 2 - *Daonella pseudomoussoni*, BES SC 1277, bed 82.
Fig. 3 - *Daonella pseudomoussoni*, BES SC 1282, bed 82.
Fig. 4 - *Daonella pseudomoussoni*, BES SC 1381, bed 82.
Scale bar equals 2 cm.

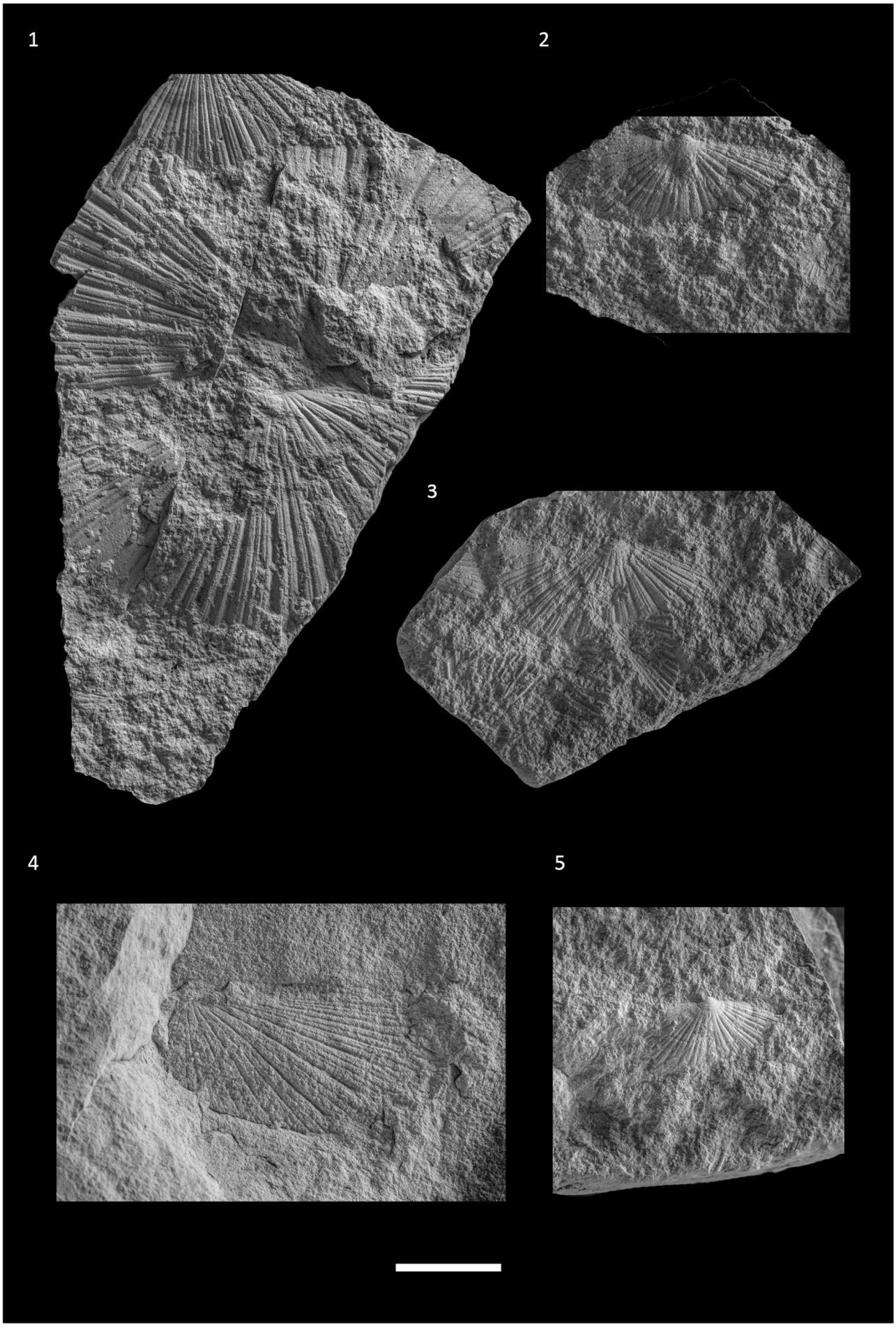
1
2
3
4
5

Plate 9

Fig. 1 - *Daonella fascicostata*, BES SC 1566, bed 94.
Fig. 2 - *Daonella fascicostata*, BES SC 1085, bed 94.
Fig. 3 - *Daonella fascicostata*, BES SC 1093, bed 94.
Fig. 4 - *Daonella fascicostata*, BES SC 1213, bed 92.
Fig. 5 - *Daonella fascicostata*, BES SC 1092, bed 94.
Scale bar equals 2 cm.

Chapter 3
A new Mesozoic scorpion from the Besano Formation (Middle Triassic, Monte San Giorgio UNESCO WHL), Italy.

*Manuscript submittted to Paläontologische Zeitschrift.
Marco Viaretti[1], Gabriele Bindellini[1], Cristiano Dal Sasso[2]
[1] Dipartimento di Scienze della Terra "Ardito Desio", Università degli Studi di Milano, Milano, Italy.
[2] Sezione di Paleontologia dei Vertebrati, Museo di Storia Naturale di Milano, Milano, Italy.

3.1 Abstract

The first Mesozoic scorpion from Italy, *Besanobuthus ziliolii* gen. nov. et sp. nov., is here described and named thanks to a single well-preserved specimen. This new taxon comes from the Besano Formation (Middle Triassic) of Monte San Giorgio, a UNESCO World Heritage Locality (WHL). The taphonomic analysis of the specimen allows interpretation of the fossil as a carcass, rather than an exuvia. Different analytical techniques, such as optical, UV and SEM microscopy reveal different characters, not visible together with a single method. The new species is assigned to the family Protobuthidae, whose diagnosis is emended to better accommodate the new taxon and possibly other ones, strengthening the family validity itself. *Besanobuthus ziliolii* represents the first arachnid report from the Besano Formation and the Mesozoic of Italy, the second genus and species of the family Protobuthidae in the world, and further corroborates the nearshore deposition previously suggested for the genesis of the upper portion of the Besano Formation.

3.2 Introduction

Terrestrial arthropods are amongst the rarest fossils in the palaeontological record (Wills 2001), and arachnids represent just a small part of this record. Dunlop et al. (2020) recognized 2531 valid species among extinct taxa; the count includes Xiphosura, which according to one of the most recent phylogenetic analyses of Chelicerata (Ballesteros and Sharma 2019) belongs to Arachnida.
The fossil record of scorpions consists of 145 valid species (Dunlop *et al.* 2020). This number - contrary to the fossil record of all other extant arachnid orders - is skewed and higher toward the Paleozoic, making scorpions the most diverse arachnids of that Era, with a total of 81 valid species. Scorpions are also the only arachnid order with a well-defined stem- and crown-group in the Paleozoic (Stockwell 1989; Jeram 1994, 1998). Compared to this great diversity, Mesozoic and Cenozoic scorpions are quite rare, counting 38 valid species in the Mesozoic and 27 in the Cenozoic. Until the discovery of large amber deposits in Myanmar and the study of their inclusions (e.g., Lourenço 2002 and subsequent

papers), the Triassic period was the richest of the Mesozoic, with 9 valid species described (Dunlop *et al.* 2020).
Here we describe in detail a new Triassic scorpion, previously only noticed (Viaretti *et al.* 2020), which represents the first from the Mesozoic of Italy. This fossil comes from the Sasso Caldo site (Besano Formation, Middle Triassic, Monte San Giorgio UNESCO WHL), located on the NW slope of Monte Pravello, between Besano and Porto Ceresio (Varese, N Italy). This contribution also represents the first report ever of an arachnid from the Besano Formation, and a step forward in the knowledge of Triassic arachnid paleobiodiversity.

3.3 Geological framework

The Besano Formation crops out on Monte San Giorgio (Lombardy, Italy; and Canton Ticino, Switzerland; Fig. 3.1), and is one of the richest and well-known sites of Middle Triassic palaeobiodiversity (e.g., Rieppel 2019) on par with more recently discovered Triassic sites in China (e.g., Benton *et al.* 2013). The Middle Triassic carbonate succession of Monte San Giorgio consists of four different formations deposited on a carbonate platform of the western margin of the Neo-Tethys (Bernasconi 1994; Furrer 1995; Röhl *et al.* 2001; Etter 2002; Stockar *et al.* 2012): these are the San Salvatore Dolomite, the Besano Formation, the San Giorgio Dolomite, and the Meride Limestone (Fig. 3.1). After the deposition of the Anisian Salvatore Dolomite, the development of a 30 to 130 m deep and approximately 20 km wide basin resulted in the deposition of the Besano Formation (e.g., Bernasconi 1991, 1994; Bernasconi and Riva 1993; Furrer 1995), from which a great part of the fossil fauna of Monte San Giorgio has been recovered (e.g., Bürgin *et al.* 1989; Furrer 2003). The Besano Formation is a 5 to 16 m thick alternation of black shales and variably laminated, organic-rich dolomitic banks; subordinate cineritic tuffs are dated as Late Anisian-Early Ladinian (Brack and Rieber 1986, 1993; Mundil *et al.* 1996; Brack *et al.* 2005; Wotzlaw *et al.* 2017).
The formation is divided into three portions (Röhl *et al.* 2001): the upper and the lower portion of the Besano Fm. represent a restricted, shallow inter- to subtidal carbonate platform, which is rich in nearshore vertebrate taxa, whereas the middle part is a slightly deeper intraplatform basin, from which a great number of ichthyosaurian remains and other pelagic vertebrates come from (e.g., Dal Sasso and Pinna 1996; Brinkmann 1997; Maish and Matzke 1998; Renesto *et al.* 2020; Bindellini *et al.* 2021). Recent biozonation of the Sasso Caldo site (Bindellini *et al.* 2019), based on index-fossil invertebrates (ammonoids and the bivalve *Daonella*), allowed confident correlation of this stratigraphic section with the stratigraphy and biozonation of the coeval Swiss localities (Rieber 1973; Brack and Rieber 1993; Brack *et al.* 2005). This means that, at Sasso Caldo, only the middle and the upper portion of the Besano Formation crop out. The scorpion comes from the upper part of the outcrop (G. Teruzzi, pers. com. 2019), which is dated back to the earliest Ladinian (Bindellini *et al.* 2019).

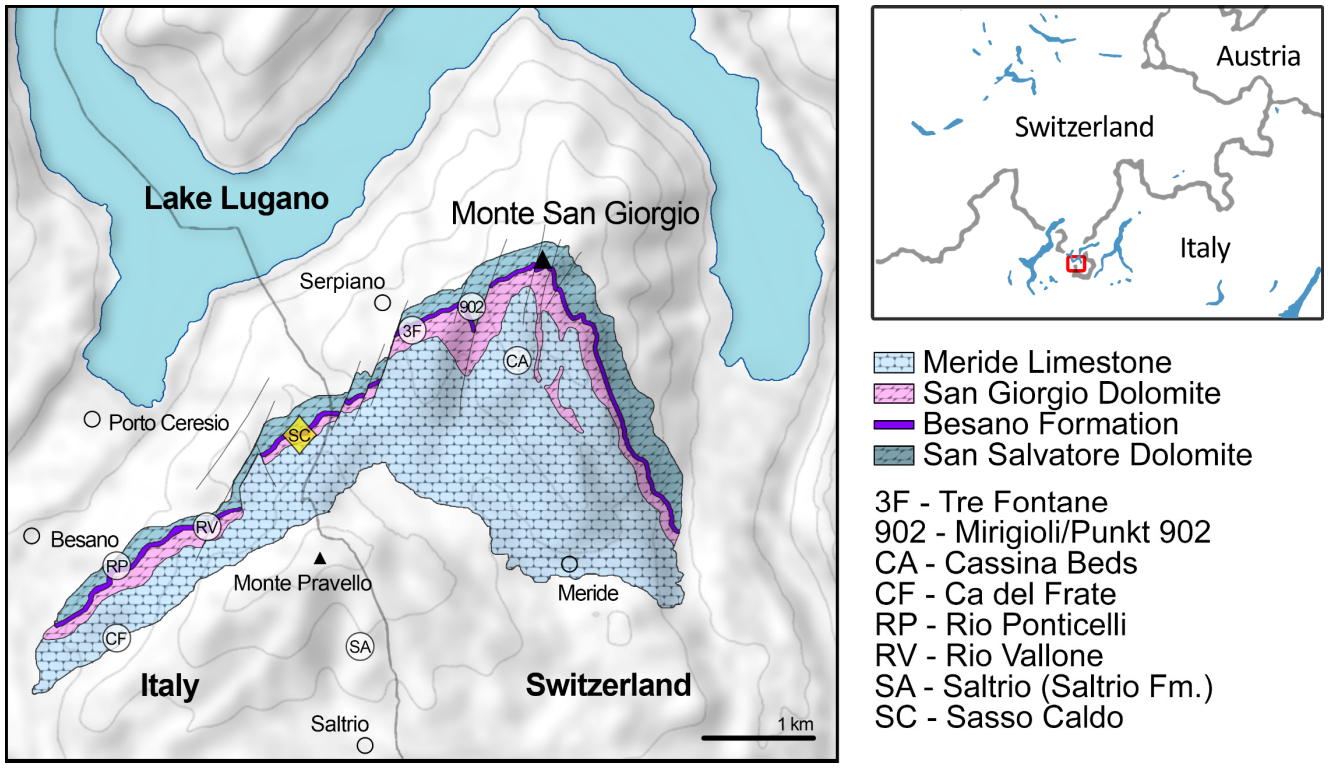

Fig. 3.1 - Map of the Monte San Giorgio area showing the Middle Triassic carbonate succession, including the major paleontological quarries in the area (white circles), and the site of origin of the fossil scorpion described in this paper (yellow rhombus).

3.4 Material and methods

3.4.1 Material

BES SC 1973, a well preserved, almost complete, fossil scorpion from the Besano Formation (Monte San Giorgio, UNESCO WHL). The specimen is deposited in the fossil collection of the Museo di Storia Naturale di Milano, is preserved as part and counterpart in two little slabs of a finely laminated, dolomitic matrix enriched in organic matter (Fig. 3.2). The length of the fossil is 43 mm.

3.4.2 Methods

To observe the anatomical features in this small-sized specimen, we used a Leica MZ9-5 stereomicroscope equipped with a plan 1.0x lens, 10/20x oculars, and a 0.63 to 6.0 zoom. A Wild Heerbrugg TYP 308700 camera lucida was mounted on top for detailed drawings. Fluorescence induced by ultraviolet light (365 nm) was used to better see organic remains and highlight their chemical compositional differences, following previous studies (e.g. Tischlinger 2002; Hone *et al.* 2010; Dal Sasso and Maganuco 2011). Scanning electron microscopy (SEM) images and elemental peaks were obtained by analysing microsamples, taken from carefully selected areas of the specimen, with a Jeol JSM 5610 LV (IXRF Systems Inc.) equipped with an EDS 500 spectrometer. Lastly, a macro-photogrammetric scan of the surface of the main slab, where most of the specimen is preserved, has been performed; this allowed the output of a DEM (Digital Elevation Model), which helped to distinguish the surface morphology of the fossil (Fig. 3.2).

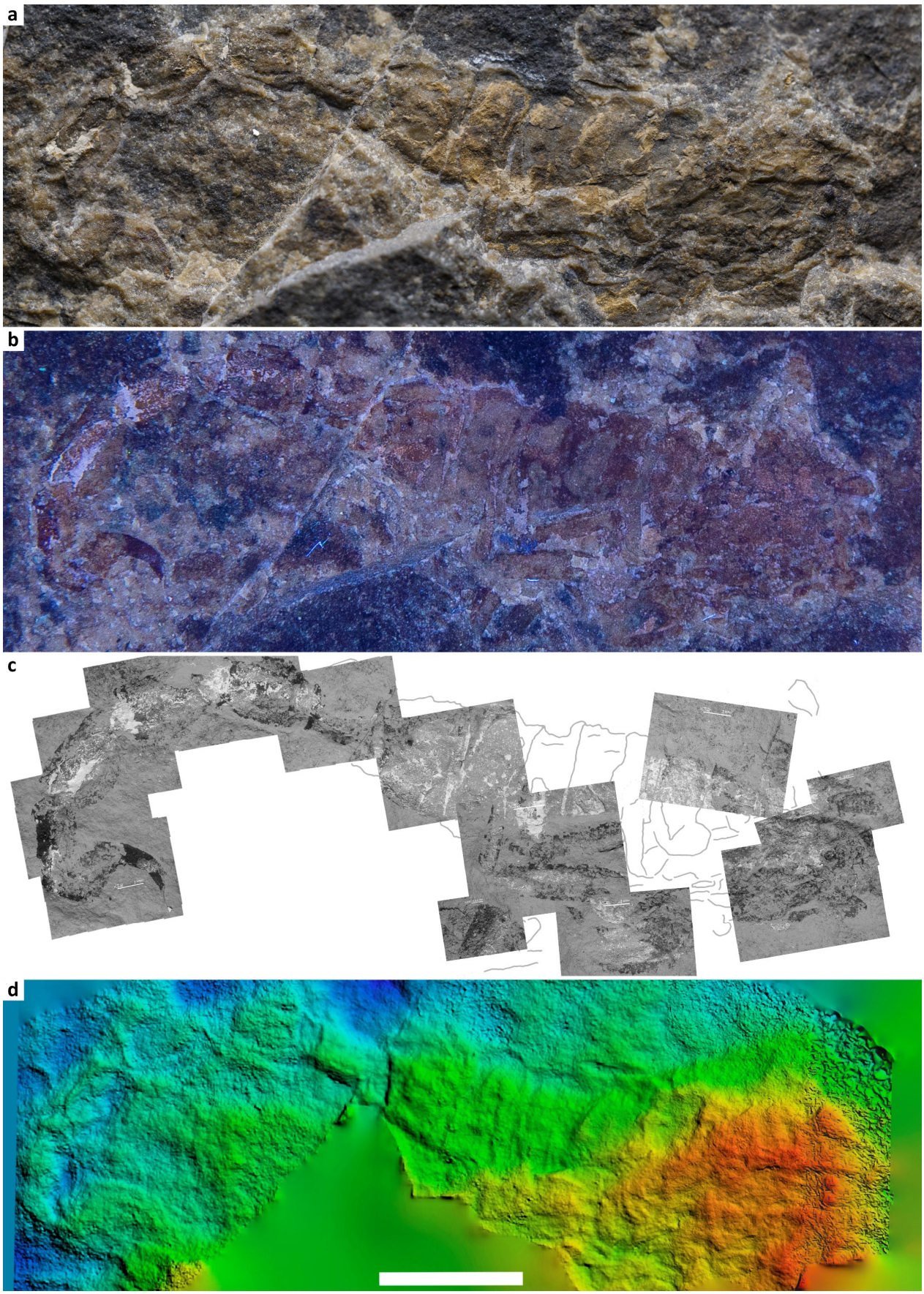

Fig. 3.2 - Specimen BES SC 1973, *Besanobuthus ziliolii* gen. et sp. nov. A, visible light photo. B, UV light photo. C, Collage of SEM images taken in BSE (Back-Scattered Electrons) mode. D, DEM obtained through photogrammetric scan of the specimen. Scale bar equals 5 mm. For further details, see Fig. 3.8.

3.5 Taphonomical remarks

The scorpion from Besano is overall well-preserved, exposed in dorsal view in the main slab (Fig. 3.2). Prosoma, mesosoma, and metasoma are preserved in their entirety, whereas the limbs are quite damaged: the preserved walking legs are folded and stacked on the back of the scorpion; only isolated parts of the pedipalps are still present.

To discriminate if the specimen was an exuvia (molt) or a carcass, we carried out a taphonomical and morphological analysis, according to the criteria established by McCoy and Brandt (2009), which use the relative position of selected anatomical elements of the scorpion body. These criteria include the integrity and posture of the body line, the relative position of the walking legs and the pedipalps, as well as the telescoping of segments. Another criterion is the relative position of the chelicerae, which was the only one impossible to evaluate because in BES SC 1973 the remains of the mouth parts are only putative (Fig. 3.3, see below). The body line is straight, with the only exception of the metasoma (i.e., the tail) which is curved. The remains of the pedipalps are retained alongside the body and there is no trace of telescoping on the segments, neither the mesosomal nor the metasomal one. The walking legs are the most damaged part of the fossil. They are visible only on the right side of the scorpion, where only one of them still shows most of the segment jointed, whereas the others consist of single or coupled segments, all lumped together on the right side of the body and overlapping the back of the scorpion.

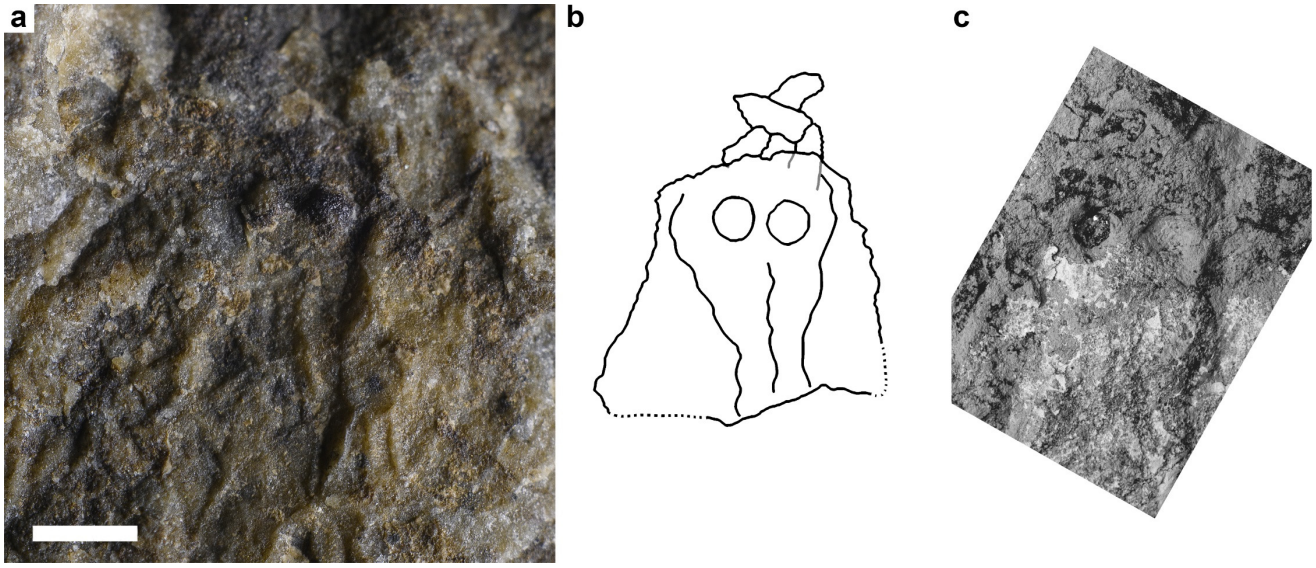

Fig. 3.3 - Prosoma of BES SC 1973. A) visible light photo and B) and interpretation of the whole prosoma; scale bar equals 1 mm. C) SEM (BSE) image of the median eyes detail on the counterpart. Scale bar equals 500 µm.

Based on these conditions, we regard specimen BES SC 1973 as a scorpion carcass (Tab. 3.1). In fact, according to the experimental data provided by McCoy and Brandt (2009), in the totality of the examined cases, the carcasses show a straight body line and no telescoped segments; the walking legs are folded against the body in most cases (77%), and the pedipalps are pulled in towards the prosoma in more than half of the cases (54%). McCoy and Brandt (2009) also showed that appendages and metasomal segments are the first parts of a scorpion carcass to disarticulate. In sum, the scorpion described in this paper, albeit not fully matching the conditions reported, can be interpreted as the remains of a carcass that was left exposed for a sufficient period of time required to degrade the appendages, which could have been affected by different biostratinomic processes like scavenging, post-mortem contractions and/or displacement due to light bottom currents.

Table 3.1 - Taphonomical criteria used to distinguish scorpion carcasses from exuviae according to McCoy and Brandt (2009), and related conditions in specimen BES SC 1973.

	Chelicerae	**Body Line**	**Pedipalps**	**Walking Legs**
Exuvia	Extended	Curved	Extended	Splayed
Carcass	Retracted	Straight	Retracted	Folded
BES SC 1973	N/A	Mesosoma straight Metasoma curved	Retracted	Folded

3.6 Systematic palaeontology

Class ARACHNIDA Lamarck, 1801
Order SCORPIONES Koch, 1837
Suborder NEOSCORPIONES Thorell and Lindström, 1885
Infraorder ORTHOSTERNI Pocock, 1911
Superfamily BUTHOIDEA Koch, 1837 (*sensu* Laurenço 2000)
Family PROTOBUTHIDAE Lourenço and Gall, 2004

Note. The definition of high-level taxonomic categories is a particularly difficult task when it comes to the study of scorpions. Soleglad and Fet (2003), in their high-level phylogeny of extant scorpions, listed all the taxonomic suprageneric categories with their diagnosis and proposed various keys to each determination. The diagnosis of the families involves various characters, such as carinae, median eyes, and overall shape of some anatomical parts, but the most used synapomorphies in the extant families definition are found in the trichobothrial pattern. In fossil specimens, the use of trichobothria is strongly limited by often poor preservation, and it is therefore preferred the use of morphological features more commonly preserved in the scorpions fossil record. Lourenço and Gall (2004) diagnosed the family Protobuthidae using all the characters present in the description of the genus *Protobuthus*. Moreover, in their character list, they included a "very incomplete" trichobothrial pattern, a "probable" composition of the dentate margins of fixed fingers, and "not observable" tibial spurs on the legs. Such extended and approximately coded diagnosis raises difficulties in the use of this taxonomic category, therefore we propose here a reviewed diagnosis for the family Protobuthidae. Accordingly, we now consider the Lourenço and Gall (2004) diagnosis of Protobuthidae as valid for the genus *Protobuthus* only.

Family PROTOBUTHIDAE Lourenço and Gall, 2004 - comb. nov.

Emended diagnosis. Small/medium-sized scorpion (up to 43 mm) with very slender body and appendages, carapace sub-trapezoidal with rounded angles, median ocular tubercle slightly anterior to the centre of the carapace, median eyes separated by less than an ocular diameter, telson with a vesicle oval in shape and with a slender aculeus longer than the vesicle, sub-aculear tooth absent.

Genus BESANOBUTHUS nov.
Figures 3.2-3.4

Type species. *Besanobuthus ziliolii* sp. nov.

Etymology. From the village of Besano (Varese Province, Lombardy, N Italy). For the etymology of *-buthus,* see Sousa *et al.* (2017).

Diagnosis. Protobuthid with a strongly carinate carapace. Three main carinae: one strong median carina starting posteriorly to the median ocular tubercle, and two specular carinae starting near the anterior prosomal margin, at the sides of the median eyes, and converging towards the posterior end of the median carina.

Remarks. Besanobuthus differs from *Protobuthus* Lourenço and Gall, 2004, because of the carinate carapace, which in *Protobuthus* has a smooth tegument and lacks carinae or clearly visible furrows (Fig. 3.3). Also, in *Besanobuthus* the shaft of the fixed finger of the chela is straight, whereas in *Protobuthus* it is slightly curved medially (Fig. 3.4).

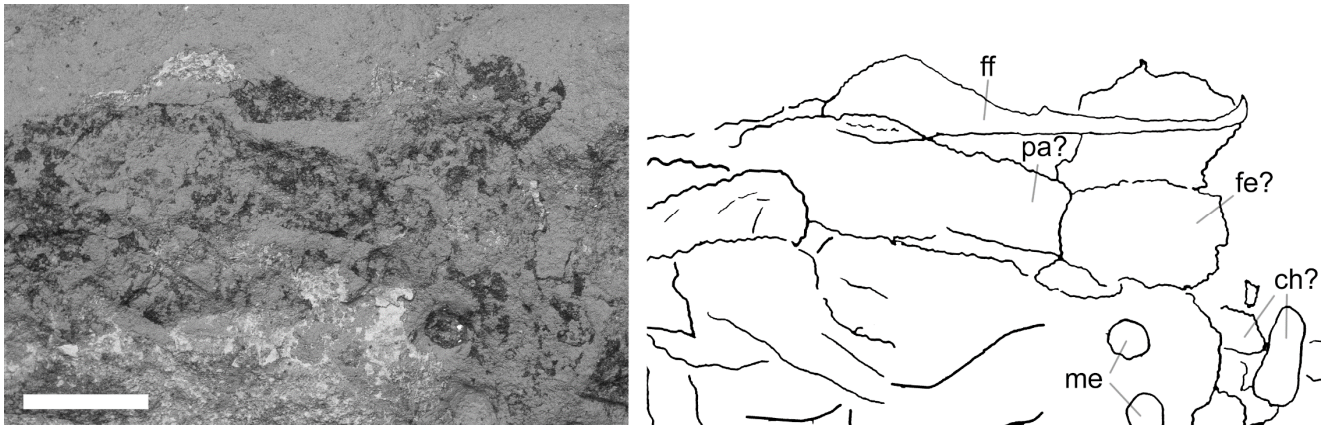

Fig. 3.4 - SEM (BSE) image of the left chela on the counterpart of *Besanobuthus* (BES SC 1973). Scale bar equals 1 mm.

Species *Besanobuthus ziliolii* sp. nov.
Figures 3.2-3.7

Etymology. The species is dedicated to Michele Zilioli (MSNM), for his skillful painstaking support to the paleontological research, which gave a fundamental contribution to exceptional discoveries about soft tissue preservation in fossils (e.g., Dal Sasso and Maganuco 2011), and to this work itself.

*Type specimen***.** Articulated almost complete fossil specimen, labeled as BES SC 1973 in the catalogue of the Museo di Storia Naturale di Milano (BES SC is acronym for Besano Sasso Caldo), and coded as 20.S288-2.5 in the Inventario Patrimoniale dello Stato (State Heritage Database).

Type locality. Sasso Caldo site, Besano, Monte San Giorgio, Varese Province, NW Lombardy, N. Italy. Geographical coordinates: 45°54'03.7"N 8°55'10.6"E, elev. 650 m.

*Type horizon and distribution***.** Upper Besano Formation (*sensu* Röhl *et al.*, 2001), uppermost Anisian/lowermost Ladinian (uppermost *N. secedensis* Zone/lowermost *E. curioni* Zone *sensu* Brack *et al.* 2005), Middle Triassic.

Diagnosis. As for the genus.

3.7 Description

Small-sized scorpion (overall length 43 mm) with a very slender body (Tab. 3.2). Metasoma made of 7 segments, mesosoma made of 5 segments. Telson slender without subaculear tooth. Appendages badly preserved, consisting in right femur and left chela of the pedipalps, and various leg segments.

Table 3.2 - Selected measurements of BES SC 1973.

Total length	43 mm		
Carapace:		**Segment III**	
length	3,6 mm	length	4,4 mm
anterior width	2 mm	width	2,9 mm
posterior width	4 mm	**Segment IV**	
Mesosoma:		length	3,6 mm
Total length	15 mm	width	3,1 mm
Metasoma		**Segment V**	
Total length	18,9 mm	length	3,2 mm
Segment I		width	1,9 mm
length	3,6 mm	**Vesicle:**	
width	3,5 mm	length	3,2 mm
Segment II		depth	2,2 mm
length	4,1 mm	**Aculeus length**	4 mm
width	3,1 mm		

Prosoma. Prosomal shield (carapace) is trapezoidal with a convex anterior margin. Three strong carinae are visible on the shield: one posterior median, located behind the median eyes, and two lateral carinae, starting at the sides of the median eyes and converging near the end of the posterior median carina. Lateral carinae have a sinuous pattern. Median ocular tubercle is located halfway between the anterior margin and the centre of the carapace; median eyes are separated by a half ocular diameter.

Mesosoma. Tergite I bears at least 7 carinae, of which the median three are in continuity with the prosomal carinae and converge at the end of the tergite. Tergites II-VII tricarinate, with three strong median carinae; one pair of secondary carinae on each side, not always visible. The surface between the carinae is rather smooth.

Metasoma. Segments II and IV show the most complete ornamentation pattern, where at least 6 carinae can be observed. Telson weakly granular, in particular the aculeus. Vesicle with an oval shape and two weak lateral carinae; aculeus slender and longer than vesicle; subaculear tooth absent (Fig. 3.5).

Pedipalps. Poorly preserved, only the right femur and the left chela are clearly recognizable (Figs. 3.4; 3.6). Trichobothrial pattern visible on the femur, and interpreted as **i1?**, **i2** and **i3?** on the internal side and **d1**, **d2?**, **d3?**, **d4?** and **d5** on the dorsal surface (sensu Vachon, 1973).

Legs. Poorly preserved, only one leg is easily recognizable unnaturally lying above the metasoma, with femur, patella, and tibia still jointed (Fig. 3.7). Each segment bears at least three carinae and, in addition, the femur shows at least two weak carinae with a transverse disposition.

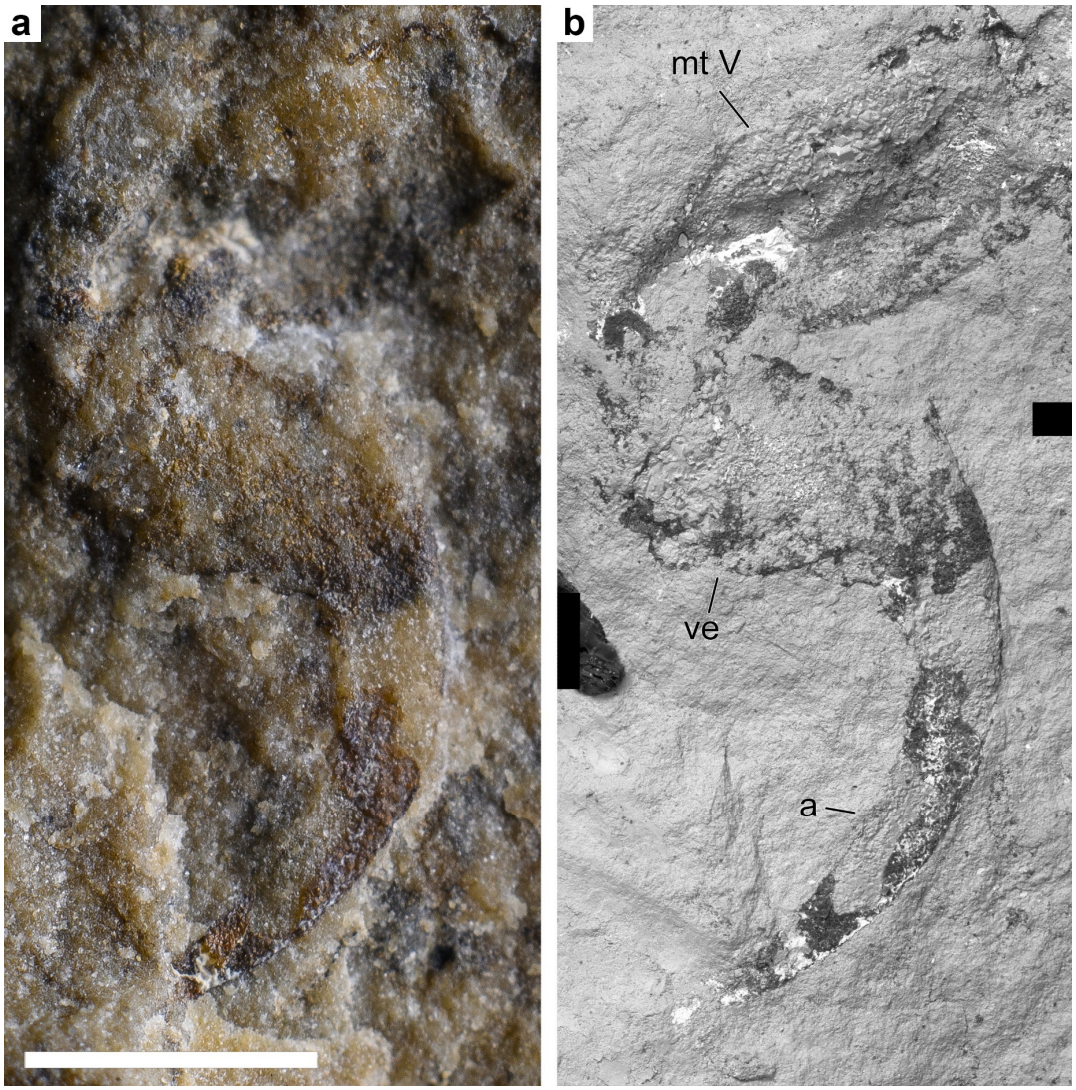

Fig. 3.5 - Telson of BES SC 1973 depicted in a classic photo (A), and in a SEM (BSE) image (B). Scale bar equals 2 mm. Anatomical abbreviations: a, aculeus; mt V, metasomal segment V; ve, vesicle.

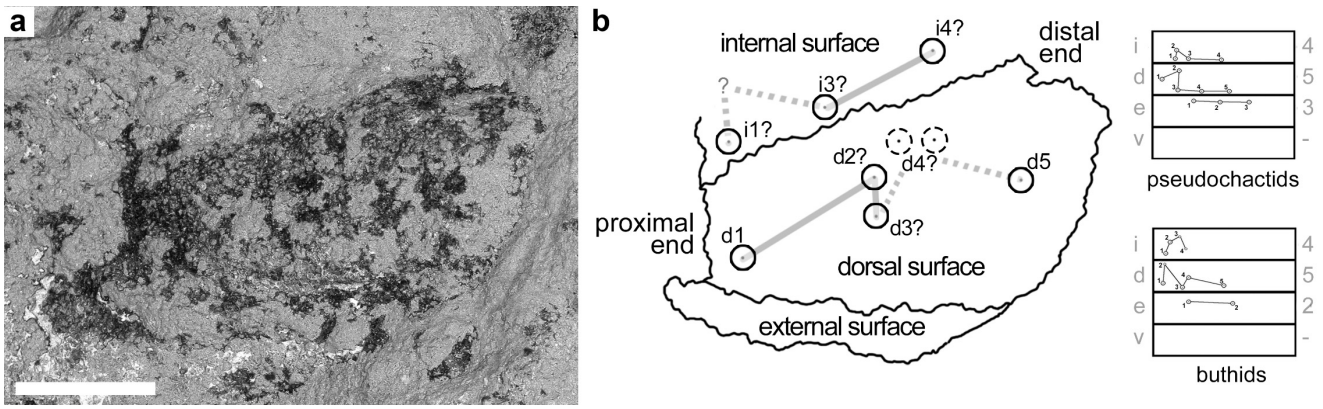

Fig. 3.6 - BES SC 1973, SEM (BSE) image of the right pedipalp femur with visible trichobothria (A), and its interpretation (B). Scale bar equals 500 µm. To the right of (B), trichobothrial pattern F1 (pseudochactids, above) and pattern A (buthids, below), modified from Soleglad and Fet (2001). Abbreviations: d, dorsal; e, external; i, internal; v, ventral. Numbers on the far right indicate the total number of trichobothria for each surface.

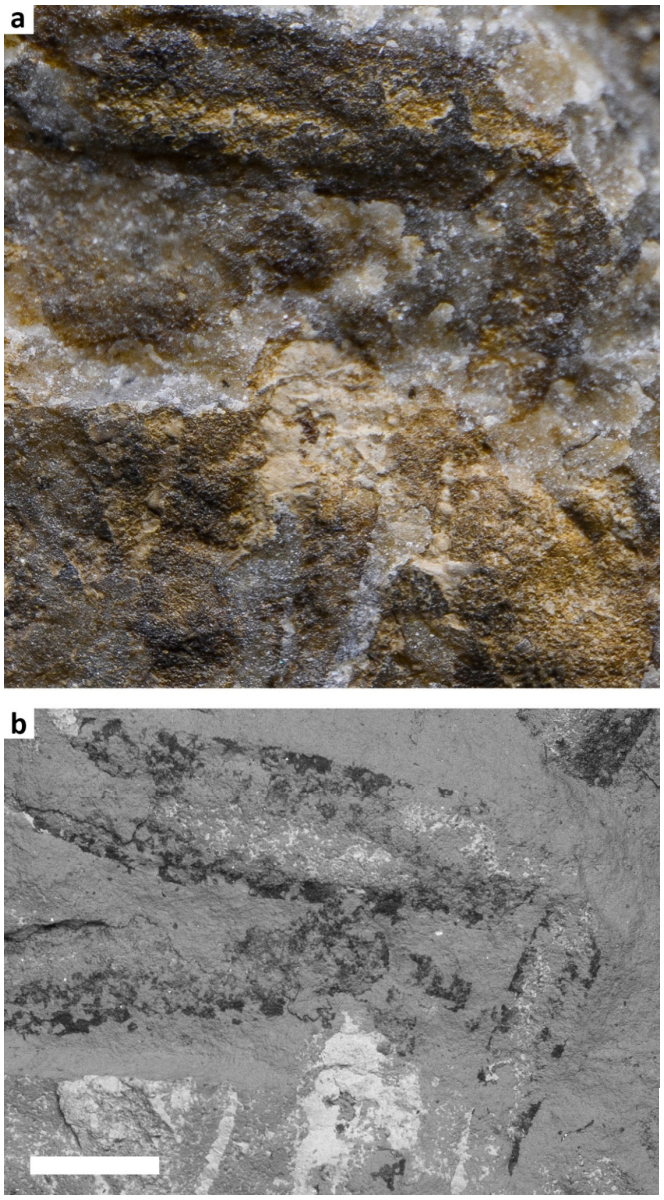

Fig. 3.7 - Jointed leg of BES SC 1973 depicted in visible light (A) and a SEM (BSE) image of the counterpart (B). Scale bar equals 1 mm. For anatomical reference see Fig. 3.8.

3.8 Discussion

There are few Triassic scorpion families that need to be evaluated to properly assess the taxonomic attribution of BES SC 1973, *Besanobuthus ziliolii*. These families are: Mesophonidae Wills, 1910, Willsiscorpionidae Kjellesvig-Waering, 1986, Gallioscorpionidae Lourenço and Gall, 2004, Stenoscorpionidae Kjellesvig-Waering, 1986, Spongiophonidae Kjellesvig-Waering, 1986, Isobuthidae Petrunkevitch, 1913 and Protobuthidae Lourenço and Gall, 2004. Comparisons with the studied specimen are made below.

Mesophonidae, Willsiscorpionidae and Gallioscorpionidae are characterized by an anterior median protrusion on the carapace which bears the median eyes or, when this structure is absent, by the median eyes located in line with the anterior margin of the carapace, as in *Willsiscorpio bromsgroviensis* (Wills, 1910). BES SC 1973 completely lacks any kind of anterior protrusion, the anterior margin of the carapace is slightly rounded, and the median eyes are located between the anterior margin and half the prosomal length. On the other hand, these characters are diagnostic of the family Protobuthidae (as stated above, see Systematic palaeontology).

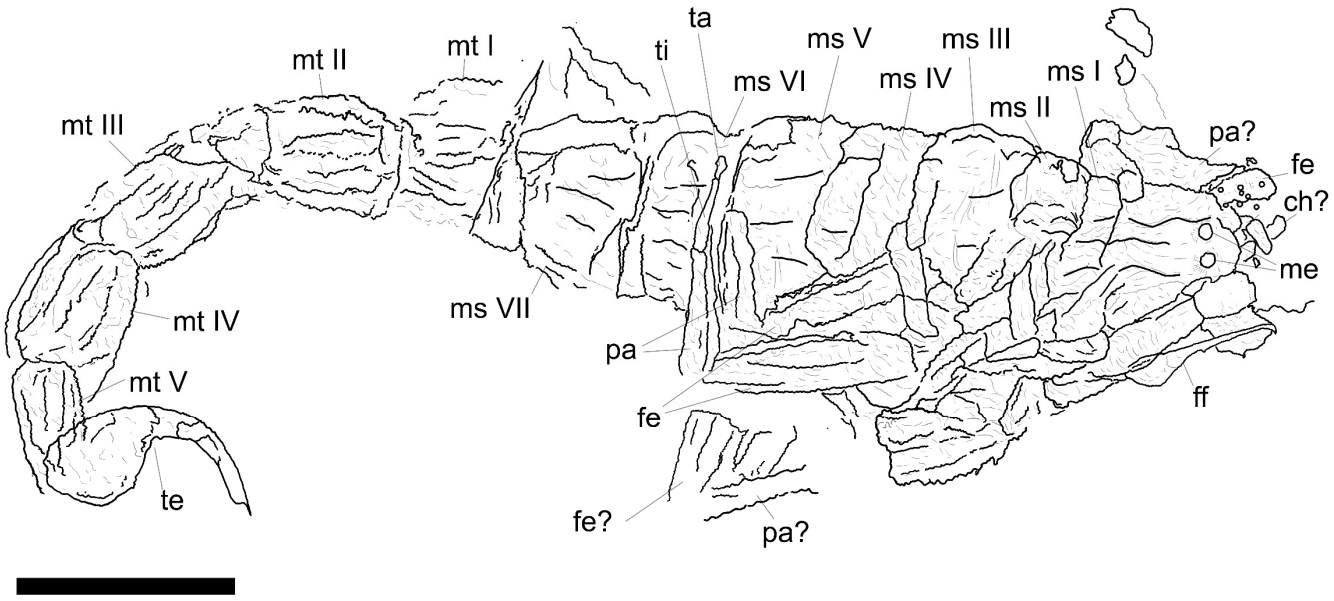

Fig. 3.8 - Interpretative drawing of BES SC 1973. Scale bar equals 5 mm. Anatomical abbreviations: ch, chelicerae; fe, femur; ff, fixed finger; me, median eyes; ms, mesosomal segment; mt, metasomal segment; pa, patella; pr, prosoma; ta, tarsus; te, telson; ti, tibia. Question marks indicate putative structures.

Any affinity of our specimen with the family Stenoscorpionidae can also be excluded since the latter is characterized by a prosomal shield divided in two halves by a longitudinal groove.

The families Spongiophonidae and Isobuthidae are both difficult to compare with the specimen here described because of the lack of diagnostic features preserved both in BES SC 1973 and in the fossil specimens assigned to the two taxa. The family Spongiophonidae is represented only by isolated tergites and a sternum articulated to four coxae, characterized by a peculiar ornamentation made of polygonal pustules (Wills 1947). Such character is absent in BES SC 1973, therefore the attribution to this family can be excluded. Finally, the family Isobuthidae includes only one Triassic scorpion, *Bromsgroviscorpio willsi* Kjellesvig-Waering, 1986, erected upon a single half abdominal plate which is impossible to compare with BES SC 1973, where this element is not preserved; the remaining taxa belonging to Isobuthidae are Paleozoic and the specimen BES SC 1973 does not bear any diagnostic character of the family, a condition which prevents any attempt of comparison.

In sum, we assign BES SC 1973 to Protobuthidae on the basis of the characters listed above in the diagnosis of the family, which has also been emended to better constrain the taxon. Based on the description reported above, specimen BES SC 1973 also represents a new taxon: *Besanobuthus ziliolii* gen. et sp. nov., a protobuthid characterized by the presence of three carinae on the prosomal shield and a straight shaft of the chela fixed finger. The assignment of *B. ziliolii* to the family Protobuthidae, and the subsequent emended diagnosis of the family, increase the relevance of this scorpionid taxon during the Triassic faunal recovery.

Lourenço and Gall, 2004, included the family Protobuthidae into the superfamily Buthoidea, but such assignment has been questioned (Baptista *et al.* 2006). The phylogenetic position of these Triassic scorpions is crucial because they bridge the Carboniferous Palaeopisthacanthidae Kjellesvig-Waering, 1986 and the Cretaceous Archaeobuthidae Lourenço, 2001, filling the absence of orthostern scorpions in the early phases of the Mesozoic (Baptista *et al.* 2006). The genus *Protobuthus* was eventually included in an unnamed group of closely related Mesozoic scorpions representing basal lineages without extant relatives, alongside *Archaeobuthus* Lourenço, 2001 and *Palaeoburmesebuthus* Lourenço, 2002 (Baptista *et al.* 2006). As a consequence, *Besanobuthus* should also be included in this group of basal scorpions. However, although

incomplete, the trichobothrial pattern of *Besanobuthus* seems to reflect an intermediate condition between two of the patterns described by Soleglad and Fet (2001) (Fig. 3.6). On the dorsal surface of the femur, we have located trichobothria **d1**, **d2?**, **d3?**, **d4?** and **d5**, with a "?" to indicate putative detections. The arrangement of these trichobothria recalls the modern pattern β of the Type A, a typical buthid pattern (Vachon 1973, 1975; Soleglad and Fet 2001). More recently, patterns α and β have been subdivided into three subpatterns by Soleglad and Fet (2003) and their evaluation here is useful to interpretat the trichobothrial pattern of *B. ziliolii*. These subpatterns are the alignment of **d1**-**d3**, the alignment of **d3**-**d4**, and the placement of **d2**; for each of them, a primitive (basal), an α, and a β arrangement were defined by the authors.

The dorsal trichobothrial pattern of the femur in *B. ziliolii* is intermediate between the primitive and the β arrangement: trichobothria **d1**-**d3** are parallel to the dorsointernal carina, and **d2** lays on the dorsal surface (primitive arrangement); on the other hand, trichobothria **d3**-**d4** point away from the dorsoexternal carina (β arrangement). In fact, the trichobothrial pattern of the dorsal surface is intermediate between the basal pattern, found in *Archaeobuthus* and *Pseudochactas*, and the modern β Type A pattern, found in buthid scorpions. The disposition of the putative trichobothria detected on the internal surface of *Besanobuthus* led us to the interpretation of **i1?**, **i3?** and **i4?**. These putative trichobothria are arranged similarly to those on the internal surface of the femur of *Pseudochactas*, where these trichobothria are somewhat in line and parallel to the dorsointernal carina. However, bad preservation of the pedipalps in BES SC 1973 prevents a confident detection of femoral trichobothria; **d1** and **d5** make an exception since their position is well-defined in our specimen. More and better preserved specimens are needed to clarify the pedipalp femur trichobothrial pattern both for genus *Besanobuthus* and family Protobuthidae.

BES SC 1973 was recovered in the upper portion of the Besano Fm. (G. Teruzzi, pers. com., 2019). According to Röhl *et al.* (2001), these sediments were deposited in a shallow inter- to subtidal carbonate platform rich in nearshore taxa, including small sauropterygians, marine gastropods, terrestrial protorosaurs, and terrestrial plants. The finding of a scorpion in this portion of the Formation at the Sasso Caldo site further corroborates the hypothesis of a near shoreline in that depositional phase, closer than during the deposition of the older middle portion of the Formation, where a pelagic influence is strongly documented (see "Geological framework").

3.9 Conclusions

After careful morphological analysis carried out through optic microscopy, UV, and SEM analysis, the specimen BES SC 1973 is assigned to the taxon *Besanobuthus ziliolii* gen. et sp. nov., included in the family Protobuthidae. This finding represents the first arachnid recorded from the Besano Fm. and the second genus attributed to the family Protobuthidae. The diagnosis of the family has been emended, in order to ensure a definition devoid of vague and preservation-linked characters. The new diagnosis highlights the characters shared by the two genera included in the Protobuthidae, *Protobuthus* and *Besanobuthus*, ignoring incomplete characters, giving room to potential new genera to be included in the family, and at the same time strengthening and stabilizing the taxon. With the description of this new species, the Triassic diversity of scorpions increases, as well as the interest towards Lower and Middle Triassic successions, which could bear other fossil scorpions.

The discovery of new specimens could clarify the characters of the new genus that are still incomplete, putative or unknown, i.e. the trichobothrial pattern and the ventral side, and shed light on the recovery and evolution of these arachnids after the end-Permian extinction.

3.10 Acknowledgements

We thank Giorgio Teruzzi (MSNM), who directed the Sasso Caldo excavations for several years, and the volunteers of the former "Gruppo paleontologico di Besano", who unearthed the specimens studied here, and many other exceptional fossils. We also thank Michele Zilioli (MSNM) for SEM analysis and macrophotography, the Italian Ministry of Culture and the "Soprintendenza Archeologia, Belle Arti e Paesaggio per le province di Como, Lecco, Monza e Brianza, Pavia, Sondrio e Varese" for permissions. This paper is part of a Ph.D. project (G. Bindellini) focusing on the Besano Formationfossil fauna, led by the Università Statale di Milano (M. Balini) in agreement with the Museo di Storia Naturale di Milano (C. Dal Sasso).

3.11 References

Ballesteros, J. A., and Sharma, P. P. 2019. A critical appraisal of the placement of Xiphosura (Chelicerata) with account of known sources of phylogenetic error. *Systematic Biology*, 68, 896-917.

Baptista, C., Santiago-Blay, J. A., Soleglad, M. E. and Fet, V. 2006. The Cretaceous scorpion genus, *Archaeobuthus*, revisited (Scorpiones: Archaeobuthidae). *Euscorpius*, 35, 1-40.

Benton, M. J., Zhang, Q., Hu, S., Chen, Z. Q., Wen, W., Liu, J., Huang, J., Zhou, C., Xie, T., Tong, J. and Choo, B. 2013. Exceptional vertebrate biotas from the Triassic of China, and the expansion of marine ecosystems after the Permo-Triassic mass extinction. *Earth Sciences Review*, 125, 199-243.

Bernasconi, S. M. 1991. Geochemical and microbial controls on dolomite formation and organic matter production/preservation in anoxic environments a case study from the Middle Triassic Grenzbitumenzone, Southern Alps (Ticino, Switzerland). D. Phil. thesis, Swiss Federal Institute of Technology Zürich, Switzerland, 196 pp.

Bernasconi, S. M. 1994. Geochemical and microbial controls on dolomite formation in anoxic environments: A case study from the Middle Triassic (Ticino, Switzerland). *Contributions to Sedimentology*, 19, 1-109.

Bernasconi, S. M. and Riva, A. 1993. Organic geochemistry and depositional environment of a hydrocarbon source rock: the Middle Triassic Grenzbitumenzone Formation, Southern Alps, Italy/Switzerland. 179-190. *In*: Spencer AM eds. *Generation, Accumulation and Production of Europe's Hydrocarbons (vol.3).* Springer, Berlin, Heidelberg, 380 pp.

Bindellini, G., Balini, M., Teruzzi, G. and Dal Sasso, C. 2019. Ammonoid and *Daonella* zonation of the Sasso Caldo quarry (Besano Formation, Middle Triassic). 87. *In*: Petti, F. M., Innamorati, G., Carmina, B. and Germani, D. Strati 2019, 3rd International Congress on Stratigraphy. ST2.4 Ammonoids in stratigraphy: Abstract book, p.87.

Bindellini, G., Wolniewicz, A. S., Miedema, F., Scheyer, T. M. and Dal Sasso, C. 2021. Cranial anatomy of *Besanosaurus leptorhynchus* Dal Sasso and Pinna, 1996 (Reptilia: Ichthyosauria) from the Middle Triassic Besano Formation of Monte San Giorgio, Italy/Switzerland: taxonomic and palaeobiological implications. *PeerJ*, 9, e11179.

Brack, P. and Rieber, H. 1986. Stratigraphy and ammonoids of the lower Buchenstein Beds of the Brescian Prealps and Giudicarie and their significance for the Anisian/Ladinian Boundary. *Eclogae Geologicae Helvetiae*, 79, 181-225.

Brack, P. and Rieber, H. 1993. Towards a better definition of the Anisian/Ladinian boundary: New biostratigraphic data and correlations of boundary sections from the Southern Alps. *Eclogae Geologicae Helvetiae*, 86, 415-527.

Brack, P., Rieber, H., Nicora, A. and Mundil, R. 2005. The Global boundary Stratotype Section and Point (GSSP) of the Ladinian Stage (Middle Triassic) at Bagolino (Southern Alps, Northern Italy) and its implications for the Triassic time scale. *Episodes*, 28, 233-244.

Brinkmann, W. 1997. Die Ichthyosaurier (Reptilia) aus der Mitteltrias des Monte San Giorgio (Tessin, Schweiz) und von Besano (Lombardei, Italien) – der aktuelle Forschungsstand. *Vierteljarsschrift der Naturforschenden Gesellschaft in Zürich*, 142, 69–78.

Bürgin, T., Rieppel, O., Sander, P. M. and Tschanz, K. 1989. The fossils of Monte San Giorgio. *Scientific American*, 260, 74-81.

Dal Sasso, C. and Pinna, G. 1996. *Besanosaurus leptorhynchus* n. gen. n. sp., a new shastasaurid ichthyosaur from the Middle Triassic of Besano (Lombardy, N. Italy). *Paleontologia Lombarda*, *Nuova serie*, 4, 3-23.

Dal Sasso, C. and Maganuco, S. 2011. *Scipionyx samniticus* (Theropoda: Compsognathidae) from the Lower Cretaceous of Italy. Osteology, ontogenetic assessment, phylogeny, soft tissue anatomy, taphonomy and paleobiology. *Memorie della Società Italiana di Scienze Naturali e del Museo di Storia Naturale di Milano*, 37, 1-282.

Dunlop, J. A., Penney, D. and Jekel, D. 2020. A summary list of fossil spiders and their relatives. *In* World Spider Catalog. Natural History Museum Bern, online at http://wsc.nmbe.ch, version 20.5, accessed on 17 May 2021.

Etter, W. 2002. Monte San Giorgio: Remarkable Triassic marine vertebrates. 220-242. *In*: Bottjer, D. J., Etter, W., Hagadorn, J. W. and Tang, C. M. eds. *Exceptional fossil preservation. A unique view on the evolution of marine life*. New York: Columbia University Press, 424 pp.

Furrer, H. 1995. The Kalkschieferzone (Upper Meride Limestone; Ladinian) near Meride (Canton Ticino, Southern Switzerland) and the evolution of a Middle Triassic intraplatform basin. *Eclogae Geologicae Helvetiae*, 88, 827-852.

Furrer, H. 2003. Der Monte San Giorgio im Südtessin-vom Berg der Saurier zur Fossil-Lagerstätte internationaler Bedeutung. *Neujahrsblatt der Naturforschenden Gesellschaft in Zurich*, 206, 1-64.

Hone, D. W. E., Tischlinger, H., Xu, X. and Zhang, F., 2010. The Extent of the Preserved Feathers on the Four-Winged Dinosaur *Microraptor gui* under Ultraviolet Light. *PLoS ONE*, 5, e9223.

Jeram, A. J. 1994. Carboniferous Orthosterni and their relationship to living scorpions. Palaeontology 37, 513–550.

Jeram, A. J. 1998. Phylogeny and classification of Palaeozoic scorpions. 17-31. *In*: Selden, P. A. (ed) *Proceedings of the 17th European Colloquium of Arachnology, Edinburgh, 1997*. The British Arachnological Society, Burnham Beeches, 350 pp.

Kjellesvig-Waering, E. N. 1986. A restudy of the fossil Scorpionida of the world. *Palaeontographica Americana*, 55, 1–287.

Koch, C. L. 1837. Scorpionen. Übersicht des Arachnidensystems. Nürnberg, C.H. *Zeh'sche Buchhandlung*, 1, 36–39.

Lamarck, J. B. P. A., 1801. *Systême des animaux sans vertèbres*. Lamarck and Deterville, Paris, viii + 432 pp.

Lourenço, W. R. 2000. Panbiogéographie, les familles des scorpions et leur répartition géographique. *Biogeographica*, 76, 21–39.

Lourenço, W. R. (2001) A remarkable scorpion fossil from the amber of Lebanon. Implications for the phylogeny of Buthoidea. *Comptes Rendus de l'Académie des Sciences Paris, Sciences de la Terre et des Planètes*, 332, 641–646.

Lourenço, W. R. (2002). The first scorpion fossil from the Cretaceous amber of Myanmar (Burma). New implications for the phylogeny of Buthoidea. *Comptes Rendus Palevol*, 1, 97-101.

Lourenço, W. R. and Gall, J. C. 2004. Fossil scorpions from the Buntsandstein (Early Triassic) of France. *Comptes Rendus Palevol*, 3, 369-378.

Maisch, M. W. and Matzke, A. T. 1998. Observations on Triassic ichthyosaurs. Part II: A new ichthyosaur with palatal teeth from Monte San Giorgio. *Neues Jahrbuch fur Geologie und Palaontologie*, 1, 26-41.

McCoy, V. E. and Brandt, D. S. 2009. Scorpion taphonomy: criteria for distinguishing fossil scorpion molts and carcasses. *The Journal of Arachnology*, 37, 312-320.

Mundil, R., Brack, P., Meier, M., Rieber, H. and Oberli, F. 1996. High resolution U-Pb dating of Middle Triassic volcaniclastics: Time-scale calibration and verification of tuning parameters for carbonate sedimentation. *Earth and Planetary Science Letters*, 141, 137-151.

Petrunkevitch, A. 1913. A monograph of the terrestrial Palaeozoic Arachnida of North America. Transactions of the Connecticut Academy of Arts and Sciences, 18, 1–137.

Pocock, R.I. 1911. A monograph of the terrestrial Carboniferous Arachnida of Great Britain. *Monographs of the Palaeontographical Society*, 64, 1–84.

Renesto, S., Dal Sasso, C., Fogliazza, F. and Ragni, C. 2020. New findings reveal that the Middle Triassic ichthyosaur *Mixosaurus cornalianus* is the oldest amniote with a dorsal fin. *Acta Paleontologica Polonica*, 65, 511-522.

Rieber, H. 1973. Die Triasfauna der Tessiner Kalkalpen. Cephalopoden aus der Grenzbitumenzone (Mittlere Trias) des Monte San Giorgio (Kt. Tessin, Switzerland). *Schweizerische Palaeontologische Abhandlungen*, 93, 1-96.

Rieppel, O. 2019. *Mesozoic Sea Dragons: Triassic Marine Life from the Ancient Tropical Lagoon of Monte San Giorgio.* Bloomington: Indiana University Press, 256 pp.

Röhl, H. J., Schmid-Röhl, A., Furrer, H., Frimmel, A., Oschmann, W. and Schwark, L. 2001. Microfacies, geochemistry and palaeoecology of the Middle Triassic Grenzbitumenzone from Monte San Giorgio (Canton Ticino, Switzerland). *Geologia Insubrica*, 6, 1-13.

Soleglad, M. E. and Fet, V. 2001. Evolution of scorpion orthobothriotaxy – A cladistic approach. *Euscorpius,* 1, 1-38.

Soleglad, M. E. and Fet, V. 2003. High-level systematic and phylogeny of the extant scorpions (Scorpiones: Orthosterni). *Euscorpius*, 11, 1-175.

Sousa, P., Arnedo, M. A. and Harris, D. J. 2017. Updated catalogue and taxonomic notes on the Old-World scorpion genus *Buthus* Leach, 1815 (Scorpiones, Buthidae). *ZooKeys*, 686, 15-84.

Stockar, R., Baumgartner, P. O. and Condon, D. 2012. Integrated Ladinian bio-chronostratigraphy and geochronology of Monte San Giorgio (Southern Alps, Switzerland). *Swiss Journal of Geosciences*, 105, 85-108.

Stockwell, S. A. 1989. Revision of the phylogeny and higher classification of scorpions (Chelicerata). Doctoral dissertation, University of California, Berkeley.

Thorell, T. and Lindström, G. 1885. On a Silurian scorpion from Gotland. *Konglige Svenska Vetenskaps-Akademiens Handlingar*, 21, 1–33.

Tischlinger, H. 2002. Der Eichstätter *Archaeopteryx* im langwelligen UV-Licht. [The Eichstätt specimen of *Archaeopteryx* under longwave ultraviolet light]. *Archaeopteryx,* 20, 21-38.

Vachon, M. 1973. [1974]. Étude des caractères utilisés pour classer les familles et les genres de scorpions (Arachnides). 1. La trichobothriotaxie en arachnologie. Sigles trichobothriaux et types de trichobothriotaxie chez les scorpions. *Bulletin du Muséum National d'Histoire Naturelle*, 3, 857–957.

Vachon, M. 1975. Sur l'utilisation de la trichobothriotaxie du bras des pédipalpes des Scorpions (Arachnides) dans le classement des genres de la famille de Buthidae Simon. *Comptes Rendus des Séances de l'Académie des Science*, 281, 1597–1599.

Viaretti, M., Bindellini, G. and Dal Sasso, C. 2020. An exceptionally well-preserved scorpion from the Besano Formation (Monte San Giorgio, Middle Triassic, Southern Alps): preliminary study. *In:* Bartolini Lucenti, S., Cirilli, O. and Pandolfi, L. *Fossilia*, Volume 2020, 53-55.

Wills, L. J. 1910. On the fossiliferous Lower Keuper Rocks of Worcestershire: with descriptions of some of the plants and animals discovered therein. *Proceedings of the Geologists' Association*, 21, 249-331.

Wills, L. J. 1947. A Monograph of British Triassic Scorpions. Part I Pages i–iv, 1–74; Plates I–VI. *Monographs of the Palaeontographical Society*, 100, i-74.

Wills, M. A. 2001. How good is the fossil record of arthropods? An assessment using the stratigraphic congruence of cladograms. *Geological Journal*, 36, 187-210.

Wotzlaw, J. F., Brack, P. and Storck, J. C. 2017. High-resolution stratigraphy and zircon U–Pb geochronology of the Middle Triassic Buchenstein Formation (Dolomites, northern Italy): precession-forcing of hemipelagic carbonate sedimentation and calibration of the Anisian–Ladinian boundary interval. *Journal of the Geological Society*, 175, 71-85.

Chapter 4
First skeletal remains of *Helveticosaurus* from the Middle Triassic Italian outcrops of the Southern Alps, with remarks on an isolated tooth.

*Manuscript in review at Rivista Italiana di Paleontologia e Stratigrafia.
Gabriele Bindellini[1], Cristiano Dal Sasso[2]
[1] Dipartimento di Scienze della Terra "Ardito Desio", Università degli Studi di Milano, Milano, Italy.
[2] Sezione di Paleontologia dei Vertebrati, Museo di Storia Naturale di Milano, Milano, Italy.

4.1 Abstract

The enigmatic marine reptile *Helveticosaurus zollingeri,* from the Middle Triassic Besano Formation of Monte San Giorgio, is known from three specimens found in Swiss territory. This paper describes the first skeletal remains of this taxon recovered from the corresponding Italian outcrops of Besano (Varese). An isolated tooth assigned to the same taxon and coming from the San Salvatore Dolomite, Rasa di Varese (Varese), is also redescribed herein. The skeletal remains have been CT scanned to inspect the preserved morphology of the bones hidden below the surface; CT data also allowed the identification of an associated ammonoid which has been crucial to determine the stratigraphic position of the studied material. The redescription of the tooth has been helped by a digital model of the specimen obtained through photogrammetry. With the additional new data obtained from the two specimens, the first skeletal reconstruction of *Helveticosaurus* is provided. This is followed by a phylogenetic test of the taxon, assessing its position among marine Triassic diapsids. Finally, in the light of recent studies we discuss the swimming mode and the possible ecological niche occupied by the animal: we suggest a distinction between the function of forelimbs and hindlimbs, and a distinction between different swimming styles likely performed by *Helveticosaurus*, depending on the speed of movements.

4.2 Introduction

Helveticosaurus zollingeri, to date, is known from three specimens housed in the Paläontologisches Institut und Museum der Universität Zürich. The holotype (PIMUZ T 4352) was collected in 1935 in the Galleria Arnaldo of Cava Tre Fontane (Monte San Giorgio, Canton Ticino, Switzerland); the preserved skeleton is 2.5 m long and has an estimated full length of 3.6 m (Kuhn-Schnyder, 1974). Earlier in 1933 a largely complete but disarticulated specimen (PIMUZ T 4353), and later in 1937 an isolated snout with 14 mesial teeth (PIMUZ T 4354), were recovered in the same locality (Rieppel, 2019). So far, the only Italian record of *Helveticosaurus* is represented by a single tooth (ST166120) from the S. Salvatore Dolomite [Dolomia

della Rasa *sensu* Airaghi (1935), Rasa di Varese, Lombardy], tentatively attributed to this genus by Pieroni (2011) and Renesto & Pieroni (2013). All these specimens are dated back to the Late Anisian (Middle Triassic).

The holotype and PIMUZ T 4353 are almost complete, although in both cases the skull is severely crushed, most of the tail is missing, and the sacral region is not well- preserved. *Helveticosaurus zollingeri* is a highly enigmatic animal. In fact, its morphology is distinct from all other known Triassic marine reptiles and its rare remains do not allow to place it in a satisfactory phylogenetic position among the Diapsida. Furthermore, for the same reasons its ecology is partly unexplored and not fully understood.The aims of this study are to describe a new specimen, recovered from the middle Besano Formation of Besano (Varese), found in 1952 and recently re-discovered in the collection of the Museo di Storia Naturale di Milano (MSNM V927 and V928); to redescribe the isolated tooth (ST166120) reported by Renesto & Pieroni (2013); to provide an updated skeletal reconstruction, and give a brief review of the swimming mode and the possible ecological role of *Helveticosaurus* in the seas where the Besano Formation was deposited during the latest Anisian.

4.3 Geological and stratigraphic context

The Middle Triassic carbonate succession of Monte San Giorgio consists of four formations that were deposited on a carbonate platform along the western margin of the Neo-Tethys (Furrer, 1995; Röhl et al., 2001; Etter, 2002; Stockar et al., 2012). Above the Anisian Lower S. Salvatore Dolomite lies the 5- to 16-meters-thick Besano Formation (also known as Grenzbitumenzone), from which the greatest part of the well-known vertebrate fauna of Monte San Giorgio has been recovered (Bürgin et al., 1989; Furrer, 2003). The Besano Formation was deposited in a shallow marine setting (30-130 m deep) and consists of an alternation of laminated dolomitic banks and bituminous shales with sparse cineritic tuffs (Bernasconi, 1991; Bernasconi & Riva, 1993, Bernasconi, 1994; Furrer, 1995; Röhl et al., 2001; Etter, 2002), which are Late Anisian-Early Ladinian in age (Brack & Rieber, 1986, 1993; Mundil et al., 1996; Brack et al., 2005; Wotzlaw et al., 2017). Recent biozonation of the Italian Sasso Caldo site (Besano, Varese) indicates that the stratigraphic section cropping out there is fairly consistent with the most recent biozonation reported from the Swiss sections (Brack et al., 2005) and allows confident correlation with the coeval Swiss localities and other Italian outcrops (Bindellini et al., 2019). The three slabs containing the bones here described come from the ammonoid-bearing layers of the Besano Formation (Fig. 4.1), since the profile of an ammonoid (with maximum diameter 71 mm) is clearly visible through computed tomography (CT) scans (Fig. 4.1C). This suggests that the fossil reptile isdated to the *Nevadites secedensis* Zone or the upper *Reitziites reitzi* Zone (Rieber, 1973; Brack et al., 2005). The ammonoid shows a platicone evolute shell, with few (eight per half turn), slightly prorsiradiate, distant but clear ribs that terminate with a rounded and prominent marginal node each (Fig. 4.1). Smaller nodes can also be identified at the umbilical margin. Although this specimen is unprepared, the combination of characters visible in the CT scan and just described is diagnostic and enough to attribute the cephalopod to the genus *Ticinites* Rieber, 1973. This genus occurs only in layer 58 of the Mirigioli section (Punkt 902) of the Besano Formation (Rieber, 1973) and defines the very base of the *N. secedensis* Zone (Brack & Rieber, 1993; Brack et al., 2005). This layer was not excavated at the Sasso Caldo quarry (Bindellini et al., 2019), but was exploited in the Piodelle-Selva Bella mine (about 1.3 km S-W of the Sasso Caldo site). Thus, MSNM V927 and V928 belong to the lowermost portion of the middle part of the Besano Formation, which following Röhl et al. (2001) coincides with the establishment of an intraplatform basin, from which a great number of ichthyosaurian remains and other pelagic vertebrates have been

recovered (e.g., Dal Sasso & Pinna, 1996; Brinkmann, 1997; Maish & Matzke, 1998; Renesto et al., 2020; Bindellini et al., 2021).

The isolated tooth crown (ST166120) from the Rasa di Varese (Varese) is preserved associated with a brachiopod referred to *Mentzelia* cfr. *mentzeli* (Renesto & Pieroni, 2013). According to these authors, in the same level the genus *Mentzelia* was found in association with the brachiopods *Punctospirella fragilis*, *Coenothyris* cfr. *vulgaris*, *Kittlidiscus lottneri*, *Trachybembyx* sp., *Macrodontella* cfr. *lamellosa*, ?*Aviculomyalina undulata*, as well as the ammonoids *Ticinites*, "*Celtites*" sp., and *Serpianites*. Therefore, the specimen has been dated to the layers of the Middle S. Salvatore Dolomite from the *N. secedensis* Zone, latest Anisian (e.g., Brack et al., 2005), which corresponds to the middle part of the Besano Formation: the San Salvatore Dolomite at Rasa di Varese (Dolomia della Rasa *sensu* Airaghi, 1935), is constituted by thick dolomite layers deposited in a carbonate platform and a reef environment (Zanin Buri, 1965; Zorn, 1971). During the latest Anisian, rising west of the Monte San Giorgio deposits, this shallow marine environment was adjacent to the basin where the Besano Formation facies were setting and the platform sediments were deposited in eteropy with the black shales, directly above the Lower S. Salvatore Dolomite (Zorn, 1971; Stockar, 2010).

Institutional abbreviations – PIMUZ, Paläontologisches Institut und Museum der Universität Zürich, Zürich, Switzerland; **MSNM**, Museo di Storia Naturale di Milano, Milan, Italy; SMF, Senckenberg Museum Frankfurt, Frankfurt, Germany; **ST**, Museo Scientifico-Naturalistico "Antonio Stoppani", Seminario Pio XI, Venegono Inferiore (Varese), Italy.

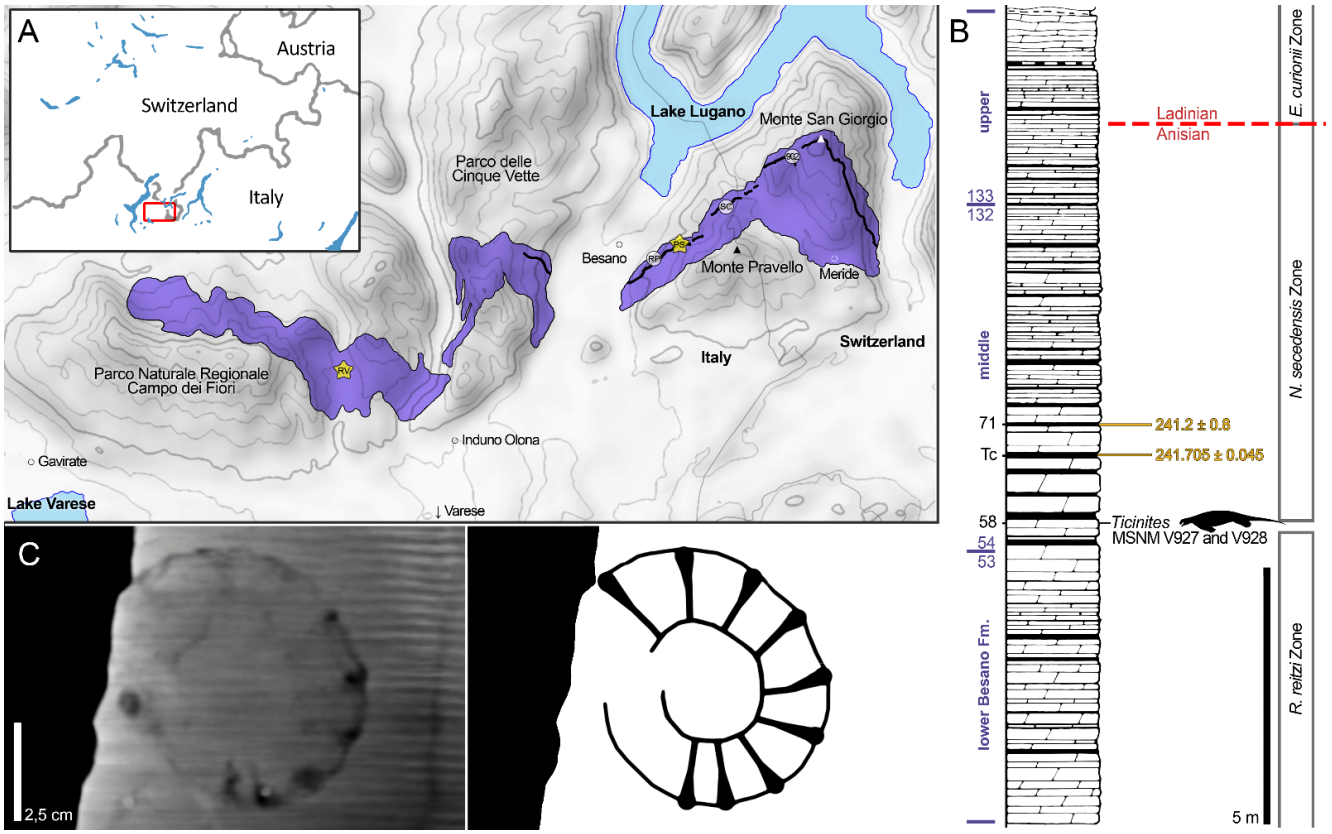

Fig. 4.1 - A) Map of the Varese Province with the Middle Triassic carbonate deposits (in purple) and the sites of origin of the specimens described in this paper (yellow stars). Localities abbreviations: 902, Punkt 902, Mirigioli; PS, Piodelle-Selva Bella mine; RP, Rio Ponticelli; RV, Rio Vallone; SC, Sasso Caldo. Outcrops of the Middle Triassic carbonate deposits modified from "Foglio 31 della Carta Geologica d'Italia (1:100.000) dell'Istituto Geografico Militare". B) simplified stratigraphic log of the Besano Formation with the inferred stratigraphic position of the new specimen described (MSNM V927+V928); log modified from Brack et al. (2005); dating (in millions of years) of layer 71 from Mundil et al. (1996); dating of Tc Tuffs (layers 66–68) from Wotzlaw et al. (2017). C) CT image and interpretative drawing of the *Ticinites* specimen associated with MSNM V927b.

4.4 Material

4.4.1 MSNM V927 and MSNM V928

Three slabs of laminated carbon-rich dolomite containing fossil bones were collected in 1952 from the waste material of the Piodelle-Selva Bella mine, near Besano (Varese), and deposited in the collections of the Museo di Storia Naturale di Milano with two different catalogue numbers (MSNM V927a,b and MSNM V928; Fig. 4.2 and Fig. 4.3). These specimens were never studied and remained indeterminate for decades. The bones pertain to the rib cage of a medium-large reptile and are included in a 12 cm-thick dolomite layer. MSNM V927a and V927b are part and counterpart, and MSNM V928 also belongs to the same individual. In fact, although the skeletal portions comprised between the two remains are missing, the bottom layer thickness and lamination in MSNM V927 and MSNM V928 are identical, the axial elements are compatible in size, and all bones show left laterodorsal exposure, the same degree of articulation, fossilisation, and diagenetic compression.

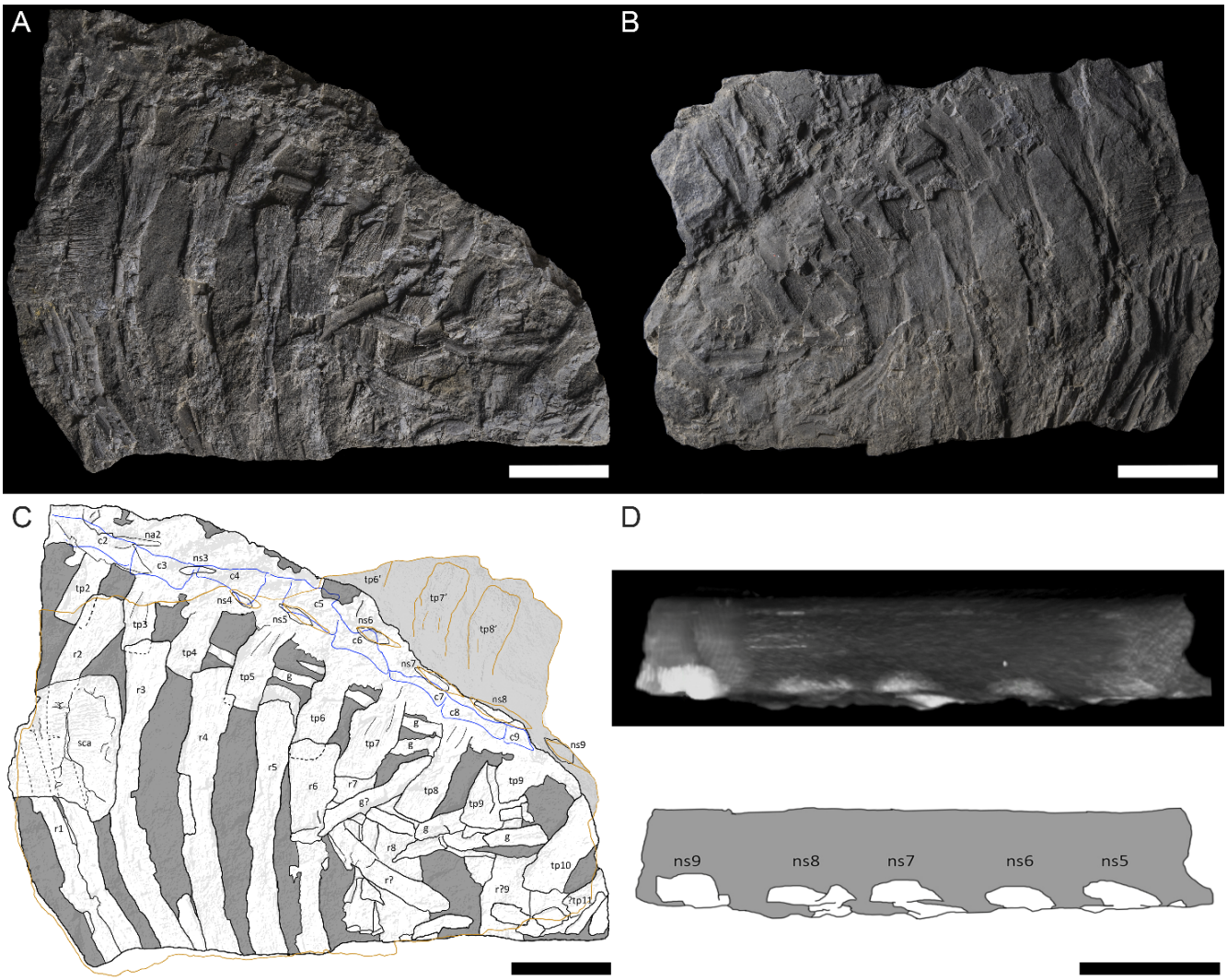

Fig. 4.2- *Helveticosaurus zollingeri*, specimen MSNM V927. A) part MSNM V927a embedding most of the anterodorsal axial elements in left laterodorsal view; B) counterpart MSNM V927b with an additional area embedding right transverse processes and neural spines; C) interpretative drawing of the bones preserved in A and B; D) CT image of the neural spines embedded in MSNM V927b as seen in cross-section (top), and their interpretative drawing (bottom). Abbreviations: c, vertebral centrum; g, gastralium; ns, neural spine; r, rib; sca, scapula; tp, transverse process. Scale bars equal 50 mm.

The main slab (MSNM V927a) contains at least eight anterodorsal vertebrae exposed in dorsal view and nine ribs in lateral view, as well as the distal end of the left scapula and fragments of several gastralia scattered under the ribs. Its counterpart (MSNM V927b) hosts fragments of the same bones, in addition to their imprints, and six neural spines visible in the CT scan, perpendicularly entering the matrix. The third slab (MSNM V928) is smaller and includes at least 10 smaller and shorter (i.e., posterodorsal) ribs in lateral view and at least nine fragmentary gastralia, tightly packed together. The preserved vertebrae are still aligned and in close contact with each other. All centra result deformed and dorsoventrally compressed in a ~10 mm-thick layer. Nonetheless, the craniocaudal length of the centra is still preserved and their average length is ~34 mm. The neural arches and most of the neural spines are crushed over their centra and the zygapophyses are not recognisable.

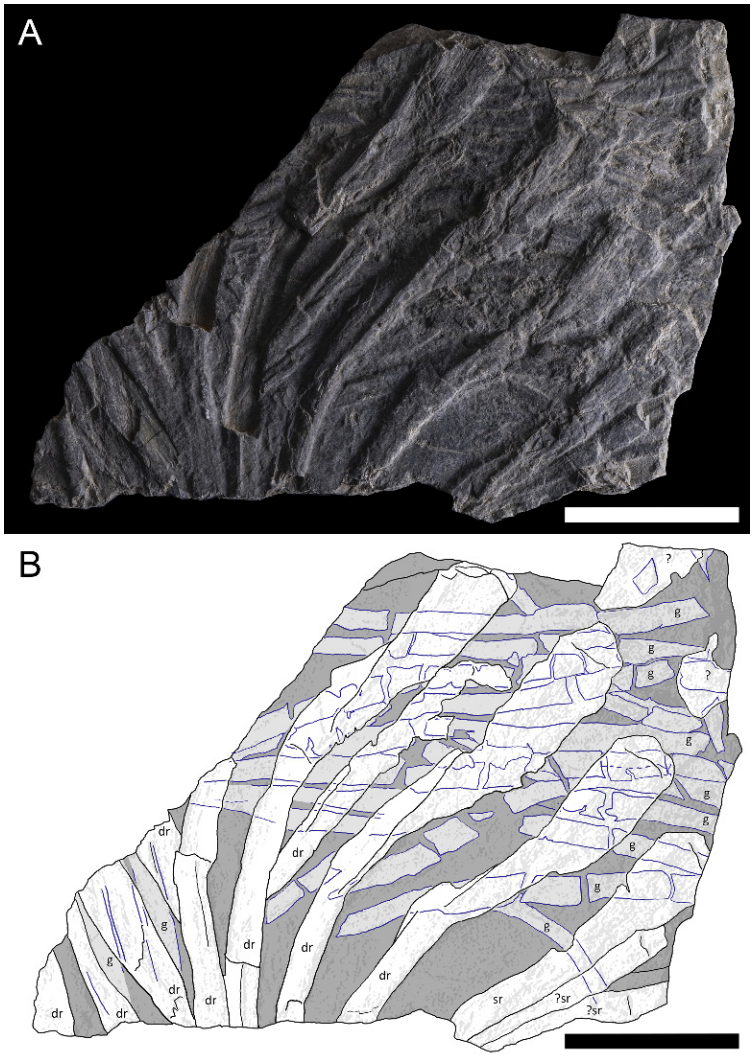

Fig. 4.3- *Helveticosaurus zollingeri*, specimen MSNM V928. A, slab embedding the axial posterodorsal (and partly sacral) elements in left laterodorsal view; B, interpretative drawing of the bones preserved in A. Abbreviations: dr, dorsal rib; g, gastralium; sr, sacral rib. Scale bars equal 50 mm.

4.4.2 ST166120

This specimen is a well-preserved isolated tooth, missing most of the root and the very tip of the crown apex (Fig. 4.4). It is partly embedded in the dolomite matrix which belongs to the San Salvatore Dolomite (Dolomia della Rasa *sensu* Airaghi, 1935) and comes from Rasa di Varese (Varese). This outcrop is located 7 km southwest of Besano.

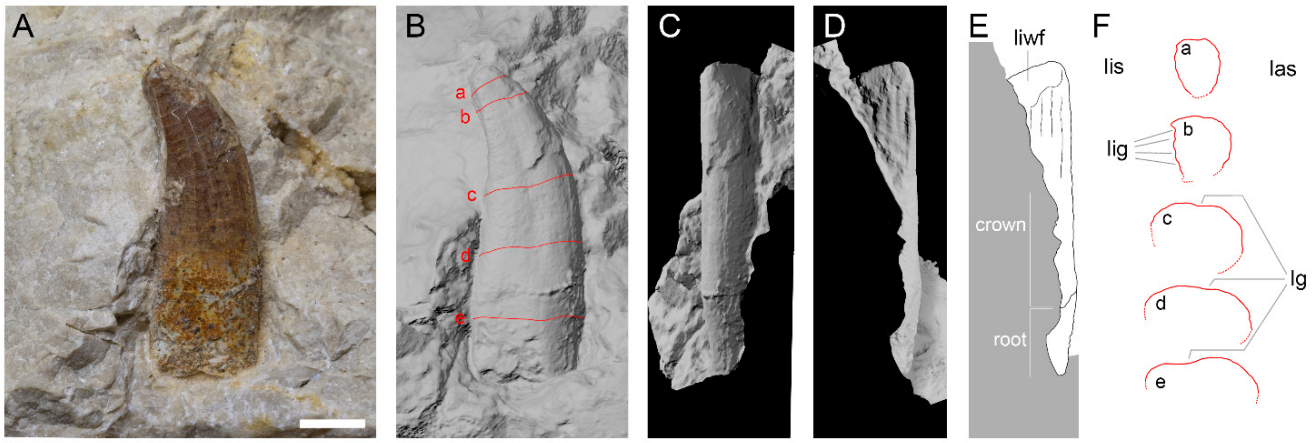

Fig. 4.4 - *Helveticosaurus zollingeri*, specimen ST166120. A) photo in distal or mesial view; B), C) e D) 3D model obtained through photogrammetry in lateral, labial and lingual view respectively; E) interpretative drawing of D; F) transverse sections of the tooth as indicated in B. Abbreviations: las, labial surface; lg, lateral groove; lig, lingual groove; lis, lingual surface; liwf, lingual wear facet. Scale bar equals 5 mm.

4.5 Methods

X-ray computed tomography (CT) was performed on MSNM V927 and MSNM V928, with a Siemens Somatom Definition Dual Source CT Scanner, at the Radiology Department of the Fondazione IRCCS "Cà Granda" Ospedale Maggiore Policlinico di Milano. The best CT imaging was obtained with a bone algorithm on transverse (axial) slices, with scan parameters 140 kV, 180-270 mA, and slice thickness of 0.5 mm. Data were exported in DICOM format using eFilm (v. 1.5.3; Merge eFilm, Toronto, Canada). Analysis and post-processing were performed with RadiAnt, 3DimViewer, and Synedra View Personal. Multiplanar reconstructions (MPR) and volume rendering reconstructions (VR) allowed us to inspect the bones hidden by other ones within the matrix, which were otherwise impossible to study without damaging the fossil.
We used photogrammetry to better study the isolated tooth ST166120 (File S1). A 3D model of the tooth was obtained with Meshroom, by processing 85 shots, following Bindellini & Dal Sasso's (2019) method. Photos of all studied specimens were taken with a Nikon D7500 camera.

4.6 Systematic paleontology

Diapsida Osborn 1903
Helveticosauridae Peyer 1955
Helveticosaurus Peyer 1955

Emended diagnosis – *Helveticosaurus* is here re-diagnosed by the combination of the following characters: marine reptile at least 2 m long; high and deep snout; strong dentition of subthecodon implantation; caniniform mesial teeth with subtriangular cross-section; alternate tooth replacement with replacement waves passing from the front to the back of the jaws; postfrontal probably forming the anterior margin of the upper temporal fossa; at least 12 cervical vertebrae; at least 44 presacral vertebrae; transverse processes of dorsal vertebrae deeply striated, and well-spaced from each other; possibly 3 sacral vertebrae; neurocentral suture persisting throughout the vertebral column; cervical ribs dicocephalous and with a free anterior

process; dorsal ribs holocephalous; lateral surfaces of the ribs deeply striated; limb girdles of generalized structure; long scapular blade with a suberectangular dorsal margin; scapula lateral surface deeply striated; pubis with open obturator foramen; limb elements poorly ossified; at least two carpal ossifications; tarsal elements reduced to a single ossification; hyperphalangy in both manus and pes.

Helveticosaurus zollingeri Peyer 1955

Holotype - PIMUZ T 4352, a nearly complete semi-articulated skeleton missing most of the tail.

Referred specimens - MSNM V927 (a and b: respectively the main slab, where the specimen is exposed dorsolaterally; and its counterpart, which includes a portion of the neural spines), anterodorsal portion of axial skeleton with distal end of scapula; MSNM V928, posterodorsal region of the same specimen including sacral ribs; ST166120, isolated tooth missing most of the root; PIMUZ T 4353, largely complete but disarticulated specimen; PIMUZ T 4354, isolated snout with 14 mesial teeth.

Locality and horizon - MSNM V927 and MSNM V 928 come from the Piodelle-Selva Bella mine, Besano, Varese (Italy); Besano Formation, *N. secedensis* Zone, level/stratum correspondent to layer 58 of the Mirigioli section, latest Anisian. ST166120 comes from Rasa di Varese (Italy); San Salvatore Dolomite (Dolomia della Rasa *sensu* Airaghi, 1935), *N. secedensis* Zone, associated with *Serpianites serpianensis* (V. Pieroni, pers. comm. 2021), latest Anisian (Renesto & Pieroni, 2013). PIMUZ T 4352, PIMUZ T 4353, and PIMUZ T 4354 were collected respectively in 1935, 1933, and 1937 in Cava Tre Fontane (Monte San Giorgio, Canton Ticino, Switzerland).

Diagnosis – Same as for genus.

4.7 Description

4.7.1 Scapula

The preserved portion of the scapula is represented only by the dorsalmost (i.e. distal) lateromedially flattened portion of the scapular blade (Fig. 4.2). The dorsal margin has a sub-squared profile, the posterior margin is concave and the exposed surface of the bone is feebly convex. This, together with its orientation and its lapping over the rib cage, indicates that is a left scapula exposed in lateral view. Mediolaterally it is very thin (from 4 to 2 mm). The sub-squared morphology of the distal end of this scapular blade is very similar to the holotype of *Helveticosaurus (*Peyer, 1955; Rieppel 1989*;* pers. obs. 2020 on PIMUZ T 4352). The preserved length of the scapular blade is 54 mm, and the maximum dorsal expansion reaches a width of 72 mm, circa 1.3 times the value of the homologous measurement in PIMUZ T 4352 (56 mm). The seemingly larger size of the MSNM specimen can be the consequence of a significant taphonomical compression, testified also by the shortened dorsoventral height of the vertebral centra and neural spines. Considering that the centra of MSNM V927 are 34.2 mm long on average (Tab. 4.1) and that the proximal ends of the ribs measure 22.4 mm on average (lengths close to those of PIMUZ T 4352 and 4353), the *in vivo* dimensions of the MSNM specimen might have been rather similar to that of PIMUZ T 4352, i.e., about 2 m of presacral length (3.6 m total body length estimated by Kuhn-Schnyder, 1974). The quadrangular profile of the dorsal

portion of the scapula is very different from *Placodus* (SMF R1035), but more similar to *Paraplacodus* (PIMUZ T 4775), although the latter is much smaller in absolute size.
The scapula of MSNM V927 shows several deep narrow longitudinal striations that cover the entire surface of the bone and are not the result of taphonomical processes. These are also clear in the holotype of *Helveticosaurus*, and to a minor extent in *Paraplacodus* (PIMUZ T 4775).

4.7.2 Dorsal vertebrae

At least eight fully articulated centra are preserved in dorsal view in MSNM V927, 11 transverse processes can be numbered in craniocaudal sequence, and six neural spines are visible still aligned in the CT scan of MSNM V927b (Fig. 4.2). No vertebrae are visible in MSNM V928. The dorsal centra do not show a parapophysis, and each diapophysis articulates with a single-headed rib. The centra are amphicoelous, slightly longer than wide, and lateromedially constricted in the middle; their height is not measurable due to diagenetic compression. The neural canal is never exposed except in the fifth vertebra, where it is 6.5 mm wide; this width is constant for all its length. Only one neural arch is visible on the surface of MSNM V927a (above the cranialmost centrum): its dorsal roof seems to be somewhat shaped as a triangle.
The transverse processes are distinctly elongate (up to 60 mm) and their distal extremities host the articulation surfaces (diapophyses) for unicapitate ribs. Transverse processes are proportionally much shorter than in *Eusaurosphargis* (Nosotti & Rieppel, 2003; Scheyer et al., 2017), but more similar in length to *Saurosphargis* (Huene, 1936) and placodonts. Each transverse process is constricted proximally, approaching the neural arch, and slightly expanded distally in rostrocaudal direction. Like the ribs and the scapula, the surface of the bone is characterised by deep striations. The distal extremity of the transverse process has an average width of 17 mm (~20 mm in PIMUZ T 4352). This width looks also larger than what can be observed in *Nothosaurus giganteus.* The ventral surface of each transverse process is characterised by the presence of an anterior and a posterior diapophyseal lamina (visible in CT data of MSNM V927a; Fig. 4.S1), which distally run parallel to the caudal and rostral margins of the process, then diverge towards the vertebral centrum, delimiting a median fossa that in ventral view appears V-shaped. This peculiar anatomy is shared by MSNM V927 with the holotype of *Helveticosaurus zollingeri* (PIMUZ T 4352), as well as with the referred specimen PIMUZ T 4353 (Peyer, 1955; Rieppel 1989). The dorsal surface of the transverse process symmetrically hosts similar laminae, although much less pronounced.
As for the zygapophyses, these are not visible in their entirety, being probably hidden by the compressed (and variably crushed) fragments of the neural arches. Above the smashed structures, at least six neural spines are preserved. Their broken bases are exposed on the surface of slab MSNM V 927a: they are compressed laterally and the cross-section on the dorsal plan results fusiform, with a thicker central portion and tapered cranial and caudal margins. The five caudalmost neural spines are completely embedded in the matrix and visible only in CT data of MSNM V 927b (Fig. 4.2D). They are not as tall as observed in PIMUZ T 4352, although – like in the centra - some diagenetic compression has occurred. Moving from the most proximal to the most caudal, the spines become gradually taller. As it occurs in the anterodorsal vertebrae of PIMUZ T 4352 and 4353, the craniocaudal length of the spines is shorter at their base, whereas it becomes longer approaching the dorsal margin. The dorsal termination of the spines is almost straight and has a quadrangular aspect if observed from the lateral side. All the spines visible in MSNM V 927b are caudally inclined. Above the neural spines, no dorsal *Placodus*-like osteoderms are visible.

4.7.3 Dorsal ribs

In MSNM V927 at least nine anterodorsal ribs are preserved (Fig. 4.2). These ribs are mildly recurved before reaching their midlength and are much thicker in craniocaudal direction than mediolaterally; the first two proximal ribs appear thinner than the other ones. Each rib possesses a slightly expanded unicipital head that articulates with the vertebral diapophysis located at the distal end of each transverse process. A groove extends proximodistally along the midline on the lateral side of the rib; this element is a biological feature and not the consequence of compression. As described for the scapula and for the transverse processes, the surface of the ribs is strongly striated, a characteristic that is typical of *Helveticosaurus*. The posterodorsal ribs, preserved in MSNM V928, are similar to the anterodorsal ribs just described, but are distinguished by a clear bend that separates the straight proximal region of the head from the curved mediodistal portion of the rib; consequently they are much thinner and more recurved than the shaft of the anterodorsal ribs. In addition, in the head region the lateral side of the rib shows a longitudinal concavity that is absent in the anterodorsal elements; a midline groove is present in the rest of the rib shaft. The distal ends of the caudalmost dorsal ribs seem to converge towards the supposed position of the pelvis, as preserved in PIMUZ T 4352 (Peyer, 1955). None of the ribs shows an uncinate process, which is present of *Paraplacodus* (Rieppel, 2000) and is also reported in *Eusaurosphargis* (Scheyer et al., 2017).

Table 4.1 - Selected measurements (in mm) of the bones preserved in MSNM V927, a referred specimen of *Helveticosaurus zollingeri* from the Middle Triassic of Besano. N.B. "Position" does not refer to the anatomical position of the elements along the axial skeleton, but is used only to number them in this specimen, from the cranialmost to the caudalmost. Abbreviations: M, mean value; n.p., not possible.

	Centra		**Transverse processes**		**Neural canal**	**Neural spines**		**Ribs**
	max. mediolateral diam. (estim.)	max. proximodistal length	mediolateral length	distal end craniocaudal width	mediolateral width	dorsoventral height	max. mediolateral length	craniocaudal width of the head
1	n.p.	n.p.	n.p.	n.p.	n.p.	n.p.	n.p.	n.p.
2	29.6	36	38	16.7	8.6	n.p.	n.p.	21.8
3	26.7	35.6	45.5	16.6	n.p.	n.p.	19.5	19.5
4	27.4	36.3	43.3	16.8	n.p.	16.1	24.5	24.3
5	28	34	51.5	17.2	6.5	13.3	34.9	22
6	27.8	32.4	58.3	18	n.p.	16.2	29.9	24.5
7	n.p.	32.1	59.5	18	n.p.	12.5	27.3	n.p.
8	n.p.	33.2	60.4	15.7	n.p.	11.4	29.3	n.p.
9	n.p.	n.p.	40.3	15.6	n.p.	n.p.	25	n.p.
10	n.p.	n.p.	44.4	18	n.p.	n.p.	n.p.	n.p.
M	27.90	34.23	49.02	16.96	7.55	13.90	27.20	22.42

4.7.4 Sacral ribs

Seemingly, the anterior margins of the caudalmost ribs preserved in MSNM V928 (Fig. 4.3) straighten and become slightly concave, a character that can be observed in the sacral region of Thalattosauria and Sauropterygia (e.g., Müller, 2005; Rieppel, 2000). Thus, the first straight rib in MSNM V928 is here interpreted as a sacral rib. Unfortunately, due to the fragmentary nature of our specimen, it is impossible to state how many sacral ribs it possessed. The distal ends of these ribs are also not preserved. Nevertheless,

given the reduced spacing of the caudalmost ribs on the surface of the slab and the fact that they seem to converge distally, we suspect that specimen MSNM V 928 possessed at least three sacral ribs. This hypothesis is consistent with the preserved portion of the sacral region of the *Helveticosaurus* holotype, PIMUZ T 4352 (pers. obs., 2019). In this specimen, the last preserved dorsal rib possesses a concavity similar to the dorsal ribs preceding it, does not show particular signs of sacralization (*sensu* Rieppel, 1994), and is followed by three straight and shorter (although poorly preserved) ribs, which we suspect to be sacrals. These three ribs do not show a clear anteroposterior thickening in comparison to the posterior dorsal ribs. Moreover, the iliac blade of PIMUZ T 4352 shows morphology and proportions more similar to *Placodus* (SMF R1035, three sacrals) than to *Eusaurosphargis* (PIMUZ A/III 4380, two sacrals).

4.7.5 Gastralia

At least five disarticulated gastralia can be numbered in MSNM V927 (Fig. 4.2), and 14 in MSNM V928 (Fig. 4.3). In the posterodorsal region, the gastralia are densely packed together, possibly still preserving their *in vivo* distribution. How many elements composed each gastral row is unclear, but since all visible elements are straight, long, and do not show any pointed end they likely represent medioventral elements. The only exception is represented by the recurved element that in MSNM V928 is partly covered by the sacral rib(s). The preserved gastralia are thinner than the ribs, dorsoventrally flattened and crossed by a median groove that extends for all of their length, both on the dorsal and on the ventral side, representing a biological feature.

4.7.6 The tooth

Specimen ST166120 (Fig. 4.4) is an isolated tooth lacking most of the root. It has already been briefly presented and figured by Pieroni (2011) and Renesto & Pieroni (2013). This tooth is 26 mm in height and has a maximum labiolingual width of 9 mm (Tab. 4.2). The tooth crown is slightly recurved lingually. The upper half of the crown is mesiodistally longer than labiolingually wide; on the other hand, the lower half of the crown and the root become more expanded labiolingually and mesiodistally compressed (Fig. 4.4F). Such variations in the shape of the cross-section, from the base to the apex of the crown, are seen also in *Paraplacodus*, despite in this taxon the teeth are proportionally longer and rounder, showing no lateral cutting edges (PIMUZ T 4773). The root of ST166120 shows a suboval section, slightly constricted in the middle by a groove on both sides. This groove extends apicobasally, becomes less pronounced on the crown surface, and disappears towards the tip. At the base of the crown, the transverse section is suboval as well; it becomes triangular above the mid-height of the crown. Here, its narrowest side, i.e., the lingual side of the tooth, is delimited laterally by two sharp edges, whereas the lateral sides converge in a rounded labial surface. At the crown tip, the apicalmost surface preserves an irregular wear surface, inclined by 45° towards one of the two sides. At the apex, the lingual surface also shows five faint striations or grooves that extend apicobasally but do not significantly affect the profile of the cross-section. These grooves delimit five visible narrow bulges that run in apicobasal direction, with the lateralmost higher than the central ones and defining one of the two lateral sharp edges of the crown.

Crown length	23 mm
Crown apex m-d Ø	4.2 mm
Crown apex la-li Ø	2.9 mm
Crown base m-d Ø	-
Crown base la-li Ø	8.1 mm
Root preserved base m-d Ø	-
Root preserved base lb-ln Ø	7.6 mm

Table 4.2 - Selected measurements of ST 166120, a referred tooth of *Helveticosaurus zollingeri* from the Middle Triassic of Dolomia della Rasa (Varese). Abbreviations: la-li, labiolingual; m-d, mesiodistal, Ø, diameter.

The triangular cross-section, associated with two sharp cutting edges (or carinae) that run in apicobasal direction for more than half the length of the crown, suggests that this tooth belonged to a carnivorous generalist and was used to pierce and cut the prey (Massare, 1987).

4.8 Discussion

4.8.1 Taxonomic identification

The most diagnostic character in the postcranial elements of MSNM V927 is the presence of straight, well-developed (~50 mm long) transverse processes, departing from amphicoelous vertebral centra at a right angle. These are similar to *Saurosphargis voltzi*, although in this taxon they are closer to each other (Huene, 1936: plate 13). In MSNM V927, the neural spines are short (~15-20 mm tall) and slightly reclined towards the tail, and all bones, including the scapula, are textured with strong striations (T. Scheyer, pers. com. 2020). All elements are comparable in size to those of the holotype of *Helveticosaurus zollingeri* (PIMUZ T 4352). Above the neural spines, no dorsal osteoderms, typical of *Placodus,* are visible in the CT scan. The dorsal spines are also shorter than in *Nothosaurus*. The anterodorsal ribs are holocephalous and there is no trace of an uncinate process as seen in *Paraplacodus*; the lateral surface of the ribs and the transverse process is deeply striated, similarly to what has been observed in *Helveticosaurus* holotype. *Saurosphargis voltzi* shares similar striations on the lateral surface of the ribs, but the ribs of this taxon show a round and slightly prominent uncinate processes (Huene, 1936: plate 13) that is absent in *Helvticosaurus*. On the other hand, in *Eusaurosphargis* the dorsal ribs are proportionally much shorter than in *Helveticosaurus* and possess uncinate processes as well (Scheyer et al., 2017)

The dorsal portion of the scapula shows a quadrangular profile, which is very different from *Placodus* (SMF R1035), where it is anteroposteriorly longer and rounded. Nevertheless, this shape recalls the morphology of *Paraplacodus* (PIMUZ T 4775), although the absolute size of this taxon is much smaller. Moreover, the scapula of MSNM V927 shows several deep narrow longitudinal striations (Fig. 4.2) covering the lateral surface of the bone; these striations are similar to those of *Helveticosaurus* holotype, and with a minor extent in *Paraplacodus* (PIMUZ T 4775).

The general morphology of the tooth described (ST166120) recalls the mesial teeth of placodonts. The profile of its transverse section is triangular, mesiodistally flattened, and delimited by sharp edges; this makes this tooth different from placodonts: *Placodus* has shorter and sturdier mesial teeth, *Paraplacodus* mesial teeth show two lateral grooves and a major medial bulge on the lingual side (e.g., Peyer 1935; Rieppel, 2000), that are absent in ST166120. In sum, the caniniform morphology of this specimen is consistent with the mesialmost maxillary teeth of *Helveticosaurus zollingeri* (Peyer, 1955: taf. 91).

Taken together, the proportions of the transverse processes, the fully striated scapula and ribs, the absence of an uncinate processes, the shape of the scapular blade, the relevant size of the bones, and the morphology of the tooth render the specimens cited herein more similar to *Helveticosaurus zollingeri* than to any other taxon.

4.8.2 Testing the phylogenetic position.

To perform the phylogenetic analysis reported below we used PAUP* 4.0 and modified Scheyer et al.'s (2017) data matrix [in turn modified from Neenan et al. (2013) - but see also Klein & Scheyer (2014)]. A heuristic search was used as search option; this was run with 100 trees set as the number of maximum trees

in memory (automatically increased by 100 if this limit was hit), 10000 random replicates, and the Tree Bisection Reconnection (TBR) mode activated. A revision of the matrix used by Scheyer et al. (2017) led us to rescore a few characters for *Helveticosaurus*: namely, character 11 from "?" to "2" and character 67 from "1" to "0", according to our interpretation of the skull; character 90 has been rescored from "?" to "0" according to our interpretation of the sacral ribs. According to our interpretation and description, specimen MSNM V928 might have possessed at least three sacral ribs; to test this hypothesis, in *Helveticosaurus* line, we modified Scheyer et al.'s (2017) character 88 from "?" to "1&2": "1" describes the condition of possessing three ribs, whereas "2" stands for four or more. Such scoring does not describe a case of polymorphism but was chosen to take into account our new observation of more than two sacral ribs (i.e., excluding state '0'), while taking into account the uncertainty of the exact number of ribs (i.e. states 1 or 2). In addition, this allows to assess the reconstructed ancestral state of this character following a parsimony criterium. This single character matters since, among the taxa closest to *Helveticosaurus*, Thalattosauria and *Eusaurosphargis* possess two sacral ribs, whereas basal sauropterygians have three sacral ribs (e.g., Neenan et al., 2013).

The new line of *Helveticosaurus* now reads as follow:
?000100???2?00???1?????????01?????????????0????????????1??1?0000000??000?00?0?010?1?10(1
2)?00101100001007100100001117110210?012112?1?11000??.

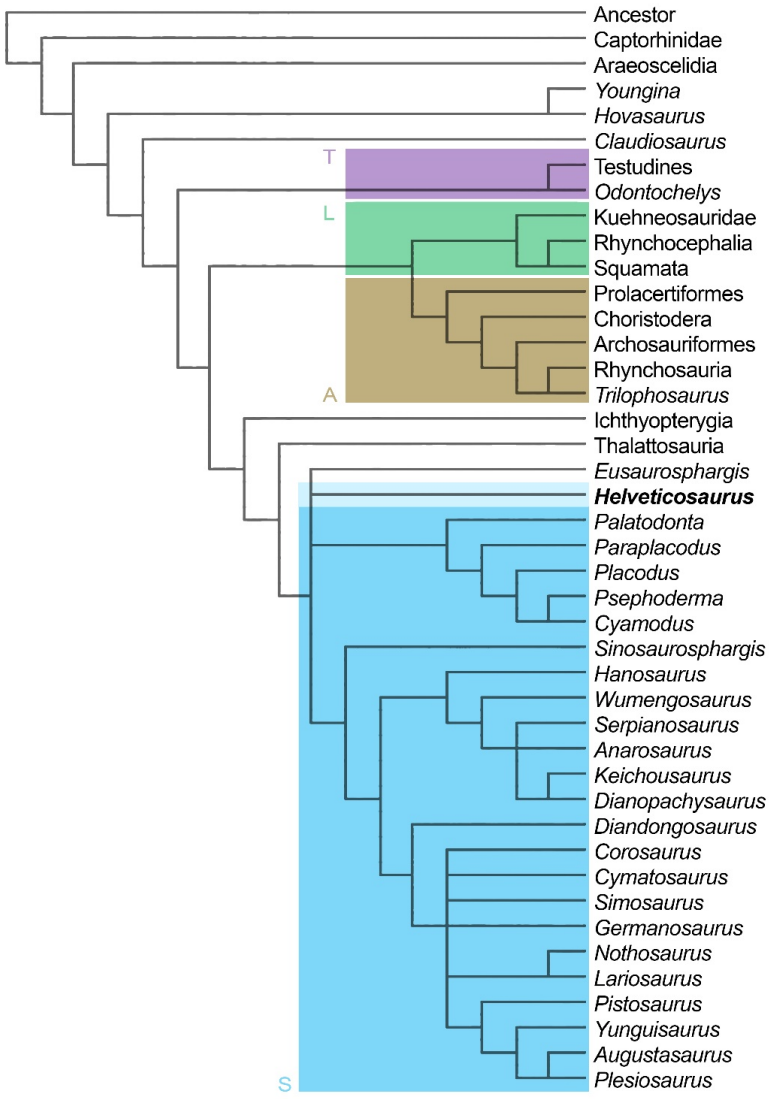

Fig. 4.5 – Strict consensus tree of 8 MPTs, obtained from Scheyer et al. (2017) modified "third matrix" (see text). In four of the MPTs, *Helveticosaurus* was recovered as sister taxon of the clade Placodontia, whereas in the remaining four it was recovered as sister taxon to the group *Eusaurosphargis*+Sauropterygia. Turtle lineage highlighted in lilac, Lepidosauromorpha in green, Arcosauromorpha in light brown, and Sauropterygia in light blue.

Our analysis resulted in 8 MPTs of score 571 (Fig. 4.S2, 4.S3). None of these trees recovered the clade "Helveticosauridae" *sensu* Nosotti & Rieppel (2003); also, *Helveticosaurus* never clustered as sister taxon of *Eusaurosphargis*, as reported by Li et al. (2014). On the other hand, in trees 1, 3, 4, and 7, *Helveticosaurus* was recovered as sister taxon of the clade Placodontia; in trees 2, 5, 6, and 8, *Helveticosaurus* was recovered as sister taxon to the group *Eusaurosphargis*+Sauropterygia, as also seen in Scheyer et al.'s (2018: fig 12b) analysis 8. The strict consensus tree is reported in Fig. 4.5. Given the topology of the 8 trees described above, in this tree a polytomy is found between *Helveticosaurus, Eusaurosphargis*, and Sauropterygia.
The PAUP* character reconstruction tool, when applied to the strict consensus tree, both with ACCTRAN (accelerated transformation) and DELTRAN (delayed transformation) character optimization, at the base of the politomy *Eusaurosphargis*+*Helveticosaurus*+Sauropterygia predicts an ancestral state of "1" for character 88, which supports the hypothesis that *Helveticosaurus* had three sacral ribs.

4.8.3 Aquatic adaptations and swimming capabilities

The presence of *Helveticosaurus* in Italy was reported for the first time by Renesto & Pieroni (2013) thanks to the isolated tooth from the Dolomia della Rasa (San Salvatore Dolomite). The occurrence of *Helveticosaurus* in both the San Salvatore Dolomite and the Besano Formation suggests that its habitat might have been related to those environments, i.e., more proximal to the shoreline than to the open sea. This hypothesis is consistent with what is known about the anatomy of *Helveticosaurus*, which will be briefly reviewed in the following paragraph.
Rieppel (1989) discussed in detail the locomotion (aquatic and terrestrial) of *Helveticosaurus*. Hyperphalangy and paedomorphosis of several skeletal elements (e.g., mostly an unossified carpus and tarsus) clearly suggest a specialisation of the limbs for underwater locomotion. The author highlighted the presence of a humerus with a well-developed entepicondyle, where the flexor tendons of the hand and digits were attached, and therefore suggested that *Helveticosaurus* had occasional excursions on land. Rieppel (1989) also noted that paedomorphosis affected the hindlimb and the pelvic girdle more than the forelimb and the pectoral girdle, thus suggesting greater functional demand imposed on the forelimbs. After comparing rowing vs subaqueous flight (Robinson, 1975; Godfrey, 1984), the author hypothesised the mode of aquatic propulsion of *Helveticosaurus* as an intermediate form of the two and referred to the "otariid model" (*sensu* Godfrey, 1984) as the most suitable to describe the swimming mode of the animal. Showing no particular specializations related either to rowing or to subaqueous flight, Rieppel (1989) suggested that the main propulsive thrust while swimming would have been provided by lateral undulation of the tail (estimated to be ~1.5 m long in the holotype) and of the distal portion of the trunk, whereas the rowing of the forelimbs in an otariid-like cycle would have greatly supported the underwater locomotion. A well-developed pectoral girdle and the inferred presence of powerful muscles could have provided these requirements. These could also have allowed the animal's locomotion during its occasional excursion on land, and strong development of the transversospinalis system should have granted the possibility to lift the anterior portion of the trunk, the neck, and the head off the ground (Rieppel, 1989).
Helveticosaurus undoubtedly had an aquatic or semiaquatic lifestyle, approaching the land only for basking, nidifying, grooming, or resting. This lifestyle is consistent with the finding of fossil specimens, such as ST166120, in a platform environment. MSNM V 927 and 928 were recovered at the base of the *N. secedensis* Zone, which chronologically coincides with the beginning of the establishment of the intraplatform basin that characterizes the middle portion of the Besano Formation (Röhl et al., 2001): likely, the carcass of the

animal has been transported from the shallow sea of the platform and sunk not far from its margin, in deeper sea.

Several adaptations to a semiaquatic lifestyle can be observed in *Helveticosaurus* (PIMUZ T 4352 and 4353); these are listed below, along with a new skeletal reconstruction of the animal (Fig. 4.6):

- elongate body shape (PIMUZ T 4352);
- laterally compressed, dorsoventrally tall tail (reported also by Peyer, 1955; PIMUZ T 4353);
- skeletal paedomorphosis (e.g., carpus and tarsus mostly unossified in PIMUZ T 4352);
- hindlimbs length reduction (humerus longer than femur both in PIMUZ T 4352 and PIMUZ T 4353);
- broadened hand and foot, possibly webbed (oar-like *sensu* Massare, 1994; PIMUZ T 4352);
- polyphalangy and elongated fingers (PIMUZ T 4352);
- well-spaced phalanges (i.e., large amount of articular cartilage; PIMUZ T 4352);

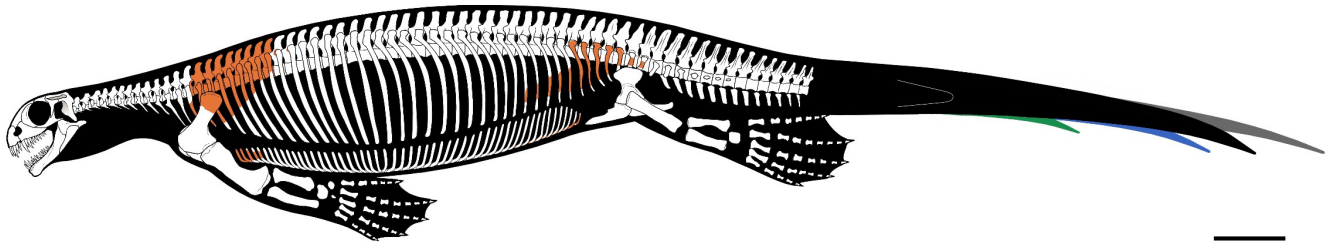

Fig. 4.6 - Skeletal reconstruction of *Helveticosaurus zollingeri*, based on all specimens known to date (Peyer, 1955; Kuhn-Schnyder, 1974; Rieppel, 1989; Renesto & Pieroni, 2013; this paper). To estimate the length of the tail, here we propose different options: in black, the original estimate of Kuhn-Schnyder (1974); the white outline is based on the body proportions of *Eusaurosphargis* (PIMUZ A/III 4380); the blue tail is based on *Placodus* (cast exposed in PIMUZ and SMF R1035); the grey tail is based on *Askeptosaurus* (Muller, 2005); the green tail represents a conservative estimate based on the mean value between the white and the blue estimate. Line drawing by Marco Auditore. Scale bar equals 20 cm.

Similar adaptations, typically acquired by convergent evolution, are variably present among vertebrates with a semiaquatic lifestyle, especially in transitional forms that secondarily moved back to water (e.g., *Ambulocetus, Spinosaurus, Thalassocnus*). In *Helveticosaurus,* carpus and tarsus are greatly unossified; their reconstruction in Fig. 4.6 is based on Rieppel's (1989: p.139-143) considerations. On the contrary, the distance among the phalanges is estimated on the basis of what is still observable in the holotype, since some fingers appear less disarticulated than the rest of the limbs (in finger IV and V of left manus and left pes, some phalanges are still in line). Phalanges result partly unossified as well, missing most of the epiphyses. To reconstruct the tail, since most of it is missing, in Fig. 4.8 we propose various options to estimate its length. The presence of a middle caudal vertebra with a tall (although incomplete) neural spine and no transverse processes, preserved in PIMUZ T 4353, suggests that, in any case, the tail was dorsoventrally tall and laterally compressed, a morphology that grants to this appendage a valuable role in generating thrust while undulating laterally (e.g., Fish et al., 2021).

According to the categories defined by Motani & Vermeij (2021), given the discussion above and the anatomy of the animal, *Helveticosaurus* should fall in the M4 category, along with sea otters and most of the pinnipeds; among extinct vertebrates, the M4 category also includes all those sauropterygians that possess a humerus longer than the femur (including, e.g., Placodontia) and likely Saurosphargidae (sister clade to Sauropterygia according to some authors, e.g., Li et al., 2014). In step "M4 vertebrates", terrestrial locomotion is limited only to exceptional cases since these animals evolved a fully marine diet and maintained water balance without

terrestrial freshwater. Among sauropterygians, *Placodus gigas* shares the most similar bauplan to *Helveticosaurus*. Carpus and tarsus are greatly unossified also in Nothosauria, although to a lesser degree than in *Helveticosaurus* (Rieppel, 1989). Taxa belonging to this clade, along with Pachypleorosauridae, possessing a humerus shorter than the femur, have been classified by Motani & Vermej (2021) in M2-3 categories, so one step back in marine adaptations in respect to Placodontia. Going further into this discussion, below we evaluate different swimming models to better define the swimming style of *Helveticosaurus*.

The otariid model, as described by Williams (2018), requires that the propulsive forces are generated almost entirely by the pectoral appendages, with the hind flippers occasionally being used for steering, as also seen in penguins and sea turtles. In this model, Feldkamp (1987) recognised three distinct stroke phases: (1) a power phase, (2) a paddle phase (during which the majority of thrust is produced), and (3) a recovery phase. Following the hypotheses of Massare (1994), the oar-like non-hydrofoil limbs of *Helveticosaurus* might have been suitable more for subaqueous rowing than for subaqueous flight. In turn, the hindlimb of *Helveticosaurus* may have had a role in creating drag and therefore steering. Actually, the otariid model describes an already highly specialised swimming style that involves the loss of the tail and does not include any kind of body undulation, which is very likely present in a secondarily aquatic reptile like *Helveticosaurus*. According to Rieppel's (1989) observations and consistently with Massare's (1994) bauplan II, the major thrust should have been produced by lateral undulation of the trunk and the tail. Therefore, the otariid model may not be entirely appropriate to describe the swimming style of *Helveticosaurus*. An array of tightly packed gastralia, as well as wide laterally projecting transverse processes, along with large ribs, may prevent a significant ability to undulate the trunk. Nonetheless, although massive, ribs and transverse processes are well-spaced (more than in some placodonts such as *Paraplacodus*), leaving room for some lateral movement of the axial skeleton in the trunk region. Consequently, some degree of lateral undulations of the trunk, at least of the posterior part (as suggested by Rieppel, 1989), should be taken into account. With respect to the gastralia, tightly packed gastralia are also found in ichthyosaurs from the Middle Triassic with an inferred anguilliform swimming style (e.g., *Cymbospondylus* and *Besanosaurus*; Merriam, 1908; Dal Sasso & Pinna, 1996).

Looking among less specialised (but still semiaquatic) vertebrates, to understand how *Helveticosaurus* could have swum, a model worth to be evaluated is the otter model. Otters can use several combinations of their appendages to paddle and generate thrust; most importantly, otters can simultaneously make use of undulatory propulsion using their elongate, flexible bodies and tails (Fish, 1994). According to Thewissen & Fish (1997), Lutrines are the best extant functional models for early cetacean locomotion: the locomotor dynamic of *Ambulocetus* may have been most similar to that of *Lutra* or, to a lesser degree, to *Pteronura*. Williams (2018) describes the stroke cycle of sea otters (*Enhydra lutris*) as made of two phases: (1) a power phase (when thrust is produced), and (2) a recovery phase (when the limb is repositioned for the next stroke). While swimming slowly and close to the surface, sea otters alternate strokes of the hindlimbs to generate thrust: since this drag-based mode of swimming is inefficient, in order to move quickly underwater otters can switch to an undulatory mode of swimming involving dorsoventral body flexion and simultaneous movements of the paired hindlimbs. In contrast to sea otters, giant river otters (*Pteronura brasiliensis*) have four webbed broad limbs and a paddle-like tail, dorsoventrally compressed (Beichman, 2019); the trunk and tail undulations and the simultaneous paddling maximise thrust production while fast swimming (Fish, 1994).

Among reptiles, short and broad limbs were cited by Massare (1994) as characteristics of smaller early mosasaurs, such as *Clidastes*. Among these, in contrast to crocodylians and bigger mosasaurs, the undulation of the entire body was likely the main propulsive action (with the amplitude increasing towards the tail; Lingham-Soliar, 1991), the limbs were probably kept close to the sides of the body while swimming and used for extra thrust only during lunges. On the contrary, among sauropterygians, large *Nothosaurus* (such as *N.*

giganteus and *N. mirabilis*) likely provided the power stroke while swimming with paired movement of the forelimbs in an underwater flight cycle or an otariid-like stroke cycle, showing biomechanical adaptations convergently evolved later in Pistosauria (Krahl et al., 2013; Zhang et al., 2014). On the other hand, Placodontia shows a plethora of different swimming styles (e.g., Scheyer & Klein, 2021): for example, it has been hypothesized that an anguilliform swimming mode for *Psephoderma* is very unlikely due to its rigid trunk and a sedentary lifestyle at the bottom of shallow waters (Renesto & Tintori, 1995; Klein et al., 2015); *Cyamodus*, still being heavily armoured, thanks to a long and massive humerus should have more likely based its swimming style on powerful stroke cycles of row-like forelimbs (Klein et al., 2015); in both *Cyamodus* and *Psephoderma* some propulsion should have been granted also by lateral undulation of the hindlimbs, thanks to the sacral gap in the dorsal armour (Renesto & Tintori, 1995; Klein et al., 2015); eventually *Placodus*, that possesses only a single row of osteoderms along the axial skeleton and among Placodontia shares the most similar bauplan with *Helveticosaurus,* has been classified as a subcarangiform swimmer (Braun & Reif, 1985), an hypothesis supported by a laterally compressed long tail (Drevermann, 1933) and bone histology (Klein et al., 2015).

Once the necessary distinctions are made, especially in the bauplan of the vertebral column of a reptile, we can postulate that the swimming style of *Helveticosaurus* might have been a unique intermediate between the otariid and the otter model. In the latter, a flattened tail assumes a major role in generating thrust, as postulated by Rieppel (1989) for *Helveticosaurus*. In any case, the swimming style of *Helveticosaurus* must have been associated with lateral undulations of the tail (of which the length is still unknown) primarily, and the trunk secondarily, as in early mosasaurs, at least for its posterior portion. Unlike early mosasaurs, the limbs of *Helveticosaurus* might have had a more important role in generating thrust, especially the forelimbs, given the robust anatomy of the humerus (Rieppel, 1989), as proposed for some nothosaurs and placodonts. Namely, while swimming at slow speed, the forelimbs could have generated thrust in a forelimb-otariid-like stroke cycle; nonetheless, the efficiency of such movements was limited by the non-hydrofoil, oar-like appendages, making a true subaqueous flight (as seen in large *Nothosaurus* and later in pistosaurs) impossible in *Helveticosaurus*. The lateral undulations of the tail should still have had an important role, whereas the hindlimbs (less robust and less ossified than the forelimbs) might have been kept close to the body or had a minor role in producing thrust in a hindlimb-otter-like stroke cycle. While swimming at high speed, lateral undulations of the body, especially of the tail, would have generated most of the thrust, as also hypothesized for *Placodus*; the limbs, kept close to the body, should have helped to minimize the drag produced during motion; the broad distal portion of the limbs could have also maximized the propulsion while undulating in concert with the body (as seen in giant river otters) and/or used for extra thrust during lunges (as postulated for early mosasaurs). The true role of the hindlimbs in generating thrust, especially at high speed, depends on the tail length, estimated to be ~1.5 m (Kuhn-Schnyder, 1974) but still unknown. Their function might have been at least similar to that of rudder blades: being broad and possibly webbed, they could have generated a considerable drag that could have been used to steer effectively and enhance maneuvrability. Having four limbs to serve with this purpose could have granted great maneuverability, especially useful in shoreline environments.

The swimming style was of course strictly related to the hunting strategies and the diet of *Helveticosaurus*. As smaller mosasaurs (Massare, 1994), *Helveticosaurus* might have been capable of rapid acceleration, typical of ambush predators. Dentition and cranial anatomy suggest that this animal should have been a generalist predator. This is strengthened by the triangular cross-section, associated with two sharp cutting edges, observed in the tooth here described. Namely, the front teeth in particular were likely used to pierce and cut soft and/or bony prey, such as cephalopods, but also small and medium-sized vertebrates (Massare, 1987).

4.9 Conclusions

The MSNM specimens, in spite of their fragmentary condition, represent an important addition to the rare fossil occurrence of *Helveticosaurus.* Besides being the first record of skeletal remains and the second of the taxon in Italy, the specimen from Besano preserves a portion of the axial skeleton that is missing in the *Helveticosaurus zollingeri* holotype, shedding some light on the anatomy of its sacral region. In fact, MSNM V928 possibly hosts a portion of three sacral ribs: due to the fragmentary remains of *Helveticosaurus*, these bones were never reported before and are described here for the first time. Among the taxa closest to *Helveticosaurus*, Thalattosauria and *Eusaurosphargis* possess two sacral ribs, whereas basal Sauropterygia have three sacral ribs. To test the presence of three or more sacral ribs in *Helveticosaurus*, we updated the phylogenetic analysis of Scheyer et al. (2017). The PAUP analysis predicted the presence of three sacral ribs in *Helveticosaurus*, supporting our claim. Furthermore, in half of the MPTs, *Helveticosaurus* was recovered as sister taxon of the clade Placodontia, whereas in the rest of the MPTs, *Helveticosaurus* was recovered as sister taxon to the group Eusaurosphargis+Sauropterygia The results also show that a loss of resolution appears at the base of the clade comprising (*Helveticosaurus*(*Eusaurosphargis*(Sauropterygia))), suggesting that, pending further material, the position of *Helveticosaurus* still needs to be fully resolved.

The redescription of ST166120, implemented by a digital model of it, helped to better understand the morphology of the *Helveticosaurus* dentition and to better define the niche occupied by this animal in the Middle Triassic pericoastal ecosystems: our results strengthen the idea that *Helveticosaurus* might have been a dweller of the carbonate platform, with an amphibious lifestyle strictly associated to the shoreline environments and a carnivorous generalistic diet.

A reappraisal of the swimming style of *Helveticosaurus* leads us to suspect that this bizarre reptile might have been a unique intermediate between the otariid and the otter model: with the lateral undulation of tail generating the main propulsive thrust, the animal while swimming at slow speed could have also generated thrust with the forelimbs in a forelimb-otariid-like (or a hindlimb-otter-like) stroke cycle, whereas while swimming at higher speeds the limbs, kept close to the body, should have helped to minimize the drag, maximized the propulsion while undulating in concert with the body, and/or used for extra thrust during lunges.

This new finding is a consequence and part of the revision of the Besano fauna of the MSNM collections. The rediscovery of this unique specimen further encourages a reanalysis of the Besano-Monte San Giorgio fossils that are housed in the historical collections of natural history museums.

4.10 Acknowledgments

We are grateful to Mr. Calligaris, who collected the MSNM specimens more than half a century ago. We also thank M. Auditore for anatomical drawings; L. Forzenigo, C. Bonelli, and G. Terribile (Fondazione IRCCS “Cà Granda” Ospedale Maggiore Policlinico di Milano) for CT analysis; the Italian Ministry of Culture and the “Soprintendenza Archeologia, Belle Arti e Paesaggio per le province di Como, Lecco, Monza e Brianza, Pavia, Sondrio e Varese” for permissions. For access to key specimens in museum collections, we thank C. Klug and T. M. Scheyer (PIMUZ), E. Gentili, and V. Pieroni (ST). We also thank M. Auditore, M. Balini, V. Buffa (Muséum National d'Histoire Naturelle, Paris), V. Pieroni, and T. Scheyer for helpful discussions. We thank T. M. Scheyer and F. Miedema (Staatliches Museum für Naturkunde, Stuttgart) for providing valuable photographic comparison material. Finally, we thank Stephan N. F. Spiekman, Silvio Renesto, an anonymous reviewer, and the RIPS editorial board for providing detailed reviews. This paper is part of a Ph. D. project (G. Bindellini) focusing on the Besano Fm. fauna, led by the Università Statale di Milano (M. Balini) in agreement with the Museo di Storia Naturale di Milano (C. Dal Sasso).

4.11 References

Airaghi C. (1935) - I fossili della dolomia triassica della Rasa (Varese). *Rendiconti del Regio Istituto Lombardo di Scienze e Lettere. Serie II*, 68: 191-196.

Bernasconi S.M. (1991) - Geochemical and microbial controls on dolomite formation and organic matter production/preservation in anoxic environments a case study from the Middle Triassic Grenzbitumenzone, Southern Alps (Ticino, Switzerland). PhD thesis, 196 pp, Swiss Federal institute Oftechnologyzürich.

Bernasconi S. M. (1994) - Geochemical and microbial controls on dolomite formation in anoxic environments: A case study from the Middle Triassic (Ticino, Switzerland). *Contributions to Sedimentology*, 19: 1–109.

Bernasconi S.M. & Riva A. (1993) - Organic geochemistry and depositional environment of a hydrocarbon source rock: the Middle Triassic Grenzbitumenzone Formation, Southern Alps, Italy/Switzerland. In: Spencer A.M. (eds) - Generation, Accumulation and Production of Europe's Hydrocarbons (vol.3): 179–190. Springer, Berlin.

Beichman A.C., Koepfli K.P., Li G., Murphy W., Dobrynin P., Kliver S., Tinker M.T., Murray M.J., Johnson J., Lindblad-Toh K., Karlsson E.K., Lohmueller K.E. & Wayne R.K. (2019) - Aquatic adaptation and depleted diversity: a deep dive into the genomes of the sea otter and giant otter. *Molecular biology and evolution*, 36: 2631-2655.

Bindellini G., Balini M., Teruzzi G. & Dal Sasso C. (2019) - Ammonoid and *Daonella* zonation of the Sasso Caldo quarry (Besano Formation, Middle Triassic). *Strati 2019, 3rd International Congress on Stratigraphy. ST2.4 Ammonoids in stratigraphy*: p.87.

Bindellini G. & Dal Sasso C. (2019) - Sauropod teeth from the Middle Jurassic of Madagascar, and the oldest record of Titanosauriformes. *Papers in Palaeontology*, 7: 137-161.

Bindellini G., Wolniewicz A.S., Miedema F., Scheyer T.M., & Dal Sasso C. (2021) - Cranial anatomy of *Besanosaurus leptorhynchus* Dal Sasso & Pinna, 1996 (Reptilia: Ichthyosauria) from the Middle Triassic Besano Formation of Monte San Giorgio, Italy/Switzerland: taxonomic and palaeobiological implications. *PeerJ*, 9: e11179.

Brack P. & Rieber H. (1986) - Stratigraphy and ammonoids of the lower Buchenstein Beds of the Brescian Prealps and Giudicarie and their significance for the Anisian/Ladinian Boundary. *Eclogae Geologicae Helvetiae*, 79: 181–225.

Brack P. & Rieber H. (1993) - Towards a better definition of the Anisian/Ladinian boundary: New biostratigraphic data and correlations of boundary sections from the Southern Alps. *Eclogae Geologicae Helvetiae*, 86: 415–527.

Brack P., Rieber H., Nicora A. & Mundil R. (2005) - The Global boundary Stratotype Section and Point (GSSP) of the Ladinian Stage (Middle Triassic) at Bagolino (Southern Alps, Northern Italy) and its implications for the Triassic time scale. *Episodes*, 28: 233–244.

Braun J., & Reif W. E. (1985) - Konstruktionsmorphologie, Nr. 169: A survey of aquatic locomotion in fishes and tetrapods. *Neues Jahrbuch für Geologie und Paläontologie*. *Abhandlungen*, 169: 307–332.

Brinkmann W. (1997) - Die Ichthyosaurier (Reptilia) aus der Mitteltrias des Monte San Giorgio (Tessin, Schweiz) und von Besano (Lombardei, Italien) – der aktuelle Forschungsstand. *Vierteljarsschrift der Naturforschenden Gesellschaft in Zürich*, 142:69–78.

Burgin T., Rieppel O., Sander P. M. & Tschanz K. (1989) - The fossils of Monte San Giorgio. *Scientific American*, 260: 74-81.

Dal Sasso C., Pinna G. (1996) - *Besanosaurus leptorhynchus* n. gen. n. sp., a new shastasaurid ichthyosaur from the Middle Triassic of Besano (Lombardy, N. Italy). *Paleontologia Lombarda*, Nuova serie, 4:3-23.

Drevermann F. R. (1933) - Die Placodontier. 3. Das Skelett von *Placodus gigas* Agassiz im Senckenberg-Museum. *Abhandlungen der Senckenbergischen Naturforschenden Gesellschaft* 38: 319-364.

Etter W. (2002) - Monte San Giorgio: Remarkable Triassic marine vertebrates. In: Bottjer D. J., Etter W., Hagadorn J.W. & Tang C.M. (eds.) - Exceptional fossil preservation. A unique view on the evolution of marine life: 220–242. Columbia University Press, New York.

Fish F.E. (1994) - Association of propulsive swimming mode with behavior in river otters (*Lutra canadensis*). *Journal of Mammalogy*, 75: 989-997.

Fish F.E., Rybczynski N., Lauder G.V. & Duff, C.M. (2021) - The Role of the Tail or Lack Thereof in the Evolution of Tetrapod Aquatic Propulsion. *Integrative and Comparative Biology*, 61: 398–413.Feldkamp S.D. (1987) - Foreflipper propulsion in the California sea lion, *Zalophus californianus*. *Journal of Zoology*, 212: 43-57.

Furrer H. (1995) - The Kalkschieferzone (Upper Meride Limestone; Ladinian) near Meride (Canton Ticino, Southern Switzerland) and the evolution of a Middle Triassic intraplatform basin. *Eclogae Geologicae Helvetiae*, 88: 827–852.

Furrer H. 2003. Der Monte San Giorgio im Südtessin-vom Berg der Saurier zur Fossil-Lagerstätte internationaler Bedeutung. Neujahrsblatt der Naturforschenden Gesellschaft in Zurich 206, Zurich, 64 pp.

Godfrey S.J. (1984) - Plesiosaur subaqueous locomotion - a reappraisal. *Neues Jahrbuch für Geologie und Paläontologie-Monatshefte*, 11: 661-672.

Huene F. v. (1936) - *Henodus chelyops* ein neuer Placodontier. *Paleontographica A*, 84: 99-148.

Klein N. & Scheyer T.M. (2013) - A new placodont sauropterygian from the Middle Triassic of the Netherlands. *Acta Palaeontologica Polonica*, 59: 887-902.

Klein N., Houssaye A., Neenan J. M. & Scheyer T. M. (2015) - Long bone histology and microanatomy of Placodontia (Diapsida: Sauropterygia). *Contributions to Zoology*, 84: 59-84.

Krahl A., Klein N., & Sander P. M. (2013) - Evolutionary implications of the divergent long bone histologies of *Nothosaurus* and *Pistosaurus* (Sauropterygia, Triassic*). BMC Evolutionary Biology*, 13: 1-23

Kuhn-Schnyder E. (1974). *Die triasfauna der tessiner Kalkalpen*. Naturforschenden Gesellschaft in Zürich, Zürich, 119 pp.

Li C., Jiang D.Y., Cheng L., Wu X.C. & Rieppel O. (2014) - A new species of *Largocephalosaurus* (Diapsida: Saurosphargidae), with implications for the morphological diversity and phylogeny of the group. *Geological Magazine*, 151: 100-120.

Lingham-Soliar T. (1991) - Locomotion in mosasaurs. *Modern Geology*: 16, 229-248.

Maisch M.W. & Matzke A.T. (1998) - Observations on Triassic ichthyosaurs. Part II: A new ichthyosaur with palatal teeth from Monte San Giorgio. N*eues Jahrbuch für Geologie und Paläontologie-Monatshefte*, 1998: 26-41.

Massare J.A. (1987) - Tooth morphology and prey preference of Mesozoic marine reptiles. *Journal of Vertebrates Paleontology*, 7: 121-137.

Massare J.A (1988) - Swimming capabilities of Mesozoic marine reptiles, implications for method of predation, *Paleobiology*, 14: 187-205

Massare J.A (1994) - Swimming capabilities of Mesozoic marine reptiles, a review. In: Maddock L., Bone Q. & Rayner J. M. (Eds.) - Mechanics and Physiology of Animal Swimming: 133–150. Cambridge University Press, Cambridge.

Motani, R., & Vermeij, G. J. (2021) - Ecophysiological steps of marine adaptation in extant and extinct non-avian tetrapods. *Biological Reviews*: 10.1111/brv.12724.

Mundil R., Brack P., Meier M., Rieber H. & Oberli F. (1996) - High resolution U-Pb dating of Middle Triassic volcaniclastics: Time-scale calibration and verification of tuning parameters for carbonate sedimentation. *Earth and Planetary Science Letters*, 141: 137-151.

Müller J. (2005). The anatomy of *Askeptosaurus italicus* from the Middle Triassic of Monte San Giorgio and the interrelationships of thalattosaurs (Reptilia, Diapsida). *Canadian Journal of Earth Sciences*, 42: 1347-1367.

Neenan J.M., Klein N. & Scheyer T.M. (2013) - European origin of placodont marine reptiles and the evolution of crushing dentition in Placodontia. *Nature Communications*, 4: 1-8.

Nosotti S. & Rieppel O. (2003) – *Eusaurosphargis dalsassoi* n. gen. n. sp., a new, unusual diapsid reptile from the Middle Triassic of Besano (Lombardy, N Italy). *Memorie della Società Italiana di Scienze Naturali e del Museo Civico di Storia Naturale di Milano*, 31: 1-33.

Peyer B. (1935) - Die Triasfauna der Tessiner Kalkalpen. VIII. Weitere Placodontierfunde. *Abhandlungen der schweizerischen Paläontologischen Gesellschaft*, 55: 1-26.

Peyer B. (1955) - Die Triasfauna der Tessiner Kalkalpen. XVIII. *Helveticosaurus zollingeri*, n.g. n.sp. *Abhandlungen der schweizerischen Paläontologischen Gesellschaft*, 72: 3-50.

Pieroni V. (2011) - La Rasa di Varese e i suoi fossili. Pietro Macchione editore, 157 pp.

Röhl H.J., Schmid-Röhl A., Furrer H., Frimmel A., Oschmann W. & Schwark L. (2001) – Microfacies, geochemistry and palaeoecology of the Middle Triassic Grenzbitumenzone from Monte San Giorgio (Canton Ticino, Switzerland). *Geologia Insubrica*, 6: 1-13.

Rieber H. (1973) - Die Triasfauna der Tessiner Kalkalpen. Cephalopoden aus der Grenzbitumenzone (Mittlere Trias) des Monte San Giorgio (Kt. Tessin, Switzerland). *Abhandlungen der schweizerischen Paläontologischen Gesellschaft*, 93: 1-96.

Renesto S., Dal Sasso C., Fogliazza F. & Ragni C. (2020) - New findings reveal that the Middle Triassic ichthyosaur *Mixosaurus cornalianus* is the oldest amniote with a dorsal fin. *Acta Paleontologica Polonica*, 65: 511-522.

Renesto S. & Pieroni V. (2013) - Middle Triassic vertebrate remains from Rasa Village (Varese, Northern Italy). In: Tanner L.H., Spielmann J.A. & Lucas S.G. (eds.) - The Triassic System: New Developments in Stratigraphy and Paleontology, Bulletin 61: 485-488. New Mexico Museum of Natural History and Science, New Mexico.

Renesto S. & Tintori, A. (1995) - Functional morphology and mode of life of the Late Triassic placodont *Psephoderma alpinum* Meyer from the Calcare di Zorzino (Lombardy, N Italy). *Rivista Italiana di Paleontologia e Stratigrafia*, 101: 37-48.

Rieppel O. (1989) - *Helveticosaurus zollingeri* Peyer (Reptilia, Diapsida): skeletal paedomorphosis; functional anatomy and systematic affinities. *Palaeontographica A*, 208:123-152.

Rieppel O. (1994) - Osteology of *Simosaurus gaillardoti*, and the phylogenetic interrelationships of stem-group Sauropterygia. *Fieldiana (Geology)*, 28: 1-85.

Rieppel O. (2000) - Part 12 A. Sauropterygia I - Placodontia, Pachypleurosauria, Nothosauroidea, Pistosauroidea. Handbook of Paleoherpetology, Verlag Dr. Friedrich Pfeil, Munchen, 134 pp.

Rieppel O. (2019) - Mesozoic Sea Dragons: Triassic marine life from the ancient tropical lagoon of Monte San Giorgio. Indiana University Press, Bloomington, 245 pp.

Robinson J.A (1975) - The locomotion of plesiosaurs. *Neues Jahrbuch für Geologie und Paläontologie*, 149: 286-332.

Scheyer T.M., Neenan J.M., Bodogan T., Furrer H., Obrist C., & Plamondon M. (2017) - A new, exceptionally preserved juvenile specimen of *Eusaurosphargis dalsassoi* (Diapsida) and implications for Mesozoic marine diapsid phylogeny. *Scientific Reports*, 7: 1-22.

Scheyer T. M., & Klein, N. (2021) - Sauropterygia: Placodontia. In Buffrénil V., Ricqlès A. J., Zylberberg L. & Padian K. (Eds.) (2021) - *Vertebrate Skeletal Histology and Paleohistology* CRC Press. Florida.Stockar R. (2010). - Facies, depositional environment, and palaeoecology of the Middle Triassic Cassina beds (Meride Limestone, Monte San Giorgio, Switzerland). *Swiss Journal of Geosciences*, 103: 101-119.

Stockar R., Baumgartner P.O. & Condon D. (2012) - Integrated Ladinian bio–chronostratigraphy and geochronology of Monte San Giorgio (Southern Alps, Switzerland). *Swiss Journal of Geosciences*, 105: 85–108.

Thewissen J.G. & Fish F.E. (1997) - Locomotor evolution in the earliest cetaceans: functional model, modern analogues, and paleontological evidence. *Paleobiology*, 23: 482-490.

Williams T.M. (1989) - Swimming by sea otters: adaptations for low energetic cost locomotion. *Journal of Comparative Physiology A*, 164: 815-824.

Williams T.M. (2018) - Swimming. In: Würsig, B., Perrin, W. F., & Thewissen, J. G. M. (Eds.) - Encyclopedia of Marine Mammals: 970–979. Academic Press, New York.

Wotzlaw J.F., Brack P. & Storck, J.C. (2017) - High-resolution stratigraphy and zircon U–Pb geochronology of the Middle Triassic Buchenstein Formation (Dolomites, northern Italy): precession-forcing of hemipelagic carbonate sedimentation and calibration of the Anisian–Ladinian boundary interval. *Journal of the Geological Society*, 175: 71-85.

Zanin Buri C. (1965) - Il Trias in Lombardia (studi geologici e paleontologici). XIII. Le alghe calcaree delle Prealpi Lombarde. *Rivista Italiana di Paleontologia e Stratigrafia*, 71: 449-544.

Zhang Q., Wen W., Hu S., Benton M. J., Zhou C., Xie T., Lü T., Huang J., Choo B., Chen Z. Q., Liu J. & Zhang Q. (2014) - Nothosaur foraging tracks from the Middle Triassic of southwestern China. *Nature communications*, 5: 1-12.

Zorn H. (1971) - Paläontologische, Stratigraphisce und Sedimentologische Untersuchungen des Salvatoredolomits (Mitteltrias) der Tessiner Kalkalpen. *Schweizerische Paläontologische Abhandlungen*, 91: 1-90.

4.12 Supplementary figures

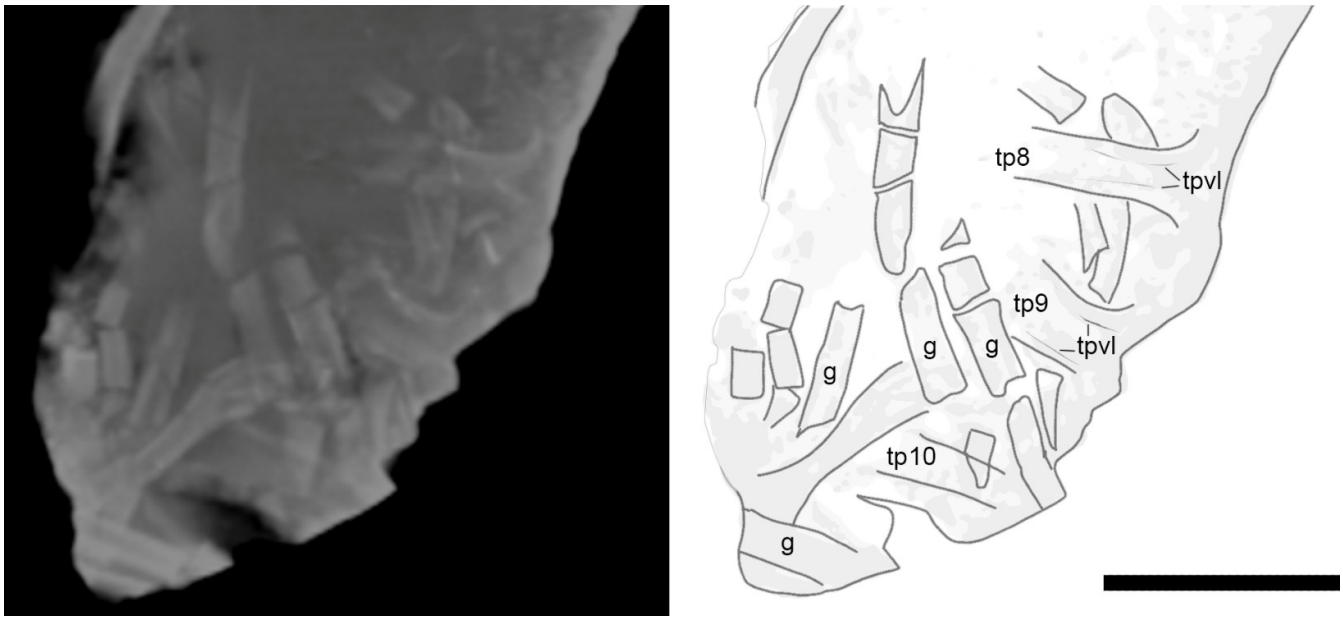

Fig. 4.S1 - Rendering of a section of the CT data showing a portion of MSNM V927a. Abbreviations: g, gastralium; tp, transverse process; tpvl, transverse process ventral lamina. Note the presence of the tpvl described in the main text. Scale bar equals 50 mm.

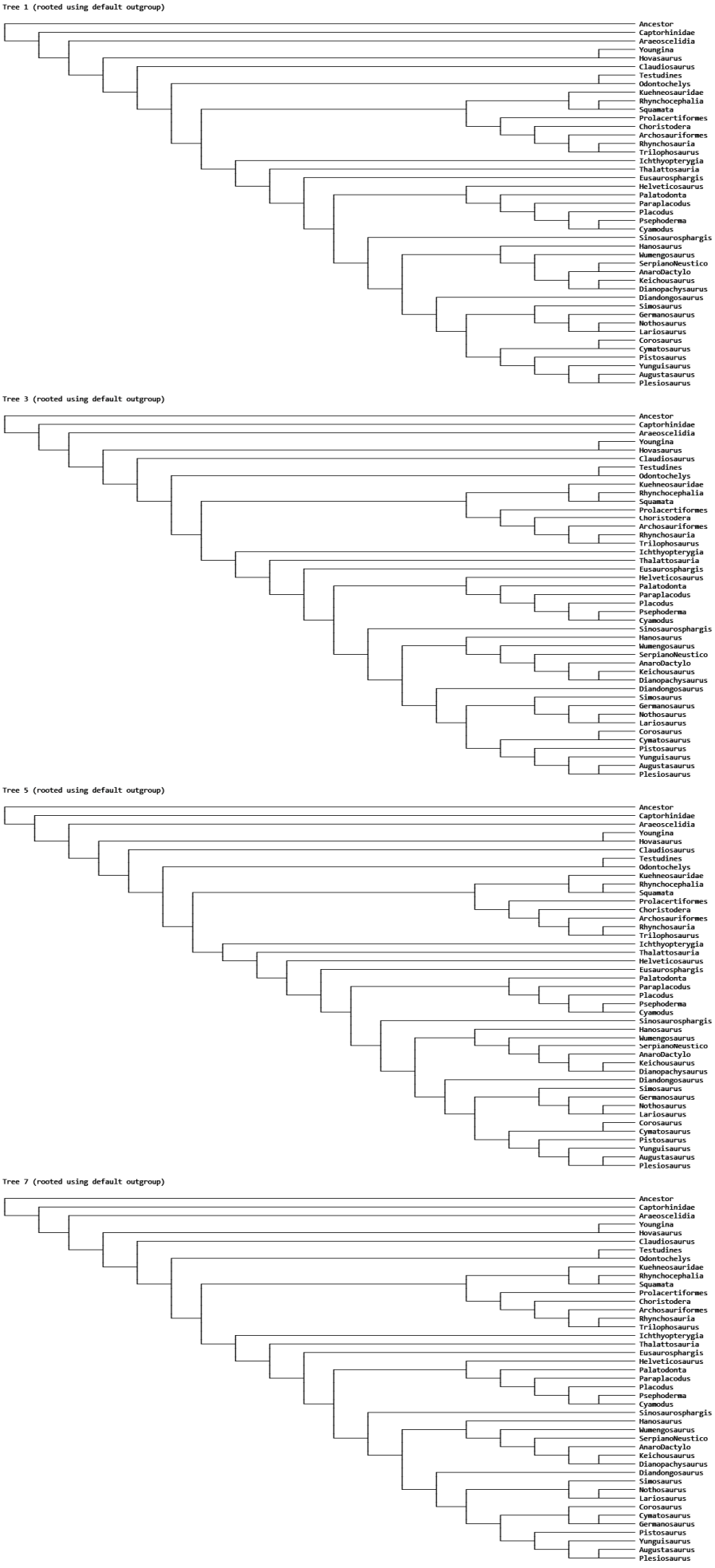

Fig. 4.S2 – Trees 1, 3, 5, 7 of the 8 MPTs (Most Parsimonious Trees) of score 571, used to build the strict consensus tree in Fig. 4.5, resulting from the phylogenetic analysis of the data matrix modified from Scheyer et al. (2017) “third matrix”, and performed in PAUP 4.0 (see text for further details).

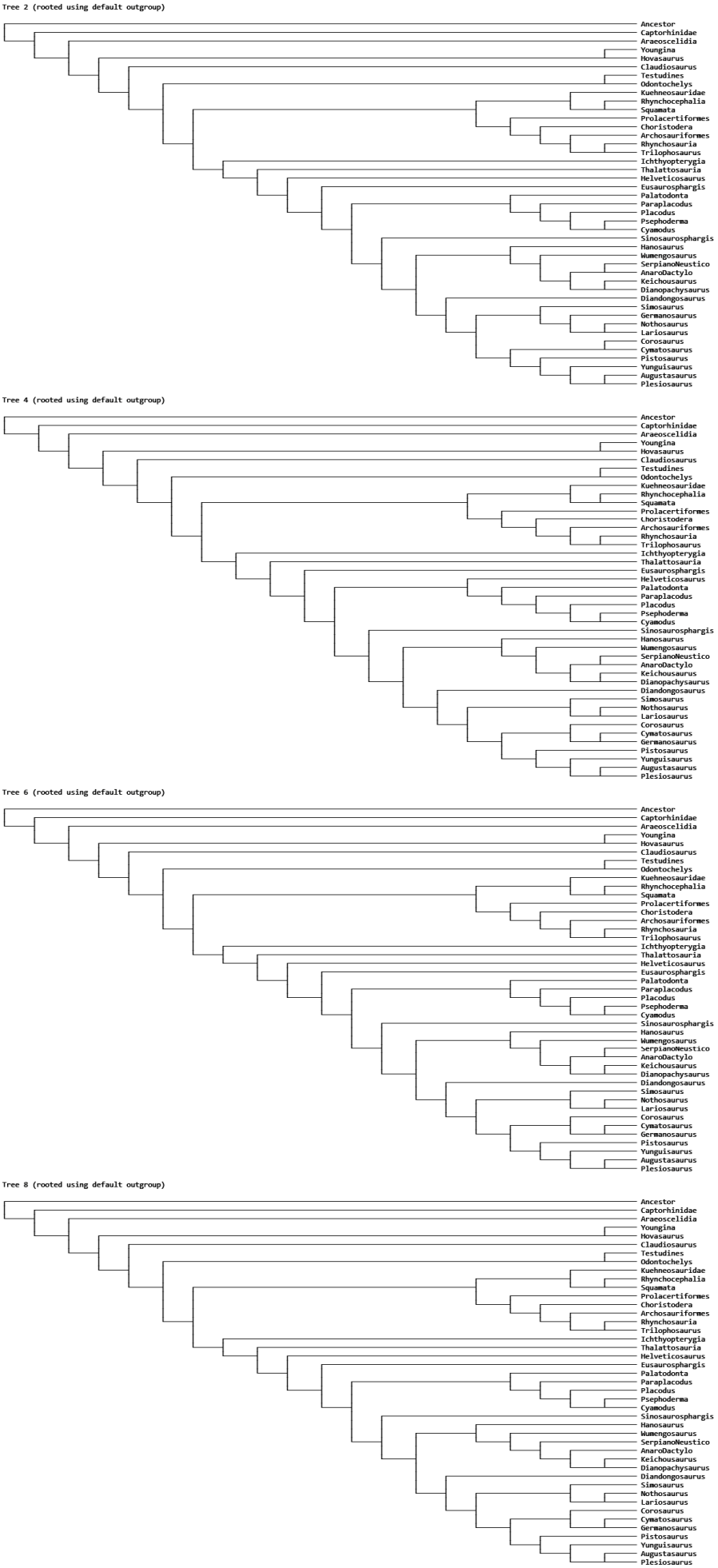

Fig. 4.S3 – Trees 2, 4, 6, 8 of the 8 MPTs (Most Parsimonious Trees) of score 571, used to build the strict consensus tree in Fig. 4.5, resulting from the phylogenetic analysis of the data matrix modified from Scheyer et al. (2017) “third matrix”, and performed in PAUP 4.0 (see text for further details).

Chapter 5
New cymbospondylid material from the Besano Formation (Middle Triassic, Monte San Giorgio)

*Draft of a manuscript to be submitted to the peer-reviewed journal Natural History Sciences.
Gabriele Bindellini[1], Cristiano Dal Sasso[2]
[1] Dipartimento di Scienze della Terra "Ardito Desio", Università degli Studi di Milano, Milano, Italy.
[2] Sezione di Paleontologia dei Vertebrati, Museo di Storia Naturale di Milano, Milano, Italy.

5.1 Abstract

Specimens MSNM V926 and SMNS 50010 are here reported and described for the first time. The former is a ribcage portion preserving at least five vertebrae and 18 ribs of a large ichthyosaur, the latter is an isolated partial forefin of a large ichthyosaur. Both of them come from the Besano Formation (Monte San Giorgio, UNESCO WHL). MSNM V926 was collected in the 1950s from the waste material of the Piodelle-Selva Bella mines, near Besano (Varese); the specimen has been recently recovered in the historical collections of the Museo di Storia Naturale di Milano. SMNS comes from P.902 dig site in Switzerland and was donated to the Stuttgart Museum für Naturkunde collection in 1976. The combination of characters observed allowed the authors to attribute the specimens to *Cymbospondylus buchseri*. Given the rarity of the taxon, known only by the holotype (the anterior half of a medium-large ichthyosaur), these specimens represent an important addition to the abundant fossil collections from the Besano Formation. In particular, MSNM V926 represents the first specimen of *Cymbospondylus buchseri* coming from the Italian side of Monte San Giorgio. The rediscovery of these specimens in museum collections gives hope for further findings in historical collections around Europe.

5.2 Introduction

A still unpublished specimen recently recovered in the collections of the Museo di Storia Naturale di Milano (MSNM V926) represents the first Italian occurrence of *Cymbospondylus buchseri* from the Middle Triassic of the Besano Formation and is described in this manuscript. *Cymbospondylus* is a medium-large ichthyosaur that belongs to one of the most basal taxa of Ichthyopterygia. It is more basal than Mixosauridae (the most common ichthyosaurs of the Besano Formation) and shastasaur-grade ichthyosaurs, to which belongs *Besanosaurus leptorhynchus*, a second medium-large ichthyosaur known from Monte San Giorgio (Dal Sasso & Pinna, 1996; Bindellini et al., 2021). The fossil here described was collected in the 1950s from the waste material of the Piodelle-Selva Bella mines, near Besano (Varese). Despite this, we can state with confidence that it comes from the ammonoid-bearing layers of

the Besano Formation (*Reitziites reizti* or *Nevadites secedensis* Zone, ~ 242 Ma), since the profiles of two ammonoids are visible on the surface and through CT scans.-.
In this chapter we also describe for the first time an isolated portion of a forefin (SMNS 50010) of an ichthyosaur from the Besano Formation, assigning it to *Cymbospondylus buchseri*. This specimen is housed at the Stuttgart Museum für Naturkunde (SMNS) and it was recovered at Punkt 902/Mirigioli dig site (Switzerland), although its exact stratigraphic position is not known.
The Besano Formation is among the most fossiliferous units of the sedimentary succession of the Monte San Giorgio site (UNESCO WHL), which has provided one of the best-preserved records of marine life in the Triassic period, including the holotype and only known specimen of *Cymbospondylus buchseri* (Sander, 1989). Nevertheless, officially no *Cymbospondylus* remains from the Italian side of Monte San Giorgio have been described yet. The early evolutionary history of ichthyosaurs was historically based almost entirely on fossil material collected from this formation, from the Muschelkalk of Germany and the Prida and Favret Formation of Nevada, USA (e.g. Bassani, 1886; Merriam, 1902; Huene, 1916). The record of genus *Cymbospondylus* is historically known from all these formations as well, but more recently new specimens have been described also from Idaho, USA, and Spitsbergen Islands (Massare & Callaway 1994; Sander, 1992; Balini & Renesto, 2012). In Italy, *Cymbospondylus* is represented by few fragmentary specimens scattered across the Alps (Pian delle Streghe, Brembana valley, Seceda and Clap di Val; Balini & Renesto 2012).

5.3 Geological setting

The Middle Triassic carbonate succession of Monte San Giorgio consists of four different formations (Fig. 5.1) deposited in an intra-platform basin in a carbonate platform on the western margin of the Neo-Tethys (Furrer, 1995; Röhl, et al. 2001; Etter, 2002; Stockar, et al. 2012). Above the Anisian Salvatore Dolomite lies the Besano Formation (Anisian/Ladinian boundary), from which the greatest part of the well-known vertebrate fauna of Monte San Giorgio has been recovered (Bürgin et al., 1989; Furrer, 2003). At the Anisian/Ladinian boundary, the development of a 30-130 m deep and approximately 20 km wide basin, at the north-western rim of the Tethys Ocean, resulted in the deposition of the Besano Formation (Bernasconi, 1994; Furrer, 1995; Röhl et al., 2001). The Besano Formation (or “Grenzbitumenzone"; Frauenfelder, 1916) is a 5 to 16 m thick alternation of black shales and variably laminated dolostones (Brack & Rieber, 1993; Brack et al., 2005). As hypothesized by Röhl et al. (2001), the uppeö and the lower portion of the Besano Formation represent a restricted, shallow inter- to subtidal carbonate platform, whereas the middle part a slightly deeper intraplatform basin, from which a great number of ichthyosaurian remains and other pelagic taxa come from (e.g., Dal Sasso & Pinna, 1996; Brinkman, 1997; Maish & Matzke, 1998; Renesto et al., 2020; Bindellini et al., 2021).
The presence of two undetermined ammonoids, associated with the bones of MSNM V926, suggests a referral to the middle portion of the Besano Formation. i.e., to the uppermost *R. reitzi* Zone or *N. secedensis* Zone, the latter dated between 241.77 ± 0.06 – 241.42 ± 0.15 Ma by Wotzlaw et al. (2017). SMNS 50010 comes from P.902 dig site in Switzerland; its precise stratigraphic position is unknown although it very likely comes from the middle Besano Formation as well, like all known ichthyosaurs taxa from the Besano Formation.

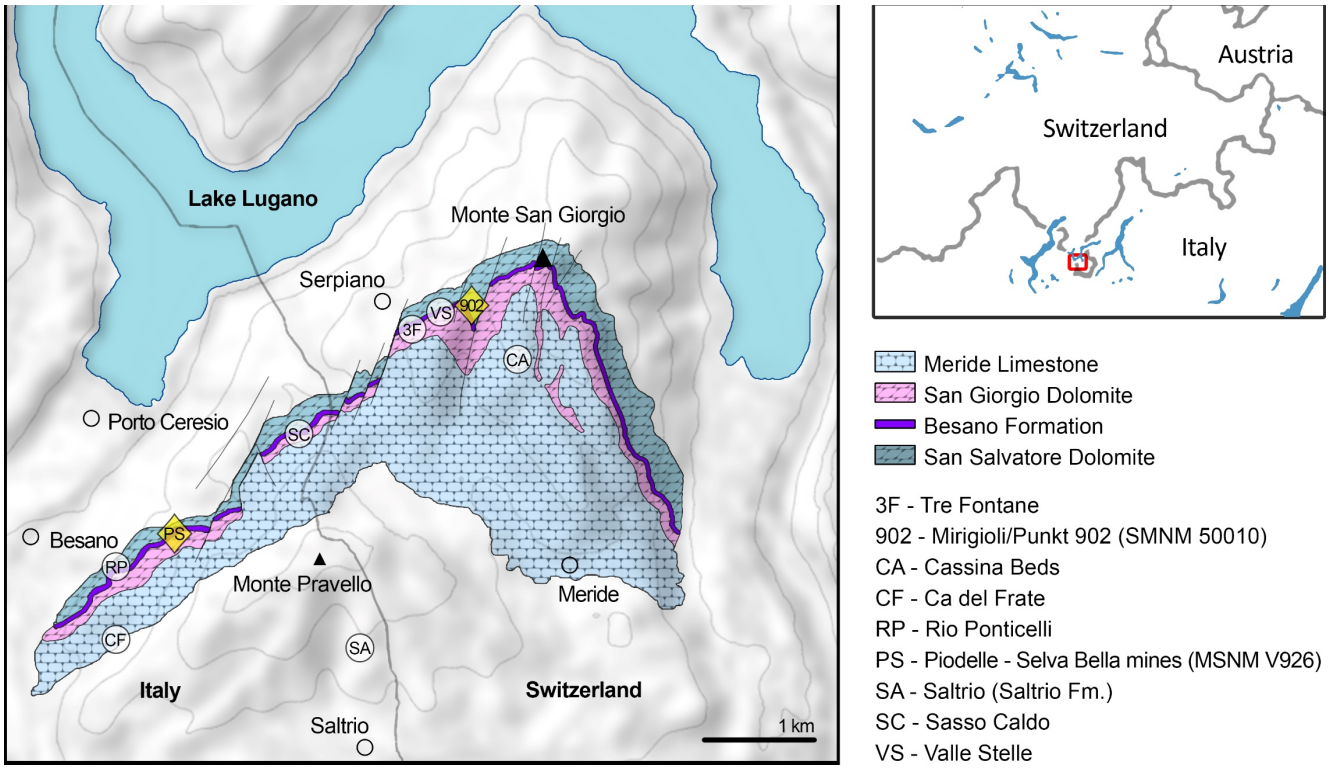

Fig. 5.1 - Map of the Monte San Giorgio area showing the Middle Triassic carbonate succession, the major paleontological quarries in the area (white circles), and the sites of origin of the specimens described in this paper (yellow rhombuses).

5.4 Materials and methods

MSNM V926 is a portion of a ribcage consisting of 3 almost complete and 2 fragmentary vertebrae, and at least 18 incomplete ribs. The vertebrae are ~5.5 cm tall and the longest rib is 41.5 cm long. Given the orientation of vertebrae and ribs, the cranial direction is on the right of the observer.

SMNS 50010 is an isolated partial forefin recovered from the Besano Formation on the Swiss side of Monte San Giorgio. Some of the preserved phalanges are still articulated. The specimen results flat and it is unclear if it is exposed in dorsal or ventral view.

Both specimens have been examined under optical microscopy and UV-induced fluorescence. In addition, X-ray computed tomography (CT) was performed on MSNM V926, with a Siemens Somatom Definition Dual Source CT Scanner, at the Radiology Department of the Fondazione IRCCS “Cà Granda” Ospedale Maggiore Policlinico di Milano. CT imaging was obtained with a bone algorithm on transverse (axial) slices, with scan parameters 140 kV, 180-270 mA, and slice thickness of 0.3 mm (Crasti, 2019). Data were exported in DICOM format using eFilm (v. 1.5.3; Merge eFilm, Toronto, Canada). Analysis and post-processing were performed with RadiAnt, 3DimViewer, and Synedra View Personal. Multiplanar reconstructions (MPR) and volume rendering reconstructions (VR) allowed the visualization of the bones below the surface (i.e., below the unprepared organic material), as well as clear images of the ammonoids associated with the specimen. Scanning electron microscopy (SEM) was also used to investigate the bone tissue and the purported presence of soft tissue in MSNM V926.

5.5 Systematic paleontology

ICHTHYOPTERYGIA Owen, 1840
ICHTHYOSAURIA Blainville, 1835
CYMBOSPONDYLIDAE Huene, 1948
CYMBOSPONDYLUS Leidy, 1868
Cymbospondylus buchseri Sander, 1989

Type and only species. *Cymbospondylus buchseri*

Type specimen. PIMUZ T 4351, slightly disarticulated anterior half of a skeleton.

Type locality. Cava Tre Fontane, Monte San Giorgio, Canton Ticino, Switzerland

Type horizon and distribution. ?Middle Besano Formation, uppermost Anisian (*N. secedensis* Zone *sensu* Brack et al. 2005), Middle Triassic.

Referred material. MSNM V926, a ribcage portion consisting of 3 complete and 2 fragmentary vertebrae, and at least 18 incomplete ribs. SMNS 50010, an isolated portion of a forefin of a large ichthyosaur.

Diagnosis. As reported by Sander (1989), Maisch & Matzke (2000), and McGowan & Motani (2003). Medium-sized *Cymbospondylus*. Shorter postorbital region of skull than in *C. petrinus*, with orbital length 170% of postorbital length. Postfrontal does not extend far beyond orbit. Scapula wider and less constricted than in *C. petrinus*. Humerus relatively wide compared to that of *C. piscosus*, nearly isometric (length/width ratio 1.16), slightly constricted. Ulna with convex posterior margin.

5.6 Description and discussion

Vertebrae – MSNM V926 includes three almost complete and two incomplete vertebrae; all of them are exposed on their right lateral side and result taphonomically compressed in mediolateral direction (Fig. 5.2 and Fig. 5.3). The height/length ratio of the centra is ~2 (Tab. 5.1), which closely matches the values reported for PIMUZ T 4351, *Cymbospondylus buchseri* holotype (Sander, 1989).
In lateral view, diapophyses occupy the middle portion of the centra and extend ventrally merging with the proximal faces of the centra. The diapophyses are long, have a concave cranial margin, and show a slight constriction in the middle. By their shape, we can infer that these vertebrae articulated with holocephalous ribs. The diapophyses are separated from the articular facets for the neural arches, a character that in *Cymbospondylus buchseri* occurs only after the 35th vertebra (Kuhn-Schnyder, 1980; Sander, 1989; Sander, 1992). A thin crest, diverging dorsally from the diapophyses and stretching toward the neural arch, but not reaching it, is clearly visible in the first two anterior-most vertebrae and is possibly absent in the third one.

Table 5.1 - Height (H) and length (L) of three centra (C, 38th, 39th, and 40th) in three specimens attributed to *Cymbosponsylus*: PIMUZ T 4351 (Sander, 1989), PIMUZ A/III 496 (Sander, 1992), MSNM V926 (this paper). If applicable, it is also reported the mean value of H and L for centra between the 35th and 42nd positions.

Specimen	C:	**38th**	**39th**	**40th**	Mean 35-42
PIMUZ T 4351 (Sander, 1989)	L	2.8	3	3.4	3.04
	H	6.1	6.1	6.2	5.78
PIMUZ A/III 496 (Sander, 1992)	L	2.95	3	3	2.95
	H	6.8	6.9	7.5	7.06
MSNM V926 (this paper)	L	2.6	2.7	2.5	not measurable
	H	5.3	5.6	5.1	

As preserved on the surface of the slab, these crests appear to be closer to the dorsal margin of the centra than they are in reality; in fact, as reported for the Seceda *Cymbospondylus* specimen (Kuhn-Schnyder, 1980), if observed in proximal view the vertebrae would result slightly rotated clockwise.
The dorsal portions of the vertebrae are very poorly preserved, so that the articular facets for the neural arches cannot be identified. In the cranialmost preserved vertebra, the dorsal portion of the lateral wall appears flat and sloping dorsally, as described for *C. buchseri* (Sander, 1989). The ventral portion of the vertebrae looks smooth and round.
The combination of characters here observed is reported in the description of the holotype of *Cymbospondylus buchseri* (Sander, 1989) as well as in the Seceda *Cymbospondylus* specimen (similar to "*Gruppe B*" in Kuhn-Schnyder, 1980). Therefore, we refer MSNM V926 to C*ymbospondylus buchseri*. Also, following Sander (1989; 1992), we assign the three well-preserved vertebrae, from the caudalmost to the cranialmost, to the 40th, 39^{th,} and 38th positions.
The anatomy of the diapophyses of MSNM V926 might result similar to what can be observed in the caudalmost dorsal vertebrae of *Besanosaurus* (BES SC 999; see chapter 7). However, the posterodorsal diapophyses of *Cymbospondylus* differ slightly in shape, extension, and disposition: in *B. leptorhynchus* they develop around and above the midline (except for the last four caudalmost dorsal vertebrae) and do not possess the ventral extension showed by C. *buchseri*. Moreover, the ribs associated with the vertebrae of MSNM V926 result proportionally too long to be attributed to the caudal portion of a *Besanosaurus* trunk, and in turn compatible with the position suggested above in *C. buchseri*.
Lastly, in *B. leptorhynchus*, the anteriormost posterodorsal vertebrae retain a thin connection between the neural arches and the diapophyses (up until at least the 49th and 50th centrum), that in *C. buchseri* is lost after the 37th position. This might reflect a different swimming style in the two ichthyosaurs, which will be investigated in chapter 7 of this thesis.

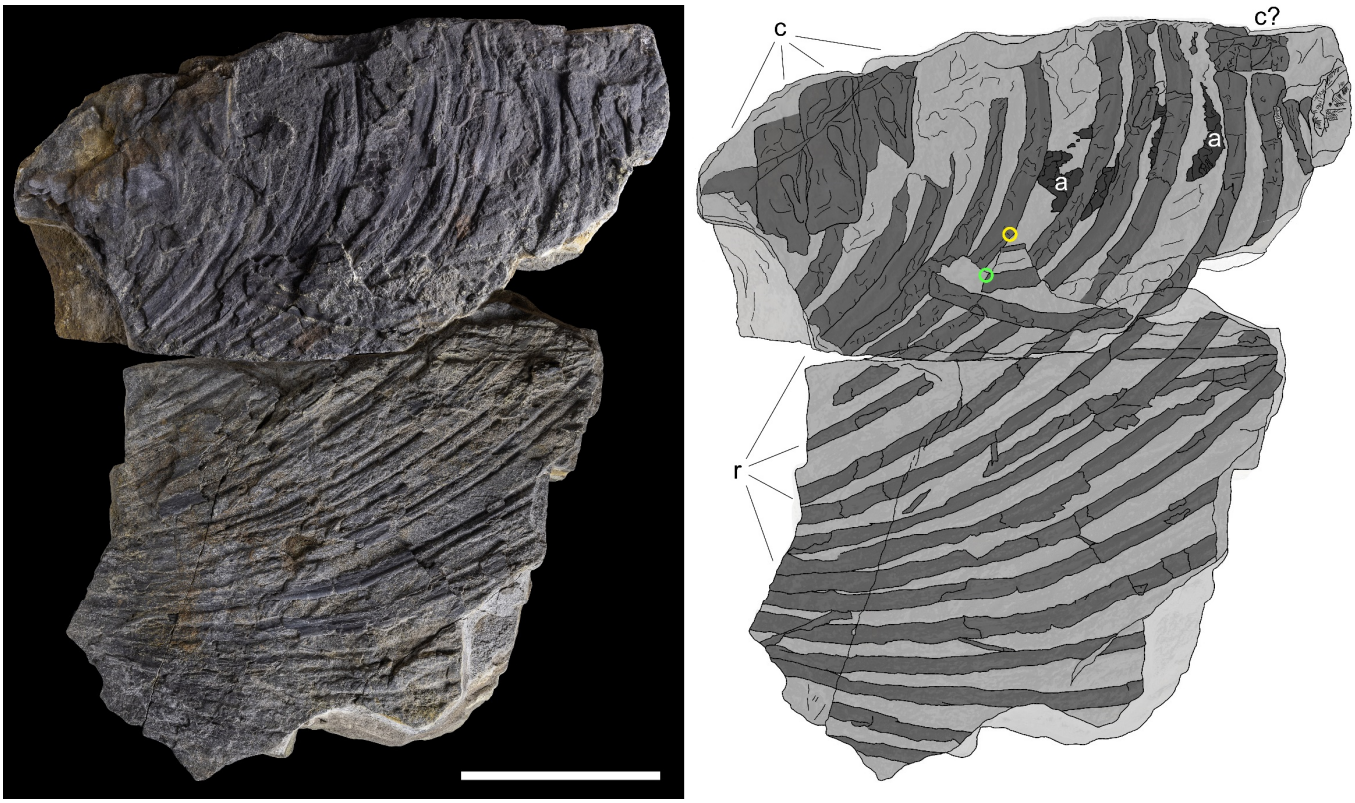

Fig. 5.2 - MSNM V926, a portion of the trunk of a *Cymbospondylus buchseri*, and its interpretative drawing. *Abbreviations*: a, ammonoid; c, vertebral centrum; r, rib. The yellow circle hightligts the point where the bone tissue has been sampled for SEM analysis (Fig. 5.4a). The green circle highligts the point where the periosteum has been sampled for SEM analysis (Fig. 5.4b). Scale bar equals 10 cm.

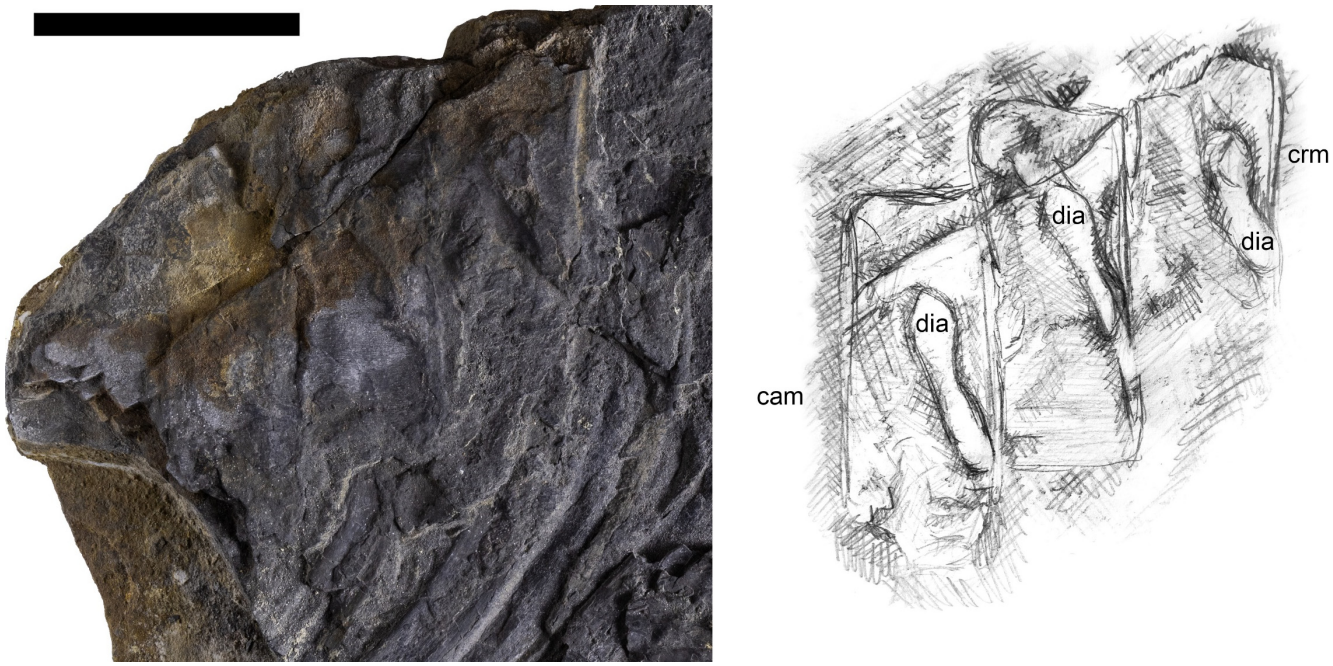

Fig. 5.3 - MSNM V926 photo and interpretative drawing of the three complete vertebrae exposed in right lateral view. Abbreviations: crm, cranial margin; cam, caudal margin; dia, diapophysis. Scale bar equals 5 cm.

Ribs – At least 18 posterodorsal ribs are preserved in cranial view. They represent a portion of the left side of the ribcage. No rib is preserved in its full length, the longest (41.5 cm) lacking its last quarter. Small fragments of right ribs lie above left ribs. The ribs are holocephalous and the heads dorsoventrally expanded, reaching proximally two-thirds of the craniocaudal length of a single centrum. The rib head, if preserved, results flattened and one-third craniocaudally wider than the rib shaft. The articular surface of the head is clearly shorter than the articular surface of the centrum, indicating that some cartilage was present between the rib head and the diapophysis. Approaching the shaft, the rib flattens and becomes thinner than the head. All the rib shafts preserved are characterized by the presence of a groove that run along the cranial side of the bone. An equivalent groove is present on the caudal side of the rib, hidden in MSNM V926 below the surface, but identifiable through CT scan or on the imprints of the caudal surface of some missing ribs.
The same characters described above are visible in the holotype of *Cymbospondylus buchseri* (Sander, 1989) and in the Seceda *Cymbospondylus* (Kuhn-Schnyder, 1980).

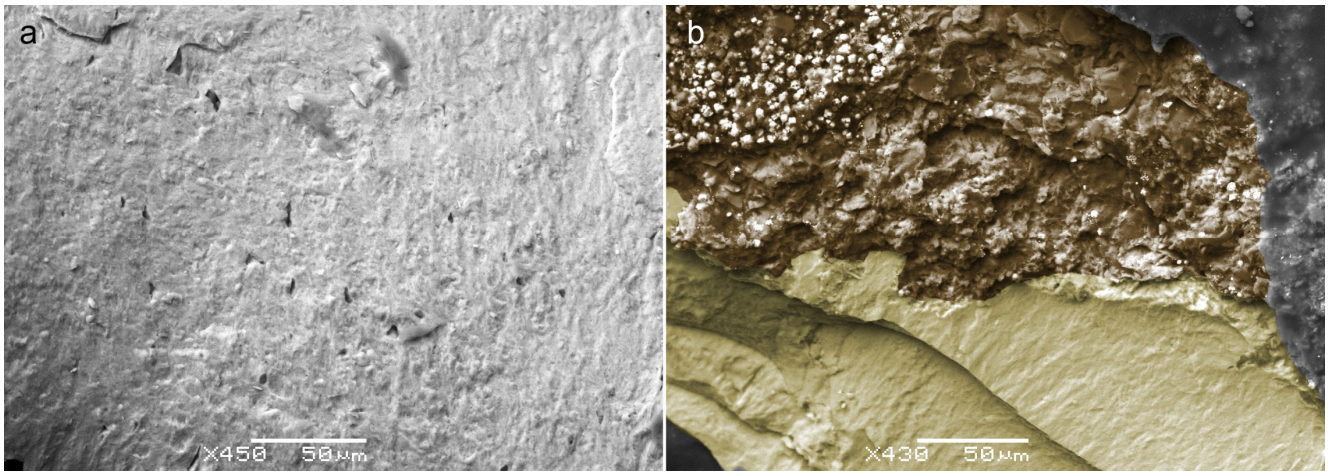

Fig. 5.4 - (a) SEM image of a dorsal rib of MSNM V926, showing a portion of the compact bone layer in transverse section, dotted by the lacunae of the osteocytes; (b) False color SEM image of a dorsal rib of MSNM V 926: the bone tissue (yellow) is covered by a patch of periosteum (brown). Paraloid (grey) used to prepare the specimen covers the fossil in the upper right corner of the image. Pyrite crystals (white), in the upper left corner of the image, cover a portion of the periosteum.

Remarks on the soft tissue remains - SEM analysis identified patches of periosteum (Fig. 5.4), preserved as a thin black patina covering the surface of some ribs. This fossilized tissue is particularly clear on the caudal side of the right rib fragments lying above the cranial sides of the left ribs.

Forefin – SMNS 50010 (Fig. 5.5) is an isolated partial forefin of which only 15 phalanges are still preserved. By judging from their relative dimensions, the fin can be orientated locating the smaller phalanges distally. The phalanges seem to be still articulated (with the exception of a single element far from the others), showing large interphalangeal spaces that in life might have been filled with cartilage. A similar feature has also been observed in the forefins of *Besanosaurus leptorhynchus* (Dal Sasso & Pinna, 1996: fig. 8; see also chapter 7 of this thesis). On the other hand, the hindfin phalanges of *Besanosaurus* are preserved close to each other and tightly packed together.
Most of the phalanges preserved possess a round profile; five of them show a concave cranial and/or caudal margin. This peculiar association of rounded phalanges adjacent to phalanges with constricted shafts has been observed solely in the forefins of *Cymbospondylus buchseri* holotype (PIMUZ T 4351). In the latter, the forefin phalanges are scattered distally to radius and ulna, not preserving their *in vivo* position, and therefore making difficult to understand which portion of the fin is preserved in SMNS 50010.

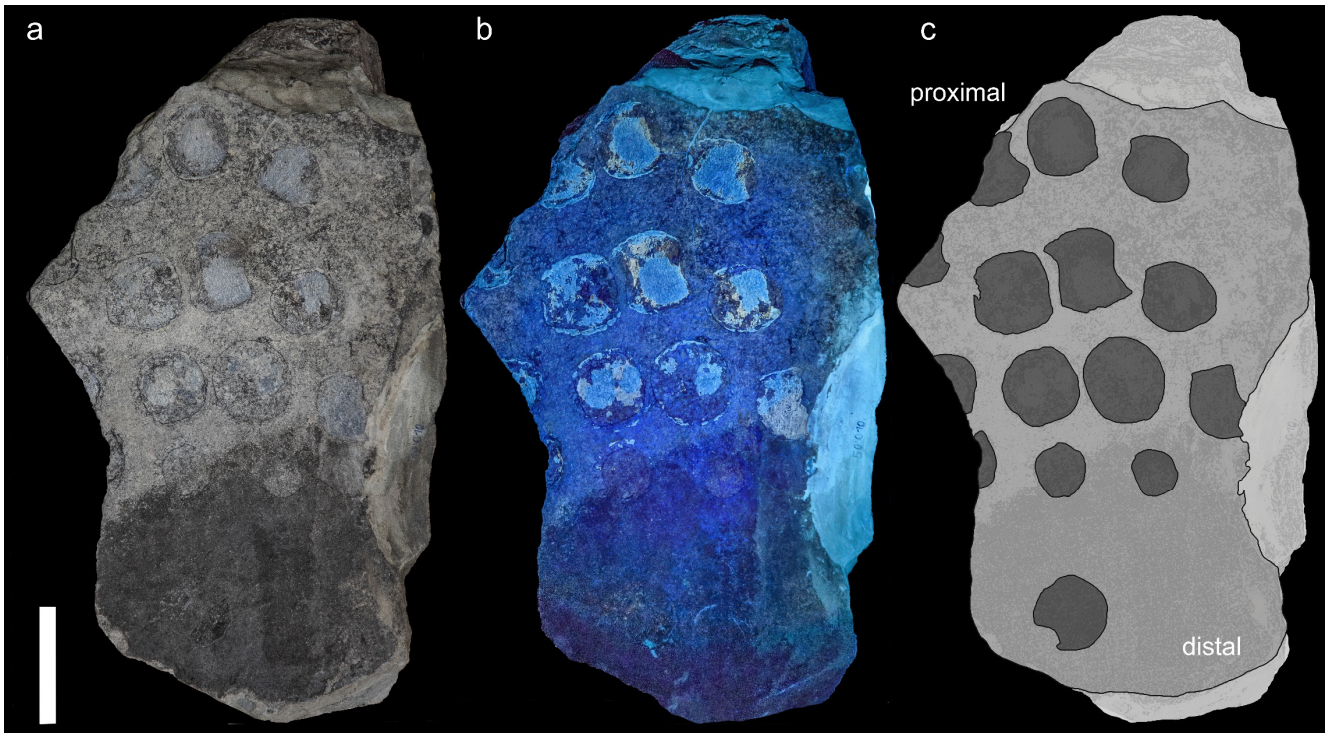

Fig. 5.5 - SMNS 50010, an isolated partial forefin attributed to *Cymbospondylus buchseri.* Photo under (a) natural and (c) UV lights; (c) interpretative drawing of the specimen, Scale bar equals 5 cm.

5.7 Conclusions

Given the combination of characters observed, both specimens MSNM V926 and SMNS 50010 are attributed to *Cymbospondylus buchseri*. Among the large ichthyosaurs of the Besano Formation, MSNM V926, can be distinguished from *Besanosaurus* by the anatomy of the diapophyses, which in this latter taxon develop around and above the midline of the centra and do not possess the ventral extension showed by *C. buchseri*. Based on the size of the centra, specimen MSNM V926 resulted ~ 90% the size

of PIMUZ T 4351, the holotype of *C. buchseri*. In SMNS 50010 is reported the association of round phalanges with adjacent phalanges possessing concave anterior and posterior margins; this character is seen only in *C. buchseri*.

Although the presence of *Cymbospondylus* was reported in the past from some Italian localities and its presence is known on the Swiss side of Monte San Giorgio, MSNM V926 represents the first specimen attributed to *C. buchseri* and recovered on the Italian side of the mountain. The attribution of MSNM V926 and SMNS 50010 to *C. buchseri* enriches the rare occurrence of the taxon in the Besano Formation and the ichthyosaurian diversity on the Italian side of Monte San Giorgio. This suggests the necessity of an in-depth reevaluation of the specimens from the Besano Formation housed and scattered in museum collections across Europe.

5.8 Acknowledgments

We are grateful to L. Forzenigo, C. Bonelli, and G. Terribile (Fondazione IRCCS "Cà Granda" Ospedale Maggiore Policlinico di Milano) for CT analysis; the Italian Ministry of Culture and the "Soprintendenza Archeologia, Belle Arti e Paesaggio per le province di Como, Lecco, Monza e Brianza, Pavia, Sondrio e Varese" for permissions. For access to key specimens in museum collections, we thank Erin Maxwell, Rainer Schoch, and Feiko Miedema (SMNS).

5.9 References

Balini, M., & Renesto, S. C. (2012). Cymbospondylus vertebrae (Ichthyosauria, Shastasauridae) from the Upper Anisian Prezzo Limestone (Middle Triassic, southern Alps) with an overview of the chronostratigraphic distribution of the group. *Rivista Italiana di Paleontologia e Stratigrafia*, 118: 155-172.

Bassani F. 1886. Sui fossili e sull'età degli schisti bituminosi triasici di Besano in Lombardia. *Atti della Società italiana di Scienze Naturali*, 29: 15-72.

Bernasconi SM. 1994. Geochemical and microbial controls on dolomite formation in anoxic environments: A case study from the Middle Triassic (Ticino, Switzerland). *Contributions to Sedimentology*, 19:1-109.

Bindellini G, Wolniewicz AS, Miedema F, Scheyer TM, Dal Sasso C. 2021. Cranial anatomy of *Besanosaurus leptorhynchus* Dal Sasso and Pinna, 1996 (Reptilia: Ichthyosauria) from the Middle Triassic Besano Formation of Monte San Giorgio, Italy/Switzerland: taxonomic and palaeobiological implications. *PeerJ*, 9:e11179

Brack P, Rieber H, 1993. Towards a better definition of the Anisian/Ladinian boundary: New biostratigraphic data and correlations of boundary sections from the Southern Alps. *Eclogae Geologicae Helvetiae*, 86:415-527.

Brack P, Rieber H, Nicora A, Mundil R. 2005. The Global boundary Stratotype Section and Point (GSSP) of the Ladinian Stage (Middle Triassic) at Bagolino (Southern Alps, Northern Italy) and its implications for the Triassic time scale. *Episodes*, 28:233-244.

Brinkmann W. 1997. Die Ichthyosaurier (Reptilia) aus der Mitteltrias des Monte San Giorgio (Tessin, Schweiz) und von Besano (Lombardei, Italien) – der aktuelle Forschungsstand. *Vierteljarsschrift der Naturforschenden Gesellschaft in Zürich*, 142:69–78.

Bürgin T, Rieppel O, Sander PM, Tschanz K. 1989. The fossils of Monte San Giorgio. *Scientific American*, 260:74-81.

Dal Sasso C, Pinna G. 1996. *Besanosaurus leptorhynchus* n. gen. n. sp., a new shastasaurid ichthyosaur from the Middle Triassic of Besano (Lombardy, N. Italy). *Paleontologia Lombarda*, Nuova serie, 4:3-23.

Etter W. 2002. Monte San Giorgio: Remarkable Triassic marine vertebrates. In: Bottjer DJ, Etter W, Hagadorn JW, Tang CM eds. *Exceptional fossil preservation. A unique view on the evolution of marine life*. New York: Columbia University Press, 220-242.

Frauenfelder A. 1916. Beiträge zur Geologie der Tessiner Kalkalpen. *Eclogae Geologicae Helvetiae*, 14: 247-367.

Furrer H. 1995. The Kalkschieferzone (Upper Meride Limestone; Ladinian) near Meride (Canton Ticino, Southern Switzerland) and the evolution of a Middle Triassic intraplatform basin. *Eclogae Geologicae Helvetiae*, 88: 827-852.

Furrer H. 2003. Der Monte San Giorgio im Südtessin-vom Berg der Saurier zur Fossil-Lagerstätte internationaler Bedeutung. *Neujahrsblatt der Naturforschenden Gesellschaft in Zurich*, 206:64.

Huene F. Von 1916. Beiträge zur Kenntnis der Ichthyosaurier im deutschen Muschelkalk. *Palaeontographica*, 62:1-68.

Kuhn-Schnyder E. 1980. Über Reste eines großen Ichthyosauriers aus den Buchensteiner Schichten (ladinische Stufe der Trias) der Seceda (NE St. Ulrich/Ortisei, Prov. Bozen, Italien). *Annalen des Naturhistorischen Museums in Wien*,83: 231-244.

Maisch MW, Matzke AT. 1998. Observations on Triassic ichthyosaurs. Part II: A new ichthyosaur with palatal teeth from Monte San Giorgio. *Neues Jahrbuch fur Geologie und Palaontologie*, 1: 26-41.

Maisch MW, Matzke AT. 2000. The Ichthyosauria. *Stuttgarter Beiträge zur Naturkunde Serie B*, 298:1-159.

Massare JA., Callaway JM. 1994. *Cymbospondylus* (Ichthyosauria: Shastasauridae) from the Lower Triassic Thaynes Formation of southeastern Idaho. *Journal of Vertebrate Paleontology*, *14*(1), 139-141.

McGowan C, Motani R. 2003. Part 8. Ichthyopterygia. In: Sues H-D, ed. *Handbook of Paleoherpetology.* Munchen: Verlag Dr. Friedrich Pfeil, 173 pp.

Merriam JC. 1902. Triassic Ichthyopterygia from California and Nevada. University of California Publications, Bulletin of the Department of Geology 3:63–108.

Renesto S, Dal Sasso C, Fogliazza F, Ragni C. 2020. New findings reveal that the Middle Triassic ichthyosaur *Mixosaurus cornalianus* is the oldest amniote with a dorsal fin. *Acta Paleontologica Polonica*, 65: 511-522.

Röhl HJ, Schmid-Röhl A, Furrer H, Frimmel A, Oschmann W, Schwark L. 2001. Microfacies, geochemistry and palaeoecology of the Middle Triassic Grenzbitumenzone from Monte San Giorgio (Canton Ticino, Switzerland). *Geologia Insubrica*, 6:1-13.

Sander PM. 1989. The large ichthyosaur *Cymbospondylus buchseri*, sp. nov., from the Middle Triassic of Monte San Giorgio (Switzerland), with a survey of the genus in Europe. *Journal of Vertebrate Paleontology*, 9:163-173.

Sander PM. 1992. *Cymbospondylus* (shastasauridae: ichthyosauria) from the Middle Triassic of spitsbergen: filling a paleobiogeographic gap. *Journal of paleontology*, 66:332-337

Stockar R, Baumgartner PO, Condon D. 2012. Integrated Ladinian bio-chronostratigraphy and geochronology of Monte San Giorgio (Southern Alps, Switzerland). *Swiss Journal of Geosciences*, 105:85-108.

Wotzlaw JF, Brack P, Storck JC. 2017. High-resolution stratigraphy and zircon U–Pb geochronology of the Middle Triassic Buchenstein Formation (Dolomites, northern Italy): precession-forcing of hemipelagic carbonate sedimentation and calibration of the Anisian–Ladinian boundary interval. *Journal of the Geological Society*, 175:71-85.

Chapter 6
Cranial anatomy of *Besanosaurus leptorhynchus* Dal Sasso & Pinna, 1996 (Reptilia: Ichthyosauria) from the Middle Triassic Besano Formation of Monte San Giorgio, Italy/Switzerland: taxonomic and palaeobiological implications

*Manuscript published on PeerJ.

Gabriele Bindellini[1], Andrzej S. Wolniewicz[2], Feiko Miedema[3,4], Torsten M. Scheyer[4], and Cristiano Dal Sasso[5]

[1] Dipartimento di Scienze della Terra "Ardito Desio", Università degli Studi di Milano, Milano, Italy

[2] Institute of Paleobiology, Polish Academy of Sciences, Warsaw, Poland

[3] Staatliches Museum für Naturkunde Stuttgart, Stuttgart, Germany

[4] Paläontologisches Institut und Museum, Universität Zürich, Zürich, Switzerland

[5] Sezione di Paleontologia dei Vertebrati, Museo di Storia Naturale di Milano, Milano, Italy

6.1 Abstract

Besanosaurus leptorhynchus Dal Sasso & Pinna, 1996 was described on the basis of a single fossil excavated near Besano (Italy) nearly three decades ago. Here, we re-examine its cranial osteology and assign five additional specimens to *B. leptorhynchus*, four of which were so far undescribed. All of the referred specimens were collected from the Middle Triassic outcrops of the Monte San Giorgio area (Italy/Switzerland) and are housed in various museum collections in Europe. The revised diagnosis of the taxon includes the following combination of cranial characters: extreme longirostry; an elongate frontal not participating in the supratemporal fenestra; a prominent 'triangular process' of the quadrate; a caudoventral exposure of the postorbital on the skull roof; a prominent coronoid (preglenoid) process of the surangular; tiny conical teeth with coarsely-striated crown surfaces and deeply-grooved roots; mesial maxillary teeth set in sockets; distal maxillary teeth set in a short groove. All these characters are shared with the holotype of *Mikadocephalus gracilirostris* Maisch & Matzke, 1997, which we consider as a junior synonym of *B. leptorhynchus*. An updated phylogenetic analysis, which includes revised scores for *B. leptorhynchus* and several other shastasaurids, recovers *B. leptorhynchus* as a basal merriamosaurian, but it is unclear if Shastasauridae form a clade, or represent a paraphyletic group. The inferred body length of the examined specimens ranges from 1 m to about 8 m. The extreme longirostry suggests that *B. leptorhynchus* primarily fed on small and elusive prey, feeding lower in the food web than an apex predator: a novel ecological

specialisation never reported before the Anisian in a large diapsid. This specialization might have triggered an increase of body size and helped to maintain low competition among the diverse ichthyosaur fauna of the Besano Formation.

6.2 Introduction

Shastasaurids were important components of Triassic marine ecosystems and represented, along with Cymbospondylidae, one of the earliest groups of medium to large-bodied ichthyosaurs. In fact, members of this varied clade ranged in size from about 6 m to more than 20 m and included the whale-sized *Shonisaurus sikanniensis*, the largest ichthyosaur known to date (Nicholls & Manabe, 2004). As defined by Ji et al. (2016), Shastasauridae include six genera of long-bodied (presacral count > 55) forms: *Shastasaurus*, *Besanosaurus*, *Guanlingsaurus*, *Guizhouichthyosaurus*, *Shonisaurus* and *'Callawayia' wolonggangense* (Camp, 1980; Dal Sasso & Pinna, 1996; Maisch & Matzke, 1997a; Li & You, 2002; Nicholls & Manabe, 2004; Maisch et al., 2006b; Pan, Jiang & Sun, 2006; Chen, Cheng & Sander, 2007; Shang & Li, 2009; Sander et al., 2011; Ji et al., 2013). The monophyly of Shastasauridae (recovered by e.g., Ji et al., 2013, 2016; Jiang et al., 2016; Motani et al., 2017; Huang et al., 2019) has often been questioned and the clade has been recovered as paraphyletic by several authors (e.g., Maisch & Matzke, 2000; Sander, 2000; Sander et al., 2011; Moon, 2017; Moon & Stubbs, 2020). The validity of some of the shastasaurid taxa has also been questioned (e.g., *Guanlingsaurus*: Sander et al., 2011; Ji et al., 2013; *Guizhouichthyosaurus*: Shang & Li, 2009; '*Callawayia*' *wolonggangense*: Chen, Cheng & Sander, 2007; Ji et al., 2016). The oldest undisputed shastasaurids are known from the Anisian (Middle Triassic) and the youngest persisted to the latest Rhaetian (Late Triassic), gaining a global distribution from present-day Europe, throughout Asia, to North America (e.g., Wiman, 1910; Storrs, 1994; Dal Sasso & Pinna, 1996; Sander, 2000; Benton et al., 2013; Maxwell & Kear, 2013; Fischer et al., 2014; Lomax et al., 2018; but see Martin et al., 2015). A considerable diversity of medium- and large-bodied ichthyosaurs, morphologically similar to shastasaurids, was also reported from the Lower to Middle Triassic of Svalbard, and possibly includes some of the earliest known shastasaurids, such as *Pessosaurus polaris* and *Pessopteryx nisseri* (e.g. Wiman, 1910; McGowan & Motani, 2003; Maxwell & Kear, 2013; Engelschiøn et al., 2018). However, due to the fragmentary nature of the specimens of these taxa, their validity and taxonomic affinity remain a matter of debate. Some of the specimens previously referred to *Pessopteryx nisseri* are morphologically very similar to *Besanosaurus leptorhynchus* (McGowan & Motani, 2003), which indicates their shastasaurid affinity, but these specimens comprise postcranial material only and will therefore not be discussed here.

Ichthyosaurs are among the most abundant fossil reptiles of the UNESCO World Heritage Site of Besano–Monte San Giorgio (Lombardy, Italy; and Canton Ticino, Switzerland; Fig. 6.1), which is one of the richest sites for Middle Triassic marine palaeobiodiversity (e.g., Rieppel, 2019). Dal Sasso & Pinna (1996) named *B. leptorhynchus* and identified it as a new shastasaurid ichthyosaur on the basis of a complete specimen (BES SC 999). It was unearthed in 1993 in the Sasso Caldo quarry near Besano, from the Anisian bituminous shales of the Besano Formation. This new ichthyosaur was clearly different from either *Mixosaurus cornalianus* (the most common ichthyosaur of the Besano Formation outcrops) and *Cymbospondylus buchseri* (the only other medium to large-sized taxon known from Monte San Giorgio), and showed a close affinity with shastasaurids, despite exhibiting several morphological differences from all other shastasaurid taxa. Nevertheless, the *Besanosaurus* specimen of the Museo di Storia Naturale di Milano (MSNM) was not the only shastasaurid uncovered by that time from Monte

San Giorgio/Besano. Two specimens, a medium-sized (PIMUZ T 4376) and a large-sized (PIMUZ T 4847) skeleton, were present in the collections of the Paläontologisches Institut und Museum der Universität Zürich (PIMUZ) since the late 1920s (PIMUZ records). Both skeletons were only briefly mentioned in 20th century literature (Kuhn-Schnyder, 1964; McGowan, 1976; Sander, 1989; Brinkmann, 1994, 1997; Cook, 1994) and the medium-sized skeleton was seemingly under study in the 1990s (Cook, 1994; Dal Sasso & Pinna, 1996; Brinkmann, 1997), but a comprehensive osteological description was never published.

The MSNM *Besanosaurus*, which represents the most complete shastasaurid from the Besano Formation discovered to date, was described in part (Dal Sasso & Pinna, 1996) when it was not yet fully prepared. Subsequent lab work confirmed the remarkable preservation of the postcranial skeleton and the presence of embryonic remains (Dal Sasso, 2001, 2004). However, the interpretation of the morphology of the holotypic skull remained problematic, due to intense overlapping and diagenetic compression of its semi-disarticulated bone elements.

Right after Dal Sasso & Pinna (1996), Maisch & Matzke (1997a) described another shastasaurid specimen (GPIT 1793/1) from the Besano Formation of Monte San Giorgio, referring it to a new genus and species, *Mikadocephalus gracilirostris*. The authors did not cite *B. leptorhynchus*, possibly because they were not aware of the existence of the specimen at that time (Sander, 2000).

Later, Maisch & Matzke (2000) and Maisch (2010) maintained the distinctness of the two genera, based on examination of GPIT 1793/1 and PIMUZ T 4376, which they referred to *Mikadocephalus gracilirostris*, and PIMUZ T 1895, which they considered a referred specimen of *B. leptorhynchus*—although the holotype was not examined personally by them (Maisch & Matzke, 2000: 7). The anatomy and taxonomy of *Mikadocephalus* and *Besanosaurus* received little attention in the late 1990s–early 2000s (but see Sander, 2000: 15; McGowan & Motani, 2003: 127), and by that time the excavations of the relevant sites at Monte San Giorgio were stopped in part in Switzerland, and totally in Italian territory. Another possible shastasaurid from Monte San Giorgio was recently identified in the collections at MSNM (BES SC 1016) and prepared for this study along with PIMUZ T 1895, which helped to clarify the anatomy of the specimens studied here.

Here, we revise the cranial anatomy of the holotype of *B. leptorhynchus* and describe for the first time the skulls of all other shastasaurid specimens from the Besano Formation. We further compare these materials with other ichthyosaurs and revise a previously-published data matrix to perform a phylogenetic analysis elucidating the position of the revised taxon. In addition, we address aspects of ontogenetic variation and palaeoecology of *Besanosaurus*.

Institutional abbreviations. GPIT, Palaeontological Collection of Tübingen University, Tübingen, Germany; GNG, Guanling National Geopark, Guanling, China; IVPP, Institute of Vertebrate Paleontology and Paleoanthropology, Chinese Academy of Sciences, Beijing, China; MSNM, Museo di Storia Naturale di Milano, Milan, Italy; PIMUZ, Paläontologisches Institut und Museum der Universität Zürich, Zürich, Switzerland; ROM, Royal Ontario Museum, Toronto, Canada; SMNS, Staatliches Museum für Naturkunde Stuttgart, Stuttgart, Germany; SPCV (currently WGSC), Wuhan Centre of China Geological Survey, Wuhan, China; TMP, Royal Tyrrell Museum of Palaeontology, Drumheller, Canada; UCMP, University of California Museum of Paleontology, Berkeley, California, USA.

Anatomical abbreviations. Osteological: ang, angular; ar, articular; at, 'anterior terrace' of the supratemporal fenestra; atl, atlas; avsc, impression of the anterior vertical semicircular canal; ax, axis;

bas, basisphenoid; bo, basioccipital; boc, basioccipital condyle; bop, basioccipital peg; bptf, basipterygoid facet; c, centrum; cl, clavicle; cop, coronoid (preglenoid) process of the surangular; d, dentary; dg, dental groove; ds, dental socket(s); dv, dividing ridge; eca, extracondylar area; en, external naris; epi, epipterygoid; exo, exoccipital; fm, foramen magnum; fmf, foramen magnum floor; fr, frontal; hsc, impression of the horizontal semicircular canal; hy, hyoid; hyf, hypoglossal foramen; icf, internal carotid foramen; icl, interclavicle; ipv, interpterygoid vacuity; j, jugal; jcr, jugal caudal ramus; jmd, jugal medial depression; jrr, jugal rostral ramus; la, lacrimal; m, maxilla; mcr, caudal ramus of the maxilla; mh, medial head of the opisthotic; mrr, rostral ramus of the maxilla; n, nasal; na, neural arch; np, notochordal pit; nuf, (remnant of a) neurovascular foramen; nvf, neurovascular foramen; opi, opisthotic; pa, parietal; pal, palatine; pas, parasphenoid; pas cup, cultriform process of the parasphenoid; pbs, parabasisphenoid; pcop, paracoronoid process; pf, parietal foramen; pm, premaxilla; pnp, postnarial process of the maxilla; po, postorbital; pop, paroccipital process; pra, prearticular; prf, prefrontal; pro, prootic; pte, pterygoid; ptf, postfrontal; pvsc, impression of the posterior vertical semicircular canal; q, quadrate; qc, quadrate condyle; qj, quadratojugal; qjce, quadratojugal covered edge; qjf, facet for the quadratojugal; qjqf, quadratojugal facet for the quadrate; sang, surangular; sbp, subnarial process of the premaxilla; sc, scleral plate; scr, sagittal crest; soc, supraoccipital; sp, splenial; spp, supranarial process of the premaxilla; sq, squamosal; st, supratemporal; sta, stapes; su, impression of the sacculus/utriculus area; tf, supratemporal fenestra; tpq, 'triangular process' of the quadrate; vk pas cup, ventral keel of the cultriform process; vo, vomer. "f", behind an abbreviation, denotes an articular facet; "p", behind an abbreviation, denotes a process. The apostrophe (') always indicates a left element.

Musculature: mAMEM, *musculus adductor mandibulae externus medialis*; mAMEP, *musculus adductor mandibulae externus profundus*; mAMES, *musculus adductor mandibulae externus superficialis*; mPSTs, *musculus pseudotemporalis superficialis*.

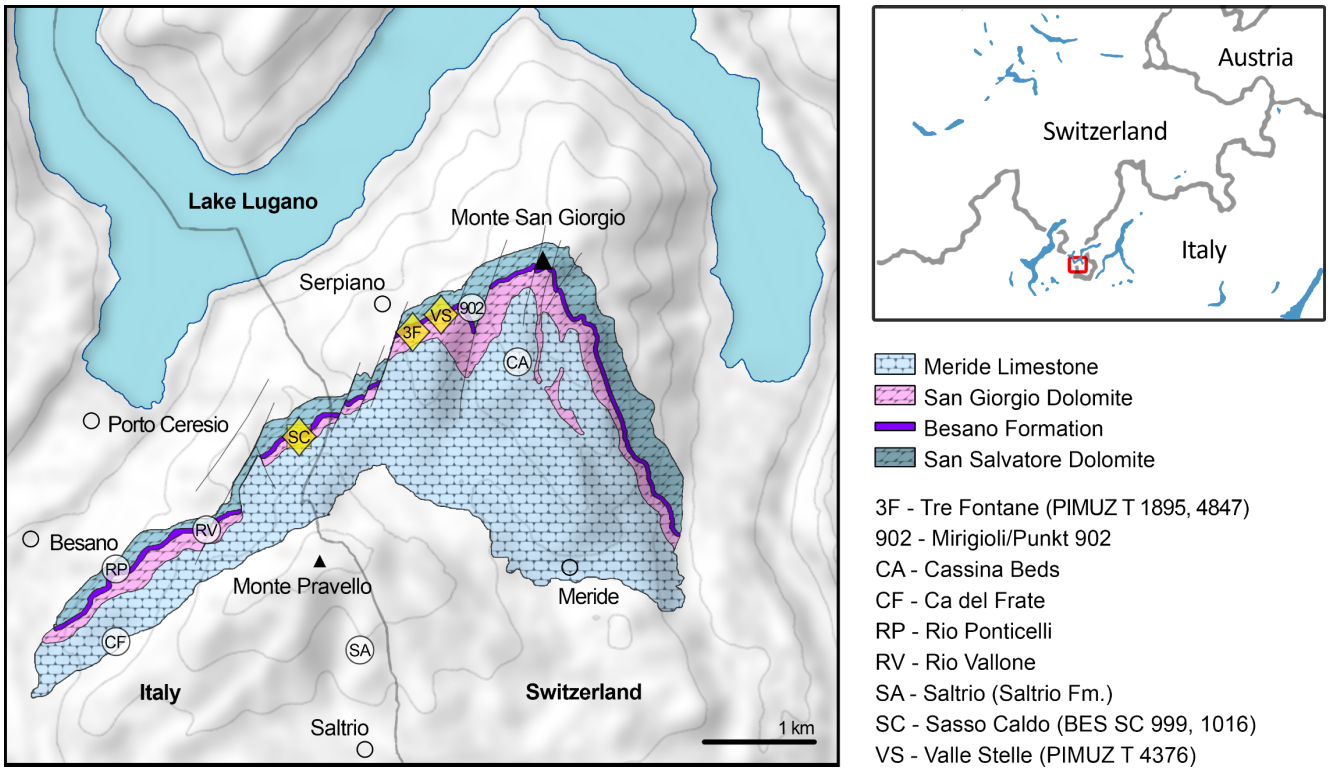

Fig. 6.1 - Relevant fossil sites in the Monte San Giorgio area. Map of the Monte San Giorgio area showing the Middle Triassic carbonate succession, the major paleontological quarries in the area (white circles), and the sites of origin of the specimens described in this paper (yellow rhombuses).

6.3 Geological setting

The Middle Triassic sedimentary succession of Monte San Giorgio consists of four different formations (Fig. 6.1) deposited on a carbonate platform along the western margin of the Neo-Tethys (Furrer, 1995; Röhl et al., 2001; Etter, 2002; Stockar, Baumgartner & Condon, 2012). Above the Anisian Salvatore Dolomite lies the 5- to 16-m-thick Besano Formation (Anisian/Ladinian boundary), from which the greatest part of the well-known vertebrate fauna of Monte San Giorgio has been recovered (Bürgin et al., 1989; Furrer, 2003).

The Besano Formation (also known as Grenzbitumenzone) consists of an alternation of variably laminated dolomitic banks and bituminous shales, and sparse cineritic tuffs that are dated as Late Anisian–Early Ladinian (Brack & Rieber, 1986, 1993; Mundil et al., 1996; Brack et al., 2005; Wotzlaw, Brack & Storck, 2017). It was deposited in a marine setting with an estimated depth of 30–130 m (Bernasconi, 1991, 1994; Bernasconi & Riva, 1993; Furrer, 1995; Röhl et al., 2001; Etter, 2002). The middle portion of the Besano Formation, which probably yielded all specimens examined herein, was deposited in an intraplatform basin (Röhl et al., 2001) and is characterized by organic-carbon rich layers, with well-preserved macro-lamination testifying very quiet hydrodynamic conditions and a lack of post-depositional bioturbation. In all studies mentioned above, it is hypothesized that such deposition took place in a basin with mostly permanent anoxic conditions at the bottom, due to restricted water circulation. The great abundance of pelagic marine vertebrates is also typical of this portion of the Besano Formation. Recent biozonation of the Sasso Caldo site (Fig. 6.2), based on index-fossil invertebrates (ammonoid and the bivalve *Daonella*), indicate that the stratigraphic section cropping out therein is fairly consistent with the most recent biozonation reported by Brack et al. (2005) and allows confident correlation with the coeval Swiss localities (Table 6.1) (Bindellini et al., 2019). The holotype of *B. leptorhynchus* (BES SC 999) was collected at the Sasso Caldo site near Besano, below the three uppermost volcanic layers and within the *N. secedensis* Zone (middle Besano Formation) from *stratum* 65 (equivalent to layer 107 of the Mirigioli Swiss section). It is of Late Anisian age and therefore the taxon represents the stratigraphically oldest shastasaurid (sensu Ji et al., 2016) known to date. The skull BES SC 1016 was collected at Sasso Caldo as well, from *stratum* 70 (equivalent to layer 96 of the Mirigioli Swiss section). The Swiss specimens were extracted from the *N. secedensis* Zone of Cava Tre Fontane (PIMUZ T 1895, 4847) and Valle Stelle (PIMUZ T 4376) mines (Figs. 6.1 and 6.2; Tab.6.1). The exact horizon of origin of the holotypic specimen of *Mikadocephalus* (GPIT 1793/1) is unknown.

Table 6.1 - Localities and horizons. Localities and horizons for each specimen described in this paper. "I" (Italy) and "CH" (Switzerland) indicate the nationality of the site. 'Stratum' or 'Layer' in squared brackets [*] was deduced following Bindellini et al. (2019), since two different methods have been used to number the layers during excavations.

Collection/specimen		Locality	Nat.	'*stratum*' (IT)	Layer (CH)
MSNM	BES SC 999	Sasso Caldo	I	65	[107]
	BES SC 1016	Sasso Caldo	I	70	[96]
PIMUZ	T 4376	Valle Stelle	CH	[82]	71
	T 4847	Cava Tre Fontane	CH	[60]	116
	T 1895	Cava Tre Fontane	CH	*N. secedensis* Zone	
GPIT	1793/1	Unknown CH site	CH	Besano Formation	

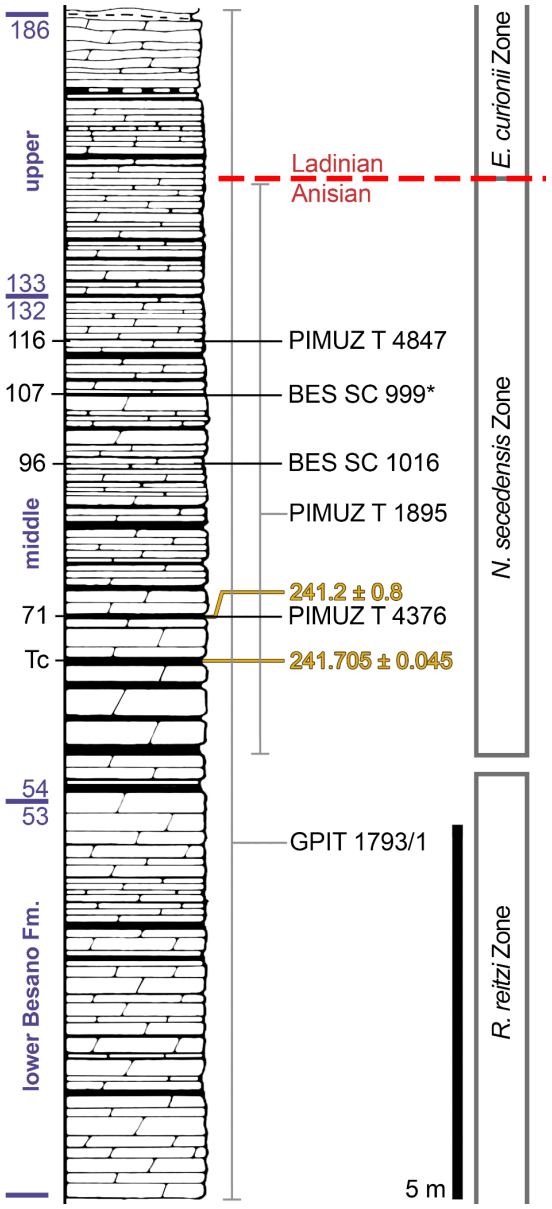

Fig. 6.2 - Stratigraphic log of the Besano Formation. Stratigraphic log of the Besano Formation at the Mirigioli/Punkt 902 outcrop, with the known stratigraphic positions of the specimens described. The stratigraphic position of PIMUZ T 1895 and GPIT 1793/1 is more uncertain, thus expressed by a range line. Log modified from Brack et al. (2005); dating (in millions of years) of layer 71 from Mundil et al. (1996); dating of Tc Tuffs (layers 66–68) from Wotzlaw, Brack & Storck (2017).

6.4 Material and Methods

6.4.1 Preservation of the studied material

All studied specimens lay in a single bedding plane and are variably compressed by diagenetic alteration (Figs. 6.3–9). The skeletons embedded in the most bituminous layers (BES SC 999, PIMUZ T 1895) demonstrate better preservation but also higher bone deformation due to more extreme diagenetic compression. The specimens embedded in bituminous dolomite (PIMUZ T 4847, BES SC 1016) show less detail but are less compressed. The preservation of specimens PIMUZ T 4376 and GPIT 1793/1 is intermediate, leading to a combination of good bone preservation and limited deformation.

Disarticulation is more common in the forefins than in the hindfins, and in the post-sacral axial skeleton (BES SC 999, PIMUZ T 4376, PIMUZ T 4847). One specimen contains embryonic and soft tissue remains (BES SC 999); the largest specimen (PIMUZ T 4847) contains a large nodule in the cranial half of the thoracic region, possibly related to visceral soft tissue.

Fig. 6.3 - The most complete skeletons of *Besanosaurus leptorhynchus* . The most complete skeletons referable to *Besanosaurus leptorhynchus*. (A) PIMUZ T 1895; (B) BES SC 999; (C) PIMUZ T 4376 (with a *Mixosaurus* specimen above it); (D) PIMUZ T 4847. Scale bars represent 50 cm.

BES SC 999. The holotype of *B. leptorhynchus* measures 5.065 m from the tip of the rostrum to the last caudal vertebra. The skeleton is virtually complete and lies in a ventrodorsal position with the paired elements symmetrically flattened along the left and right sides of the body. In the presacral region the vertebrae and the rib cage are nearly as articulated as in vivo; in the caudal region, the elements associated with the vertebral centra (neural spines and chevrons) are relatively close to their in vivo position, but slight wave action may have displaced them to some degree. The skull is detached and set at an approximately right angle in relation to the body, and mostly exposed in left lateral view. The original fossil of BES SC 999 is stored in a special climate-controlled cabinet within the MSNM collections, still divided in 25 slabs (Dal Sasso & Pinna, 1996: fig. 5); a recomposed cast of the skeleton and the surrounding matrix is on display in the MSNM paleontological hall n°5.
PIMUZ T 4376. The best-preserved specimen, it measures 2.12 m from the tip of the rostrum to the last preserved caudal vertebra (the distalmost caudals are missing). The skull and most of the presacral axial skeleton are exposed in right laterodorsal view, and are mostly articulated; the rest of the vertebrae and ribs, as well as the limb bones, are disarticulated and variably clustered on both sides of the vertebral column.
PIMUZ T 1895. Incomplete and mostly unprepared skeleton, lacking most of the tail and the limbs, except for the tailbend (preserved in a separate slab) and the very proximal elements (girdle bones). The specimen is exposed in left laterodorsal view and semi-articulated. The preserved presacral length is around 1.40 m. The associated skull is preserved on a separate slab and the tip of the rostrum was recently prepared and transferred from a minor counterslab to the main slab for this study.
PIMUZ T 4847. The largest specimen, it has a presacral length of 3.28 m but lacks most of the post-sacral skeleton and most of the limb bones. In life, this individual likely reached a length of about 8 m, being one of the biggest among Middle Triassic ichthyosaurs. It is exposed in left lateroventral view, and only the rib cage is preserved semi-articulated. All other bones are scattered along the body profile, and only the longest skull elements retain some original orientation. The inferior quality of preservation of this specimen is partially related to the more difficult preparation of the hard dolomite layers.
GPIT 1793/1. This specimen is the holotype of *Mikadocephalus gracilirostris* (Maisch & Matzke, 1997a). It is preserved in three slabs that can be easily reassembled in their original position. It consists of a partial skull and lower jaw, both almost entirely disarticulated, with the exception of the dorsal bones of the dermal skull (see the description below for further information). These are exposed in ventral (internal) view. The specimen has undergone some diagenetic compression but is still relatively well preserved in 3D in comparison to the rest of the material described herein.
BES SC 1016. Collected in several elongate slabs fractured perpendicular to the rostrocaudal axis of the skull and reassembled during preparation, this specimen consists of a partially disarticulated skull and lower jaw exposed in left laterodorsal view, missing the tip of the rostrum and the caudal portion of the occipital region. The bone elements are embedded in a hard layer of dolomite, show medium–low diagenetic compression, and are crossed by several lines of fracture.

6.4.2 The cranial material

BES SC 999. The skull of BES SC 999 (Fig. 6.4) is preserved mostly on slab n°1, but a few fragmentary bones are also preserved on slab n°2 (see slab numbers in Dal Sasso & Pinna, 1996: fig. 5). The entire skull is extremely compressed measuring only 15 mm in mediolateral thickness and it is fossilised in a very peculiar position: the rostrum, the left orbit, left postorbital, and the bones of the left lower jaw are well-exposed in lateral view and are still semi-articulated whereas the rest of the bones have been displaced and rotated in a puzzling way.

In detail, part of the left maxilla is covered by fragments of the left and right nasal bones, obscuring the caudal end of the external naris. Part of the nasals, the frontals, the parietals, the right prefrontal, the right postfrontal, and the supratemporals have been overturned relative to the other elements, exposing their internal surface. Due to this displacement of the skull roof, the right side elements are now adjacent to the left ones, which are exposed in lateral (external) view. The right nasal is still partially articulated with the right frontal, whereas the left nasal is no longer articulated with the rest of the skull, being caudally separated from the left frontal by the left prefrontal. The long rostral processes of the nasals are deformed, fractured, and partly hidden in between the two premaxillae.

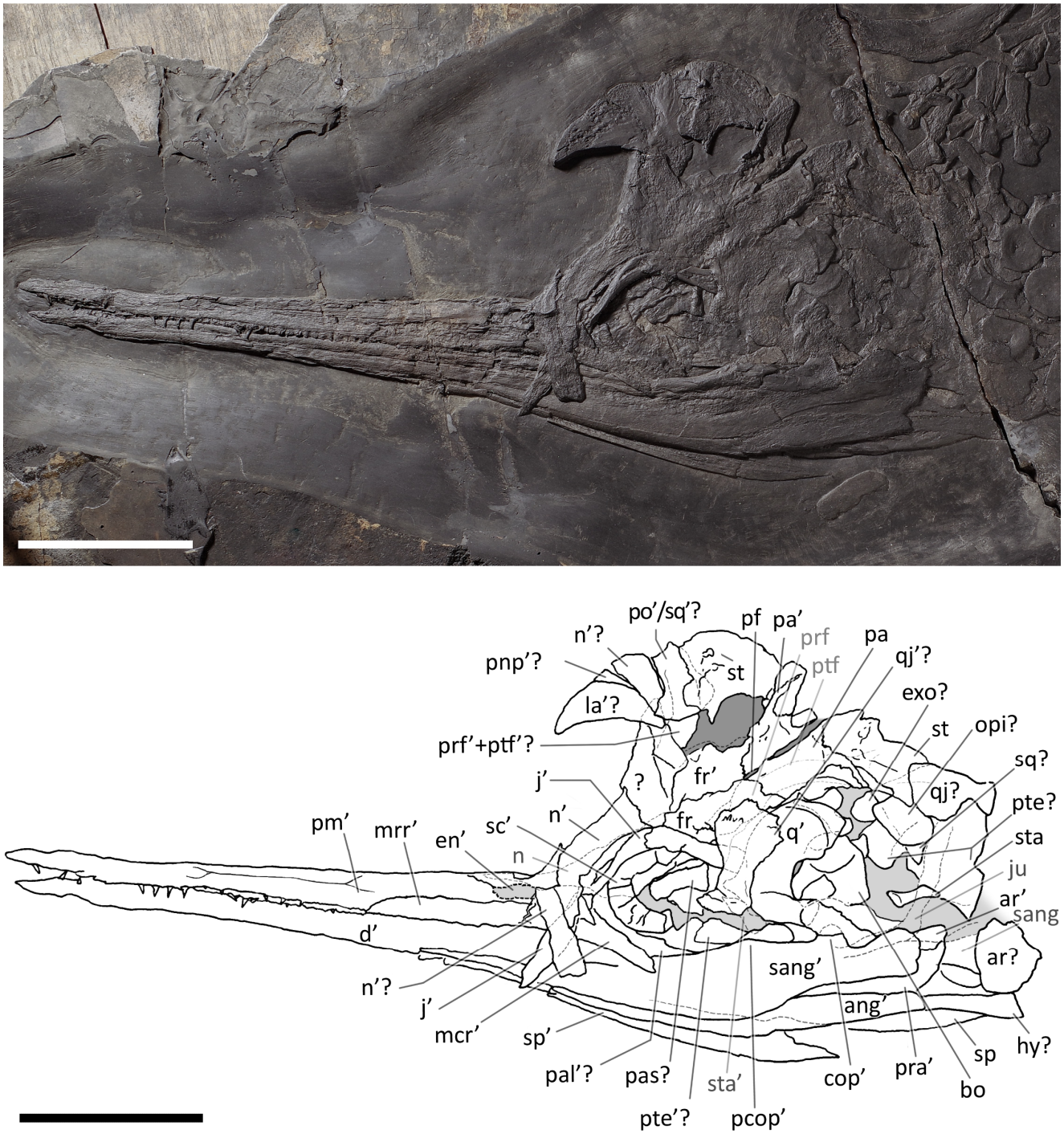

Fig. 6.4 - Skull and mandible of Besanosaurus leptorhynchus holotype BES SC 999, and their interpretative drawings. Grey dashed lines and grey labels indicate elements not visible on the surface, grey areas indicate background sediment, light grey areas indicate background bone. Abbreviations: see text. Scale bar represents 10 cm.

The left jugal is rotated relative to the orbit so that its medial surface is exposed. It now occupies a position above the left orbit, so that in the previous description of *B. leptorhynchus* it was misinterpreted as the prefrontal-postfrontal complex (Dal Sasso & Pinna, 1996). Likely, the jugal has been displaced in this position as a result of the disarticulation and displacement of the skull roof. Subsequently, the rostral portion of the jugal has been covered and then compressed below a disarticulated fragment of the left ?nasal.
The quadrate is exposed in caudolateral view; the basioccipital, the right stapes, the putative right opisthotic, and right exoccipital are exposed in occipital (caudal) view and clustered close to one another. Several bones are hidden under the elements exposed on the surface. These include the left stapes, the right prefrontal and postfrontal (located under the right parietal and frontal), a small part of the basioccipital, the right squamosal, still articulated with the right jugal, the right elements of the lower jaw, the right maxilla, the right premaxilla, and the palatal elements (vomers, palatines and pterygoids). A great portion of the right nasal is covered by the left sclerotic ring, the left jugal, and the left nasal, but it is exposed caudally adjacent to the right frontal.

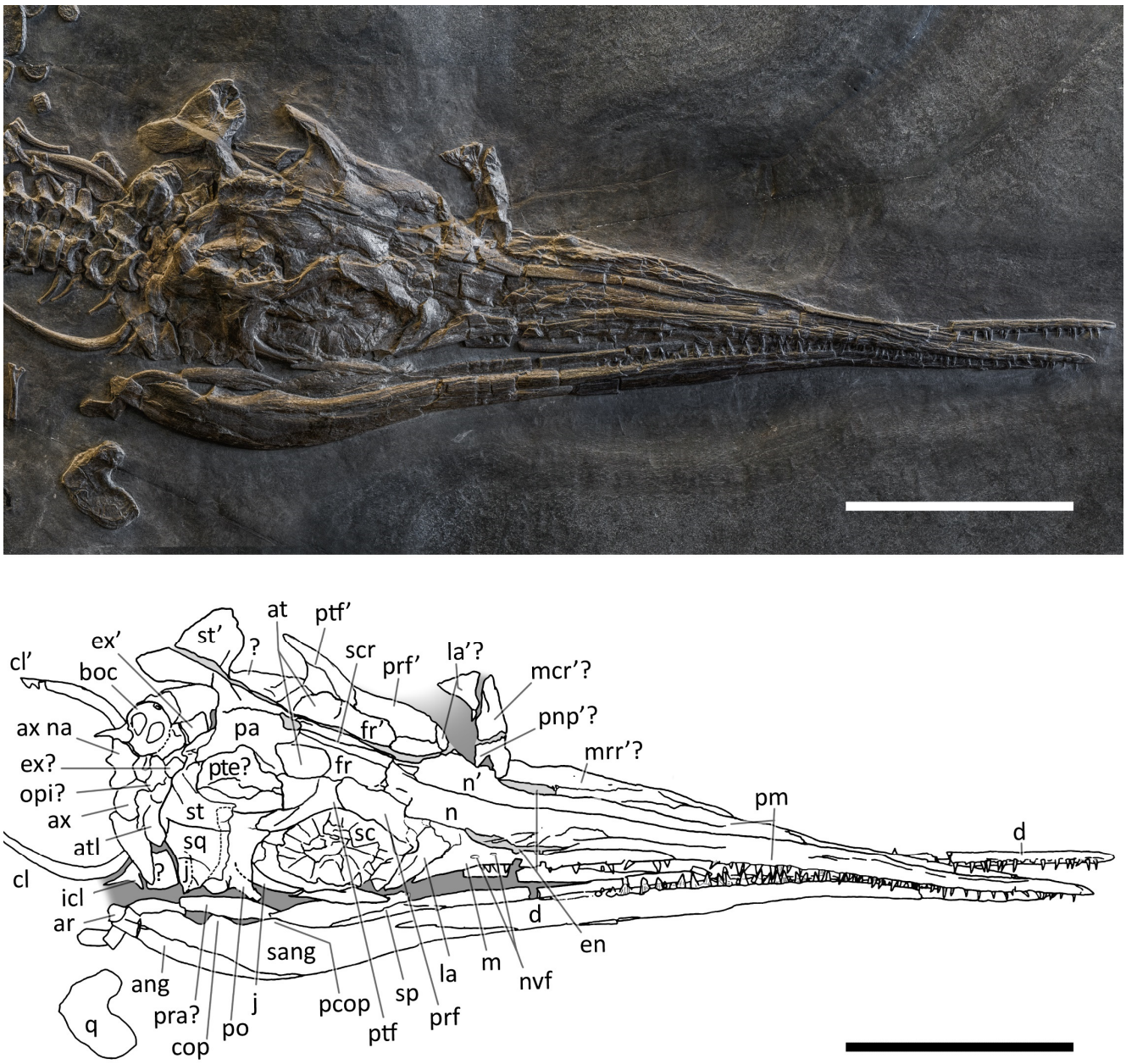

Fig. 6.5 - Skull and mandible of PIMUZ T 1895, and their interpretative drawings. Grey dashed lines indicate portions of missing elements preserved as counterprints, grey areas indicate background sediment, light grey areas indicate background bone. Abbreviations: see text. Scale bar represents 10 cm.

PIMUZ T 4376. This is the best articulated and least deformed skull (Fig. 6.5). Almost all elements from both sides of the skull roof are visible, thanks to a dorsal rotation that likely occurred during very slow plastic deformation of a soupy sea bottom substrate. Symmetric positions with respect to the sagittal line are retained by all bones, except for the caudal-most portion of the left ?lacrimal. The right supratemporal shows the medial process still connected to the right parietal, which preserves the sagittal crest, and the lateral portion of the bone, still in articulation, delimits the caudodorsal and the caudolateral margin of the supratemporal fenestra. The occipital area is disarticulated, with the basioccipital rotated and covering the paired elements of the left side. The right orbit and the bones bordering its caudoventral margin are slightly displaced dorsoventrally; the same has happened to the right narial opening. Only the lower right jaw is exposed and well visible in lateral view, with an unusual upside-down rotation of the detached rostral tip (rotated by 180° and curiously parallel to the right premaxilla).

PIMUZ T 1895. This specimen (Fig. 6.6) is mainly exposed on its left side, but is in a way very similar to PIMUZ T 4376, i.e., with the skull roof well-exposed in dorsal view, the circumnarial and orbital regions slightly compressed but visible in lateral view, and the lower jaw mediolaterally compressed and visible in lateral aspect. The bones of the latter are more displaced, so that the main elements of both sides can be seen for most of their length. Just caudal to the orbit, a vertical fracture in the bituminous matrix crosses the skull, leaving a gap of missing bone pieces. In contrast to PIMUZ T 4376, here the occipital region is not fully preserved.

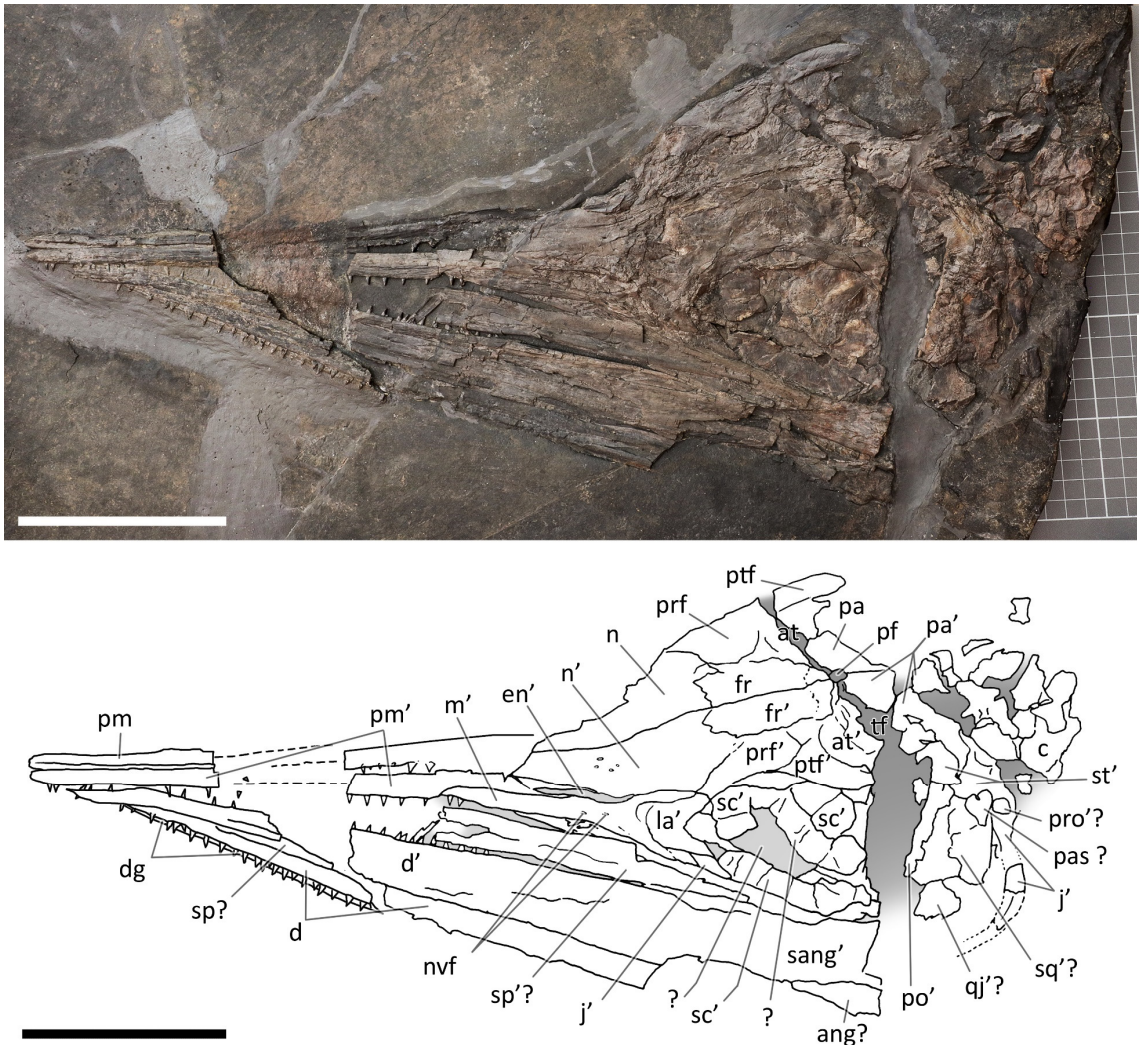

Fig. 6.6 - Skull and mandible of PIMUZ T 1895, and their interpretative drawings. Grey dashed lines indicate portions of missing elements preserved as counterprints, grey areas indicate background sediment, light grey areas indicate background bone. Abbreviations: see text. Scale bar represents 10 cm.

PIMUZ T 4847. The skull of PIMUZ T 4847 (Fig. 6.7) is detached from the body, exposed in ventral view, and mostly disarticulated. The lower jaw bones lay on the two sides of the skull at some distance, partly still articulated. Unfortunately, most elements of the skull roof and the occipital region have been dispersed and lost. Both jugals are exposed in medial view and the left one is close to its original position, although missing its rostral tip. From the postorbital region of the skull only the left quadrate, the right articular and the right quadratojugal are clearly identifiable. Some bones of this specimen are impossible to identify due to its poor preservation.

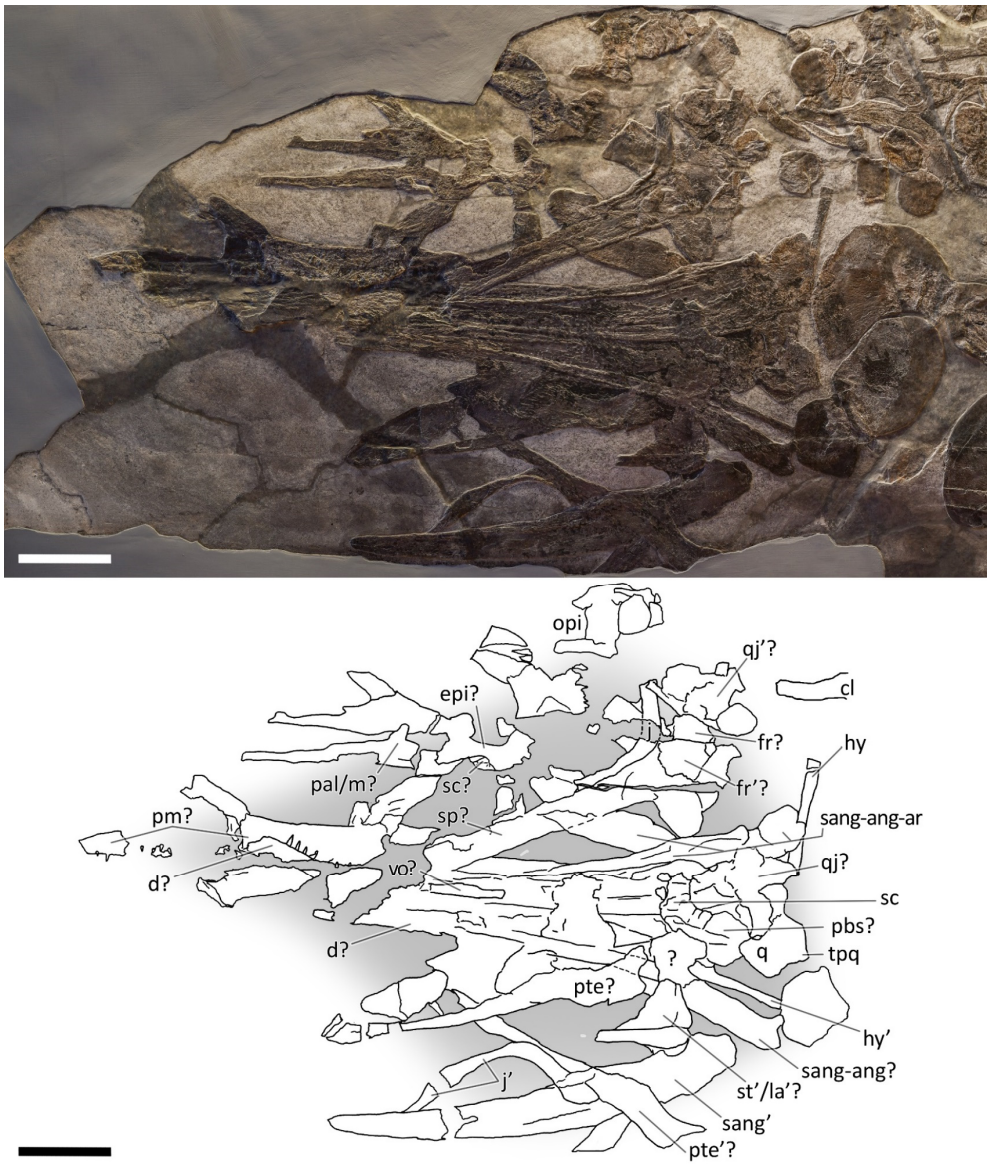

Fig. 6.7 - Skull and mandible of PIMUZ T 4847, and their interpretative drawings. Grey areas indicate background sediment. Abbreviations: see text. Scale bar represents 10 cm.

GPIT 1793/1. This skull was described and designated as the holotype of *Mikadocephalus gracilirostris* by Maisch & Matzke (1997a). The cranial elements are mostly disarticulated and scattered on the three slabs of the bituminous matrix (Fig. 6.8). Despite this, the dorsal-most bones of the skull roof are still in articulation (part of the nasals, frontals, prefrontals, postfrontals and parietals), and are exposed in internal view. In addition, on both sides of the skull, the lateral portions of the prefrontals and postfrontals (i.e. supraorbital arches) are broken and dislocated, so that their dorsolateral surfaces are exposed lying on top of the internal surface of the skull roof. In our paper we propose a new interpretation of this specimen (Fig. 6.8 and description below), which allows for the attribution of GPIT 1793/1 to *B. leptorhynchus*.

BES SC 1016. This specimen lacks the tip of the rostrum and some occipital elements (Fig. 6.9). The skull is partly disarticulated and incomplete. Some of the right dorsal elements of the skull roof (prefrontal, postfrontal, frontal and parietal) can be recognized; they delimitate a very deformed orbit and temporal fossa. The left jugal and maxilla are preserved in lateral view and are almost complete. The left premaxilla is also preserved in lateral view but it is missing the rostral tip; at its caudal end, the supranarial and subnarial processes are clear and intact, well-defining the rostral portion of the left external naris. The left dentary is exposed laterally, whereas the left surangular is exposed in medial view; the right lower jaw is visible in dorsal view. Remarkably, this specimen preserves both pterygoids which are well exposed and still articulated with each other.

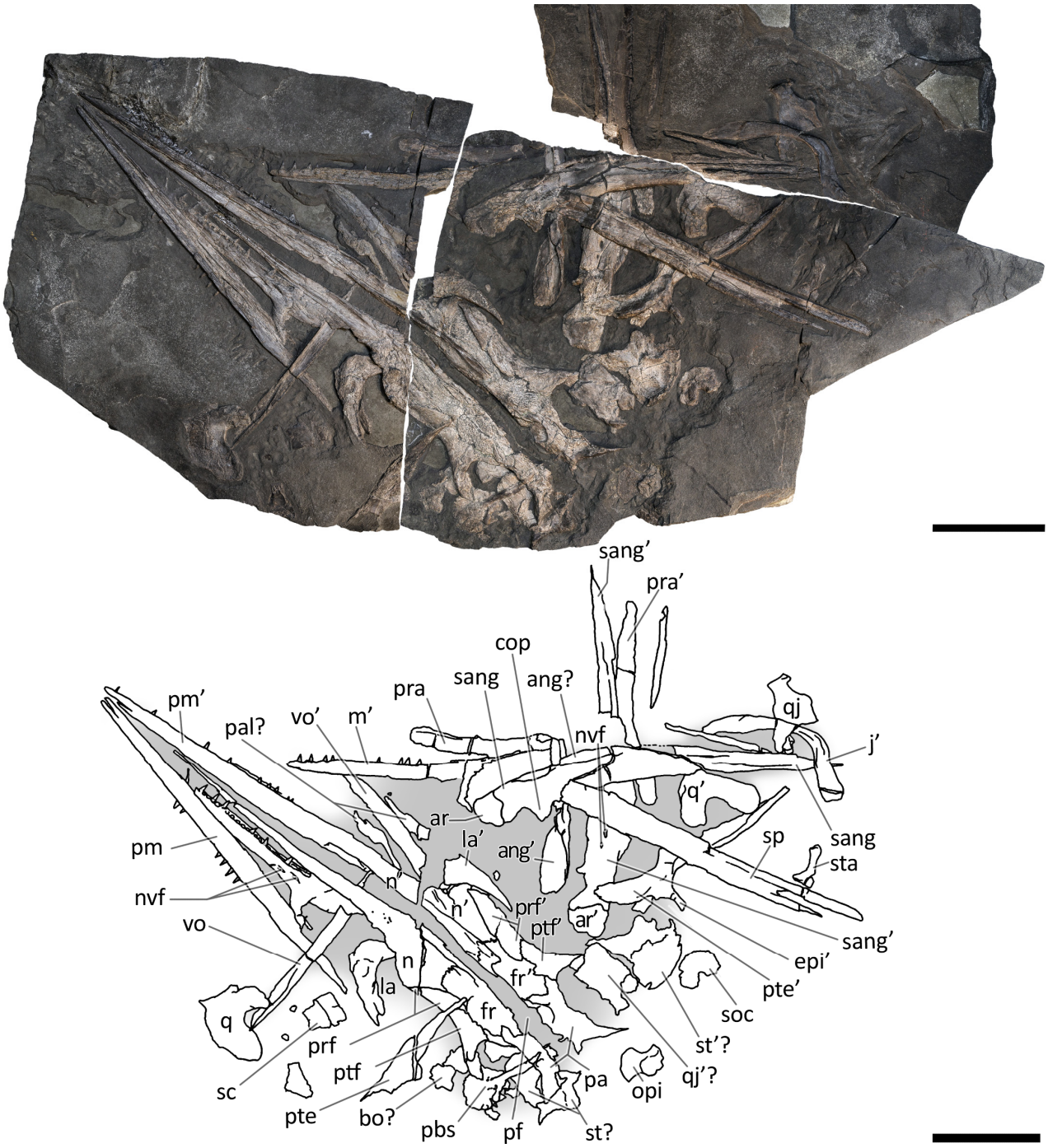

Fig. 6.8 - Skull and mandible of GPIT 1793/1, and their interpretative drawings. Grey dashed lines and grey labels indicate elements not visible on the surface, grey areas indicate background sediment, light grey areas indicate background bone. Abbreviations: see text. Scale bar represents 10 cm.

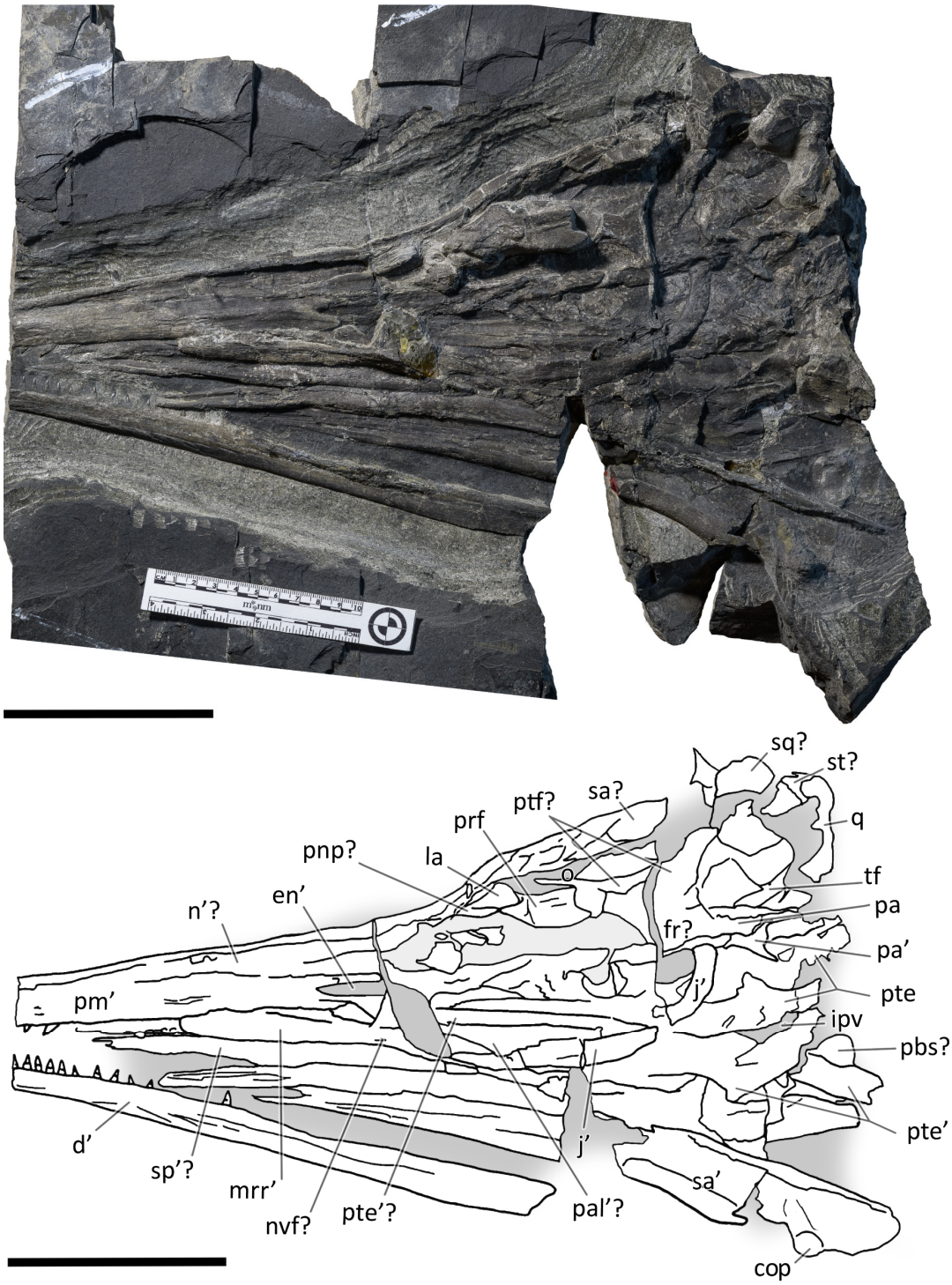

Fig. 6.9 - Skull and mandible of BES SC 1016, and their interpretative drawings. Grey areas indicate background sediment, light grey areas indicate background bone. Abbreviations: see text. Scale bar represents 10 cm.

6.4.3 Methods

X-ray computed tomography (CT) was performed on the whole skeleton of the holotype of *B. leptorhynchus* and on BES SC 1016 with a Siemens Somatom Definition Dual Source CT Scanner at the Radiology Department of the Fondazione IRCCS "Cà Granda" Ospedale Maggiore Policlinico di Milano. The best CT imaging was obtained with a bone algorithm on transverse (axial) slices with 140 kV voltage and 180–270 mA current and a slice thickness of 0.3 mm (Crasti, 2019). Data were exported in DICOM format using eFilm (v. 1.5.3; Merge eFilm, Toronto, ON, Canada). Analysis and post-processing were performed with RadiAnt, 3DimViewer, and Synedra View Personal. Multiplanar reconstructions (MPR) and volume

rendering reconstructions (VR) allowed to inspect the bones hidden under other ones within the matrix, otherwise impossible to study without damaging the fossil (Fig. 6.10).

We used photogrammetry to visualise the cranial anatomy of specimens BES SC 999, PIMUZ T 4376, and GPIT 1793/1 (File S1, S2, and S3). 3D models of the skulls were obtained with Meshroom by processing around 100 shots for each specimen. Photos of all studied specimens were taken with a Nikon D3500 camera.

To test the phylogenetic position of *Besanosaurus leptorhynchus* we used a modified matrix (see discussion) from Huang et al. (2019). This was analysed in TNT 1.5 (Goloboff et al, 2008; Goloboff & Catalano, 2016), with memory set to hold 99,999 trees. The New Technology search option (a combination of Sectorial Search, Ratchet, Drift, and Tree fusing, with 100 random addition sequences) was used, followed by a round of TBR branch-swapping. Bremer support values were calculated in TNT 1.5 using the built-in Bremer Support tool.

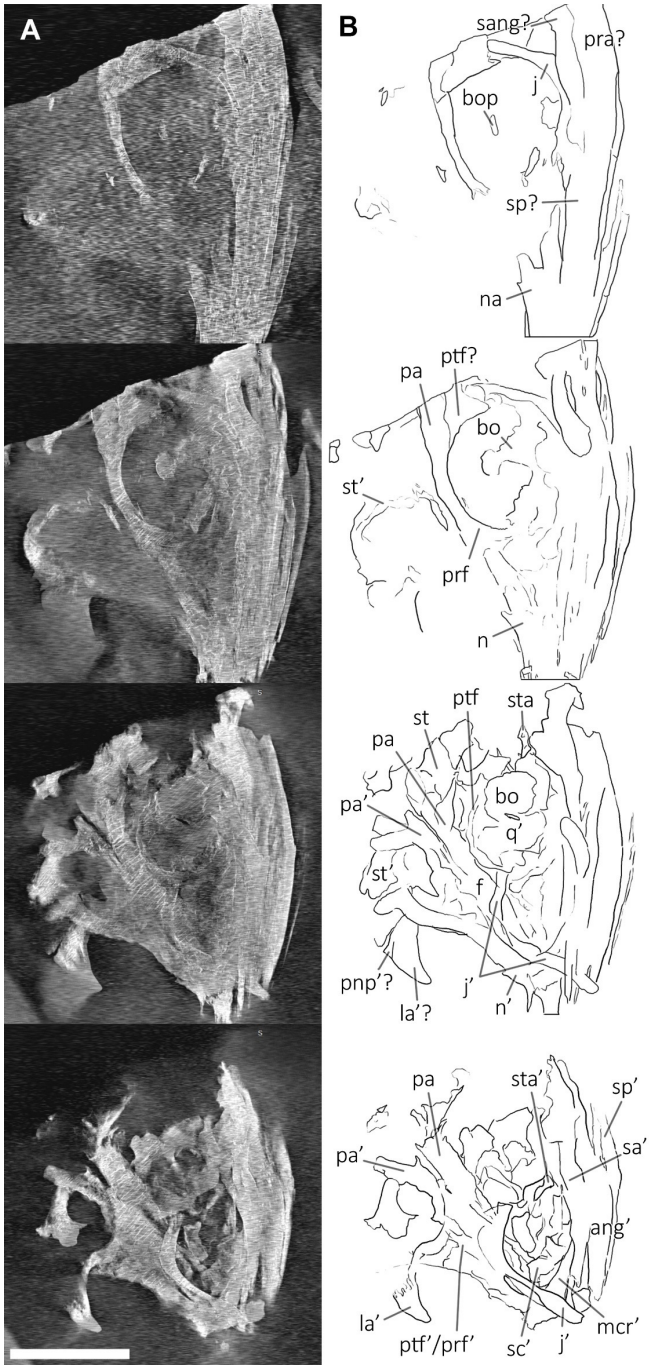

Fig. 6.10 - Selected (most informative) CT slices of the postnarial region of the holotype of *Besanosaurus leptorhynchus* (BES SC 999), ordered by depth (top to bottom, from the deepest to the most surface level). (A) original slices; (B) slices interpretations. Abbreviations: see text. Scale bar represents 10 cm.

6.5 Results: revised taxonomy of *Besanosaurus leptorhynchus*

6.5.1 *Mikadocephalus gracilirostris* as a junior synonym of *Besanosaurus leptorhynchus*

Maisch & Matzke (1997*a*) recognized the following characters as possible autapomorphies of *Mikadocephalus gracilirostris*: 1) exceedingly slender and gracile snout; 2) presence of a triangular medioventral process on the quadrate; 3) a very large and well-developed coronoid process on the surangular; 4) an elongated quadrate process of the pterygoid; 5) maxillary teeth implantation thecodont anteriorly, aulacodont posteriorly; 6) large body size. On the basis of our observations (detailed in the bone-by-bone descriptions below), specimen GPIT 1793/1 shares all these characters with the holotype of *B. leptorhynchus* (except character 4, not visible in the latter) and with all other specimens examined (BES SC 1016, PIMUZ T 4376, PIMUZ T 4847 and PIMUZ T 1895), wherever the characters are preserved (e.g., the pterygoid character is shared by GPIT 1793/1, PIMUZ T 4847 and BES SC 1016).
In general, no autapomorphies supporting and justifying a distinction of *Mikadocephalus gracilirostris* from *Besanosaurus leptorhynchus* can be found in GPIT 1793/1 and BES SC 999. For these reasons we consider *Mikadocephalus gracilirostris* a junior synonym of *Besanosaurus leptorhynchus*, as previously hypothesized by Sander (2000:15) and McGowan & Motani (2003:127). Consequently, subsequent assignment of the PIMUZ shastasaurid material to *Mikadocephalus gracilirostris* (i.e., PIMUZ T 4376; Maisch & Matzke, 2000) must be rejected, and the valid taxon name for all the referred material remains by priority *Besanosaurus leptorhynchus* Dal Sasso & Pinna, 1996, according to the ICZN (1999).
Maisch & Matzke (2000) deemed the relative size of the skulls of *Cymbospondylus* and *Besanosaurus* as very small when compared to body length, equaling about “one-quarter of the presacral length”; the authors then considered this character to be in stark contrast to the condition in *Mikadocephalus gracilirostris*, whose skull,referring to PIMUZ T 4376 was “more than half the length of the presacral vertebral column”. This has been regarded by Maisch & Matzke (2000) as a valid diagnostic character, reported as clearly unrelated to ontogeny and distinguishing *Besanosaurus* from *Mikadocephalus*, and *Mikadocephalus* from other shastasaurids known at that time. However, given that in most ichthyosaurs the cranium displays negative allometry vs body size during growth (McGowan, 1973), we deem it plausible that this difference can be attributed to ontogeny, and therefore we consider the six specimens described as a possible ontogenetic series of *B. leptorhynchus* (discussed below).
Moreover, our analysis shows that there are no observable qualitative characters of the skull and mandible that differ between the proposed holotypes: treating the proposed taxa as synonymous is therefore logical. In addition, Maisch & Matzke (2000) compared two different (i.e., non-homologous) lengths (presacral vertebral column vs presacral length) to highlight that anatomical difference between *Besanosaurus* and *Mikadocephalus* as diagnostic: it is true that the skull of PIMUZ T 4376 is a few centimeters longer than half the length of the presacral vertebral column, but is also true that the holotypic skull of *Besanosaurus* is around one-third of the presacral length of the vertebral column (which equals, as the authors stated, “one-quarter of the presacral length”, a length that includes the skull itself and not just the presacral vertebral column). This different ratio can be explained by intraspecific (possibly ontogenetic) variation, as we demonstrate below.
Maisch & Matzke (1997*a*) also mentioned that the interpterygoid vacuity of *Mikadocephalus* must have been large, and similar to post-Triassic ichthyosaurs. In reality, this cannot be unambiguously determined since a good portion of the medial border of the left pterygoid in GPIT 1793/1 has been

broken and dislocated above the rest of the bone. On the other hand, in BES SC 1016, where the two pterygoids are still semi-articulated, the interpterygoid vacuity is narrower than that hypothesized for the holotype of *Mikadocephalus*. This space is actually larger than in *Mixosaurus*, showing an intermediate condition between Lower Triassic ichthyosaurs and post-Triassic taxa. It is also comparable in size and morphology to other shastasaurids (*Guizhouichthyosaurus tangae*, IVPP V11853; '*Callawayia*' *wolonggangense*, SPCV 10305; pers. obs.).

Finally, Maisch & Matzke (1997*a*) considered the 'triangular process' of the quadrate (Maisch & Matzke, 1997:fig. 7) as a diagnostic character of *Mikadocephalus gracilirostris*. Interestingly, the right quadrate of a referred specimen of *Guanlingsaurus liangae* (SPCV 03107; pers. obs.) also shows such a 'triangular process' (Fig. 6.S4). Furthermore, the *B. leptorhynchus* holotype (BES SC 999), and referred specimens PIMUZ T 4376 and T4847, also possess this character (see quadrate description). Therefore, we consider it more plausible to provisionally treat this character as a possible shastasaurid synapomorphy, rather than a *Besanosaurus* apomorphy (presence/absence of 'triangular process' not determined for other shastasaurids except *Besanosaurus* and *Guanlingsaurus*).

Given that our comparison with the former holotype of *M. gracilirostris* found a substantially identical osteology, both in the shape and interrelationships of the bones, we propose the junior synonymy of the taxon with respect to *B. leptorhynchus*. As a consequence, the former holotype and only specimen of *M. gracilirostris* is here redescribed and discussed together with all other *Besanosaurus* material.

6.5.2 Systematic palaeontology

ICHTHYOPTERYGIA Owen, 1840
ICHTHYOSAURIA Blainville, 1835
MERRIAMOSAURIA Motani, 1999
BESANOSAURUS Dal Sasso & Pinna, 1996
Besanosaurus leptorhynchus Dal Sasso & Pinna, 1996

Type and only species. *Besanosaurus leptorhynchus* Dal Sasso & Pinna, 1996; middle Besano Formation (uppermost Anisian, Middle Triassic), Monte San Giorgio, Italy/Switzerland.

Type specimen. Complete semi-articulated skeleton, labelled as BES SC 999 in the catalogue of the MSNM (BES SC is an acronym for Besano Sasso Caldo), and coded as 20.S288-2.2 in the Inventario Patrimoniale dello Stato (State Heritage Database).

Type locality. Sasso Caldo site, Besano, Varese Province, NW Lombardy, N. Italy. Geographical coordinates: 45°54'03.7"N 8°55'10.6"E, elevation 650 m.

Type horizon and distribution. middle Besano Formation (*sensu* Bindellini et al., 2019), uppermost Anisian (*N. secedensis* Zone *sensu* Brack et al., 2005), Middle Triassic.

Referred material. PIMUZ T 4376 (complete semi-articulated skeleton with the best-preserved skull of the taxon), PIMUZ T 1895 (incomplete semi-articulated skeleton with well-preserved skull), PIMUZ T 4847 (incomplete semi-disarticulated skeleton with disarticulated skull), GPIT 1793/1 (disarticulated

skull, formerly the holotype of *Mikadocephalus gracilirostris*), BES SC 1016 (incomplete semi-disarticulated skull; the specimen is coded as 20.S288-2.6 in the Inventario Patrimoniale dello Stato - State Heritage Database);

Emended cranial diagnosis. Large ichthyosaur with one possible autapomorphy – a caudoventral exposure of the postorbital in the temporal region – and the following combination of cranial characters: extremely long, slender, and gracile snout; frontal rostrocaudally elongate and relatively flat; frontal participation in the temporal fossa but not to the temporal fenestra; L-shaped jugal; 'triangular process' on the medioventral border of the quadrate; prominent coronoid (preglenoid) process of the surangular, distinctly rising above the dorsal margin of the surangular; tiny conical teeth with a coarsely-striated crown surface and deeply striated roots; mesial maxillary teeth set in sockets; distal maxillary teeth set in a groove shorter than half of the rostral ramus of the maxilla.

6.6 Results: revised cranial osteology of B*esanosaurus leptorhynchus*

6.6.1 Cranial openings

External naris. It is difficult to infer the shape of the external naris on the holotype of *B. leptorhynchus* BES SC 999 (Fig 4). In GPIT 1793/1 the naris is not clearly preserved since the rostrum is disarticulated and the caudal ends of the premaxillae are likely incomplete. In PIMUZ T 4376, although the skull is in very good condition, the rostral portion of the right naris is damaged and the elements bordering it are severely crushed. The best-preserved naris can be seen in specimen PIMUZ T 1895 (Fig. 6.11): it is long and slender. The dorsal margin of the naris is built by the caudodorsal process of the premaxilla and by a short portion of the lateroventral margin of the nasal, whereas the ventral margin is made by the premaxilla, rostrally, and the maxilla, mediocaudally. The external naris is pointed into a sharp apex rostrally and its rostral and caudal margins are formed, respectively, by two short and sharp caudal processes of the premaxilla (supranarial and subnarial processes, the latter being shorter in length); by the nasal (caudodorsal half) and by the postnarial process of the maxilla (caudoventral half). The caudal portion of the external naris is dorsoventrally wider. In PIMUZ T 1895 and BES SC 1016 the rostral margin of the left naris is more intact than in all other specimens, showing that the supranarial process of the premaxilla covers approximately 50% of the dorsal margin of the external naris, whereas the subnarial process likely covers one-third of the ventral margin of the external naris. The processes are not well-preserved in PIMUZ T 4376, but in GPIT 1793/1 and BES SC 999 (Fig. 6.12) the subnarial process is partially preserved and similar in length to PIMUZ T 1895 and BES SC 1016, whereas the supranarial processes are broken off. Therefore, very likely all specimens originally possessed the same morphology as that seen in PIMUZ T 1895 and BES SC 1016.
In well-preserved skulls of *Guizhouichthyosaurus tangae* (IVPP V11869, pers. obs.; Maisch et al., 2006*b*; Fig. 6.S1) and in the type specimen of '*Callawayia' wolonggangense* (SPCV 10306; pers. obs.) the external naris is bordered by the premaxilla rostrodorsally and rostroventrally, the nasal caudodorsally, and the maxilla caudoventrally: the premaxilla bifurcates caudally into a prominent supranarial process and a smaller subnarial process, thus contributing also to the rostroventral margin of the external naris, with the maxilla not forming the entire ventral margin. In *Shonisaurus* sp. (Callaway & Massare, 1989: fig. 3; Motani, 1999) the anatomy is very similar, except that the nasal is excluded from the caudodorsal margin of the external naris by the premaxilla. In all three taxa, as in *Besanosaurus*,

the external naris is proportionally long rostrocaudally and narrow dorsoventrally, especially in its rostral portion. The circumnarial region of *Besanosaurus* is more similar to *Guizhouichthyosaurus* and '*Callawayia' wolonggangense*, as a nasal contribution is visible caudodorsally, and the ventral margin is formed by the premaxilla and the maxilla. In *Guizhouichthyosaurus* (IVPP V11869; Fig. 6.S1) the supranarial process is more dorsoventrally expanded than in *Besanosaurus* and rostrocaudally reaches approximately 50% of the length of the external naris, whereas the subnarial process is slightly shorter and smaller than the supranarial process; in '*Callawayia' wolonggangense* (SPCV 10306; pers. obs.) the supranarial process is stouter than in *Besanosaurus*, extending at least up to approximately 50% of the dorsal length of the external naris, and the subnarial processes almost reaches the caudal margin of the external naris.

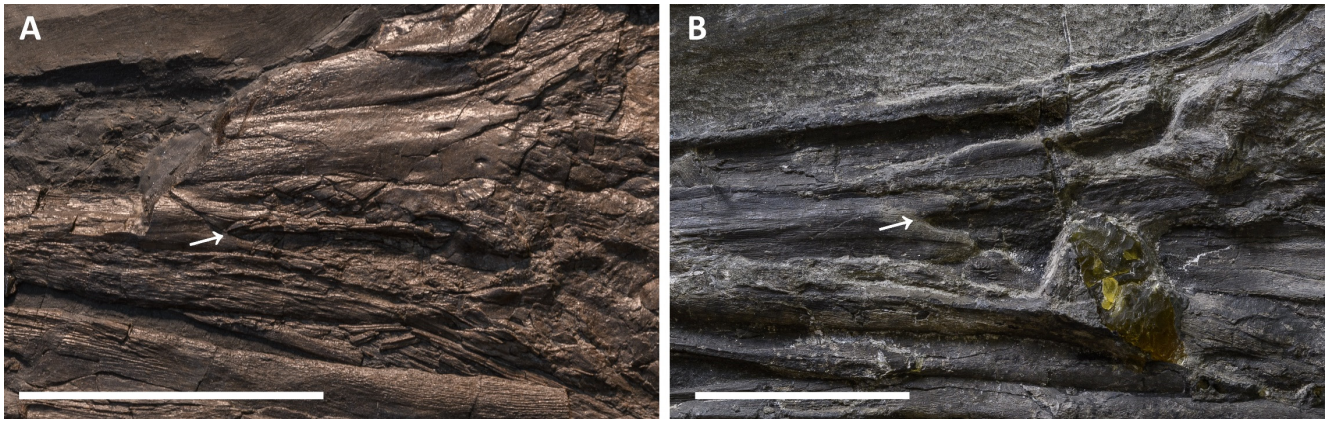

Fig. 6.11 - External naris and perinarial region of *Besanosaurus leptorhynchus*. (A) PIMUZ T 1895; (B) BES SC 1016. The white arrows point to the rostral tip of the external naris in both specimens. Scale bars represent 5 cm.

Orbit. The orbit is the largest cranial opening. In *Besanosaurus* it is oval-shaped, as tall as the scleral ring and 4/3 rostrocaudally longer than high. It is bordered by the jugal ventrally, the postorbital caudally, the postfrontal dorsally, the prefrontal rostrodorsally, and the lacrimal rostrally. The best-preserved orbit can be observed in specimen PIMUZ T 4376, where almost all the bones are still articulated, or semi-articulated (jugal, lacrimal). In PIMUZ T 1895 the contacts of the elements are the same, and in all other specimens that we refer to *B. leptorhynchus* the disarticulated circumorbital elements show very similar shapes and proportions. The anatomy of the orbit of *Besanosaurus* is more similar to that in *Guizhouichthyosaurus* (IVPP V11869; Maisch et al., 2006*b*) than to '*Callawayia' wolonggangense* (SPCV 10306; Chen et al., 2007), in which all the bones that border the orbit seem to be reduced to accommodate a bigger orbit.

Supratemporal fossa. The supratemporal fossa, that includes the supratemporal fenestra, is built by a portion of the parietal medially, of the frontal rostromedially, of the postfrontal rostrolaterally, of the postorbital laterally, and of the supratemporal laterocaudally and caudomedially. In *Besanosaurus* the supratemporal fossa includes a wide semioval rostral terrace ('anterior terrace' of Motani 1999:char. 14), almost as long as the supratemporal fenestra. This terrace is composed of the caudal two-fifths of the frontal, a medial flange of the postfrontal, and in minor part by a rostrolateral process of the parietal. The supratemporal terrace is nicely preserved almost in 3D in specimen PIMUZ T 4376, well-exposed in PIMUZ T 1895, but not visible in the rotated skull roof of BES SC 999 and GPIT 1793/1. The supratemporal fossa seems to be proportionally smaller in *Besanosaurus* than in *Guizhouichthyosaurus tangae* (IVPP V11865; pers. obs.) and *Guanlingsaurus liangae* (SPCV03107; pers. obs.); on the other

hand, *Besanosaurus* 'anterior terrace' is bigger than in *Shastasaurus* (UCMP 9017; Sander et al. 2011) and proportionally similar in size to that in '*Callawayia' wolonggangense* (SPCV 10306; pers. obs.).

Supratemporal fenestra. This fenestration, seen in dorsal view, occupies half the area of the supratemporal fossa and opens on its caudolateral border. The best articulated specimens (PIMUZ T 4376 and PIMUZ T 1895) clearly show that it is bordered by the parietal medially, the postfrontal rostrally, the postorbital laterally, and the supratemporal laterocaudally. The frontal does not directly build the profile of the temporal fenestra, although it indeed builds a great portion of the 'anterior terrace' of the supratemporal fossa. The same can be observed in GPIT 1793/1 and BES SC 999, although the fenestration is exposed in ventral (internal) view. The lateral margin of the supratemporal fenestra coincides with that of the supratemporal fossa. The supratemporal fenestra of *Besanosaurus* is one of the smallest observed in the clade Shastasauridae, comparable to that in '*Callawayia*' *wolonggangense* (SPCV 10305; Chen et al., 2007). As in *Guizhouichthyosaurus* (Maisch et al., 2006*b*), but unlike '*Callawayia' wolonggangense* (Chen et al., 2007), and *Guanlingsaurus liangae* (Sander et al., 2011), the frontal does not contribute to the rostral border of the fenestra.

Parietal foramen. In *Besanosaurus* the parietal foramen is located between the two parietals and the two frontals. It opens along the medial sagittal line at about the level of the caudal margin of the scleral rings, and its rostral border is at the level of the rostral border of the supratemporal fenestrae. This is best seen in PIMUZ T 1895 and PIMUZ T 4376, but a small elongate parietal foramen, positioned across the parietals and the frontals, is also preserved in BES SC 999, and in GPIT 1793/1. In PIMUZ T 4376 the parietal foramen is rostrally bordered by the caudal-most ends of the frontals and is positioned mainly between the rostromedial processes of the parietals, which do not contact each other on the midline. This condition differs from the one observed in *Guanlingsaurus liangae* (Sander et al., 2011), where the parietal foramen is placed more caudally and it is fully enclosed in between the two rostromedial processes of the parietal. For this reason, the parietal foramen of *Besanosaurus* is more similar to that of *Guizhouichthyosaurus tangae* and *'Callawayia' wolonggangense*, although it is proportionally slightly smaller than in the latter taxon. In contrast, in some Parvipelvia, the frontals form most of the rostral and lateral margins of the parietal foramen, only leaving the caudal-most margin to the parietal (McGowan, 1973; Kear, 2005).

Foramen magnum. The preservation of the foramen magnum is exceedingly rare in ichthyosaurs due to the nature of the ossification of the braincase; in fact, it is not preserved in its integrity in any of the examined fossils of *Besanosaurus*. Nevertheless, its profile can be inferred from two specimens: PIMUZ T 4376, where the basioccipital shows its dorsal surface and very well-preserved facets for the exoccipitals; and GPIT 1793/1, where the supraoccipital forms the dorsal margin of the foramen magnum. In caudal view, it should possess a sub-pentagonal profile, with rounded margins and equal sides, possibly being slightly taller than wide. These margins are defined by four different bones, which in clockwise order are the supraoccipital, the right exoccipital, the basioccipital, and the left exoccipital.

6.6.2 Scleral plates

The sclerotic ring is complete and well-preserved in PIMUZ T 4376; it is also almost complete, although partially disarticulated, in PIMUZ T 1895. At least seven distinct scleral plates, of which six are in

articulation (and somewhat imbricate), are still positioned in the left orbit of BES SC 999, only partially covered by a fragment of the putative left palatine, and slightly displaced rostrally with respect to their original position inside the orbit. These plates form almost one half of the entire sclerotic ring that occupied a major part of the orbit. On the whole, we can thus calculate that the sclerotic ring of *Besanosaurus* was composed of approximately 15 to 17 plates.
Each scleral plate is subrectangular to trapezoidal and characterised by fine, sometimes undulating striations that radiate from the base to the lateral surface. Here the plates bend medially at about 45°, showing a short peripheral surface measuring about 1/3 of the lateral surface.
Compared to Parvipelvia, the sclerotic ring of the *Besanosaurus* holotype is proportionally smaller if normalised to the body length of the animal (see Motani et al., 1999 for the discussion of this ratio), albeit being bigger than that in *Cymbospondylus* (PIMUZ T 4351; Sander, 1989) and similar in size to *Mixosaurus* (BES SC 1000). The number of sclerotic plates in *Besanosaurus* is also similar to that in *Mixosaurus* (McGowan & Motani, 2003:24).

6.6.3 Dermal skull roof

Premaxilla. The holotype of *B. leptorhynchus* (BES SC 999) preserves complete and articulated rostral elements. The slender rostrum which inspired its specific name entirely comprises narrow and elongate dentary and premaxillary bones. The latter likely overlap for some extent the lateral surface of the maxillae, and caudomedially accommodate equally narrow and very elongate vomers, as shown by the disarticulated vomers exposed in specimen GPIT 1793/1, and by the articular surfaces of the almost identical premaxillae. Complete premaxillae are also preserved in PIMUZ T 4376, where both the left and right elements are visible.
In both BES SC 999 and PIMUZ T 4376, the premaxilla rostrally terminates in a rounded tip, which extends more rostrally than the tip of the dentary, thus resulting in an overbite of less than one cm (some postmortem deformation might have occurred). The tips of the premaxillae are missing, like most of the rostral halves of the jaws, in BES SC 1016, which in turn helps to describe the premaxillary-maxillary contacts.
In the holotype of *B. leptorhynchus,* the ventral surface of the premaxilla hosts several deep sockets that are also clearly visible in BES SC 1016 (Fig. 6.10). The premaxilla of BES SC 999 hosts at least 35 (estimated) teeth that interlock with the dentary teeth.
The left premaxilla in this specimen still articulates caudoventrally with the left maxilla and dorsomedially with a long and slender rostral process of the left nasal. The premaxilla terminates caudally with very thin supranarial and subnarial processes (better described above).
In the holotype BES SC 999, a caudorostrally extended area of collapsed premaxillary bone is visible in front of the naris; this possibly highlights the presence of an internal weak point. Something similar can also be observed in PIMUZ T 4376 and T 1895 and, curiously, in the same area, the right premaxilla of GPIT 1793/1 is also collapsed and fractured along a horizontal line that was described by Maisch & Matzke (1997*a*) as the anterior (i.e., rostral) margin of the external naris. This, actually, could represent the rostral-most extension of a possible pneumatic recess of the internal naris (as seen, for instance, in the aquatic adaptations of *Spinosaurus*; Dal Sasso et al., 2014, Ibrahim et al., 2014). The subnarial and supranarial processes, described by Maisch & Matzke (1997*a*) for GPIT 1793/1 are here considered taphonomic artefacts. If the relative lengths of the supranarial and subnarial processes in PIMUZ T 4376 were similar to those reconstructed by Maisch & Matzke (1997*a*), the external naris of the specimen would be unnaturally long, proportionally even longer than in the reconstruction published by Maisch & Matzke (2000).

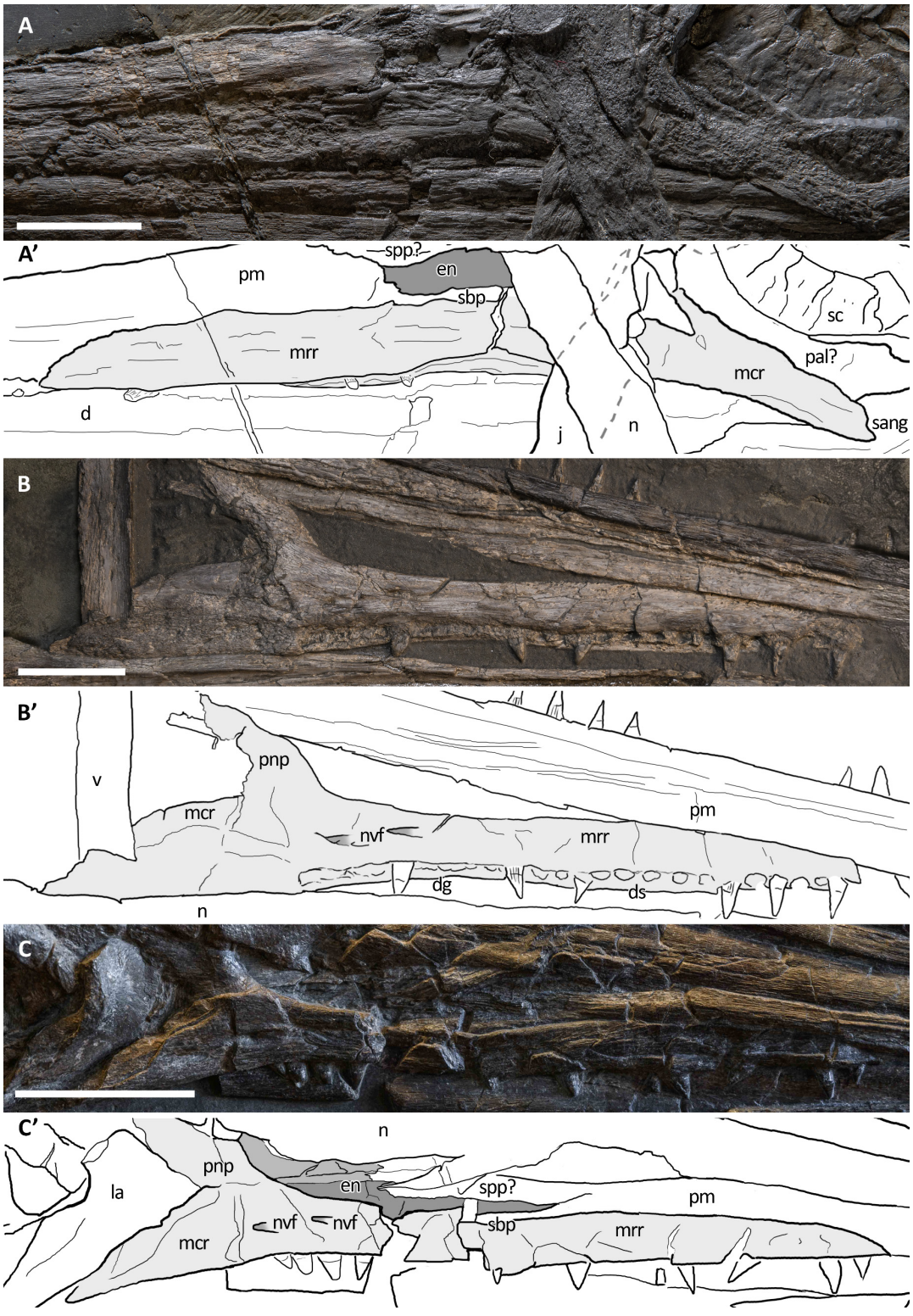

Fig. 6.12 - Maxillae of *Besanosaurus leptorhynchus*. Maxillae referable to *Besanosaurus leptorhynchus*. (A and A′) BES SC 999; (B and B′) GPIT 1793/1; (C and C′) PIMUZ T 4376. Light gray areas highlight the maxilla, darker gray areas pinpoint the external naris, when preserved. Abbreviations: see text. Scale bars represent 2.5 cm.

Maxilla. The maxilla of *Besanosaurus* (Fig. 6.12) is a craniocaudally elongate triradiate bone, as in the majority of the other Triassic ichthyosaurs (e.g., Ji et al., 2016: figs. 3–4). It is well-exposed in most of the specimens examined here, with some variation in the shape and height of the postnarial process, that we interpret as intraspecific or taphonomic variation (it is more pronounced in GPIT 1793/1 and BES SC 1016). Similarly, in BES SC 999 the main body of the maxilla looks dorsoventrally taller than in the other specimens, due to taphonomic mediolateral compression. In the holotype, the long and slender

rostral ramus of the maxilla bears around 20 (estimated) teeth that are present along the dentigerous margin from the rostral tip of the bone to the level of the rostral border of the naris. The caudal-most, tooth-bearing portion of the maxilla, below the external naris hosts the teeth in a short groove (aulacodont implantation), although 70% of the maxillary teeth are set in distinct alveoli (subthecodont implantation) well visible in GPIT 1793/1. The caudodorsally directed and curved postnarial process delimits the caudal border of the external naris and accommodates the convex rostral margin of the lacrimal. This process projects toward the prefrontal forming a contact point (PIMUZ T 4376), excluding the lacrimal from contact with the nasal. Similarly, the postnarial process forms a point contact with the prefrontal in *Guizhouichthyosaurus tangae* (IVPV 11869; pers. obs.) and *'Callawayia' wolonggangense* (SPCV 10306; pers. obs.), a condition contrasting with *Guanlingsaurus liangae* where this process is short and well separated from the prefrontal (SPCV 03107; pers. obs., Sander et al., 2011). The caudal ramus of the maxilla, which measures three-fifths the length of the rostral ramus, is toothless and in BES SC 999, PIMUZ T 4376, and T 1895 slightly bends caudally below the lacrimal, also following the natural bend of the dentary and surangular below the orbit. In GPIT 1793/1, as reported by Maisch & Matzke (1997*a*), the caudal rami of both maxillae are incomplete and are therefore shorter than in the *Besanosaurus* holotype, and toothless as well.

Specimens GPIT 1793/1, PIMUZ T 1895, and PIMUZ T 4376 clearly show two maxillary foramina below the naris, which extend rostrally into shallow, rostrocaudally elongate grooves (best preserved in GPIT 1793/1). Similar foramina are present in *Guizhouichthyosaurus tangae* (IVPP V11869, pers. obs.; GNG dq-46, Maisch et al. 2006b; Fig. 6.S1) below the postnarial process of the maxilla. Neurovascular foramina, albeit larger and more rounded in outline, are also present in the maxilla of *Guanlingsaurus liangae* (SPCV 03107; pers. obs.).

On the whole, the maxilla of *Besanosaurus* maintains similar proportions to those observed in *'Callawayia' wolonggangense* (SPCV 10306; pers. obs.), being relatively thin and slender, clearly less robust than in *Shonisaurus popularis* and *Cymbospondylus* (Camp, 1980; Sander et al., 2011). The caudal ramus of the maxilla slightly bends ventrally as in *Shastasaurus pacificus* (Sander et al., 2011). However, the postnarial process is absent in *Shonisaurus popularis* (Camp, 1980; Callaway & Massare, 1989).

Nasal. The left and right nasal bones are best preserved in PIMUZ T 4376 and GPIT 1793/1, exposed in dorsal and ventral view, respectively; in BES SC 999 they are severely deformed and fractured. The nasals of *Besanosaurus* are very slender elongate elements. They are triangular in shape and taper extremely towards the rostral region in between the premaxillae. The caudal-most portion of the bone is broader than the rostral, reaching its maximum mediolateral width at the straight lateral margin that contacts the dorsal edge of the postnarial process of the maxilla (PIMUZ T 4376). Rostrally to that edge, the nasal shows a small facet where a portion of the dorsal tip of the postnarial process of the maxilla is housed (GPIT 1793/1 and PIMUZ T 1895). The nasal borders the caudalmost dorsal edge of the naris and contributes to the dorsal side of the rostrum with a very long premaxillary contact. The nasal contacts the prefrontal laterally, but does not contact the postfrontal. Dorsocaudally the nasal forms an interdigitating suture with the frontal.

In dorsal view, the surface of the best-preserved nasal (PIMUZ T 4376) appears convex and shows sub-longitudinal striations. In ventral (i.e., internal) view (GPIT 1793/1) the nasal shows a concave smooth surface for most of its length, and a flat rugose texture in the area of the suture with the frontal; a medial dorsocaudally elongate and thin vertical process might represent the contact with the vomer.

Interestingly, the nasals of BES SC 999 and PIMUZ T 4376 are fractured where they begin to narrow rostrally, becoming thinner and slender; similar fractures are also observed in PIMUZ T 1895. This feature highlights the presence of a distinct constriction separating the gracile rostrum from the rest of the skull, as seen in BES SC 999 and PIMUZ T 4376. Just rostrally to this constriction, at least four neurovascular foramina are present in PIMUZ T 1895; similar foramina are also visible in *Guizhouichthyosaurus tangae* (IVPP V11869, pers. obs., Fig. 6.S1; GNG dq-46, Maisch et al., 2006b).

Lacrimal. The lacrimal of *Besanosaurus leptorhynchus* is approximately comma-shaped in outline in lateral view. This element displays a convex rostral margin, a concave caudal edge, and a caudoventrally pointed tip. This morphology is best seen in the right lacrimal of PIMUZ T 4376 and the left lacrimal of T 1895, which also preserve them in articulation with all other elements: the dorsal margin contacts the rostroventral process of the prefrontal; the convex rostral margin articulates with the postnarial process and a portion of the caudal ramus of the maxilla; and the caudoventral tip contacts the rostral tip of the jugal, ventrally. The concave caudal edge marks the rostral limit of the orbit.
In GPIT 1793/1 the lacrimal bones are semi-articulated and exposed in medial (internal) view, showing a concave surface and a ridged margin arising towards the pointed tips, which represents the contact with the caudal ramus of the maxilla. In BES SC 999, the putative (and deformed) left lacrimal does not show a clear articulation with the other bones.
The lacrimal of *Besanosaurus* is similar to *Guizhouichthyosaurus tangae* (GNG dq-46; Maisch et al., 2006*b*) and '*Callawayia' wolonggangense*, which namely shows a less robust anatomy (more elongate overall shape, more slender, curved and pointed tips) linked to the presence of a larger orbit (SPCV 10306; Chen et al., 2007; pers. obs.). *Platypterygius australis* shows a lacrimal semilunateshape (Kear 2005), somewhat similar to that in *Besanosaurus*, although its caudoventral extension is less developed.

Prefrontal. Although in the holotype of *B. leptorhynchus* the anatomy of the prefrontal is unclear, this bone is well-preserved in three other specimens (PIMUZ T 1895, T 4376, and GPIT 1793/1). The prefrontal in lateral view is a comma-shaped bone angled by 45°, with a rostroventrally tapered tip contacting the dorsal end of the lacrimal and the caudal end of the maxillary postnarial process. The larger caudal portion contacts the postfrontal caudolaterally, and the frontal mediodorsally. The lateroventral margin of the prefrontal is part of the orbital rim, whereas the rostromedial margin is sutured to the nasal. The lateral portion of the prefrontal is mediolaterally thickened and separated from the medial portion by a rounded ridge, that becomes even more pronounced caudally, at the level of the 'anterior terrace' of the temporal fenestra. This thickened area continues along the dorsal border of the orbit towards the postfrontal, building a prominent supraorbital crest. As a result, the cross-section of the whole skull looks roughly hexagonal-shaped, with a rounded, slightly protruding crest at the lateral edges of the prefrontal and the postfrontal.

Postfrontal. The anatomy of the postfrontal is best observed in specimen PIMUZ T 4376, although it is also visible on the left and right sides in PIMUZ T 1895 and GIPT 1793/1 (in ventral view, Fig. 6.13). The postfrontal occupies a surface of the skull roof immediately caudal to the prefrontal and is contacted by this bone rostrally. Its lateral edge is thick and sigmoid in dorsal view. This area is separated by a clear step from the medial, triangular-shaped, rostromedial process of the postfrontal. Its rostral part is elevated in comparison to its caudal part, which contributes to the rostrolateral half of the 'anterior terrace' of the supratemporal fenestra. Medially the rostromedial process contacts the caudal half of the

frontal bone, with an irregularly-shaped suture that in ventral view appears deeply interdigitating (GIPT 1793/1). Caudomedially the caudomedial process contacts the rostrolateral ramus of the parietal. The stout pointed caudal ramus of the postfrontal has a minor contribution to the lateral border of the temporal fenestra and contacts the dorsal portion of the postorbital (PIMUZ T 4376). Here, the suture is sharp and oblique, with the postfrontal laterally overlapping part of the postorbital, which possesses a concave facet that houses the caudal end of the postfrontal.

Unlike in Euichthyosauria, the postfrontal does not exclude the postorbital from bordering the temporal fenestra, a condition which is in contrast with a recent interpretation given for *Cymbospondylus duelferi*, *Cy*. *petrinus*, and *Cy*. *nichollsi* (Klein et al., 2020).

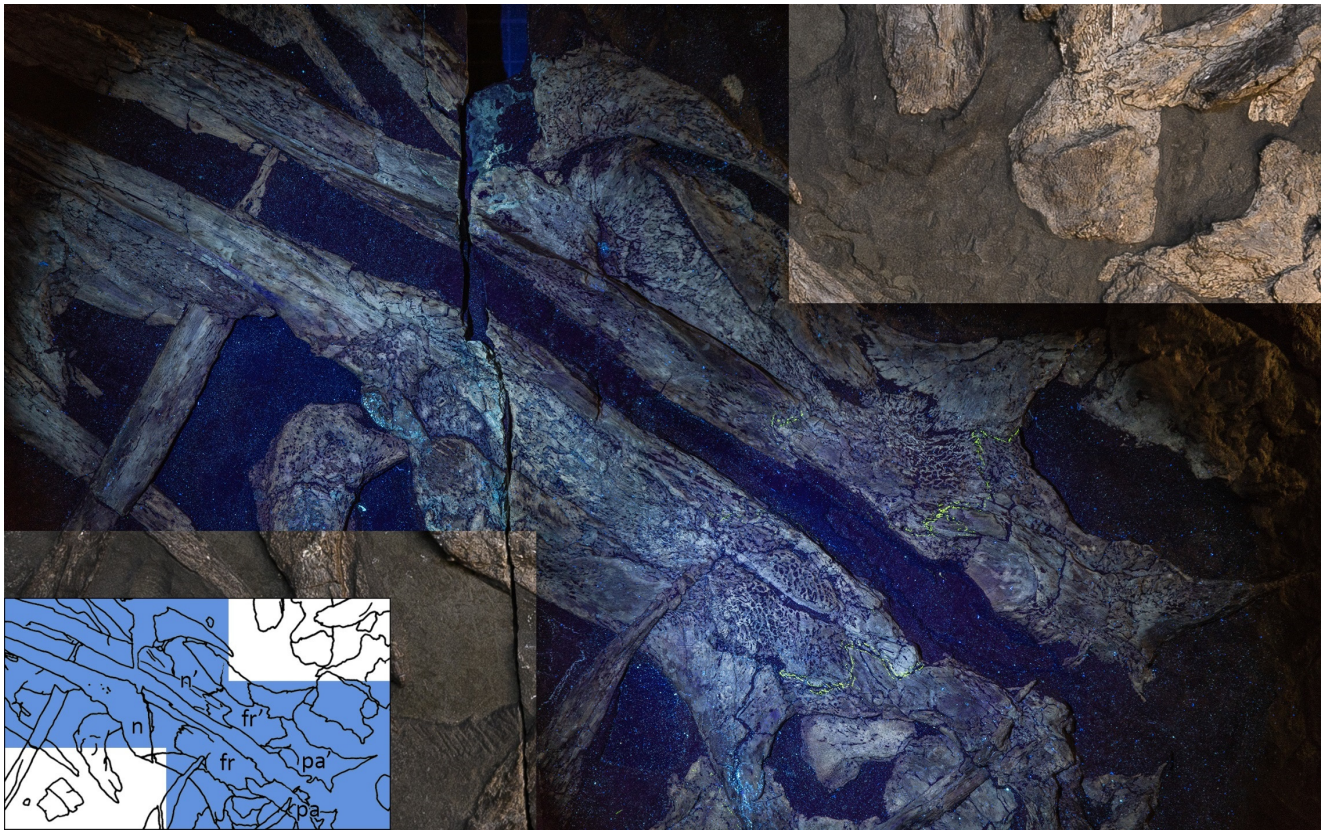

Fig. 6.13 - GPIT 1793/1, partly under visible, partly under UV light (365 nm), highlighting the sutures, otherwise not easily distinguishable from fractures, of frontals and adjacent bones on the ventral (internal) side of the skull roof: the extent of the frontals is greater internally than externally (see Figs. 4–6). Scale bar represents 5 cm.

Postorbital. A purported postorbital in the holotype of *B. leptorhynchus* (Dal Sasso & Pinna, 1996: fig. 10; Fig. 6.4) is here regarded as a possible quadratojugal (see below). The only certain postorbital is seen in PIMUZ T 4376, still articulated to adjacent elements of the left temporal region. It produces a somewhat hourglass-shaped lateral surface, an approximately trapezoidal dorsolateral exposure, and a caudoventral exposure which tapers into a distinct apex. Distinct striations radiate from the rostrolateral corner of the bone to the whole surface of this element, distinguishing it from the rugose surfaces of the postfrontal, the supratemporal and the squamosal, with striations parallel to the lateral margin of the temporal fossa. The caudal and the rostral borders of the postorbital are concave, with the latter forming the caudal margin of the orbital rim and the dorsomedial margin contributing to part of the supratemporal fossa and fenestra. In PIMUZ T 4376 the caudal contact with the squamosal is extensive, where its rostral margin seems to overlap the caudal margin of the postorbital.

The bulky aspect of the postorbital of *Besanosaurus* differs from the thin more "semilunar-shaped" postorbital of more derived Euichthyosauria, being more similar in shape to that of *Shastasaurus pacificus* (Sander et al., 2011) or *Guizhouichthyosaurus tangae* (Maisch et al., 2006*b*; IVPP V11865 and V11869, pers. obs.; Fig. 6.S1), with which in particular it shares a comparable anatomy, showing a similar profile and the same bone contacts. As in the latter, but with lesser extent, in *Besanosaurus* the postorbital contributes to the lateral border of the temporal fenestra, preventing the postfrontal-supratemporal contact. In *Shastasaurus* (Sander et al., 2011), the caudolateral process of postfrontal is longer, but the postorbital still contributes to the lateral margin of the supratemporal fenestra. In '*Callawayia' wolonggangense* (SPCV 10305; pers. obs.), and in a single specimen referred to *Guizhouichthyosaurus tangae* (GNG dq-41, Maisch et al., 2006*b*), the postorbital is excluded from the lateral margin of the supratemporal fenestra by an extension of the laterocaudal process of the postfrontal contacting the supratemporal.
The base of the postorbital certainly contacts the horizontal ramus of the jugal, but this articulation cannot be seen in any *Besanosaurus* specimens, because all jugals are more or less displaced from their original position. In PIMUZ T 4376, the postorbital forms a ventrocaudal exposure in the temporal region – a possible autapomorphy of *B. leptorhynchus* (difficult to compare with other shastasaurids, in which the temporal region is often deformed or incompletely preserved).

Jugal. The jugal is preserved in all specimens, although variably – and sometimes bizarrely (BES SC 999) – disarticulated. It is almost in place in PIMUZ T 4376, in which it is slightly shifted caudodorsally. It is disarticulated, well-visible and exposed in medial view in GPIT 1793/1 (Fig. 6.8). The jugal is a mediolaterally compressed, L-shaped bone, with a proportionally long horizontal suborbital ramus and a shorter vertical postorbital ramus. The two rami are orientated at an angle of almost 90°, which accommodates the ventrocaudal border of the orbit. In our interpretation, the rostral tip of the jugal –which is triangularly tapering into two oblique facets – is situated between the caudal tip of the lacrimal dorsally and the caudal ramus of the maxilla ventrally; on the other hand, the postorbital (dorsal) ramus enters the postorbital region and is thereby partially hidden by the postorbital and the squamosal contacting them with its smooth lateral surface. Such a loose articulation seems to be a natural condition, with the postorbital ramus of the jugal possibly interposed between the quadratojugal medially and the squamosal laterally. In fact, excluding PIMUZ T 4376, in all the specimens assigned here to *B. leptorhynchus*, the jugal is disarticulated from the other elements and does not show any apparent suture or scar on the surface of the caudal ramus; even in PIMUZ T 4376 it seems to be slightly displaced dorsally.
The suborbital (ventral) ramus varies quite in cross-sectional shape: it is dorsoventrally expanded rostrally, but it tapers into a smooth and suboval shape in its caudal half. The jugal has a concavity on its medioventral side in the area rostral to the bend of the postorbital ramus. This morphology is exposed in the holotype (BES SC 999), in PIMUZ T 4876, and in GPIT 1793/1. In this medioventral concavity, or groove, the surangular was likely housed while the animal was keeping its jaws closed. Judging from the position of the jugals, this feature can also be seen in *Guizhouichthyosaurus tangae* (Maisch et al., 2006*b*:fig. 2) and *Utatsusaurus hataii* (Motani et al., 1998:fig. 2).

Squamosal. The shape of the squamosal is clearly visible in specimen PIMUZ T 4376 and partly visible in PIMUZ T 1895, whereas in the holotype BES SC 999 this element seems to be present below the slab surface, visible only through CT scans. It is an approximately quadrangular-shaped, mediolaterally flat bone, proportionally bigger than the quadratojugal (with a greater external exposure than the

quadratojugal), and dorsoventrally shorter than the postorbital. Dorsally it contacts the supratemporal and rostrally the postorbital, whereby it overlaps its caudal margin. On its medial side, the squamosal contacts the quadratojugal, and rostrally these two bones are separated by the postorbital ramus of the jugal (Figs. 6.4–6.6), as seen in *Guizhouichthyosaurus tangae* (IVPP V11865, pers. obs.; Fig. 6.S2). Several fine striations project dorsoventrally from the dorsocaudal edge of this element. The ventral margin of the squamosal bears two short processes: the caudal process is slightly longer and is directed caudoventrally, the rostral process is shorter and directed ventrally. The cranioventral edge of the quadratojugal is visible laterally below the processes. The large size of the squamosal and its prominence in the cheek region is a common feature of Shastasauridae as seen in *Guanlingsaurus liangae* (Sander et al., 2011), *Guizhoichthyosaurus tangae* (IVPPV 11869, pers. obs.; Maisch et al. 2006*b*)*, Shastasauruc pacificus* (Sander et al., 2011) and possibly *Shonisaurus* (Callaway & Massare, 1989). However, the element seems to be more quadrangular in *Besanosaurus* than in these taxa. The element becomes reduced in size throughout ichthyosaur phylogeny. As the cheek region becomes less prominent in Parvipelvia, the squamosal adopts a more triangular morphology as seen in e.g., *Ichthyosaurus* and *Hauffiopteryx* (e.g., Marek et al., 2015). Similarly, the squamosal seems to be more triangular in '*Callawayia' wolonggangense*, but its caudal margins are broken in SPCV 10306, which might affect the perceived shape (pers. obs.).

Frontal. The frontal bones are preserved, co-articulated, and exposed in dorsal view in PIMUZ T 4376 and PIMUZ T 1895, and in ventral view in the holotype BES SC 999 and in GPIT 1793/1. A pair of putative frontals are also visible in PIMUZ T 4847 (albeit these fragments may represent only a portion of the 'anterior terrace' of the temporal fenestra since they show the same radiate bone texture as on the dorsal surface of the skull roof in PIMUZ T 4376 and PIMUZ T 1895). In *Besanosaurus* the frontal contacts the nasal rostrally, the parietal caudally, the prefrontal rostrolaterally, and the postfrontal caudolaterally. The frontal also borders the very rostral edge of the parietal foramen. The frontals contact each other at the midline; this contact is characterized by the presence of a prominent sagittal crest, which starts rostrally to the parietal foramen and becomes less prominent approaching the nasals. In the most 3D-preserved specimen (PIMUZ T 4376), the sagittal crest of the frontals is the continuation of the more prominent sagittal crest of the parietals, the two being separated only by the opening of the parietal foramen.
In ventral view the frontal bone is slightly longer than in dorsal view, where it expands mediolaterally: due to oblique sutural contacts, the prefrontal and the postfrontal overlap the dorsolateral surface of the frontal. Rostrodorsally there is a similar slight overlapping with the nasal, whereas caudodorsally the frontal is overlapped by the rostromedial and rostrolateral rami of the parietal. In GPIT 1793/1, on the ventral side of the frontals, there are remnants of the putative olfactory lobes, partially hidden by broken and ventrally dislocated rostromedial portions of the frontals (Fig. 6.13). These lobes define a clear step between the rostral half and the caudal half of the frontals; for this reason, the caudal halves are thicker dorsoventrally. As in *Besanosaurus,* the frontal contributes to the supratemporal fossa in *Guizhouichthyosaurus tangae* (Maisch et al., 2006*b*), in '*Callawayia*' *wolonggangense* (Chen et al., 2007), *Guanlingsaurus liangae* (Sander et al., 2011) and *Shastasaurus pacificus* (Sander et al., 2011).

Parietal. Similarly to the frontals, the parietals are preserved articulated in dorsal view in specimens PIMUZ T 4376 and T 1895 and in ventral view in GPIT 1793/1 and BES SC 999 (although are quite damaged in the latter specimen). The parietal bone contacts the frontal rostrally, the postfrontal rostrolaterally, the supratemporal caudolaterally, and the supraoccipital caudally. Medially the two

parietals contact each other and form a prominent sagittal crest (only visible in PIMUZ T 4376). The two rostral rami of the parietal slightly overlap the caudal edge of the frontal, so that on the ventral side of the skull they seem rostrocaudally longer than on the dorsal side.
The parietal of *Besanosaurus* is a highly three-dimensional element of the skull roof. The lateral side of the parietal possesses a smooth, concave, and almost vertical wall, which borders the temporal fenestra medially and where the rostral portion of the *musculus adductor mandibulae externus profundus* (mAMEP) and the ventral half of the *musculus pseudotemporalis superficialis* (mPSTs) may have attached (as reported in *Sphenodon*, e.g., Jones et al., 2009). In PIMUZ T 4376 this wall is separated from the prominent sagittal crest by a narrow and short flat surface, in continuity with the 'anterior terrace' of the temporal fenestra. The rostral portion of the *musculus adductor mandibulae externus medialis* (mAMEM) and the dorsal half of the mPSTs may have attached on this flat surface and on the sagittal crest (Jones et al., 2009). Compared to *'Callawayia' wolonggangense* (SPCV 10306; pers. obs.) and *Guanlingsaurus liangae* (SPCV 03107; pers. obs., Fig. 6.S4), the sagittal crest of *B. leptorhynchus* seems more prominent and more similar to that of *Guizhouichthyosaurus tangae* (IVPP V11865; pers. obs.), albeit is not as prominent as in mixosaurids (e.g., MSNM V 455) and *Cymbospondylus* (PIMUZ T 4351).
Remarkably, in GPIT 1793/1 the parietals exposed in ventral (internal) view display a deep ovoid-shaped concavity that would have accommodated the rostral region of the cerebral hemispheres, possibly including or even exclusively including the optic lobes (Marek et al., 2015; Fig. 6.13), apparently even more prominent than what is preserved in the *Callawayia neoscapularis* holotype (ROM 41993; McGowan 1994). There is no apparent epipterygoid facet on the ventral side of the parietal. Distinct epipterygoid facets are observed in *Ichthyosaurus* and *Platypterygius australis* as ventrally directed extensions lateral to the indentation of the rostral region of the cerebral hemisphere (McGowan, 1973; Kear, 2005). It is possible this facet is only ossified in parvipelvian ichthyosaurs. This leads to the hypothesis that there was no (ossified) connection between the epipterygoid and skull roof in *Besanosaurus*.

Supratemporal. The supratemporal, clearly visible in PIMUZ T 4376, is a triradiate complex bone. The rostrolateral ramus develops on the dorsolateral side of the skull roof and contacts the postorbital rostroventrally, and the squamosal ventrally. A process in the form of a descending ramus functions as a major part of the caudolateral side of the skull and envelops the dorsal head of the quadrate caudally, as seen in *Guanlingsaurus liangae* (SPCV 03107; pers. obs.; Fig. 6.S3). The rostromedial ramus is directed rostromedially and contacts, on its rostromedial side, the caudolateral process of the parietal. On the caudal side a facet for the opisthotic is not visible. We interpret the "supratemporal antero-medial extension" (Motani et al., 2017: char. 12) as short on the basis of specimens PIMUZ T 4376 and BES SC 999, as their morphology is short compared with *Cymbospondylus* (Motani, 1999). This morphological difference has been used as a character in recent phylogenetic analyses (Ji et al., 2016; Huang et al., 2019).
In BES SC 999, both supratemporals show their internal (rostromedial) aspect, characterized by a rugose texture. An apparent L-shaped concavity is also present, in which the dorsal portion of the quadrate head was likely housed; this concavity is dorsally demarcated by two conical prominences, connected by a ridge, and laterally by a longer ridge, descending from the lateral-most prominence. The putative left supratemporal in GPIT 1793/1 is also preserved in rostromedial view: the surface is concave and two prominences, closely resembling the one described above, are visible as well.

6.6.4 Braincase

Supraoccipital. This bone is clearly preserved only in GPIT 1793/1, exposed in caudal view. The supraoccipital is represented by an inverted U-shaped "massively built arched bone" (Maisch & Matzke, 1997a). The inner ventral arch of this bone delineates the upper margin of the foramen magnum, whereas the outer dorsal arch (Fig. 6.14A) contacted the caudoventral margins of the parietals. Lateral to the foramen magnum, the ventral edges of the supraoccipital arch contain small facets for the exoccipitals. Curiously, the left dorsolateral margin of the supraoccipital hosts a notch that seems absent on the right side of the bone, likely due to oblique compression. This was also noted by Maisch & Matzke (1997*a*), who suspected this notch to be a neurovascular foramen similar to those described in *Ophthalmosaurus icenicus* and *Ichthyosaurus* (Andrews, 1910; McGowan, 1973). This morphology is most similar to *Stenopterygius*, as that taxon also lacks distinct supraoccipital foramina in most observed specimens, but contrasts with the morphology of most other Euichthyosauria in which the supraoccipital is known, as many taxa have two distinct foramina on the lateral sides of the element (Miedema & Maxwell, 2019).

Exoccipital. Only one clear exoccipital is present, close to its original position, in specimen PIMUZ T 4376 (Fig. 6.14D). A putative right exoccipital is partially exposed in rostral view in BES SC 999. This bone in *Besanosaurus* appears slightly dorsoventrally taller than rostrocaudally long and shaped as a column, with a constricted central body and wider ends. It possesses a ventral facet for the basioccipital and a dorsal facet for the supraoccipital. The latter is smaller, occupying an area that is two-thirds the size of the one occupied by the ventral facet. There is one small indentation in its rostral side, which we interpret as the original location of the hypoglossal foramen, although the opening is now closed due to sediment infill and other diagenetic processes. One hypoglossal foramen is usually present in the exoccipital of Ichthyosauria, although there can be more, as seen in e.g., *Temnodontosaurus* and *Ophthalmosaurus icenicus* (Maisch, 1997; 2002).

Prootic. A possible prootic is exposed as a small isolated element in the occipital region of PIMUZ T 1895 and GPIT 1793/1 (Fig. 6.14C). In each of these specimens, this bone has a size comparable to that of a single scleral plate, and the shape of a discoidal capsule. Rearticulated in anatomical position (e.g., McGowan & Motani, 2003), this bony capsule would have been convex rostrally and concave caudally and, on the caudal side, it would have contacted a cartilaginous otic capsule along its external circumference. The capsule is not preserved in any of the specimens we examined. The prootic in specimen GPIT 1793/1 tentatively displays a V-shaped indentation (although heavily flattened) in which the otic capsule would have fit. The degree of prominence of a possible dividing ridge between the major areas of the indentation is unclear due to the compression. The prootic of *Besanosaurus* is more similar to that of Lower Jurassic ichthyosaurs than to that of *Mixosaurus* and cymbospondylid ichthyosaurs, which have a more elongated and quadrangular morphology and are larger in comparison to their opisthotic – a morphology which resembles a condition similar to their diapsid ancestors (Maisch & Matzke, 2006; Maisch et al., 2006*a*).

Opisthotic. A well-preserved right opisthotic is exposed in rostral (internal) view in GPIT 1793/1 (Fig. 6.14D), which was not described by Maisch & Matzke (1997*a*), because it was unprepared at the time. A putative opisthotic is also preserved in BES SC 999. The opisthotic consists of a rectangular to oval medial head with indentations that accommodated the caudal region of the semicircular canals, a stout paroccipital process, and a clear basioccipital facet.

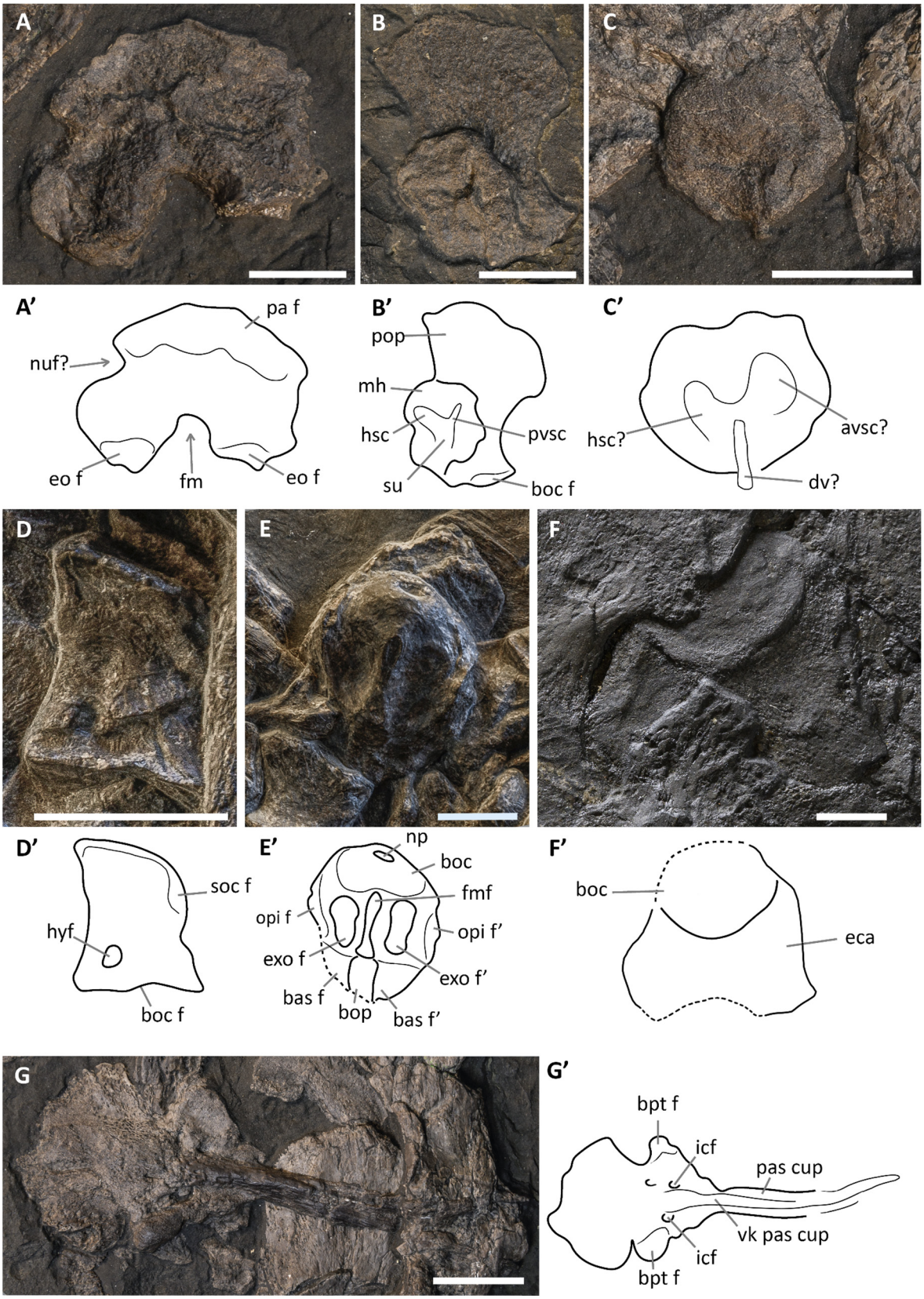

Fig. 6.14 - Braincase elements of *Besanosaurus leptorhynchus*. Disarticulated braincase elements of *Besanosaurus leptorhynchus* GPIT 1793/1 (A–C, G), PIMUZ T 4376 (D and E), and BES SC 999 (F). Interpretative drawings are denoted by apostrophes. (A and A′) supraoccipital in posterior view; (B and B′) opisthotic in rostromedial view. (C and C′) prootic in caudal view. (D and D′) exoccipital in rostral? view; (E and E′) basioccipital in dorsal view; (F and F′) basioccipital in caudal view; (G and G′) parabasisphenoid in ventral view. Dashed lines indicate portions of bones not visible on the surface, thin lines indicate bone structures. Abbreviations: see text. Scale bars represent 1 cm.

The paroccipital process is roughly as wide as it is tall when measured at its widest position. This morphology resembles the condition in more derived Euichthyosauria, in which the paroccipital process is usually stouter (e.g., *Stenopterygius*; Miedema & Maxwell, 2019) and *Temnodontosaurus trigonodon* (Maisch, 2002), than in the more basal *Mixosaurus cornalianus* or *Phantomosaurus neubigi* (Maisch & Matzke, 2006). In these latter taxa the paroccipital process is longer than wide and tapers distally, which is not the case in the opisthotic associated with GPIT 1793/1 (Maisch et al., 2006*a*; Maisch & Matzke, 2006). The paroccipital process heavily resembles the morphology described for *Shonisaurus* (Camp, 1980). In GPIT 1793/1 the basioccipital facet is distinctly offset from the paroccipital process and medial head due to the curved convex morphology of the ventral margin of the opisthotic. The morphology of the medial head and shape of the indentations for the semicircular canals are thus far not known in any other Triassic ichthyosaur. The indentations are V-shaped as in all other adult ichthyosaurs in which this morphology is known. The angle between the indentation of the horizontal semicircular canal and caudal vertical semicircular canal are roughly similar to those in other ichthyosaurs. There may be a high degree of conservatism in the inner-ear shape of ichthyosaurs, although this needs further study. The shape of the indentation is different from the early adult morphology in *Stenopterygius*, although it is unsure whether the shape of the inner ear or the shape of the enclosing opisthotic is more affected by ontogeny (Miedema & Maxwell, 2019). The indentation for the caudal vertical semicircular canal does not reach higher than the dorsal margin of the medial head – this leads to a morphology which differs from many post-Triassic taxa in which this indentation creates a second "process" as visible in caudal view (clearly present in *Stenopterygius* and *Platypterygius australis* and to some degree in *Ichthyosaurus* and *Temnodontosaurus* [McGowan, 1973; Maisch, 2002; Kear, 2005; Miedema & Maxwell, 2019]).

Stapes. The stapes is elongated and slender. Both stapedes are present disarticulated in the holotype of *B. leptorhynchus* (Fig. 6.4): the right one is exposed in rostrolateral view, not obscured by other bones, close to its original position but rotated 180° along the horizontal plane; the left one is partly hidden by the postorbital but visible through CT scans. One stapes is also visible in GPIT 1793/1. All stapedes of *Besanosaurus* are slender and subcylindrical in shape, with expanded ends and constrained shafts. Both in BES SC 999 and GPIT 1793/1 the lateral articulation for the quadrate is wider and cup-shaped, whereas the sigmoidal medial portion tapers towards the basioccipital, as described by Camp (1980: fig. 12) for *Shonisaurus*. The stapedes of *Besanosaurus*, unlike those of Merriamosauria, seem to lack a facet for the opisthotic on their dorsomedial end.

Basioccipital. Two specimens expose the basioccipital close to its original position: the holotype BES SC 999 (Fig. 6.14F) preserves this bone heavily compressed and exposed in caudal view, whereas in PIMUZ T 4376 (Fig. 6.14E) the basioccipital is preserved in dorsal view. In caudal view (BES SC 999) a wide extracondylar area is visible below the condyle (Fig. 6.14F). The area is slightly convex ventrally resembling *Ichthyosaurus*, but not as convex as in, e.g., *Phantomosaurus* (Maisch & Matzke, 2006). A wide extracondylar area is characteristic of more basal ichthyosaurs, as the extracondylar area is severely reduced in *Stenopterygius* and virtually absent in Ophthalmosauridae (Miedema & Maxwell, 2019). The convex occipital condyle is located above this area and occupies a medial portion of the basioccipital bone that is half the size of the extracondylar area. In PIMUZ T 4376 (Fig. 6.14E) the rostrocaudal length of the basioccipital appears close to its transverse length, which is consistent with the typical robust aspect of this element. On the dorsal surface of the bone, the two facets for the exoccipitals are well-defined; these are represented by two shallow drop-shaped depressions, tapered rostrally. The two

exoccipital facets are also parallel and very close to each other, as seen in *Stenopterygius* (Miedema & Maxwell, 2019), and are separated by a dorsal median ridge (i.e., the floor of the foramen magnum). Rostral to the medial ridge a prominent basioccipital peg emerges, laterally delimiting two subtriangular articular facets for the basisphenoid. Through CT scans, the basioccipital peg is also visible in the *Besanosaurus* holotype (Fig. 6.10).

Parabasisphenoid. GPIT 1793/1 preserves an almost intact parabasisphenoid exposed in ventral view (Fig. 6.14D), although it is disarticulated from the rest of the skull and the cultriform process is likely incomplete rostrally. In general, the parabasisphenoid has a piriform profile, being wider caudally than rostrally. In fact, a deep constriction is present in the middle of its dorsoventrally compressed body, just caudal to the articular surface of the basipterygoid process, as also seen in *Phantomosaurus neubigi* (Maisch & Matzke, 2006). This well-developed articular surface demonstrates that *Besanosaurus* also retained a functional basicranial articulation, although this process seems shorter in *Besanosaurus* than in *Phantomosaurus*. The caudal profile of the parabasisphenoid is characterized by a pair of caudolateral shallow natural notches and a slightly more evident median depression. On the ventral surface of the parabasisphenoid there is a clear bulge; this becomes more developed rostrally, where it tapers and becomes the cultriform process. In GPIT 1793/1, to the left side of this process, two carotid foramina are clearly visible; the cultriform process separates the carotid foramina as in *Callawayia neoscapularis* (ROM 41993; pers. obs.), *Guizhouichthyosaurus tangae* (IVPP V11853; pers. obs.), *Macgowania janiceps* (TMP 2009.121.1; pers. obs.) and *Temnodontosaurus* (Maisch, 2002), but differs from parvipelvians, in which a single carotid foramen is present (e.g., Maisch & Matzke, 2000).
Interestingly, PIMUZ T 1895 exposes a parasphenoid element, which forms a single ossification, not co-ossified with the basisphenoid. In fact, judging by the relative size of the specimen, PIMUZ T 1895 is osteologically less mature, and therefore likely ontogenetically younger than GPIT 1793/1. In PIMUZ T 1895 the cultriform process is preserved as a mediolaterally thin, median process pointing downwards; paired foramina for the carotid artery are present at its base, and the lateral extensions represent the basipterygoid processes.
We did not find any isolated basisphenoid in the examined specimen. A putative basisphenoid was mentioned by Maisch & Matzke (1997*a*) as present in GPIT 1793/1 as a separate ossified element, lying adjacent to the complete parasphenoid described above. It was originally described as having a "grossly triangular shape with a narrow anterior extension, and two lateral flanges [that] reminds of the general outline of the basal plate of the parasphenoid, being distinctly smaller, however". We interpret this element as a broken piece of the basioccipital exposed in rostroventral view, possibly showing the basisphenoid facet.

6.6.5 Palatoquadrate complex

The palatal bones are preserved in between the flattened dermal skull elements in most of the specimens examined here. Some palatal elements are detectable through CT scans in BES SC 999, although the resolution is not good enough for us to describe their morphology. Therefore, the anatomy of the vomers, the palatines, and the pterygoids is based on specimens GPIT 1793/1, BES SC 1016, and PIMUZ T 4748 (Figs. 6.6, 6.8 and 6.10). These specimens are disarticulated and likely incomplete but do preserve palatal elements. For this reason, the reconstruction we propose (see "Cranial reconstruction" section below) is also based on *Mixosaurus* (Huene 1916, Riess, 1986:fig. 5), *Stenopterygius* (McGowan & Motani,

2003:fig. 40), as well as pers. obs. of '*Callawayia*' *wolonggangense* (SPCV 10305; Fig. 6.S5) and *Guizhouichthyosaurus tangae* (IVPP V11853).

Vomer. In the holotype of *B. leptorhynchus* the vomers are not clearly detectable through CT scans. Possible vomers are exposed and disarticulated in PIMUZ T 4748 and GPIT 1793/1, in which they appear to constitute long, slender, and thin sheets of bone, slightly thicker caudally and pointed rostrally. *In vivo*, the vomers are partly articulated with each other, with the premaxillae and with the nasals, via long sutures that are partly preserved in GPIT 1793/1. In fact, in the right vomer exposed in lateral view the dorsal margin (partly covered) bear a thin vertical lamella of bone, which likely contacted similar median vertical processes of the other rostral bones. The lateral surface of the bone is concave all along its length. As noted by Maisch & Matzke (1997*a*), the anterior third of the ventral margin is reinforced by a ridge, whereas caudally another prominent ridge possibly represents the lateral facet for the palatine.

Palatine. In the holotype BES SC 999, a portion of the putative left palatine emerges within the left orbit, and a big portion of the right palatine is detectable through CT scans. However, these cannot be unambiguously identified . In GPIT 1793/1 we confirm the presence of two small splinters of bone, which lie adjacent to the elongate plate of the ?left vomer (Maisch & Matzke, 1997*a*), possibly representing incomplete portions of both palatines. In PIMUZ T 4748, possible fragmentary palatines are disarticulated from the other elements of the skull.

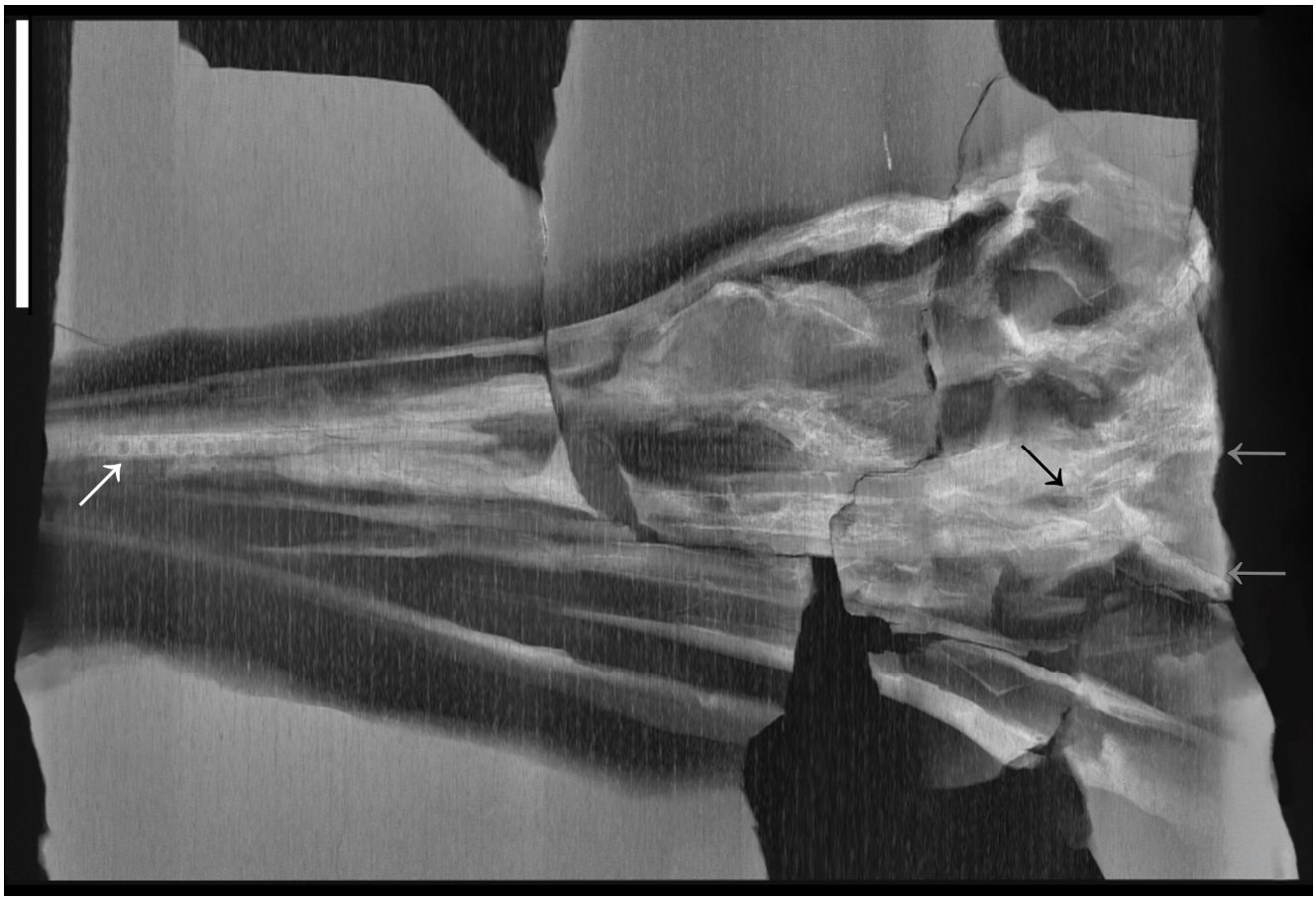

Fig. 6.15 - CT image of BES SC 1016. CT image of specimen BES SC 1016. Note the pterygoids still in articulation and the relatively narrow interpterygoid vacuity (black arrow). The caudal extremities of the pterygoids are marked by grey arrows (full extent of the pterygoids is visible in Fig. 9). Note also the implantation of the mesialmost (caudalmost) premaxillary teeth, that are nested in separate sockets (white arrow). Scale bar represents 10 cm.

Pterygoid. The paired pterygoids are well-preserved in BES SC 1016, still semi-articulated and exposed in ventral view, separated caudally by the interpterygoid vacuity (Figs. 8 and 15). The left pterygoid is also partly preserved in 3D in GPIT 1793/1, where it is exposed in dorsal view, with the medial border of the rostral half partly folded onto the lateral portion of the bone and overlain by the right splenial. Remarkably, the pterygoid of GPIT 1793/1 also preserves the ascending process for the epipterygoid, which runs rostrocaudally, for at least the caudal half of the bone. Possible pterygoids are also preserved, albeit quite damaged, in specimen PIMUZ T 4748. As in other taxa, the pterygoid of *Besanosaurus* can be divided into two different halves. The rostral half tapers rostrally into a pointed tip, whereas caudally it becomes mediolaterally expanded, until reaching its maximum mediolateral width at its caudal end. The lateral margin of this second half hosts a wide concavity, in which the *adductor mandibulae* muscular complex would have been attached. In the caudalmost half of the pterygoid, three processes radiate in three different planes (see also Maisch & Matzke, 1997*a*): a caudolateral quadrate process, a caudomedial small bony flange, and a medial vertically ascending ridge that contacted the epipterygoid. Unlike in *Mixosaurus* (SMNS 15378, pers. obs.; Maisch & Matzke, 1997*b*), the two pterygoids were not in close contact caudally in *B. leptorhynchus*, but slightly diverged from the midline leaving a narrow interpterygoid vacuity, which was definitely smaller than the wide opening observed in *Guizhouichthyosaurus tangae* (IVPP V 11853, Shang & Li, 2009). The median bulge of the parasphenoid may have emerged ventrally through this opening.

Epipterygoid. We agree with the interpretation of the epipterygoid given by Maisch & Matzke (1997*a*) for GPIT 1793/1. In this specimen, the epipterygoid is still articulated with the left pterygoid, although taphonomically compressed and slightly dislocated on its dorsal surface. The epipterygoid ventrally contacted the pterygoid with a large base that becomes much thinner (rostrocaudally reduced and mediolaterally very slim) approaching the dorsal end. The dorsal tip of this bone is missing, likely not preserved, although there is no apparent epipterygoid facet on the parietal roof. The presence of an ossified epipterygoid is significant as so far it was only reported in one other ichthyosaur: *Ichthyosaurus* (McGowan, 1973). The 2D nature of most preserved ichthyosaur specimens and the internal position of the epipterygoid hinders its identification in ichthyosaurs in general.

Quadratojugal. Putative quadratojugals are visible in the holotype of *B. leptorhynchus* BES SC 999. The right one is quite compressed and poorly preserved; the left one (formerly thought to be the left postorbital) lies on the rostral half of the left quadrate and is more complete. The only specimen in which the anatomy of the quadratojugal is clear is GPIT 1793/1 (Maisch & Matzke, 1997*a*; Fig. 6.16). In this specimen, the right quadratojugal is fully disarticulated and exposed in medial (internal) view. It has the shape of a trapezoidal plate with slightly convex cranial and caudal margins, and with a large flat triangular process that might have intruded dorsocranially between the postorbital and the squamosal, as in *Temnodontosaurus* (Maisch & Matzke, 1997), likely contacting also the caudal end of the jugal (see also jugal). At the other end, i.e., in the caudoventral direction, the quadratojugal terminates in a prominent and thickened process, clearly offset from the main body of the bone and bearing a robust oblong articular facet for the quadrate. This facet, directed caudomedially, is similar to that in *Phantomosaurus neubigi* (Maisch & Matzke, 2006).
In articulated skulls, the quadratojugal was almost entirely overlapped by the squamosal, emerging laterally only with its stout quadrate process (Fig. 6.17) that recalls the morphology of *Guizhouichthyosaurus tangae* (IVPP V11869; pers. obs.) and *Guanlingsaurus liangae* (SPCV 03107;

pers. obs.).. The concave internal space left between the quadratojugal and the quadrate+pterygoid was likely occupied by the *adductor mandibulae* muscular complex (mAMES, mAMEM, mAMEP) (Jones et al., 2009).

As in many non-euichthyosaurian ichthyosaurs, the temporal region is proportionally long (Ji et al., 2016:char. 31.0). Despite this, compared to *Guizhouichthyosaurus tangae* (IVPP V11865, pers. obs.; Fig. 6.S2), where most of the left squamosal is broken off, and the left quadratojugal is almost entirely exposed, the quadratojugal of *Besanosaurus* looks slender and proportionally smaller, although its general anatomy is not so different. In turn, the quadratojugal in *Besanosaurus* closely resembles the one of *Shonisaurus* (Nicholls & Manabe, 2004:fig. 6).

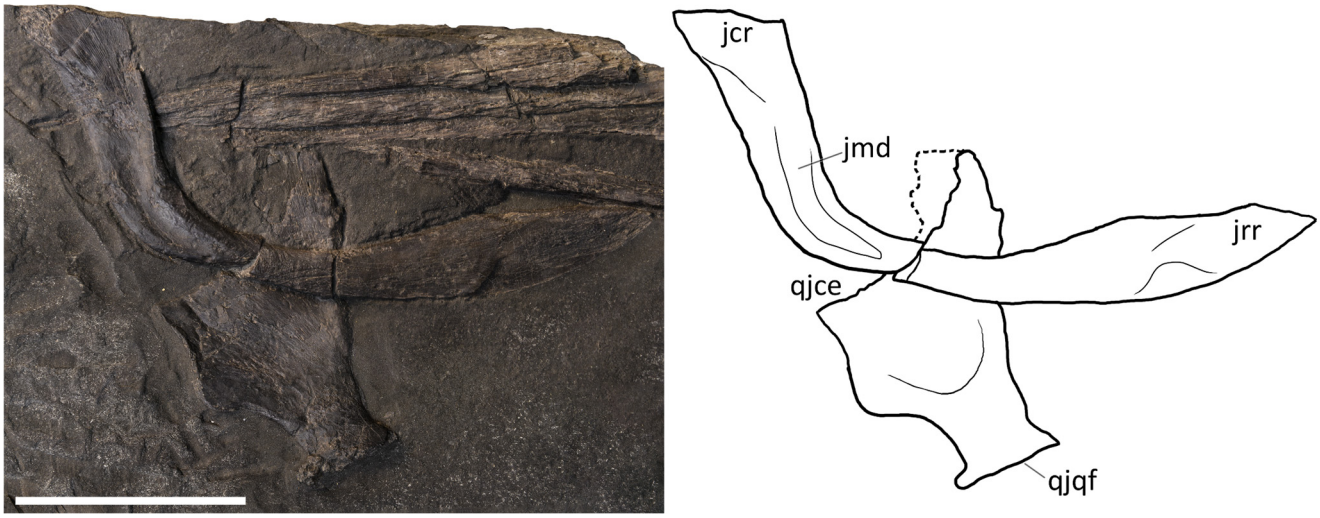

Fig. 6.16 - Jugal and quadratojugal of GPIT 1793/1. Specimen GPIT 1793/1, left jugal in medial view (top) and right quadratojugal in lateral view (bottom). Dashed lines indicate portions of missing elements preserved as counterprints, thin lines indicate bone depressions. Abbreviations: see text. Scale bar represents 5 cm.

Quadrate. The left quadrate of BES SC 999 (partly hidden by the left postorbital) and the right quadrate of GPIT 1793/1 are preserved in rostrolateral view and are nearly identical; the incomplete ?right quadrate of PIMUZ T 4847 is also preserved but disarticulated (Fig. 6.17). Based on these specimens, the quadrate of *B. leptorhynchus* can be described as a relatively large element, kidney-shaped in outline, with a well-expressed lateroventral condyle for the articulation with the lower jaw and a stout dorsal head inserting in a proper "L-shaped" notch of the medial surface of the supratemporal vertical descending wall. The condyle is well developed on the rostrolateral side of the bone; just dorsal to the neck of the condylar process there is a rectangular articular facet for the quadratojugal. Along its concave lateral margin, the quadrate is thickened, whereas the convex side is tabular. On the medioventral border of the latter, there is a small triangular projection ("triangular process of the quadrate", TPQ of Maisch & Matzke, 1997*a*) which has previously not been described in any other ichthyosaur, but we confirm it is also present in *Guanlingsaurus liangae* (SPCV 03107, pers. obs.; Fig. 6.S3). This is the reason why we suggest to treat this character as a possible shastasaurid synapomorphy, rather than an autapomorphy of *Mikadocephalus gracilirostris* (see above). Medially, this process contacts the caudolateral edge of the pterygoid. In BES SC 999, the 'triangular process' of the right quadrate is located below the left ?quadratojugal (Fig. 6.10 and 6.17), and is therefore not visible on the surface but only through CT. This 'triangular process' may have had a structural-mechanical function, helping to hold in place, on its caudal side, the caudolateral flange of the pterygoid. On the caudomedial side, matching the anatomy of the adjacent skull elements, the quadrate likely bears a concave facet for the opisthotic, a small rounded and flat facet for the stapes, and a ventral large facet for the pterygoid, mediolaterally extending from the TPQ to the condyle for the lower jaw.

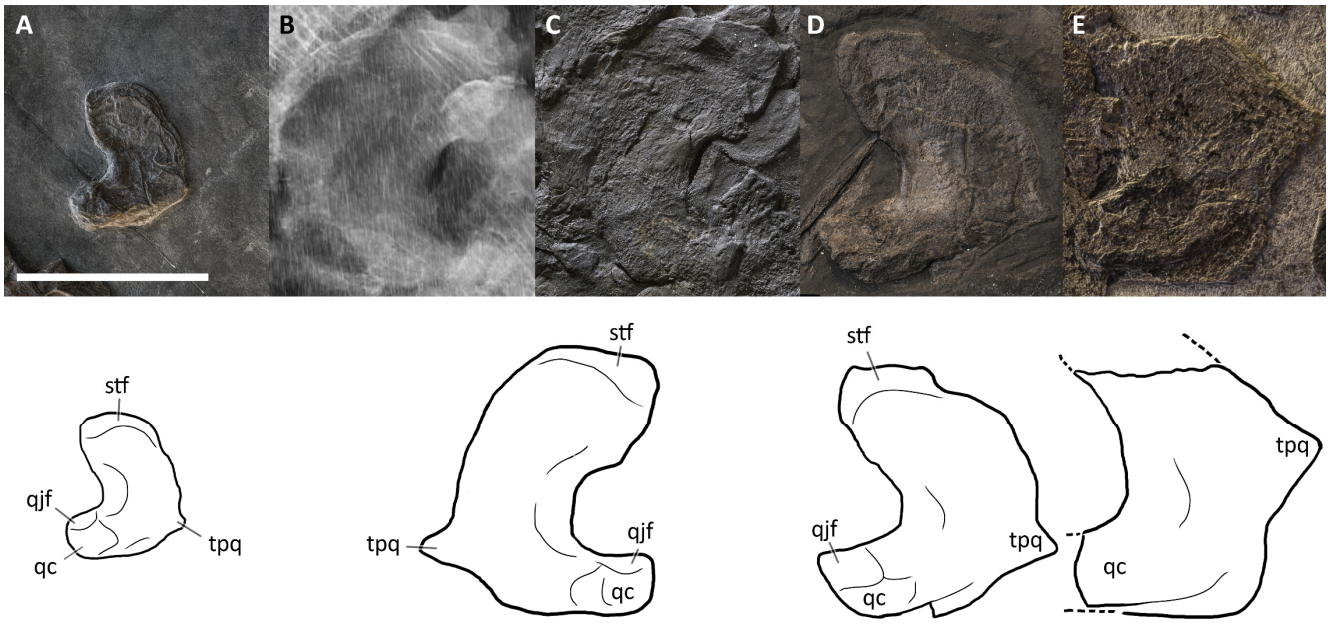

Fig. 6.17 - Quadrates of *Besanosaurus leptorhynchus*. Quadrates of *Besanosaurus leptorhynchus*. (A) right quadrate of PIMUZ T 4376 in rostrolateral (anterior) view; (B) CT scan of the left quadrate area of BES SC 999; (C) left quadrate of BES SC 999 in rostrolateral view, under visible light; (D) right quadrate of GPIT 1793/1 in rostrolateral view; (E) right quadrate of PIMUZ T 4847 in rostrolateral view; the upper half of the quadrate is missing, as well as most of its lateral portion. Interpretative drawings below. Dashed lines indicate portions of missing elements, thin lines indicate bone structures. Abbreviations: see text. Scale bar represents 5 cm.

6.6.6 Mandible

Dentary. The dentary bones of *Besanosaurus* are well-preserved in BES SC 999 and PIMUZ T 4376, in which they are completely exposed in lateral view and still articulated. In both specimens the dentary is an extremely slender, narrow, elongate and approximately triangular bone that makes up almost three-quarters of the lower jaw length. The ventral margin of the dentary is straight rostrally and slightly concave caudally, whereas the dorsal (dentigerous) margin is straight all along its length. Each dentary contacts its contra-lateral element in a long symphysis mediorostrally, the surangular laterocaudally and the splenial mediocaudally, forming a pair of long oblique straight sutures that face ventrally. Both in BES SC 999 and PIMUZ T 4376, a narrow groove runs at mid-height on the lateral side of the dentary, from the caudal end towards the rostral tip, for four-fifths of the bone length. Above this mid-height line, the dorsal surface rostrally hosts a long dental groove and caudally a few teeth sockets (at least six). The labial shelf is partially exposed in PIMUZ T 4376, where it appears slightly concave. The 3D preservation of PIMUZ T 4376 also shows the aspect of the dentary-surangular suture, which is visible both on the lateral and the dorsal (buccal) surface of the lower jaw. This suture rostrally begins below the last five maxillary tooth positions and continues to the caudal end of the bone below the caudal margin of the lacrimal.

The very slender shape and the very gradual tapering towards the rostral tip of the dentary seen in *Besanosaurus* are similar to the dentary of '*Callawayia' wolonggangense* (SPCV 10306; Chen et al. 2007). On the other hand, contrary to *Guizhouichthyosaurus tangae*, the caudal end of the *Besanosaurus* dentary does not reach the midline of the orbit (Pan et al., 2006), ranging from the rostral limit (PIMUZ T 4376, ?T 1895) to the rostral third of its length (BES SC 999). This slight variation may be due to ontogeny-related allometry, or to different preservation.

Splenial. This bone contributes to more than a half of the maximum height of the lower jaw, although in *Besanosaurus* the splenial looks less dorsoventrally expanded and straighter than in *Ichthyosaurus* (McGowan & Motani, 2003:fig. 41). It contributes to the medial (internal) wall of the lower jaw and is best observed in the holotype BES SC 999, where the lower jaw bones have been disarticulated and arranged in a fan-shape so that the caudal tip of the left splenial is almost entirely exposed. The splenial is long and slender and dorsoventrally taller than the angular. A small portion of the left splenial is visible, although largely obscured by adjacent elements, in PIMUZ T 4376.
The splenial contacts the dentary rostrally, the angular laterocaudally, the surangular laterodorsally, and a small portion of the prearticular caudodorsally. This is partially visible in medial view in the better exposed (right) splenial of GPIT 1793/1, and – to a lesser extent – in those of BES SC 999 and BES SC 1016. In all cases, the rostral end is thinner than the rest of the bone, and divided into two processes: a shorter, less robust dorsal one, and a longer, thicker ventral one. The latter possesses a slightly curved, concave facet that has been interpreted as the surface of contact for the dentary (Maisch & Matzke, 1997*a*), as in other taxa such as *Ophthalmosaurus icenicus* and *lchthyosaurus* (Andrews, 1910; Sollas, 1916). Both rostral tips of the two processes also show a rugose surface facing medially, which has been interpreted as contributing to the mandibular symphysis in *Stenopterygius* (SMNS 81961, pers. obs.) and *Platypterygius australis* (Kear, 2005). Given that this element is a left splenial exposed in medial view, we think this is also the case for GPIT 1793/1. The Meckelian groove of the splenial is represented by a long, slender, longitudinal depression, that gradually terminates rostrally in between the two processes.

Surangular. The lateral side of the articulated right and left surangular bones is well-visible in PIMUZ T 4376 and in the holotype BES SC 999. On the other hand, the disarticulated surangulars of GPIT 1793/1 and BES SC 1016 are exposed in medial view, and those of PIMUZ T 4847 are possibly exposed in medial view as well, although they are not much informative due to poor preservation. The surangular articulates with the dentary rostrodorsally and with the angular caudoventrally; caudomedially, the surangular is very often preserved in articulation with the articular.
In *Besanosaurus* the surangular is a robust and long bone, although shorter than the dentary. It possesses a relatively slender rostral process, whereas its main shaft becomes taller and thicker before reaching the coronoid (or preglenoid) process, its tallest point being at the level of the caudal end of the orbit. In medial view (GPIT 1793/1), a large elliptical neurovascular foramen opens here, at the center of the bone concavity, and a second much smaller foramen opens 1 cm caudal to it. In front and just caudal to the coronoid (preglenoid) process, the surangular of *Besanosaurus* narrows, expanding dorsoventrally again at its caudal end, in correspondence with the articulation with the articular bone.
Maisch and Matzke (1997*a*) described a separate coronoid in GPIT 1973/1, but we argue that a broken bone fragment was likely erroneously identified as the coronoid and that the coronoid in *B. leptorhynchus* was fused with the surangular, like in more derived ichthyosaurs. One specimen of the early-diverging ichthyopterygian *Chaohusaurus brevifemoralis* (Huang et al., 2019) has a separate coronoid on one side of the mandible, and a coronoid fused with the surangular on the other side. The coronoid in that specimen forms a distinct, pointed process in the caudal portion of the mandible - the coronoid process. In *B. leptorhynchus* (BES SC 999, PIMUZ T 4376) and all other more derived ichthyosaurs (see McGowan 1973; Moon & Kirton, 2016) the mandible bears two distinct processes located in its caudal portion: a caudally located, pointed process - which corresponds in shape and

position to the coronoid process in *Chaohusaurus brevifemoralis* (preglenoid process of Moon & Kirton, 2016), and a more dorsoventrally shallow process located rostrally to it - which Moon & Kirton (2016) described as the paracoronoid process. In light of the anatomy seen in *Chaohusaurus brevifemoralis* and the presence of two distinct mandibular processes in *B. leptorhynchus*, *Ichthyosaurus* and *Ophthalmosaurus icenicus*, we conclude that the coronoid likely became fused to the surangular in Merriamosauria (Ji et al. 2016), and formed a caudally located coronoid (preglenoid) process, with the surangular forming an additional, paracoronoid process, more rostrally.
The coronoid (preglenoid) process is thus remarkably large, distinctly rising above the dorsal margin of the surangular with a robust, rounded, and roughened dorsal tip, which probably served as attachment for an efficient mAMEM and mAMEP (Jones et al., 2009). The lateral wall of the surangular hosts a large longitudinal rough area, which is particularly well-visible in the holotype. This area is situated between upper and lower thicker and convex borders, resulting in a sligh depression on the lateral side of this bone; it likely served as the attachment of the externalmost mAMES, which was likely well-developed.
Interestingly, the caudal half of the surangular of *B. leptorhynchus* closely resembles that of *Phantomosaurus neubigi* (Sander, 1997), which has been recovered within Cymbospondylidae as the sister taxon to *Cymbospondylus* (Maisch & Matzke, 2000). Except for *P. neubigi*, no other ichthyosaur shows such a pronounced coronoid (preglenoid) process. However, since in many ichthyosaurs the jaws interlock tightly with each other, or are crushed on top of each other, this feature might be more widespread than currently established.
The anatomy of the surangular is more similar to '*Callawayia' wolonggangense* (SPCV 10306; Chen et al., 2007) than *Guizhouichthyosaurus* (Pan et al., 2006), and also shows an intermediate condition between *Cymbospondylus* and more derived Merriamosauria.

Angular. The angular is preserved articulated with the rest of the lower jaw in PIMUZ T 4376 and disarticulated in GPIT 1793/1. In BES SC 999 the rostral tip of the angular occupies its original position, whereas the caudal end is displaced in a more ventral position, being taphonomically dislocated much like the splenial. In lateral view, the angular of *Besanosaurus* appears as a very elongate arched element that tapers rostrally to a gently curved, pointed end, with concave and convex dorsal and ventral margins respectively. Consequently, the angular forms its major contribution to the lateral side of the lower jaw in its caudal half, whereas rostrally the bone is overlapped by the surangular and forms the ventral side of the jaw. The contribution to the medial side of the lower jaw is represented by a low, long, rostrocaudally directed bony flange. The caudal end has a suboval outline in the sagittal plane, although it terminates with a straight suture for the articular. The angular is U-shaped in cross-section, contacting the surangular within its dorsal concavity, and the prearticular and the splenial medially. A well-preserved, three-dimensional facet for the surangular is exposed in medial view in GPIT 1793/1. The medial contact of the angular with the splenial is particularly thin and persists up to the rostral tip.
The overall shape if the angular, as well as the contacts with the adjacent bones, are more similar to '*Callawayia' wolonggangense* (SPCV 10306; Chen et al., 2007) and *Guizhouichthyosaurus* (Pan et al., 2006), than to *Ichthyosaurus*, as pointed out for the latter by Maisch & Matzke (1997*a*).

Prearticular. In the best-preserved specimen (PIMUZ T 4376), the prearticular is situated at the caudal ends of the lower jaws, together with the articular. In the holotype, BES SC 999, the left prearticular is compressed and therefore larger than in life. In PIMUZ T 4847 a potential prearticular appears disarticulated from the

surangular, but still partially articulated with the articular. In GPIT 1793/1, the prearticulars are fully disarticulated but fragmentary, both missing their rostral ends, and probably exposed in medial (internal) view. Maisch & Matzke (1997*a*) described them as thin, slender, crescent-shaped elements with a concave dorsal and convex ventral margin. Based on our observations of GPIT 1793/1 and all other specimens, we disagree with the statement on their "crescent-shape", as the concavo-convex condition appears to be very faint, albeit present. When articulated, this bone contacted the angular caudoventrally and the articular medially, until its caudal end. In fact, the corresponding facets for the prearticular are preserved in the right prearticular of GPIT 1793/1. The prearticular of *Besanosaurus* looks very similar to that in other ichthyosaurs, such as *Ichthyosaurus* (McGowan, 1973) and *Stenopterygius* (pers. obs.), but it is different from *Platypterygius australis,* in which it is more angled caudodosally (Kear, 2005).

Articular. The articular is the most caudal and the most compact element of the lower jaw, forming the mandibular portion of the craniomandibular joint. This is reflected by its complex dorsomediolateral articular surface for the quadrate, rooted on a subrectangular base that is firmly sutured to the caudal end of the surangular (laterally) and of the prearticular (mediodorsally). This is best seen in PIMUZ T 4376 and GPIT 1793/1. The concavo-convex articular surfaces of the articular bone allow wide mobility around the condyle of the quadrate. The surface texture of the articular is also peculiar, being rather roughened and granular. As noted by Maisch & Matzke (1997*a*), the caudal positioning of the articular indicates that the retroarticular portion of the mandible was short.
As described for the holotype of *Phantomosaurus neubigi* by Maisch & Matzke (2006), a portion of the articular is exposed on the lateral surface of the lower jaw, posterior to the surangular, although this may be an effect of taphonomical compression in both cases.

Hyoid. Hyoid elements are visible in PIMUZ T 4847, and possibly BES SC 999. As in most vertebrates, the hyoid bones appear short if compared to the total length of the skull and lower jaw, but most of the hyoid apparatus is cartilaginous and thus not represented in fossils. If our identification is correct, the two symmetrical elements we see disarticulated in PIMUZ T 4847 are the first ceratobranchial pair, which are commonly preserved in the majority of ichthyosaurs as the only ossified hyoid elements (Motani et al., 2013). They are straight, rostrocaudally elongated, slender bones, a little shorter than the horizontal ventral ramus of the jugal. They are flattened mediolaterally and bear symmetrical subsquared rostral and caudal ends, that are slightly wider than the midshaft of the bone. This morphology can also be seen in the exposed caudal half of the possible right ceratobranchial I of BES SC 999. The first pair of ceratobranchials of *Besanosaurus* are very similar to those of *Guanlingsaurus liangae* (GNG dq-50; Ji et al., 2013) and *Shonisaurus sikanniensis* (TMP 94.378.2; Nicholls & Manabe, 2004) in being elongated, narrow in the middle, and broader at the extremities. The 3D structure is not preserved in the hyoids of *Besanosaurus*, so that they appear taphonomically straight.

6.6.7 Dentition

The dentition is visible in all examined specimens, although the most complete tooth rows are preserved in the holotype BES SC 999, in PIMUZ T 4376, in GPIT 1793/1, and in PIMUZ T 1895. Well-preserved premaxillary sockets are also visible in the CT of BES SC 1016 (Fig. 6.15). The teeth of *B. leptorhynchus* are typically small (if compared to the jaw length and width; File S4: char. 68), conical, without carinae, pointed, and widely spaced. The crown surface shows very fine apicobasal striations, which become more pronounced on the root surface, especially in the distalmost dentary teeth (PIMUZ T 4376; Fig 18).

The premaxilla hosts at least 35 (estimated) teeth that interlock with the dentary teeth; the mesial-most premaxillary teeth are slightly curved , longer, and more slender than the distalmost teeth, which are broader, shorter, and with bulkier roots. The ventral surface of the premaxilla is flat and hosts several deep sockets, in which the teeth are implanted.

The maxillary teeth (11 preserved in PIMUZ T 4376) are shorter than the premaxillary teeth, and the distal-most ones are stouter with larger diameters but never blunt. The distalmost teeth are located almost below the caudal end of the external naris; the rostral (mesial) maxillary teeth are set in sockets, whereas the caudal (distal) teeth are set in a short groove, which is shorter than half of the rostral ramus of the maxilla as noted by Maisch & Matzke (1997*a*).

The dentary carries 38 (estimated) teeth, with the distalmost ones located below the rostral half of the rostral ramus of the maxilla. The dentary teeth show deeply striated roots, a feature that is more pronounced in the distalmost teeth. Also, the latter are much shorter and broader than the more mesial teeth (Fig. 6.18). In the dentary, the rostral (mesial) teeth are implanted in a long groove (PIMUZ T 1895), whereas the caudalmost (distalmost) teeth are set/implanted in deep sockets.

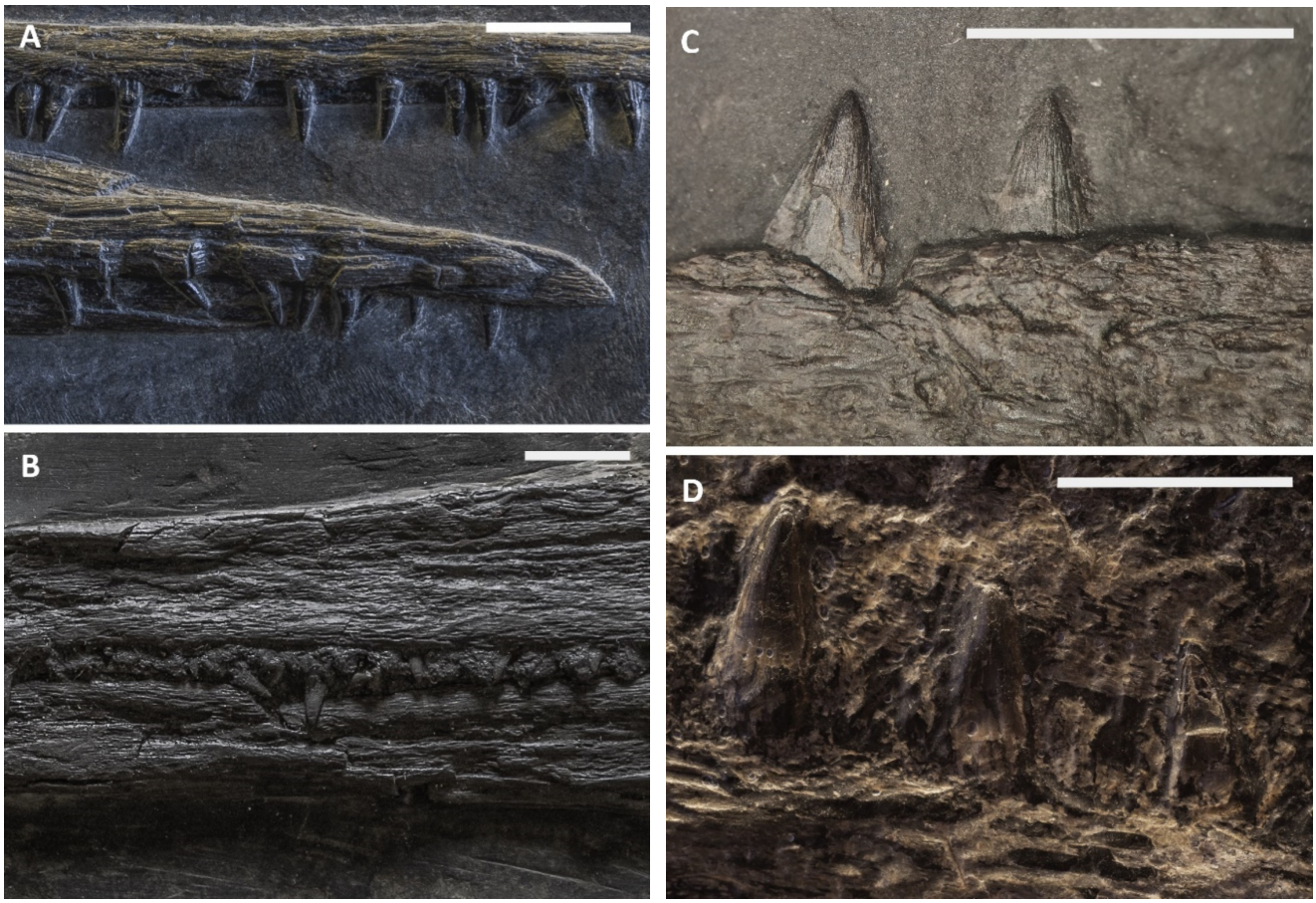

Fig. 6.18 - Teeth of the specimens referable to *Besanosaurus leptorhynchus*. (A) PIMUZ T 4376: rostralmost (mesialmost) teeth of the dentary (above, turned upside down) and the premaxillae (below); (B) BES SC 999: premaxillary teeth at mid-length of the rostrum; (C) GPIT 1793/1: rostralmost teeth of the right maxilla; (D) PIMUZ T 4847: ?dentary teeth at mid-length of the rostrum. Scale bars represent 1 cm.

6.7 Discussion

6.7.1 Remarks on specimen size and intraspecific variation

The specimens we assigned to *B. leptorhynchus* can be ordered by size (skull length), from the smallest to the largest, as follows: PIMUZ T 4376 (405 mm), PIMUZ T 1895 (455 mm), BES SC 999 (522 mm), BES SC 1016 (530 mm), GPIT 1793/1(585 mm), PIMUZ T 4847 (710 mm). Table 6.2 reports the main cranial measurements, which were taken by all of the authors from the original fossils.

Given that no significant qualitative and quantitative anatomical differences in the cranium are found between all specimens of *B. leptorhynchus* we examined, and given that the few discrepancies are probably due to taphonomical deformation, the measurements plotted in Table 6.2 likely directly correlate to size variation only. Therefore, we consider that the resulting signal indicates that all of the specimens of *B. leptorhynchus* examined here represent a possible ontogenetic series.

The skull length, together with the orbital diameter and the lower jaw length (Fig. 6.19 B and C), increases with a constant slope through the possible ontogenetic stages. However, if compared to the presacral length (Fig. 6.19A), it appears that the body length grows much faster than the skull. This is more apparent once the animal has reached the reproductive ontogenetic stage, represented in *Besanosaurus* by the holotype BES SC 999.

Table 6.2 - Selected numbers and measurements. Note: Selected numbers and measurements of each specimen of *Besanosaurus leptorhynchus*. Craniometric measures 1–10 are from McGowan & Motani (2003), 11–15 and 22–26 are from Dal Sasso & Pinna (1996), 16–21 are newly defined. Round brackets (*) indicate preserved but incomplete or deformed elements, square brackets [*] indicate estimated measurements of reconstructed elements.

	Measure/number/ratio specimen	PIMUZ T 4376	PIMUZ T 1895	BES SC 999	BES SC 1016	GPIT 1973/1	PIMUZ T 4847
1	Skull length: distance between tip of snout and caudal edge of articular surface of quadrate	405	[455]	522	[530]	[585]	(710)
2	Jaw length: distance between tip of mandible and caudal edge of surangular	412	[475]	532	[550]	[600]	(743)
3	Snout length: distance between tip of snout and rostral border of orbit	309	[320]	[366]	[368]	384	[590]
4	Premaxillary length: distance between tip of snout and rostral tip of maxilla	184	[196]	214	[220]	/	/
5	Prenarial length: distance between tip of snout and rostral border of external naris	224	[238]	270	[275]	/	/
6	Snout ratio: snout length divided by jaw length	0,75	0,67	0,69	0,67	0,59	0,79
7	Premaxillary ratio: premaxillary length divided by jaw length	0,45	0,41	0,40	0,40	/	/
8	Prenarial ratio: prenarial length divided by jaw length	0,54	0,51	0,51	0,50	/	/
9	Orbital diameter: maximum (rostrocaudal) internal diameter of orbit	67	[78]	[88]	[92]	[98]	[130]
10	Orbital ratio: orbital diameter divided by jaw length	0,16	0,16	0,17	0,17	0,16	0,17
11	Estimated number of sclerotic plates	[15]	[16]	[16]	/	/	[17]

	Measure/number/ratio specimen	PIMUZ T 4376	PIMUZ T 1895	BES SC 999	BES SC 1016	GPIT 1973/1	PIMUZ T 4847
12	Internal diameter of the sclerotic ring (rostrocaudal)	21	[25]	[32]	/	/	[50]
13	External diameter of the sclerotic ring (rostrocaudal)	51	[58]	[63]	/	/	[80]
14	Internal diameter of the sclerotic ring (dorsoventral)	17	[26]	[28]	/	/	[45]
15	External diameter of the sclerotic ring (dorsoventral)	38	[58]	[57]	/	/	[73]
16	Parietal lenght along the midline	36	(45)	(48)	[50]	58	/
17	Frontal length along the midline	49	55	(61)	/	71	[110]
18	Lenght of caudal ramus of maxilla	(26,5)	38	[57]	(45)	(45)	/
19	Length of rostral ramus of maxilla	81	83	[110]	(95)	138	/
20	Lower jaw height at coronoid process	27	/	(59)	[57]	47	[69]
21	Surangular height at notch for the jugal	25,5	/	(43)	42	41,5	[56]
22	Length from the caudal margin of the naris to the rostral margin of the lower jaw	156	[220]	237	[300]	/	/
23	Length of the cheek region	43	[60]	64	[75]	/	/
24	Jaw depth at mid-length of the jaw	14	23	22	/	/	/
25	Sclerotic ratio (sclerotic diameter 13 divided by orbital diameter)	0,31	0,32	0,36	/	/	0,38
26	Mandibular ratio (jaw depth divided by jaw length)	0,03	0,05	0,04	/	/	/
28	Overall body length	(2,124)	/	5,065	/	/	/
29	Presacral length	[1,215]	[1,406]	2,052	/	/	(3,280)

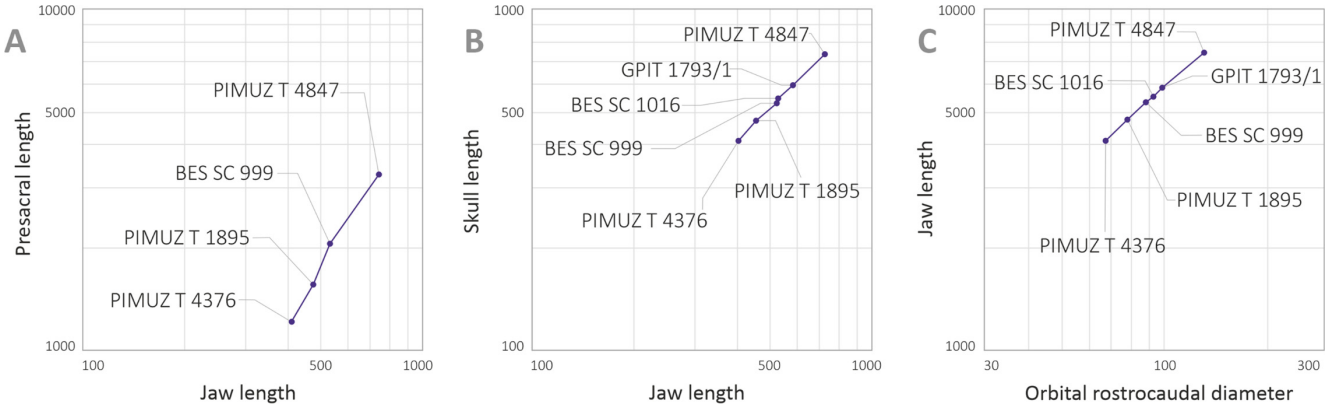

Fig. 6.19 - Selected plots showing relevant cranial ratios across studied specimens. Selected plots showing relevant cranial ratios across studied specimens supporting that they represent an ontogenetic series. (A) Presacral length/jaw length; (B) orbital rostrocaudal diameter/Jaw length; (C) jaw length/orbital rostrocaudal diameter.

6.7.2 Reconstruction

Although the holotype of *B. leptorhynchus* (BES SC 999) preserves very little three-dimensional information, together with information from the referred specimens, it provides enough anatomical detail allowing us to infer most of the three-dimensional anatomy of the skull of the taxon. The reconstruction proposed in Fig. 6.20 depicts the bone proportions in the holotype, although much of the 3D anatomyhas been inferred primarily from the best-preserved referred specimen (PIMUZ T 4376) and only a small

portion of 3D anatomical information was obtained from other shastasaurid specimens (e.g., the arrangement of the palatal elements in '*Callawayia*' *wolonggangense* [SPCV10305]; Fig. 6.S5). The unpreserved osteological features, represented in Fig. 6.20, were inferred following the methodology proposed by Bryant & Russell (1992), i.e., based on the cladistic distribution of known features in related taxa. A 3D 1:1 model of the skull was first reconstructed from thin cardboard based on the 2D drawings of the specimens (Figs. 6.4–6.9) and used as a reference for the main spatial distribution of the bones. Shapes, dimensions, and proportions of the skull roof bones are mostly based on PIMUZ T 4376. The morphology of the internal side of these bones is very well expressed in GPIT 1793/1.

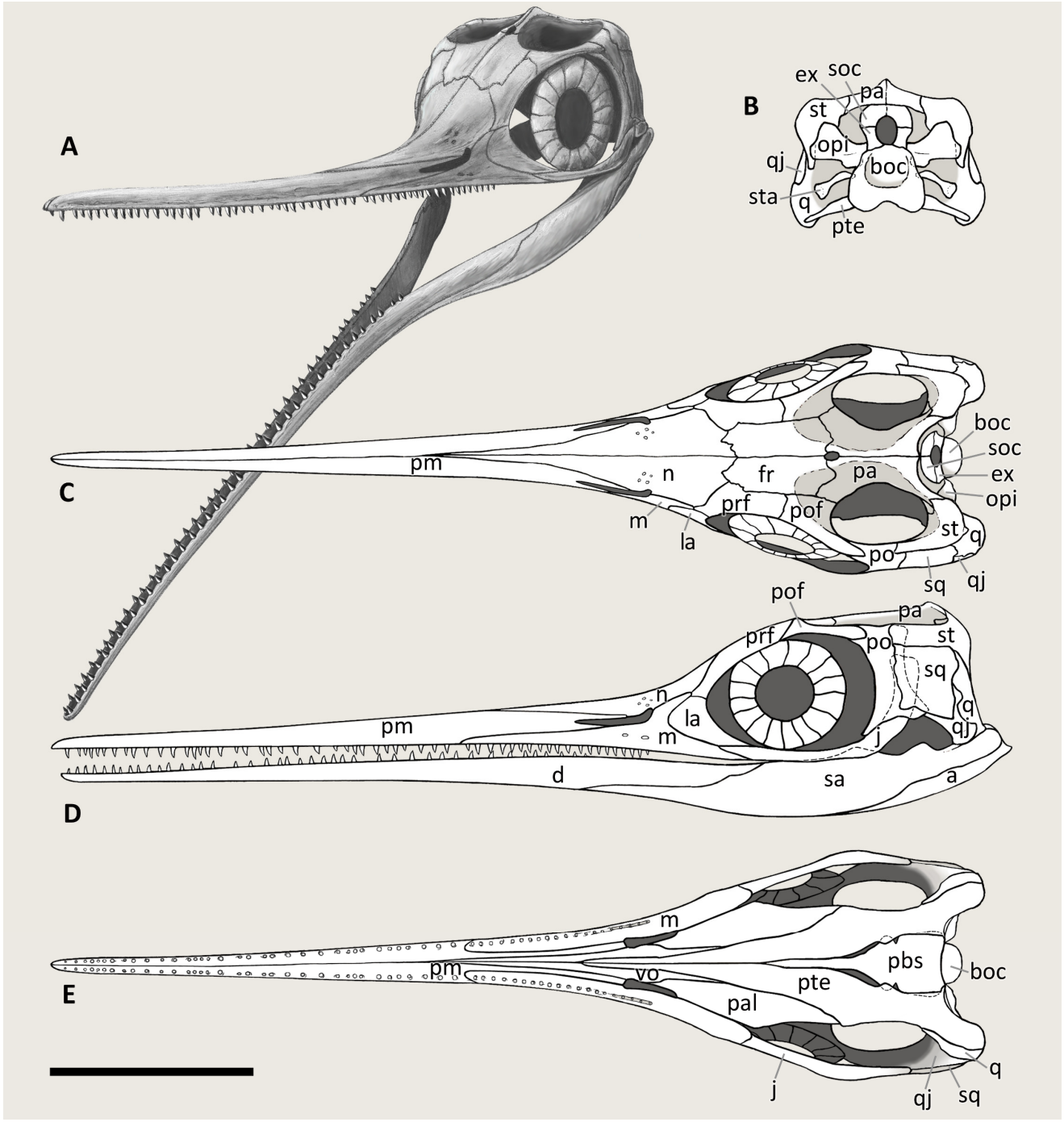

Fig. 6.20 - Cranial reconstruction of *Besanosaurus leptorhynchus*. Articulated skull and mandible in (A) left rostrolateral, (B) caudal (occipital), (C) dorsal, (D) left lateral, and (E) ventral (palatal) view. Abbreviations: see text. Line drawings by Marco Auditore.

The distinct curvature of the nasal, separating the gracile rostrum from the rest of the skull is inferred by the presence of extensive fractures in this region, observed in BES SC 999, PIMUZ T 4376, and PIMUZ T 1895, which, in particular, also shows similar additional fractures laterally, pointing out the presence of a short descending bony flange of the nasal, dorsally to the naris.
The proportions of the sclerotic ring are those of the holotype, however the anatomy of scleral plates is deducted from PIMUZ T 4376 and PIMUZ T 1895, since in BES SC 999 only half of the ring is preserved.
The lower jaw of BES SC 999 is unnaturally expanded dorsoventrally and the caudal elements have been partly disarticulated; to reconstruct the correct height and arrangement of the lower jaw, the model in Fig. 6.20 was based on the articulated lower jaw of PIMUZ T 4376.
The jugal turned out to be one of the most difficult bones to rearticulate with the rest of the skull. This bone is often found completely or partially disarticulated in the specimens described, and in any case, its caudal ramus is always loose from the adjacent bones. Based also on its remarkable length, we assumed that the caudal end of the jugal was simply juxtaposed, unsutured, medially to the squamosal and the postorbital, as seen also in *Guizhouichthyosaurus tangae* (IVPP 11896; pers. obs.) (Fig. 6.S2).
The postorbital region is longer than tall in *Besanosaurus* and other shastasaurids, with the exception of '*Callawayia wolonggangense*', in which the postorbital region is short, like in other post-Triassic ichthyosaurs.
The reconstruction in caudal view is based on BES SC 999, for the basioccipital; PIMUZ T 4376, which preserves the facets for the exoccipital on the basioccipital, and the quadrate; and GPIT 1793/1, which possesses the best preserved supraoccipital and opisthotic.
The 3D anatomy of the supratemporal and the way the quadrate articulates with the adjacent bone elements are inferred from the elements that articulate with them and based on comparison with, a referred specimen of *Guanlingsaurus liangae* (SPCV 03107, pers. obs.) (Fig. 6.S3).
The palatal view was based on BES SC 1016, which preserves paired pterygoids; GPIT 1793/1, that shows a finely 3D preserved left pterygoid and putative palatines; and through observation of *Guizhouichthyosaurus tangae* (IVPP V 11853; pers. obs.) and *'Callawayia' wolonggangense* (SPCV 10305, pers. obs.) (Fig. 6.S5). The reconstruction we propose in Fig. 6.20E is also based on Huene (1916), Riess (1986: fig. 5), and McGowan & Motani (2003: fig. 40) for the general anatomy of the skull.

6.7.3 Phylogeny

In order to test the phylogenetic placement of *B. leptorhynchus* within Ichthyosauromorpha, we used the phylogenetic matrix of Huang et al. (2019), the most recently updated version of the phylogenetic matrix of Ji et al. (2016), a comprehensive dataset of 218 morphological characters scored for 73 ichthyosauromorph taxa. Even though the recently published character-taxon matrix of Moon (2017) is broader in scope, containing 287 characters scored for 116 taxa, we decided the matrix of Huang et al. (2019) was a more appropriate basis for performing a phylogenetic analysis as it focusses on non-parvipelvian ichthyosaurs. Our decision was motivated by the fact that Moon (2017) scored only 25 taxa (including only 3 non-parvipelvian taxa) (~22%) based on personal observation of fossil specimens, whereas Huang et al. (2019) scored the majority of taxa based on personal observation of relevant specimens, including all of the Chinese and American shastasaurids, and almost all Triassic ichthyosauromorphs in general (see Ji et al., 2016; Jiang et al., 2016; Motani et al., 2017).

B. leptorhynchus was scored on the basis of personal observation of the type and all referred specimens described in this study. In addition, the scorings of several cranial characters modified for the following shastasaurids, based on personal observation of fossil specimens, aided with relevant literature: *Guizhouichthyosaurus tangae* (IVPP V11865, IVPP V11869; Maisch et al., 2006), '*Callawayia' wolonggangense* (SPCV 10305, SPCV 10306; Chen et al., 2007), *Guanlingsaurus liangae* (SPCV 03107; Sander et al., 2011) and *Shastasaurus pacificus* (UCMP 9017; Sander et al., 2011). All characters were treated as unordered and carrying equal weights.

The modified phylogenetic matrix (File S4) was analysed in TNT 1.5 (Goloboff et al., 2008; Goloboff & Catalano, 2016), with memory set to hold 99,999 trees. The New Technology search option (a combination of Sectorial Search, Ratchet, Drift, and Tree fusing, with 100 random addition sequences) was used, followed by a round of TBR branch-swapping. Bremer support values were calculated in TNT 1.5 using the built-in Bremer Support tool from trees resulting from TBR branch swapping, by holding trees suboptimal by ten steps.

The analysis resulted in 14,480 most parsimonious trees (MPTs) of 713 steps (CI = 0.363, RI = 0.788). The phylogenetic analysis caused a loss of resolution at the base of Merriamosauria (last common ancestor of *Shastasaurus pacificus* and *Ichthyosaurus communis* and all of its descendants; Ji et al., 2016), with a strict consensus topology recovering a polytomy formed by all genera recovered in a monophyletic Shastasauridae in the analysis of Huang et al. (2019), *Californosaurus perrini*, *Callawayia neoscapularis*, Toretocnemidae and Parvipelvia. In 60% of the MPTs, *B. leptorhynchus* was recovered as the earliest-diverging representative of a 'shastasaurid' grade, but other possible resolutions of the Merriamosauria node recovered *B. leptorhynchus* as either the most basal taxon within a monophyletic Shastasauridae (as in Huang et al.,2019), or in a shastasaurid sub-clade comprising ((*B. leptorhynchus*, *Guizhouichthyosaurs tangae*), '*Callawayia*' *wolonngangensis*) (Fig. 6.21).

The majority (60%) of MPTs resulting from our analysis recovered 'Shastasauridae' as a paraphyletic group at the base of Merriamosauria, which is in agreement with some other large-scale studies of ichthyosaur phylogeny that also recovered 'shastasaurids' as a grade (Callaway, 1989; Maisch & Matzke, 2000; Sander, 2000; Fröbisch et al., 2013; Moon, 2017). However, the remainder of the resulting MPTs recovered a monophyletic Shastasauridae, similar to the results obtained by Huang et al. (2019), Motani et al. (2017), Jiang et al. (2016), Ji et al. (2016) and Motani (1999). As a consequence, we do not consider the results of our analysis as conclusive for solving the controversy around shastasaurid monophyly/paraphyly. Because the introduction of new phylogenetic data from *B. leptorhynchus* and the revision of several cranial character states for other shastasaurids in the dataset of Huang et al. (2019) caused a loss of phylogenetic resolution at the base of Merriamosauria, it is expected that revisions of shastasaurid postcranial character scores, as well as the revision of character scores for other Triassic ichthyosaurs in general, might result in further changes to the topology obtained by Huang et al. (2019). Similarly, the relative phylogenetic position of *B. leptorhynchus* within Shastasauridae remains ambiguous, as in the subset of MPTs which recovered a monophyletic Shastasauridae, *B. leptorhynchus* was recovered as either the earliest-diverging shastasaurid, or forming a clade with the Ladinian–Carnian Chinese taxon *Guizhouichthyosaurus* (e.g., Maisch et al., 2006; Jiang et al., 2020) and the Carnian Chinese taxon '*Callawayia*' *wolonggangense*. Further studies of the taxonomy and phylogenetic relationships of Triassic ichthyosaurs are needed in order to unambiguously resolve the relationships at the base of Merriamosauria, but the results of our phylogenetic analysis, which recovered *B. leptorhynchus* as an early-diverging merriamosaurian, confirm its importance for our understanding of the early evolutionary and biogeographic history of shastasaurids, in particular, and merriamosaurians, more generally.

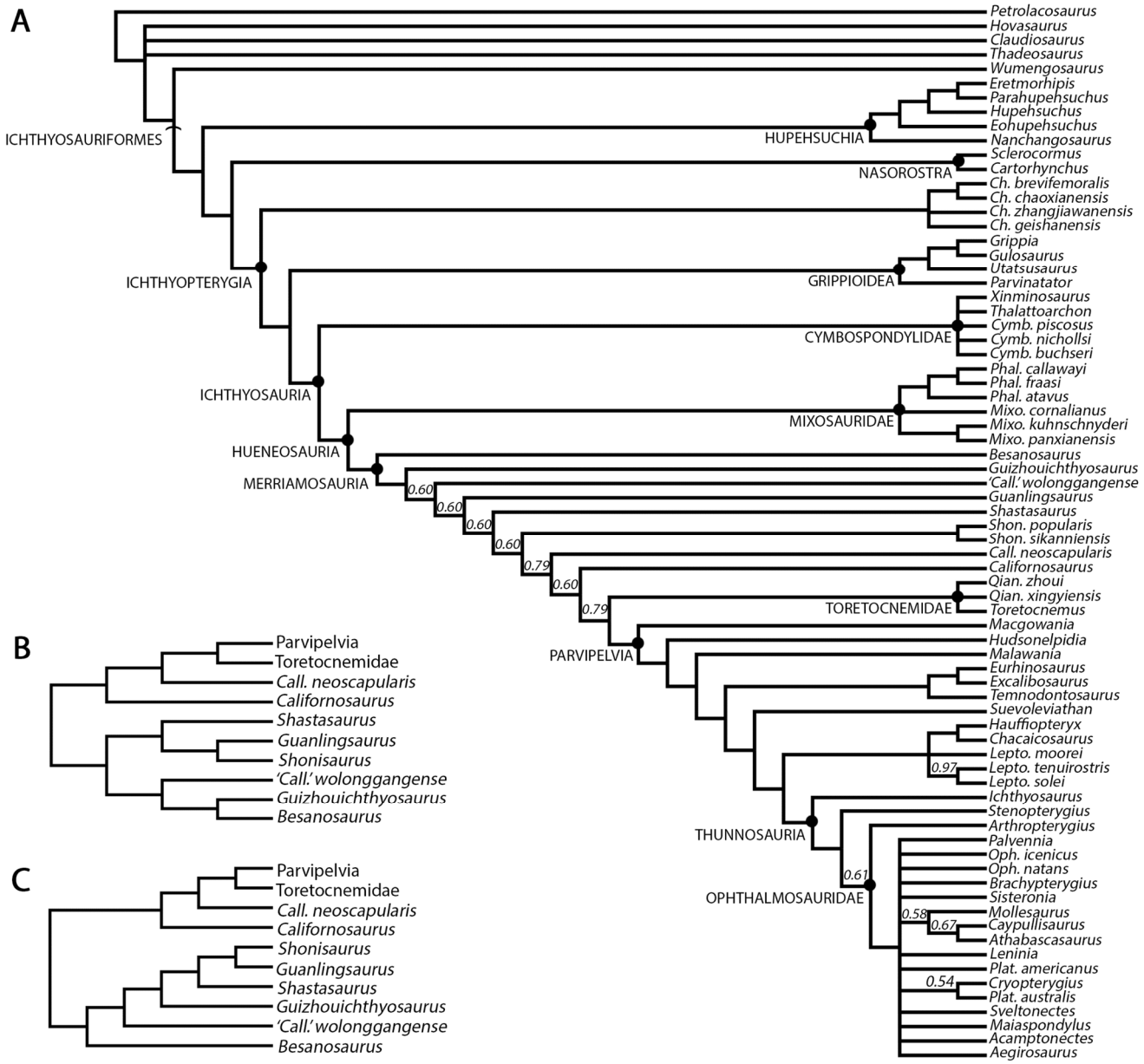

Fig. 6.21 - Cladogram of Ichthyosauriformes and phylogenetic position of *Besanosaurus*. (A) 50% Majority rule consensus of 14,480 MPTs of 713 steps (CI = 0.363, RI = 0.788) obtained from parsimony analysis of the character-taxon matrix of Huang et al. (2019). Note that 'shastasaurids' are recovered as a grade at the base of Merriamosauria. Numbers above nodes indicate proportion of MPTs with specific node resolution. (B) Alternative resolution of Merriamosauria, with Shastasauridae recovered as a clade, and *Besanosaurus leptorhynchus* being the sister taxon of *Guizhouichthyosaurus*. (C) Alternative resolution of Merriamosauria, with Shastasauridae recovered as a clade, and *Besanosaurus leptorhynchus* being the earliest-diverging shastasaurid. Abbreviations: *Call., Callawayia; Ch., Chaohusaurus; Cymb., Cymbospondylus; Lepto., Leptonectes; Mixo., Mixosaurus; Oph., Ophthalmosaurus; Qian., Qianichthyosaurus; Phal., Phalarodon; Shon., Shonisaurus*.

6.7.4 Feeding ecology of *Besanosaurus*

Ichthyosaurs appeared in the Early Triassic, just after the Permo-Triassic extinction event, and by the Middle Triassic they achieved a great taxonomic and ecomorphological diversity (Scheyer et al., 2014; Stubbs & Benton, 2016). The diversity in ichthyosaur taxa in the Besano Formation is a good example of this event, even in a relatively small marine basin. Indeed, we may assume the establishment of a niche partitioning between the ichthyosaurian taxa belonging to the Besano fauna: mixosaurids (with different ecologies), *Cymbospondylus buchseri*, and *Besanosaurus leptorhynchus*. Direct dietary

evidence exists for *Mixosaurus* and *Cymbospondylus*. The holotype of *Cymbospondylus buchseri* shows a gastrointestinal content consisting exclusively of hooklets of soft-bodied coleoid cephalopods (Rieber, 1970; Sander, 1989).A recent case of dietary preference has been described for *Mixosaurus cornalianus* (Renesto et al., 2020), where the authors found tiny coleoid hooklets in the gut content of one specimen (BES SC 1000), which also preserves tiny fish vertebrae and scales from at least three different taxa. Hooklet dimensions suggest a partitioning driven by the size of the prey items in these two groups, and the additional presence of small fish in the *Mixosaurus* diet strengthens the idea that the two taxa relied on different food sources. In addition, mixosaurids and *Cymbospondylus* often seem to occur together, and with almost a global distribution (Nevada, Svalbard, and Monte San Giorgio). This may explain how these two ichthyosaur taxa could share the same open marine environment. In fact, following the conclusions of Renesto et al. (2020), *Mixosaurus cornalianus* was likely an efficient open water swimmer and maneuvering exploiting BCF (body/caudal fin) periodic propulsion, and thus able to coexist with the bigger *Besanosaurus* and *Cymbospondylus*, occupying its own niche.

C. buchseri has been considered an apex predator (Fröbisch et al., 2006; Pardo-Perez et al., 2020). However, its known gut contents show that this animal could fed lower in the food web, although this "last meal" does not exclude the possibility of a larger prey selection, consistently with its skull anatomy and tooth morphology.

The skull of an adult *Besanosaurus leptorhynchus* appears quite small, if compared to the overall body length, even smaller than in *Guizhouichthyosaurus tangae* (Pan et al., 2006; Shang & Li, 2009). Jiang et al. (2020) recently described a thalattosaurian trunk in the stomach region of a *Guizhouichthyosaurus,* inferring macropredation in this taxon. The authors further hypothesized this behaviour for other large-bodied shastasaurids, including *Besanosaurus*. Given its longirostrine morphology, it is unlikely that *Besanosaurus* was a macropredator *sensu* Jiang et al. (2020). The rostrum of *B. leptorhynchus* is remarkably long and slender and equipped with several almost homodont, relatively tiny teeth, ornamented by faint grooves running from the tip to the base of the crown. The small skull and slender rostrum would have allowed rapid lateral or vertical movements of the head and would have been fairly hydrodynamic (at least in the cranialmost portion of the body), as suggested, e.g., for teleosaurids (Pierce et al., 2009). Dal Sasso & Pinna (1996) reported that the teeth of *Besanosaurus* are more similar to that of Jurassic ichthyosaurs, such as *Stenopterygius* (see for example Dick & Maxwell, 2015: fig. 1), than to other Triassic ichthyosaurs known at that time, and hypothesized that *Besanosaurus* fed nearly exclusively on small coleoid cephalopods. The minute teeth and slender rostrum suggest that *Besanosaurs* was a "soft-prey specialist" sensu Fischer et al. (2016). Also, following Massare (1987) and Pierce et al. (2009), the mesial (rostral) teeth of *Besanosaurus* can be defined as the "pierce 1 guild" (long, delicate, and sharply pointed teeth for piercing small fish and soft cephalopods), and the distal (caudal) teeth as the "smash guild" (teeth bearing rounded points for grasping belemnoids and soft cephalopods), with the middle teeth showing an intermediate condition. This morphology and size do not change with skull and specimen size increase, unlike what was observed in *Stenopterygius* (Dick & Maxwell, 2015; Dick et al., 2016).

A single coleoid cephalopod hooklet surrounded by other gastric material is preserved in the thoracic region of the holotype of *B. leptorhynchus*, positioned 215 mm caudal to the right coracoid and 55 mm ventral to the vertebral column (Fig. 6.22). The hooklet is 2 mm long, has a robust shaft and a very curved uncinate tip, a central ridge, and a long articular process at the base, similar to the type C and D hooklets described by Pollard (1968: fig. 2). Among the known Middle Triassic (Monte San Giorgio) forms, the hooklet found in *Besanosaurus* is consistent in shape (but twice the size) with a mid-arm

element of a specimen of *Phragmoteuthis ?ticinensis* (Rieber, 1970: figs. 1-3). Comparable hooklets are those recently found in the stomach region of a *Mixosaurus cornalianus* (Renesto et al., 2020: fig. 7A). In modern cetaceans, a long and slender rostrum with several small conical and homodont teeth is often coupled with a raptorial snap feeder-like hunting strategy, associated with a mostly piscivore diet (e.g., *Stenella longirostris*, *Pontoporia*, *Inia* and *Platanista;* Marx et al., 2016; Marshall & Pyenson, 2019). A longirostrine skull enables high velocity at the jaw tips, at the expense of biting forces, which is advantageous for capturing small elusive prey if combined to a rapid snapping of the jaws and fast lateral or vertical movements of the rostrum. *Besanosaurus* could fall into this category.
The inferred presence of well-developed jaw muscles (see surangular description) leads us to assume an efficient and fast jaw-closing movement, which is consistent with this hypothesis. That these muscles could have also generated strong biting forces is unlikely, given the thin and slender anatomy of the rostrum.

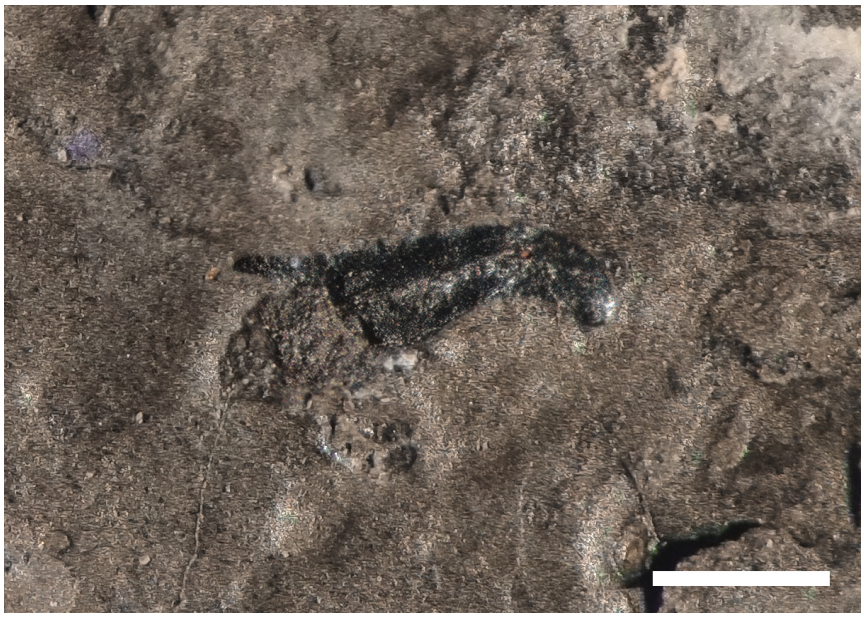

Fig. 6.22 - Isolated hooklet of a coleoid cephalopod preserved in the thoracic region of BES SC 999, holotype of *Besanosaurus leptorhynchus*. Scale bar represents 1 mm.

The convergence of a longirostrine skull morphology between diapsids and cetaceans (gharials and river dolphin, which primarily feed on small fishes) has been discussed by McCurry et al. (2017), who proposed that this convergence is driven by prey morphology and the methods of prey capture. Longirostrine morphology in river dolphins is also associated with a large degree of movement in the cervical vertebrae, more than in other oceanic species (Cassens et al., 2000; McCurry et al., 2017).
Piscivory for *Besanosaurus* would be further consistent with a prey driven niche partitioning among the Besano Formation ichthyosaurs. In any case, it appears that *Besanosaurus* would have preferred small, soft-bodied, and elusive prey which may have included coleoids. Unlike *Besanosaurus*, *Cymbospondylus* may have used a more forceful feeding strategy (slower feeding cycle and higher biting forces), given its less slender and more robust rostrum. Aside from the nature of the prey, it is clear that different hunting strategies, given by very different skull morphologies and dimensions, may have helped to maintain low competition among such a diverse ichthyosaur fauna, cohabitating the same ecosystem. Interestingly, in the southeastern Chinese Carnian faunas, in absence of a large cymbospondylid, the Shastasauridae diversity (three taxa with very different rostrine morphology and

ecologies; see for example Chen et al., 2006; Sander et al., 2011; Jiang et al., 2020) is greater than in the Besano Fauna.

If all three ichthyosaur taxa from the Besano Formation preyed on coleoids, we would expect a more abundant number of specimens and/or diversity in dibranchiate taxa. Such a diversity – also in term of ontogenetic stages – is not reported in the fossil record, but the lack of coleoids in the Besano Formation (with the exception of those in the gut contents) could be explained by particular bottom conditions of the basin not allowing the preservation of the cephalopod soft tissue.

To date, the Anisian record of a true ichthyosaurian apex predator in the form of a *Thalattoarchon saurophagis*-like animal (Fröbisch et al., 2013) is missing in the Besano Formation or in the broader Tethys realm. *Cymbospondylus* might have filled this gap, nevertheless no specimens larger than *C. buchseri* holotype (~5,5 m; Sander, 1989) have been reported from the Besano Formation to date. *Nothosaurus giganteus* might have had this role as well, however very few specimens have been reported from the middle part of the Besano Formation (e.g., PIMUZ T 4829), whereas most specimens are from the Muschelkalk deposits of the Germanic Basin (e.g., Rieppel, 2000; Klein et al., 2015). This sauropterygian was therefore presumably a dweller of nearshore environments. The ecological role of the three known ichthyosaurian taxa of the Besano Formation is still not fully understood, especially their swimming style, and still under examination, pending a detailed description of the postcranial osteology of *Besanosaurus* (under study elsewhere).

6.7.5 Longirostry and large size in *Besanosaurus*

Besanosaurus represents the earliest known large-sized marine diapsid (~ 8 m) that acquired an extreme longirostrine skull morphology: prior to *Besanosaurus*, marine reptiles possessing a longirostrine morphology never reached such size (Fig. 6.23).

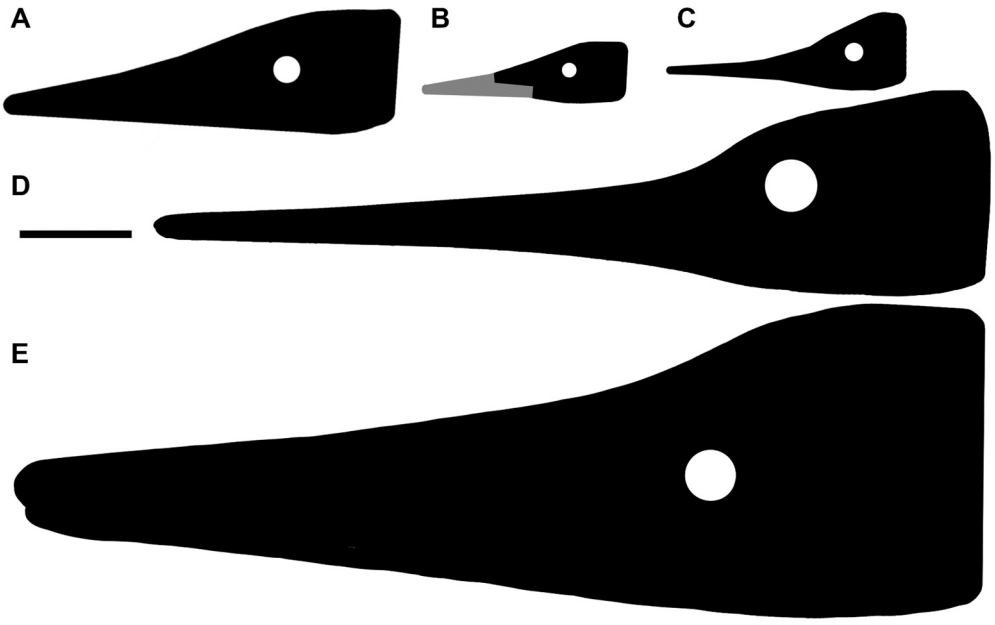

Fig. 6.23 - Early and Middle Triassic ichthyopterygian heads possessing longirostry. Simplified outlines of four different Early and Middle Triassic ichthyopterygian heads possessing a long and slender rostrum. Specimens are at the same scale. (A) *Utatsusaurus hataii* (UHR 30691, Motani, Minoura & Ando, 1998); (B) *Grippia longirostris* (PMU R445, Motani, 2000); (C) *Mixosaurus cornalianus* (BES SC 1000, Renesto et al., 2020); (D) *Besanosaurus leptorhynchus* (PIMUZ T 4847, this paper); (E) *Cymbospondylus buchseri* (PIMUZ T 4351, Sander, 1989). Scale bar represents 10 cm.

The idea that a longirostrine skull ensures high velocity at the jaw tips, which is advantageous for capturing small elusive prey is also consistent with Pierce et al. (2009) discussion about the morpho-functional significance of the longirostrine anatomy in teleosaurids (e. g., *Plagiophthalmosuchus gracilirostris*, Johnson et al., 2020). An increased skeletal mass in teleosaurids, exemplified by a low pneumaticity and the development of thick osteoderms, would have resulted in an increased high body inertia (Hua & Buffrénil, 1996; Pierce et al., 2009). The mentioned authors suggested that a high body mass would also have permitted the body to remain stationary during rapid and precise movements of the head and neck. If we apply this to *Besanosaurus* we can infer that a longirostrine morphology may have reasonably coevolved with a high body mass, granting great benefits to the fishing ability of this animal. In addition, as discussed in the previous paragraph, foraging lower in the food web, together with an increased feeding efficiency, could have contributed to the appearance of remarkable large body size. In fact, following the model of Ferrón et al. (2018) on gigantism in active marine predators, an increased feeding efficiency should have led to a more efficient way of consuming metabolic resources, triggering the possibility to acquire bigger body sizes without shifting to a higher metabolic level. A similar increase of body size, triggered by the acquisition of a more efficient feeding mode (although very different from longirostry), occurred in Mysticeti (Marx et al., 2016) and possibly happened at a higher metabolic level than in ichthyosaurs (Ferrón et al., 2018). A similar process may have resulted in the appearance of Late Triassic truly giant forms (> 20 m), such as *Shonisaurus sikanniensis* (Nicholls & Manabe, 2004). Interestingly, some giant penguins (e.g., *Icadyptes,* Clarke et al., 2007) do also show a remarkable longirostrine beak. Indeed, the acquisition of longirostry, enabling to reach large sizes, should not have been the only ecological pathway to gigantism.
Undoubtedly, gigantism may have granted many other advantages, such as a reduced vulnerability against predators, and possibly a more efficient body heat preservation, that in turn could have represented itself an intrinsic factor promoting gigantism, fueling positive feedback.

6.8 Conclusions

In general, the specimens here described preserve and represent a remarkably complete cranial anatomy, so that *Besanosaurus leptorhynchus* now is among the best-understood Middle Triassic Ichthyosaur taxa to date. Our revision of the skull morphology of this taxon clarified long-standing controversies regarding its cranial anatomy and the taxonomy of shastasaurids from Monte San Giorgio. Based on this rich fossil material, we have demonstrated that *Mikadocephalus gracilirostris* (GPIT 1793/1) is a junior synonym of *Besanosaurus leptorhynchus*, providing evidence to refute previous hypotheses (Maisch & Matzke, 1997, 2000; Maisch, 2010) about the co-occurrence of two different shastasaurid taxa (*Besanosaurus* and *Mikadocephalus*) in the Besano Formation.
The six specimens here described represent a potential ontogenetic series covering a certain size range of mainly adult and potentially subadult specimens (Fig. 6.19), ordered by increasing size as follows: PIMUZ T 4376, PIMUZ T 1895, BES SC 999, BES SC 1016, GPIT 1793/1, PIMUZ T 4847. An allometric growth signal, yet to be fully tested, has also been detected. Other sources of intraspecific variation such as sexual dimorphism, cannot be ruled out, however, partly due to the limited dataset. Here we also report evidence that *Besanosaurus* was the largest Middle Triassic ichthyosaur taxon of the Western Tethys since we confidently estimate a full adult size of about 8 m for specimen PIMUZ T 4847.

Besanosaurus possesses an extremely long, slender, and gracile snout, representing an ecological specialization never seen before the Anisian in a large sized (~ 8 m) diapsid. The diagnostic, prominent coronoid (preglenoid) process of the surangular and a large rugose area for the attachment of the mAMES allow to infer the presence of well-developed jaw closing muscles, which likely had an important functional role: we assume an efficient and fast jaw closing movement and hypothesize a snap-feeder-like hunting strategy, with a specific preference for small and elusive prey (such as coleoids and/or small fishes). Among the ichthyosaurian Besano-Monte San Giorgio Fauna (*Cymbopondylus,* mixosaurids, and *Besanosaurus*), different hunting strategies, demonstrated by different morphologies and dimensions of the rostra, should have led to the maintenance of low interspecific competition (i.e., niche partitioning). We also hypothesize that the specialization represented by a longirostrine morphology might have been driven by prey preference and the methods of prey capture. *Mixosaurus* and *Cymbospondylus* show almost a global distribution; on the contrary, *Besanosaurus* is known only from the Besano Formation (Italy and Switzerland). A wider distribution of this genus is expected (and supported by McGowan & Motani, 2003: 135-136): it seems unlikely to us that *Besanosaurus* would be represented only in the Alpine Tethys realm.
Last but not least, the importance of *Besanosaurus* is not only given by the completeness and remarkable preservation of its remains, and its ecological role, but also by the key phylogenetic position occupied by the taxon in the ichthyosaurian phylogeny: our analysis, performed with a matrix that includes around 90% of unambiguous scores for *B. leptorhynchus* and revised scores for other Triassic taxa, shows that this taxon represents the basalmost member of Shastasauridae.

6.9 Acknowledgments

We thank the volunteers of the former “Gruppo paleontologico di Besano”, who unearthed the holotype of *Besanosaurus leptorhynchus*, and many other exceptional fossils. We also thank F. Fogliazza (MSNM) and C. Egli (PIMUZ) for preparation of the two new skulls; M. Auditore for anatomical drawings; L. Forzenigo, C. Bonelli, and G. Terribile (Fondazione IRCCS “Cà Granda” Ospedale Maggiore Policlinico di Milano) for CT analysis of the whole holotype of *B. leptorhynchus*; the Soprintendenza Archeologica della Lombardia for permissions. For access to key specimens in museum collections we thank T. Goller and I. Werneburg (GPIT), R. B. Hauff (Urweltmuseum Hauff, Holzmaden), C. Klug (PIMUZ), E. Maxwell (SMNS), L. Cheng and X.-H. Chen (WGSC), C. Li and Q. Shang (IVPP), Pat Holroyd (UCMP), Kevin Seymour and Brian Iwama (ROM). We also thank M. Auditore, M. Balini, S. Maganuco and G. Teruzzi, for helpful discussions. This paper is part of a Ph.D. project (G. Bindellini) focusing on the Besano Formation fauna, led by the Università Statale di Milano (M. Balini) in agreement with the Museo di Storia Naturale di Milano (C. Dal Sasso). Comparative data collection by ASW was funded by a Natural Environment Research Council (NERC) Ph.D. Studentship (cohort grant NE/L501530/1) carried out at the Department of Earth Sciences, University of Oxford (2013–2017). TMS acknowledges support by Swiss National Science Foundation (grant no. 31003A_179401) and the late Max Kuhn (Uster) is warmly acknowledged for having generously supported the preparation of PIMUZ specimens. Finally, we thank the editor Mark T. Young, Neil Kelley and an anonymous reviewer for their constructive comments.

6.10 References

Andrews CW. 1910. *A descriptive catalogue of the marine reptiles of the Oxford Clay, part 1*. British Natural History Museum, London, 215 pp.

Benton MJ, Zhang Q, Hu S, Chen ZQ, Wen W, Liu J, Huang J, Zhou C, Xie T, Tong J, Choo B. 2013. Exceptional vertebrate biotas from the Triassic of China, and the expansion of marine ecosystems after the Permo-Triassic mass extinction. *Earth Sciences Review*, 125:199-243.

Bernasconi SM. 1991. Geochemical and microbial controls on dolomite formation and organic matter production/preservation in anoxic environments a case study from the Middle Triassic Grenzbitumenzone, Southern Alps (Ticino, Switzerland). D. Phil. thesis, Swiss Federal Institute of Technology Zürich, Switzerland, 196 pp.

Bernasconi SM. 1994. Geochemical and microbial controls on dolomite formation in anoxic environments: A case study from the Middle Triassic (Ticino, Switzerland). *Contributions to Sedimentology*, 19:1-109.

Bernasconi SM, Riva A. 1993. Organic geochemistry and depositional environment of a hydrocarbon source rock: the Middle Triassic Grenzbitumenzone Formation, Southern Alps, Italy/Switzerland. In: Spencer AM eds. *Generation, Accumulation and Production of Europe's Hydrocarbons (vol.3).* Springer, Berlin, Heidelberg, pp. 179-190.

Bindellini G, Balini M, Teruzzi G, Dal Sasso C. 2019. Ammonoid and *Daonella* zonation of the Sasso Caldo quarry (Besano Formation, Middle Triassic). Strati 2019, 3rd International Congress on Stratigraphy. ST2.4 Ammonoids in stratigraphy: Abstract book, p.87.

Brack P, Rieber H. 1986. Stratigraphy and ammonoids of the lower Buchenstein Beds of the Brescian Prealps and Giudicarie and their significance for the Anisian/Ladinian Boundary. *Eclogae Geologicae Helvetiae*, 79:181-225.

Brack P, Rieber H, 1993. Towards a better definition of the Anisian/Ladinian boundary: New biostratigraphic data and correlations of boundary sections from the Southern Alps. *Eclogae Geologicae Helvetiae*, 86 (2):415-527.

Brack P, Rieber H, Nicora A, Mundil R. 2005. The Global boundary Stratotype Section and Point (GSSP) of the Ladinian Stage (Middle Triassic) at Bagolino (Southern Alps, Northern Italy) and its implications for the Triassic time scale. *Episodes*, 28:233-244.

Brinkmann W. 1994. Paläontologisches Museum der Universität Zürich: Führer durch die Ausstellung, Zürich, 108 pp.

Brinkmann, W. 1997. Die Ichthyosaurier (Reptilia) aus der Mitteltrias des Monte San Giorgio (Tessin, Schweiz) und von Besano (Lombardei, Italien) – der aktuelle Forschungsstand. *Vierteljarsschrift der Naturforschenden Gesellschaft in Zürich*, 142:69–78.

Bryant HN, Russell AP. 1992. The role of phylogenetic analysis in the inference of unpreserved attributes of extinct taxa. *Philosophical Transactions of the Royal Society, Series B,* 337:405-418.

Bürgin T, Rieppel O, Sander PM, Tschanz K. 1989. The fossils of Monte San Giorgio. *Scientific American*, 260:74-81.

Callaway JM, Massare JA. 1989. *Shastasaurus altispinus* (Ichthyosauria, Shastasauridae) from the Upper Triassic of the El Antimonio district, northwestern Sonora, Mexico. *Journal of Paleontology,* 63:930-939.

Camp CL. 1980. Large ichthyosaurs from the Upper Triassic of Nevada. *Paleontographica*, 170:139-200.

Cassens I, Vicario S, Waddell VG, Balchowsky H, Van Belle D, Ding W, Fan C, Lal Mohan RS, Simoes-Lopes PC, Bastida R, Meyer A, Stanhope MJ, Milinkovitch MC. 2000. Independent adaptation to riverine habitats allowed survival of ancient cetacean lineages. *Proceedings of the National Academy of Sciences*, 97:11343-11347.

Chen XH, Cheng L, Sander P. 2007. A new species of *Callawayia* (Reptilia: Ichthyosauria) from the Late Triassic in Guanling, Guizhou. *Geology in China*, 34:974-982.

Cook DHN. 1994. A new ichthyosaur genus from the Middle Triassic of Monte San Gorgio, Switzerland. *Journal of Vertebrate Paleontology*, 14:21-22.

Crasti A. 2019. La tomografia computerizzata applicata allo studio osteologico dell'olotipo di *Besanosaurus leptorhynchus*. Unpublished master thesis, Università degli Studi di Milano, Milano, 43 pp.

Dal Sasso C. 2001. Dinosauri italiani. Marsilio, Venezia, 256 pp.

Dal Sasso C. 2004. Dinosaurs of Italy. Indiana University Press, Bloomington and Indianapolis, 216 pp.

Dal Sasso C, Pinna G. 1996. *Besanosaurus leptorhynchus* n. gen. n. sp., a new shastasaurid ichthyosaur from the Middle Triassic of Besano (Lombardy, N. Italy). *Paleontologia Lombarda*, Nuova serie, 4:3-23.

Dal Sasso C, Maganuco S, Iurino DA. 2014. Update on the internal structure of the snout of *Spinosaurus aegyptiacus*. Second North African Vertebrate Palaeontology Congress - NAVEP2, 1-7 September 2014, Ouarzazate (Morocco). Abstract book:26.

Dick DG, Maxwell EE. 2015. Ontogenetic tooth reduction in *Stenopterygius quadriscissus* (Reptilia: Ichthyosauria): negative allometry, changes in growth rate, and early senescence of the dental lamina. *PloS one*, 10:e0141904.

Dick DG, Schweigert G, Maxwell EE. 2016. Trophic niche ontogeny and palaeoecology of early Toarcian *Stenopterygius* (Reptilia: Ichthyosauria). *Palaeontology*, 59:423-431.

Engelschiøn VS, Delsett LL, Roberts AJ, Hurum JH. 2018. Large-sized ichthyosaurs from the Lower Saurian niveau of the Vikinghøgda Formation (Early Triassic), Marmierfjellet, Spitsbergen. *Norwegian Journal of Geology*, 98:239-266.

Etter W. 2002. Monte San Giorgio: Remarkable Triassic marine vertebrates. In: Bottjer DJ, Etter W, Hagadorn JW, Tang CM eds. *Exceptional fossil preservation. A unique view on the evolution of marine life*. New York: Columbia University Press, 220-242.

Fischer V, Capetta H, Vincent P, Garcia G, Goolaerts S, Martin JE, Roggero D, Valentin X. 2014. Ichthyosaurs from the French Rhaetian indicate a severe turnover across the Triassic–Jurassic boundary. *Naturwissenschaften*, 101:1027-1040.

Fischer V, Bardet N, Benson RB, Arkhangelsky MS, Friedman M. 2016. Extinction of fish-shaped marine reptiles associated with reduced evolutionary rates and global environmental volatility. *Nature communications*, 7:1-11.

Ferrón HG, Martínez-Pérez C, Botella H. 2018. The evolution of gigantism in active marine predators. *Historical Biology*, 30:712-716.

Fröbisch NB, Sander PM, Rieppel O. 2006. A new species of *Cymbospondylus* (Diapsida, Ichthyosauria) from the Middle Triassic of Nevada and a re-evaluation of the skull osteology of the genus. *Zoological Journal of the Linnean Society*, 147:515-538.

Furrer H. 1995. The Kalkschieferzone (Upper Meride Limestone; Ladinian) near Meride (Canton Ticino, Southern Switzerland) and the evolution of a Middle Triassic intraplatform basin. *Eclogae Geologicae Helvetiae*, 88:827-852.

Furrer H. 2003. Der Monte San Giorgio im Südtessin-vom Berg der Saurier zur Fossil-Lagerstätte internationaler Bedeutung. *Neujahrsblatt der Naturforschenden Gesellschaft in Zurich*, 206:64.

Goloboff PA, Farris JS, Nixon KC. 2008. Cladistics TNT, a free program for phylogenetic analysis. *Cladistics*, 24:774-786.

Goloboff PA, Catalano SA, 2016. TNT version 1.5, including a full implementation of phylogenetic morphometrics. *Cladistics,* 32:221-238.

Hua S, De Buffrenil V. 1996. Bone histology as a clue in the interpretation of functional adaptations in the Thalattosuchia (Reptilia, Crocodylia). *Journal of Vertebrate Paleontology*, 16, 4, 703-717.

Huang JD, Motani R, Jiang DY, Tintori A, Rieppel O, Zhou M, Ren X-X, Zhang R. 2019. The new ichthyosauriform *Chaohusaurus brevifemoralis* (Reptilia, Ichthyosauromorpha) from Majiashan, Chaohu, Anhui Province, China. *PeerJ*, 7:e7561.

Huene F. Von 1916. Beiträge zur Kenntnis der Ichthyosaurier im deutschen Muschelkalk. *Palaeontographica*, 62:1-68.

Huene F. Von 1931. Neue Ichthyosaurier aus Württemberg. *Neues Jahrbuch für Mineralogie, Geologie und Paläontologie B*, 65:305-320.

ICZN 1999. International Code of Zoological Nomenclature. Fourth Edition. The International Trust for Zoological Nomenclature, London, UK, 306 pp.

Ibrahim N, Sereno PC, Dal Sasso C, Maganuco S, Fabbri M, Martill DM, Zouhri S, Myhrvold N, Iurino DA. 2014. Semiaquatic adaptations in a giant predatory dinosaur. *Science*, 345:1613-1616.

Jones ME, Curtis N, O'Higgins P, Fagan M and Evans SE. 2009. The head and neck muscles associated with feeding in Sphenodon (Reptilia: Lepidosauria: Rhynchocephalia). *Palaeontologia Electronica*, 12.2.7A

Johnson MM, Young MT and Brusatte SL. 2020. The phylogenetics of Teleosauroidea (Crocodylomorpha, Thalattosuchia) and implications for their ecology and evolution. *PeerJ*, 8:e9808.Ji C, Jiang DY, Motani R, Hao WC, Sun ZY, Cai T. 2013. A new juvenile specimen of *Guanlingsaurus* (Ichthyosauria, Shastasauridae) from the Upper Triassic of southwestern China. *Journal of Vertebrate Paleontology*, 33:340-348.

Ji C, Jiang DY, Motani R, Rieppel O, Hao WC, Sun ZY. 2016. Phylogeny of the Ichthyopterygia incorporating recent discoveries from South China. *Journal of Vertebrate Paleontology*, 36:e1025956.

Jiang DY, Motani R, Huang J, Tintori A, Hu Y, Rieppel O, Fraser NC, Ji C, Kelley NP, Fu W, Zhang R. 2016. A large aberrant stem ichthyosauriform indicating early rise and demise of ichthyosauromorphs in the wake of the end-Permian extinction. *Scientific reports*, 6:26232.

Jiang DY, Motani R, Tintori A, Rieppel O, Ji C, Zhou M, Wang X, Lu H, Li ZG. 2020. Evidence Supporting Predation of 4-m Marine Reptile by Triassic Megapredator. *iScience.* DOI: 10.1016/j.isci.2020.101347.

Kear BP. 2005. Cranial morphology of *Platypterygius longmani* Wade, 1990 (Reptilia: Ichthyosauria) from the Lower Cretaceous of Australia. *Zoological Journal of the Linnean Society*, 145:583-622.

Klein N, Voeten DFAE, Lankamp J, Bleeker R, Sichelschmidt OJ, Liebrand M, Nieweg DC, Sander PM. 2015. Postcranial material of *Nothosaurus marchicus* from the Lower Muschelkalk (Anisian) of Winterswijk, The Netherlands, with remarks on swimming styles and taphonomy. *Paläontologische Zeitschrift*, 89:961-981.

Klein N, Schmitz L, Wintrich T, Sander PM. 2020. A new cymbospondylid ichthyosaur (Ichthyosauria) from the Middle Triassic (Anisian) of the Augusta Mountains, Nevada, USA. *Journal of Systematic Palaeontolo*gy, 18:1167-1191.

Kuhn-Schnyder, E. 1964. Die Wirbeltierfauna der Tessiner Kalkalpen. *Geologische Rundschau* 53:393–412.

Li C, You H. 2002. *Cymbospondylus* from the Upper Triassic of Guizhou, China. *Vertebrata Palasiatica*, 40:9-16.

Lomax DR, De La Salle P, Massare JA, Gallois R. 2018. A giant Late Triassic ichthyosaur from the UK and a reinterpretation of the Aust Cliff 'dinosaurian' bones. *PloS one*, 13:e0194742

Maisch MW. 1997. Variationen im Verlauf der Gehirnnerven bei *Ophthalmosaurus* (Ichthyosauria, Jura). *Neues Jahrbuch für Geologie und Paläontologie-Monatshefte*, 7:425-433.

Maisch MW. 2002. A braincase of *Temnodontosaurus* cf. *trigonodon* (von Theodori, 1843) (Ichthyosauria) from the Lower Jurassic of Germany. *Geologica et Palaeontologica*, 36:115-122.

Maisch MW. 2010. Phylogeny, systematics, and origin of the Ichthyosauria. The state of the art. *Palaeodiversity*, 3:151-214.

Maisch MW, Matzke AT. 1997*a*. *Mikadocephalus gracilirostris* n. gen., n. sp., a new ichthyosaur from the Grenzbitumenzone (Anisian-Ladinian) of Monte San Giorgio (Switzerland). *Paläontologische Zeitschrift*, 71:267-289.

Maisch MW, Matzke AT. 1997*b*. Observations on Triassic ichthyosaurs. Part I: Structure of the palate and mode of tooth implantation in *Mixosaurus cornalianus* (BASSANI, 1886). *Neues Jahrbuch fur Geologie und Palaontologie - Monatshefte*, 12.

Maisch MW, Matzke AT. 2000. The Ichthyosauria. *Stuttgarter Beiträge zur Naturkunde Serie B*, 298:1-159.

Maisch MW, Matzke AT. 2006. The braincase of *Phantomosaurus neubigi* (Sander, 1997), an unusual ichthyosaur from the Middle Triassic of Germany. *Journal of Vertebrate Paleontology*, 26:598-607.

Maisch MW, Matzke AT, Brinkmann W. 2006*a*. The otic capsule of the Middle Triassic ichthyosaur *Mixosaurus* from Monte San Giorgio (Switzerland): new evidence on the braincase structure of basal ichthyosaurs. *Eclogae geologicae helvetiae*, 99:205-210.

Maisch MW, Pan XR, Sun ZY, Cai T, Zhang DP, Xie JL. 2006*b*. Cranial osteology of *Guizhouichthyosaurus tangae* (Reptilia: Ichthyosauria) from the Upper Triassic of China. *Journal of Vertebrate Paleontology*, 26:588-597.

Marek RD, Moon BC., Williams M, Benton MJ. 2015. The skull and endocranium of a Lower Jurassic ichthyosaur based on digital reconstructions. *Palaeontology*, 58:723-742.

Marshall CD, Pyenson ND. 2019. Feeding in aquatic mammals: an evolutionary and functional approach. In: Bels V, Whishaw IQ, eds. *Feeding in Vertebrates*. Springer, Cham, pp. 743-785.

Marx FG, Lambert O, Uhen MD. 2016. *Cetacean paleobiology*. John Wiley & Sons, Chichester, 319 pp.

Martin JE, Vincent P, Suan G, Sharpe T, Hodges P, Williams M, Howells C, Fischer V. 2015. A mysterious giant ichthyosaur from the lowermost Jurassic of Wales. *Acta Palaeontologica Polonica*, 60:837-842.

Massare JA. 1987. Tooth morphology and prey preference of Mesozoic marine reptiles. *Journal of Vertebrates Paleontology*, 7:121-137.

Massare JA, JM. Callaway. 1990. The affinities and ecology of Triassic ichthyosaurs. *Geological Society of America Bulletin,* 102:409-416.

Maxwell EE, Kear BP. 2013. Triassic ichthyopterygian assemblages of the Svalbard archipelago: a reassessment of taxonomy and distribution. *GFF*, 135:85-94.

McCurry MR, Evans AR, Fitzgerald EM, Adams JW, Clausen PD, McHenry CR. 2017. The remarkable convergence of skull shape in crocodilians and toothed whales. *Proceedings of the Royal Society B: Biological Sciences*, 284:20162348.

McGowan C. 1973. The cranial morphology of the Lower Liassic latipinnate ichthyosaurs of England. *Bulletin of the British Museum (Natural History), Geology*, 24:1-109.

McGowan, C. 1976. The description and phenetic relationships of a new ichthyosaur genus from the Upper Jurassic of England. *Canadian Journal of Earth Sciences*, 13: 668–683.

McGowan C. 1994. A new species of *Shastasaurus* (Reptilia: Ichthyosauria) from the Triassic of British Columbia: the most complete exemplar of the genus. *Journal of Vertebrate Paleontology*, 14:168-179.

McGowan C, Motani R. 2003. Part 8. Ichthyopterygia. In: Sues H-D, ed. *Handbook of Paleoherpetology.* Munchen: Verlag Dr. Friedrich Pfeil, 173 pp.

Miedema F, Maxwell EE. 2019. Ontogeny of the braincase in *Stenopterygius* (Reptilia, Ichthyosauria) from the Lower Jurassic of Germany. *Journal of Vertebrate Paleontology*, 39:e1675164.

Moon BC. 2017. A new phylogeny of ichthyosaurs (Reptilia: Diapsida). *Journal of Systematic Palaeontology*, 17:129-155.

Moon BC, Stubbs TL. 2020. Early high rates and disparity in the evolution of ichthyosaurs. *Communications biology*, 3:1-8.

Motani R. 1999. Phylogeny of the Ichthyopterygia. *Journal of Vertebrate Paleontology*, 19:473-496.

Motani R, Ji C, Tomita T, Kelley N, Maxwell EE, Jiang DY, Sander PM. 2013. Absence of suction feeding ichthyosaurs and its implications for Triassic mesopelagic paleoecology. *PLoS One*, 8:e66075.

Motani R, Jiang DY, Tintori A, Ji C, Huang JD. 2017. Pre-versus post-mass extinction divergence of Mesozoic marine reptiles dictated by time-scale dependence of evolutionary rates. *Proceedings of the Royal Society B: Biological Sciences*, 284:20170241.

Motani R, Minoura N, Ando T. 1998. Ichthyosaurian relationships illuminated by new primitive skeletons from Japan. *Nature*, 393:255-257.

Motani R, Rothschild BM, Wahl W. 1999. Large eyeballs in diving ichthyosaurs. *Nature*, 402:747-747.

Mundil R, Brack P, Meier M, Rieber H, Oberli F. 1996. High resolution U-Pb dating of Middle Triassic volcaniclastics: Time-scale calibration and verification of tuning parameters for carbonate sedimentation. *Earth and Planetary Science Letters*, 141:137-151.

Nicholls EL, Manabe M. 2004. Giant ichthyosaurs of the Triassic. A new species of *Shonisaurus* from the Pardonet Formation (Norian: Late Triassic) of British Columbia. *Journal of Vertebrate Paleontology*, 24:838-849.

Pan X, Jiang D, Sun Z. 2006. Discussion on *Guizhouichthyosaurus tangae* Cao and Luo in Yin et al., 2000 (Reptilia, Ichthyosauria) from the Late Triassic of Guanling County, Guizhou. *Acta Scientiarum Naturalium Universitatis Pekinensis*, 42:697.

Pardo-Pérez JM, Kear BP, Maxwell EE. 2020. Skeletal pathologies track body plan evolution in ichthyosaurs. *Scientific reports*, 10:1-7

Pierce SE, Angielczyk KD, Rayfield EJ. 2009. Shape and mechanics in thalattosuchian (Crocodylomorpha) skulls: implications for feeding behaviour and niche partitioning. *Journal of Anatomy*, 215:555-576.

Pollard JE. 1968. The gastric contents of an ichthyosaur from the lower Lias of Lyme Regis, Dorset. *Palaeontology,* 11:376-388.

Renesto S, Dal Sasso C, Fogliazza F, Ragni C. 2020. New findings reveal that the Middle Triassic ichthyosaur *Mixosaurus cornalianus* is the oldest amniote with a dorsal fin. *Acta Paleontologica Polonica*, 65: 511-522.

Rieber H. 1970. *Phragmoteuthis* ?*ticinensis* n. sp., ein Coleoida-Rest aus der Grenzbitumenzone (Mittlere Trias) des Monte San Giorgio (Kt. Tessin, Schweiz). *Paläontologische Zeitschrift,* 44:32-40.

Rieppel O. 2000. Part 12 A. Sauropterygia I - Placodontia, Pachypleurosauria, Nothosauroidea, Pistosauroidea. In: Wellnhofer P, ed. *Handbook of Paleoherpetology*, Munchen: Verlag Dr. Friedrich Pfeil, 134 pp.

Rieppel O. 2019. *Mesozoic Sea Dragons: Triassic Marine Life from the Ancient Tropical Lagoon of Monte San Giorgio*. Bloomington: Indiana University Press, 256 pp.

Riess J. 1986. Fortbewegungsweise, Schwimmbiophysik und Phylogenie der Ichthyosaurier. *Palaeontographica. Abteilung A, Paläozoologie, Stratigraphie*, 192:93-155.

Röhl HJ, Schmid-Röhl A, Furrer H, Frimmel A, Oschmann W, Schwark L. 2001. Microfacies, geochemistry and palaeoecology of the Middle Triassic Grenzbitumenzone from Monte San Giorgio (Canton Ticino, Switzerland). *Geologia Insubrica*, 6:1-13.

Sander PM. 1989. The large ichthyosaur *Cymbospondylus buchseri*, sp. nov., from the Middle Triassic of Monte San Giorgio (Switzerland), with a survey of the genus in Europe. *Journal of Vertebrate Paleontology*, 9:163-173.

Sander PM. 1997. The paleobiogeography of *Shastasaurus*. In: Callaway JM, Nicholls EL, eds. *Ancient marine reptiles*. Academic Press, pp. 17-43.

Sander PM. 2000. Ichthyosauria: their diversity, distribution, and phylogeny. *Paläontologische Zeitschrift*, 74:1-35.

Sander PM, ChenX, Cheng L, Wang X. 2011. Short-snouted toothless ichthyosaur from China suggests Late Triassic diversification of suction feeding ichthyosaurs. *PLoS One*, 6:e19480.

Scheyer TM, Romano C, Jenks J, Bucher H. 2014. Early Triassic Marine Biotic Recovery: The Predators' perspective. *PLoS One*, 9:e88987.

Shang QH, Li C. 2009. On the occurrence of the ichthyosaur *Shastasaurus* in the Guanling biota (Late Triassic), Guizhou, China. *Vertebrata PalAsiatica*, 47:178-193.

Sollas WJ. 1916. The skull of *Ichthyosaurus* studied in serial sections. *Philosophical Transactions of the Royal Society of London B*, 208:63-126.

Stockar R, Baumgartner PO, Condon D. 2012. Integrated Ladinian bio-chronostratigraphy and geochronology of Monte San Giorgio (Southern Alps, Switzerland). *Swiss Journal of Geosciences*, 105:85-108.

Storrs GW. 1994. Fossil vertebrate faunas of the British Rhaetian (latest Triassic). *Zoological Journal of the Linnean Society*, 112:217-259.

Stubbs TL, Benton MJ. 2016. Ecomorphological diversifications of Mesozoic marine reptiles: the roles of ecological opportunity and extinction. *Paleobiology*, 42:547-573.

Wiman C. 1910. Ichthyosaurier aus der Trias Spitzbergens. *Bulletin of the Geological Institution of the University of Upsala*, 10:124-148.

Wotzlaw JF, Brack P, Storck JC. 2017. High-resolution stratigraphy and zircon U–Pb geochronology of the Middle Triassic Buchenstein Formation (Dolomites, northern Italy): precession-forcing of hemipelagic carbonate sedimentation and calibration of the Anisian–Ladinian boundary interval. *Journal of the Geological Society*, 175:71-85.

6.11 Supplementary figures

Fig. S1 - Perinarial region of *Guizhouicthyosaurus tangae*. Perinarial region of a 3D-preserved referred specimen of *Guizhouicthyosaurus tangae* (IVPP V11869) in left lateral view. For bone interpretation, see Li & You (2002: fig. 2). Scale bar represents 5 cm.

Fig. S2 - Postorbital region of *Guizhouicthyosaurus tangae.* Postorbital region of a 3D-preserved referred specimen of *Guizhouicthyosaurus tangae* (IVPP V11865) in left lateral view. Abbreviations: see text. Scale bar represents 5 cm.

Fig. S3 - Postorbital region of *Guanlingsaurus liangae.* Postorbital region of a 3D-preserved referred specimen of *Guanlingsaurus liangae* (SPCV 03107) in left lateral view. For bone interpretation, see Sander et al. (2011: fig. 2b).

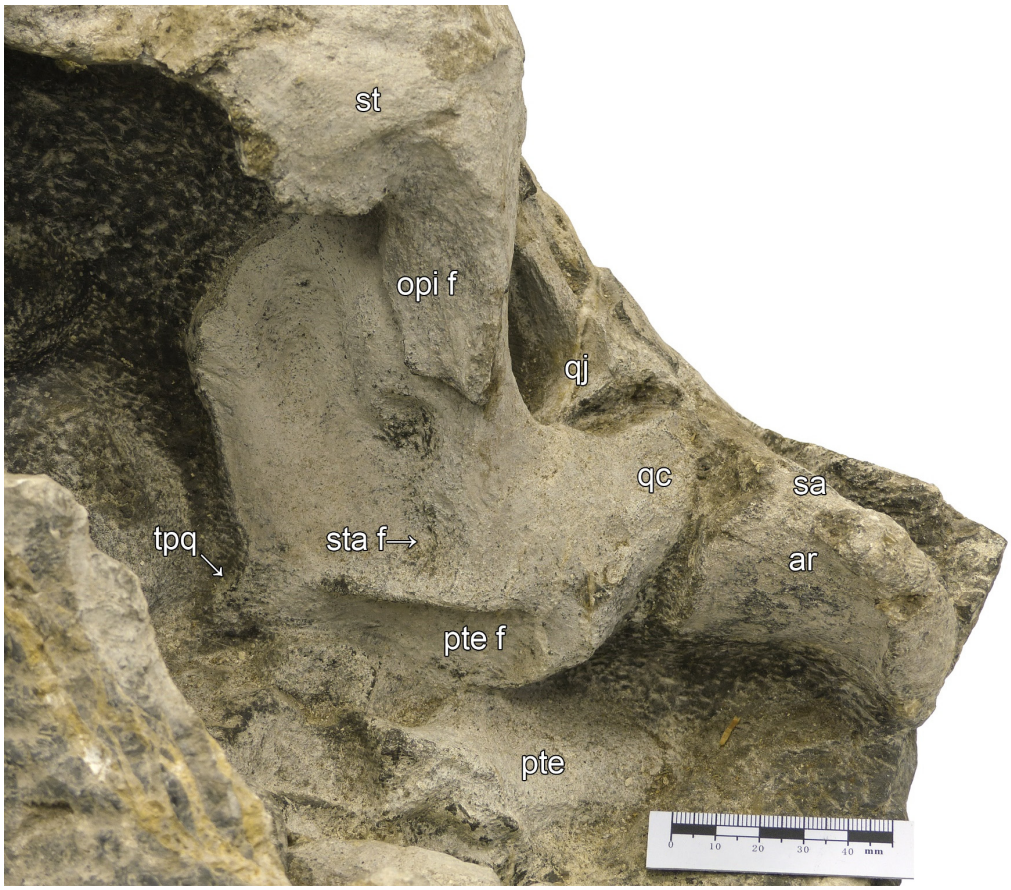

Fig. S4 - Occipital region of *Guanlingsaurus liangae.* Occipital region of a 3D-preserved referred specimen of *Guanlingsaurus liangae* (SPCV 03107) in caudomedial view. Note the presence of the triangular process of the quadrate, which helps to hold the caudolateral flange of the pterygoid. Abbreviations: see text. Scale bar represents 5 cm.

Fig. S5 - Palatal view of '*Callawayia' wolonggangense*. Palatal view of a referred specimen of '*Callawayia' wolonggangense* (SPCV 10305). For bone interpretation, see Chen et al. (2007: fig. 2D).

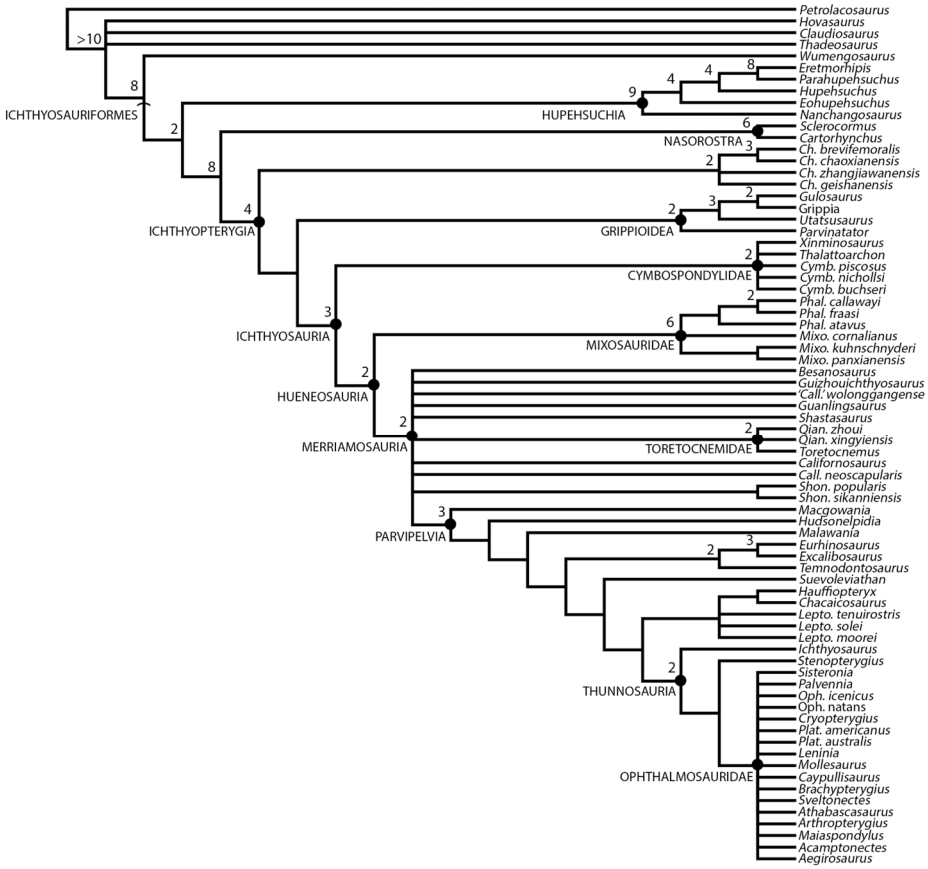

Fig. S6 - Strict consensus tree of Ichthyosauriformes.Strict consensus of 14,480 MPTs of 713 steps (CI=0.363, RI=0.788) obtained from parsimony analysis of the character-taxon matrix of Huang et al. (2019). Note large polytomy at the base of Merriamosauria. Numbers above nodes indicate Bremer support values. Abbreviations: *Call.*, *Callawayia*; *Ch.*, *Chaohusaurus*; *Cymb.*, *Cymbospondylus*; *Lepto.*, *Leptonectes*; *Mixo.*, *Mixosaurus*; *Oph.*, *Ophthalmosaurus*; *Qian.*, *Qianichthyosaurus*; *Phal.*, *Phalarodon*; *Shon.*, *Shonisaurus*.

Chapter 7
Postcranial anatomy of *Besanosaurus leptorhynchus* (Reptilia: Ichthyosauria) from the Middle Triassic Besano Formation of Monte San Giorgio, Italy/Switzerland, and implications for reconstructing the swimming styles of Triassic ichthyosaurs

*Manuscript to be submittted to PeerJ.

Gabriele Bindellini[1], Andrzej S. Wolniewicz[2, 3], Feiko Miedema[4], Cristiano Dal Sasso[5], Torsten M. Scheyer[6]

[1] Dipartimento di Scienze della Terra "Ardito Desio", Università degli Studi di Milano, Milano, Italy

[2] School of Resources and Environmental Engineering, Hefei University of Technology, Hefei, China

[3] Institute of Paleobiology, Polish Academy of Sciences, Warsaw, Poland

[4] Staatliches Museum für Naturkunde Stuttgart, Stuttgart, Germany

[5] Sezione di Paleontologia dei Vertebrati, Museo di Storia Naturale di Milano, Milano, Italy

[6] Paläontologisches Institut und Museum, Universität Zürich, Zürich, Switzerland

7.1 Abstract

Besanosaurus leptorhynchus Dal Sasso & Pinna, 1996 was described on the basis of a single fossil excavated near Besano (Italy). A recent revision of the taxon and a reexamination of its cranial osteology allowed the assignment of five additional specimens to it (Bindellini et al., 2021). In this manuscript we proceed to analyze, describe and discuss the postcranial anatomy. Results show that *Besanosaurus leptorhynchus* possesses a peculiar bauplan that in body proportions fits in between *Cymbospondylus* and shastasaur-grade ichthyosaurs. The vertebral count consists of 61 presacral, two sacral, and at least 138 caudal elements; the caudal series represents 55% of the whole axial skeleton. We found unambiguous evidence for the presence of a taibend in *Besanosaurus leptorhynchus* that forms an angle of ~30 degrees. Remarkably, the pedal phalanges retain a rudimentary, but still distinctive, shaft. This condition is more similar to mixosaurids, but distinctly differs from all other shastasaur-grade ichthyosaurs, in which the pedal phalanges are circular in outline. On the other hand, well-separated round phalanges are found in the hindfins. These are particularly long and therefore we suggest that this condition might have enhanced maneuverability. Round hindfin phalanges in shastasaurs recall the condition of some cetaceans such as orcas; as in the latter, we suggest a complete or almost complete loss of secondary ossification centers in *Besanosaurus*. In the pubis, the obturator foramen opens to the caudal margin in all examined specimens. showing an elongated sub-oval outline.

To test the swimming capabilities of *Besanosaurus leptorhynchus* we expanded the dataset of Motani et al. (1996): B*esanosaurus* plots in between anguilliform swimmers, such as *Cymbospondylus*, and shastasaur-grade ichthyosaurs. These results allowed further discussion on the swimming style differences among Middle Triassic Ichthyosaurs. Here we suggest that mixosaurids, supposedly independently, and convergently to Jurassic taxa, evolved for the first time a combination of adaptations that would have appeared later in Parvipelvia. Moreover, different swimming styles for *Cymbospondylus,* Mixosauridae*,* and *Besanosaurus* are found and strenghten the previously suggested niche partitioning of the three taxa from the Besano Formation (Bindellini et al., 2021). Eventually, we discuss the similarities of *Besanosaurus* with *Pessopteryx* and *Pessosaurus* and conclude that *Besanosaurus* is not a junior synonym of either of the two taxa.

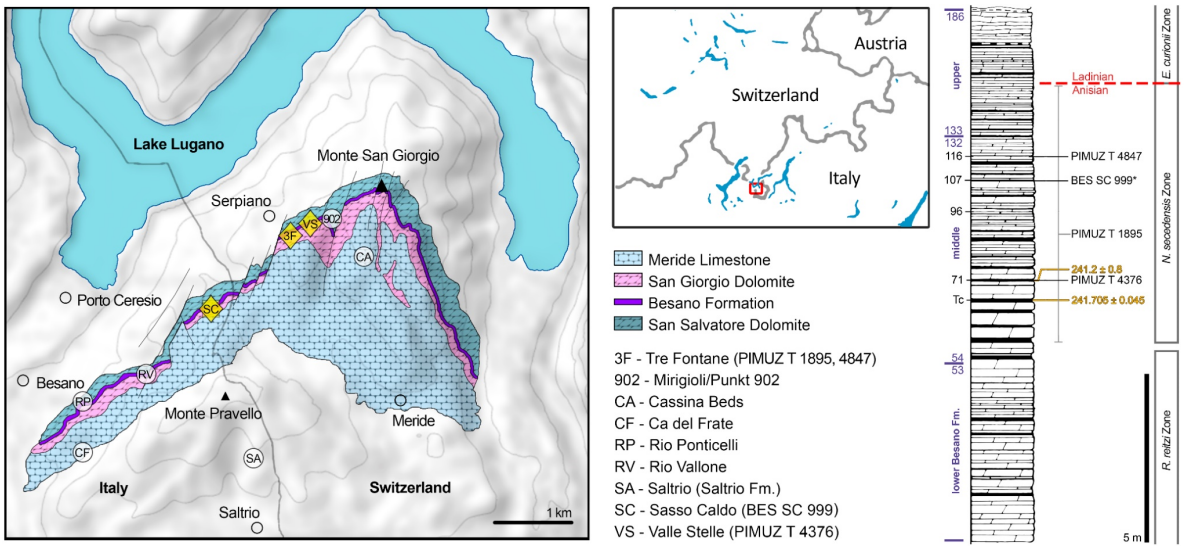

Fig. 7.1- Map of the Monte San Giorgio area (left) showing the Middle Triassic carbonate succession, the major paleontological quarries in the area (white circles), and the sites of origin of the specimens described in this paper (yellow rhombuses). Stratigraphic log of the Besano Formation at the Mirigioli/Punkt 902 outcrop (right), with the known stratigraphic positions of the specimens described. The stratigraphic position of PIMUZ T 1895 and GPIT 1793/1 is more uncertain, thus expressed by a range line. Log modified from Brack et al. (2005); dating of layer 71 from Mundil et al. (1996); dating of Tc Tuffs (layers 66-68) from Wotzlaw et al. (2017).

7.2 Material and Methods

7.2.1 Material

All studied specimens lay in a single bedding plane and are variably compressed by diagenetic alteration (Fig. 7.2 and Fig. 7.3). Disarticulation is more common in the forefins than in the hindfins, and in the post-sacral axial skeleton (BES SC 999, PIMUZ T 4376, PIMUZ T 4847). One specimen contains embryonic and soft tissue remains (BES SC 999); the largest specimen (PIMUZ T 4847) contains a large nodule in the cranial half of the thoracic region, possibly related to visceral soft tissue. According to increasing body size, the studied specimens can be ordered as follows.

PIMUZ T 4376 – the smallest specimen. It measures 2.12 m from the tip of the rostrum to the last preserved caudal vertebra (the distalmost caudals are missing).

PIMUZ T 1895 – the specimen is incomplete (lacking most of the tail and the limbs, except for the tailbend) and semiarticulated. The preserved presacral length is around 1.40 m.

BES SC 999 – a sexually mature small adult. The holotype of *B. leptorhynchus* measures 5.065 m from the tip of the rostrum to the last caudal vertebra. The skeleton is virtually complete and lies in a ventrodorsal position.

PIMUZ T 4847 – a large adult. It has a presacral length of 3.28 m but lacks most of the post-sacral skeleton and most of the limb bones. In life, this individual likely reached a length of about 8 m.

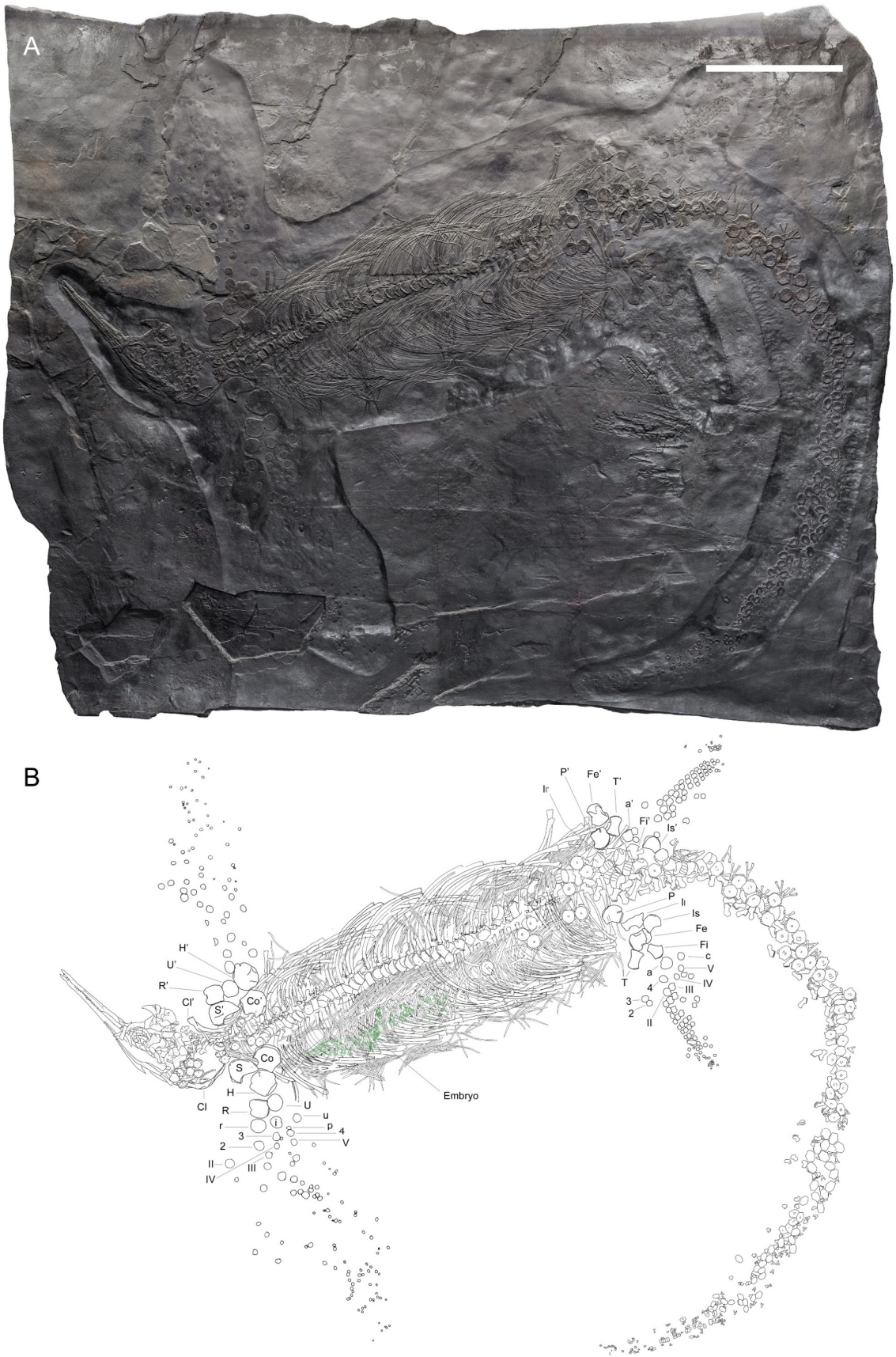

Fig. 7.2 - (A) BES SC 999 *Besanosaurus leptorhynchus* cast and (B) interpretative drawing (modified from Dal Sasso & Pinna, 1996). *Abbreviations*: a, astragalus; c, calcaneum; Cl, clavicle; Co, coracoid; Fe, femur; Fi, Fibula; H, humerus; i, intermedium; Il, Ilium; Is, Ischium; P, pubis; p, pisiform; R, radius; r, radiale; S, scapula; T, Tibia; U, Ulna; u, ulnare; 2, 3, and 4, distal carpals or tarsals; II, III, IV, IV, and V metacarpals or metatarsals. The apostrophe (‘) always indicates a left element. Scale bar represents 50 cm.

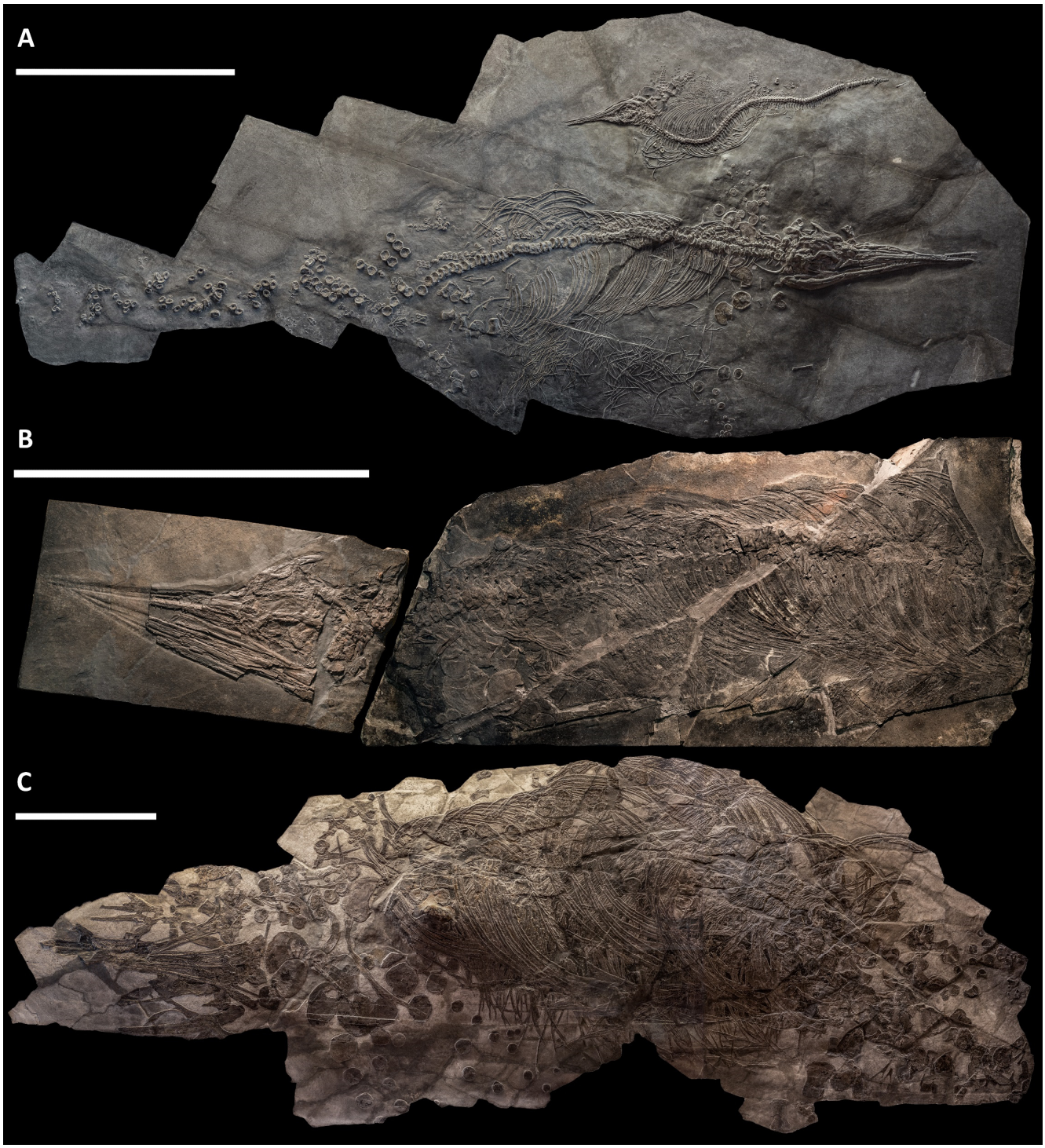

Fig. 7.3- Three additional skeletons referred to *Besanosaurus leptorhynchus*. (A) PIMUZ T 1895; (B) PIMUZ T 4376; (C) PIMUZ T 4847. Scale bars represent 50 cm.

7.2.2 Methods

X-ray computed tomography (CT) was performed on the whole skeleton of the holotype of *B. leptorhynchus* with a Siemens Somatom Definition Dual Source CT Scanner at the Radiology Department of the Fondazione IRCCS "Cà Granda" Ospedale Maggiore Policlinico di Milano. The best CT imaging was obtained with a bone algorithm on transverse (axial) slices with 140 kV voltage and 180–270 mA current

and a slice thickness of 0.3 mm (Crasti, 2019). Data were exported in DICOM format using eFilm (v. 1.5.3; Merge eFilm, Toronto, ON, Canada). Analysis and post-processing were performed with RadiAnt, 3DimViewer, and Synedra View Personal. Multiplanar reconstructions (MPR) and volume rendering reconstructions (VR) allowed to inspect the bones hidden under other ones within the matrix, otherwise impossible to study without damaging the fossil.
We used photogrammetry to visualize the postcranial anatomy of specimens BES SC 999 and PIMUZ T 4376 (Files S1 and S2). Photos of all studied specimens were taken with a Nikon D3500 camera.

7.3 Systematic paleontology

ICHTHYOPTERYGIA Owen, 1840
ICHTHYOSAURIA Blainville, 1835
SHASTASAURIDAE Merriam, 1902
BESANOSAURUS Dal Sasso & Pinna, 1996
Besanosaurus leptorhynchus Dal Sasso & Pinna, 1996

Type and only species. *Besanosaurus leptorhynchus* Dal Sasso & Pinna, 1996; Middle Besano Formation (uppermost Anisian, Middle Triassic), Monte San Giorgio, Italy/Switzerland.

Type specimen. Complete semi-articulated skeleton (Fig. 7.2), labeled as BES SC 999 in the catalogue of the MSNM (BES SC is acronym for Besano Sasso Caldo), and coded as 20.S288-2.2 in the Inventario Patrimoniale dello Stato (State Heritage Database).

Type locality. Sasso Caldo site, Besano, Varese Province, NW Lombardy, N. Italy. Geographical coordinates: 45°54'03.7"N 8°55'10.6"E, elev. 650 m.

Type horizon and distribution. Middle Besano Formation (*sensu* Bindellini et al. 2019), uppermost Anisian (*N. secedensis* Zone *sensu* Brack et al. 2005), Middle Triassic.

Referred material. PIMUZ T 4376 (complete semi-articulated skeleton with the best-preserved skull of the taxon; Fig. 7.3A), PIMUZ T 1895 (incomplete semi-articulated skeleton with well-preserved skull; Fig. 7.3B), PIMUZ T 4847 (incomplete semi-disarticulated skeleton with disarticulated skull; Fig. 7.3C), GPIT 1793/1 (disarticulated skull, formerly the holotype of *Mikadocephalus gracilirostris*), BES SC 1016 (incomplete semi-disarticulated skull; the specimen is coded as 20.S288-2.6 in the Inventario Patrimoniale dello Stato - State Heritage Database).

Emended diagnosis. Large ichthyosaur with one possible autapomorphy – a caudoventral exposure of the postorbital in the temporal region – and the following combination of characters: extremely long, slender, and gracile snout; frontal rostrocaudally elongate and relatively flat; frontal participation in the temporal fossa but not to the temporal fenestra; L-shaped jugal; 'triangular process' on the medioventral border of the quadrate; prominent coronoid (preglenoid) process of the surangular, distinctly rising above the dorsal margin of the surangular; tiny conical teeth with a coarsely-striated crown surface and deeply striated roots; mesial maxillary teeth set in sockets; distal maxillary teeth set in a groove shorter than half of the rostral ramus of the maxilla; 61 presacral, two sacral, and at least 138 caudal vertebrae; tailbend forming an angle

of ~30°; apical wedge-shaped caudal centra located in between the 56-60th position circa in the caudal series, possessing small and rounded articular surfaces for possibly unossified ribs; caudal series equals ~1,2 times the length of the rest of the axial skeleton in adults; round manual phalanges; pedal phalanges retaining reduced shafts in adults; obturator foramen with a sub-oval outline, open in juveniles and almost entirely enclosed within the pubis in adults.

7.4 Description

7.4.1 Axial skeleton

Vertebrae

In the axial skeleton of *Besanosaurus leptorhynchus* we numbered 12 cervical, 49 dorsal, at least two sacral, and at least 138 caudal centra. The holotype, therefore, possesses 201 vertebrae in total. The overall count of presacral vertebrae is at least 61. Cervical, dorsal, and proximal caudal centra are generally subcircular; mid-distal tail centra become ovoidal and mediolaterally compressed; all the centra possess a typical hourglass-shaped sagittal cross section.

Cervical centra – In PIMUZ T 4376, the specimen in which the neck region is best preserved, 12 cervical centra are present (Fig. 7.4A). These are exposed in lateroventral view and show facets for dichocephalous ribs, therefore we regard them as cervical vertebrae. BES SC 999 also shows 12 cervical centra possessing both a diapophysis and a parapophysis (Fig. 7.4C). The cervical centra are generally circular on the transverse plane, but the cranialmost centra show a triangular ventral outline that becomes rounder towards the dorsal region. The height/length ratio of the cervical vertebrae equals ~1.5.

The atlas and axis seemingly do not show distinctive differences when compared to the other cervical vertebrae. The cranial and caudal articular surfaces of the atlas are concave similar to those in other centra. The atlas and axis are separate both in PIMUZ T 4376 and BES SC 999. The neural arches and neural spines of the atlas and axis are fused into a single element, well visible in PIMUZ T 4376. No intercentra can be identified in any of the studied specimens. Diapophyses and parapophyses are always present in the cervical centra and project distally from the centra (more markedly in the adults than in the small specimens). The diapophyses increase in size posteriorly towards the dorsal region, gradually assuming a reniform outline, whereas the parapophyses decrease in size maintaining a rounded outline. Anteriorly, the diapophyses and parapophyses are clearly separated from each other, they become closer posteriorly, and the parapophyses are no longer present in the 13th centrum, in which only an enlarged diapophysis is visible. The diapophyses always contact the facets for the neural arch.

In BES SC 999, the 12th centrum possesses a parapophysis that is extremely reduced in size (Fig. 7.4B). A similar condition has been described in *Guizhouichthyosaurus tangae* (IVPP V 11853; Shang & Li, 2009) and S*hastasaurus pacificus* (Merriam, 1902: pl. 8, fig. 3). In *Shonisaurus sikanniens* there is a parapophysis in the first 10 and in the 12th presacral centra, whereas the 11th centrum only shows a single rib facet (Nicholls & Manabe, 2004). Around 10 cervical centra have also been recorded for *Guanlingsaurus liangae* (Ji et al., 2013), whereas in Camp (1980: fig. 28), in the cervical series of *Shonisaurus popularis*, a parapophysis is visible up until the 9th centrum. Sander (1989) recorded six cervical vertebrae in *Cymbospondylus buchseri*; Merriam (1908: fig. 58) reports the presence of a parapophysis in the first 12 centra of *Cymbospondylus petrinus*; Fröbisch et al. (2006) note the presence of a tiny parapophysis in the 8th vertebra of *Cymbospondylus nichollsi* and suggest the 9th to have only a rudimentary parapophysis.

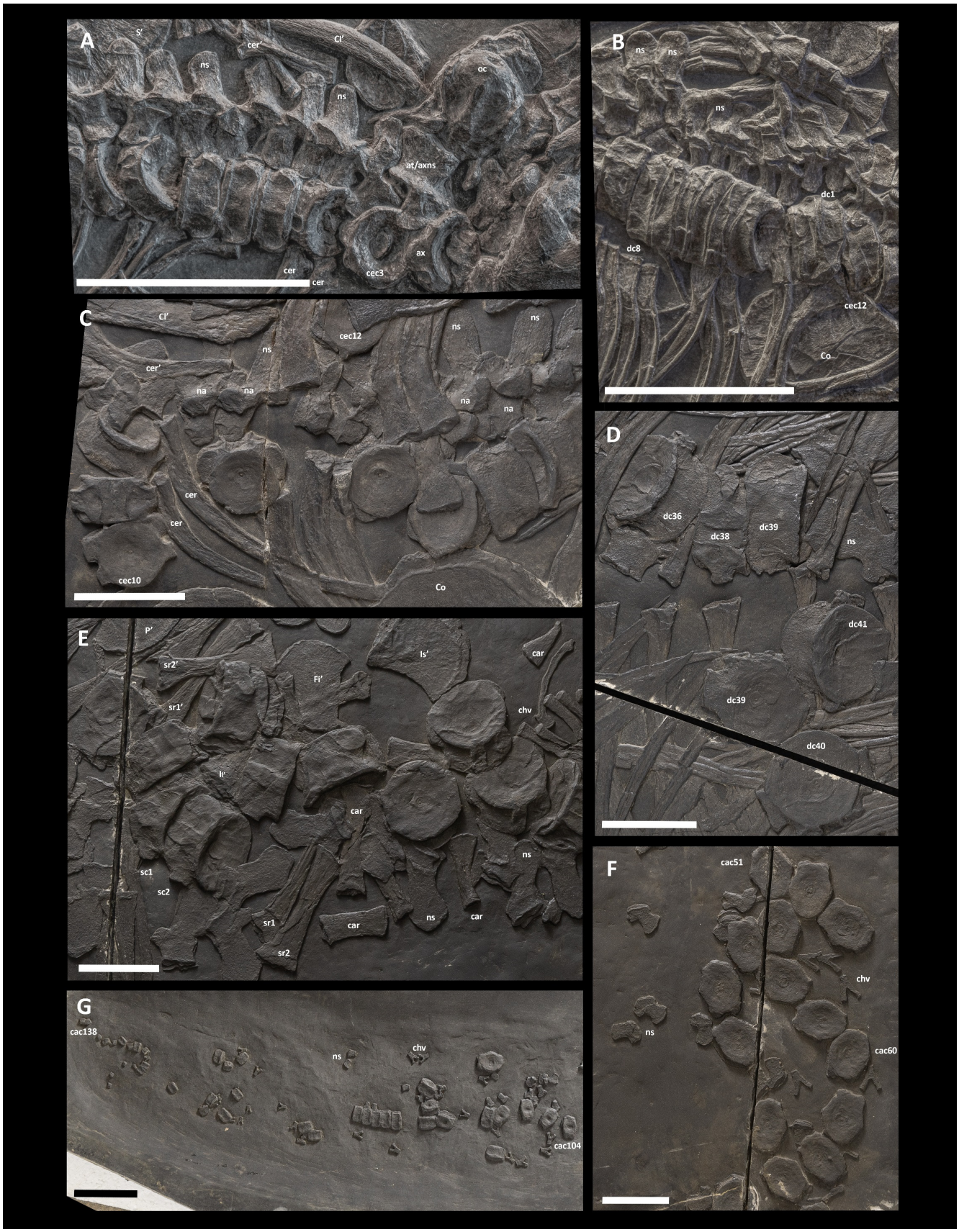

Fig. 7.4 - Selected elements of the axial skeleton of *Besanosaurus leptorhynchus*. (A, B) PIMUZ T 4376; (C-G) BES SC 999. *Abbreviations*: at, atlas; ax, axis; cac, caudal centrum; car, caudal rib; cec, cervical centrum; cer, cervical rib; chv, chevron; Cl, clavicle; Co, coracoid; dc, dorsal centrum; Fi, fibula; Il, ilium; Is, ischium; na, neural arch; ns, neural spine; oc, occipital condyle; P, pubis; S, scapula; sc, sacral centrum; sr, sacral rib. Numbers indicate the position of the centra relatively to the section referred (ce, cervical; d, dorsal; ca, caudal). The apostrophe (‘) always indicates a left element. Scale bars represent 5 cm.

Dorsal centra – Dorsal centra (i.e, non-cervical presacral centra) are generally circular in articular view, showing a regular and constant morphology along the vertebral column. The height/ length ratio of the dorsal centra is almost constant along the trunk region (~1.5 for the cranialmost dorsal centra; ~1.75 for the caudalmost dorsal centra), although the overall size of the vertebrae slightly increases from the neck towards the pelvis (height of the 10th cervical centrum equals 31 mm; height of the 46th dorsal centrum equals 49 mm). On the lateral side, the dorsal centra have only one articular facet, for holocephalous ribs. The diapophysis is long, has a concave cranial margin, and shows a slight constriction in the middle (Fig. 7.4). It is always confluent with the anterior face of the centrum and contacts the facet for the neural arch up until at least the 37th or 38th dorsal centrum (the 49th and 50th centrum, respectively; Fig. 7.4D). In comparison, in *Cymbospondylus buchseri* the connection between the rib facet and the neural arch is lost at the 29th dorsal centrum (35th centrum; Sander, 1989), in *Cymbospondylus petrinus* is lost between the 24th and 26th dorsal centrum (36th-38th Merriam 1908), in *Californosaurus perrini* is lost at the 27th dorsal centrum, and in *Shonisaurus* popularis it is already lost anterior to the 23rd dorsal centrum (Camp, 1980). *Besanosaurus* dorsal centra differ greatly from *Mixosaurus* dorsal centra: the latter are relatively longer and two facets for the articulation of the ribs are visible on the lateral side of the centra close to the pelvic region (Brinkman, 2004; BES SC 1000; Renesto et al., 2020). In lateral view, the dorsal centra of *Besanosaurus* and *Cymbospondylus buchseri* are very similar. However, unlike *Cymbospondylus buchseri*, the posterior dorsal vertebrae of *Besanosaurus*, except for the last four caudalmost elements, possess a diapophysis located around or above the mid-height of the centrum, and that never shows the anteroventral extension visible in the dorsal centra of the caudal half of the trunk in *Cymbospondylus buchseri* (pers. obs.). In addition, the typical triangular shape of the posterior dorsals in craniocaudal view of *Cymbospondylus* petrinus (Merriam, 1908) and likely *C. buchseri* (Sander, 1989) differs from *Besanosaurus*, in which the centra are sub-pentagonal in shape.

Aberrant dorsal centra – In PIMUZ T 4376, the first eight dorsal centra (13–20; Fig. 7.4B) are remarkably narrow in lateral view in comparison with the preceding and following elements of the vertebral column. Each of these centra measures about a half of a normal centrum. We rule out the possibility that taphonomical compression selectively and plastically reduced the craniocaudal length of these eight centra since the adjacent elements (ribs, neural arches, and spines) maintain typical proportions. On the other hand, these centra are preserved packed closely to each other. To explain this particular condition, we tentatively suggest the existence of a developmental abnormality that affected the craniocaudal length of centra 13–18 in PIMUZ T 4376.

Sacral centra – We distinguish at least two sacral vertebrae in BES SC 999, designated by the presence of at least two large disarticulated but still parallel ribs, with clearly enlarged distal articulations, located in proximity to the ilia (Fig. 7.4E). Both in the holotype and in PIMUZ T 4376, two further pairs of ribs with enlarged proximal articulations can be recognized, but their intermediate morphology (see description below) leads us to treat them as indeterminate. The left ilium is hidden by other bones but is well visible in CT images (Fig. 7.4). Sacral centra are also preserved in PIMUZ T 4376, but are not visible in PIMUZ T 1895 and T 4847. The sacral centra in *Besanosaurus leptorhynchus* occupy the 62nd and 63rd position (and possibly two more caudal positions), so that the presacral vertebral count can be determined as 61. Even though the ilium is preserved adjacent to sacral vertebrae in BES SC 999, likely close to its in vivo position, the sacral centra do not show diagnostic characters that can differentiate them from the caudalmost dorsal centra and the cranialmost caudal centra. A gradual, slight increase in size in caudal direction of the precaudal

vertebrae, makes the two sacral centra the largest in the entire axial skeleton (52 mm in lateral width and 25 mm in craniocaudal length).
In lateral view, both sacral vertebrae show a long reniform synapophysis and large facets for neural arches. The same number of sacral centra has been reported in *Shonisaurus popularis* (Camp, 1980) and *Guizhouichthyosaurus tangae* (Shang & Li, 2009).

Caudal centra – BES SC 999 is the only specimen that possesses a complete, partially articulated tail (Fig. 7.2, Fig. 7.4, and Fig. 7.5). In this specimen, the caudal series (possessing at least 138 vertebrae), measures ~280 cm, which is ~1.2 times the length of the rest of the body and accounts for 55.3% of the entire axial skeleton length. This length was measured along the direction of the vertebral column, without taking the tailbend into account. In the holotype the tailbend is inferred to be present 155 cm caudally to the sacrum, based on the tailbend preserved in PIMUZ T 1895 that possesses an angle of ~30°. PIMUZ T 4376 also has an almost complete tail, albeit mostly disarticulated; this still preserves at least 105 caudal centra, missing only the distalmost ones, and measuring ~104 cm.
The size of the caudal centra starts decreasing immediately posterior to the sacrum. Moreover, the postsacral centra gradually become more and more mediolaterally compressed. Centra clearly laterally wider than dorsoventrally tall are visible posterior to the 30th caudal centrum of BES SC 999 tail (Fig. 7.5). From the cranialmost to the caudalmost position, the height/length ratio in preflexural centra ranges from ~1.8 to ~2.8, whereas in the caudalmost preserved centra it is ~1.65.
Apical wedge-shaped centra are visible on one of the slabs comprising PIMUZ T 1895, whereat least five centra with a trapezoidal outline in lateral view can be recognized (Fig. 7.5A). The neural spines corresponding to these centra are shorter than the preflexural ones and oriented vertically (Fig. 7.5F). Neural spines positioned caudal to the tailbend become even shorter and cranially oriented. Despite the absence of soft tissue in the caudal peak region of the examined specimens, the presence of a dorsal lobe of the caudal fin in *Besanosaurus* may be inferred, based on the recent discoveries concerning *Mixosaurus* (Renesto et al., 2020). Based on the inferred position of the caudal bend, the tail of *Besanosaurus* possesses a markedly heterocercal fin.
In BES SC 999 the cranialmost 4/5 caudal centra, unlike the following, lack haemal arches (Fig. 7.5D). The sixth caudal centrum likely articulated with the last ossified caudal ribs. In BES SC 999, PIMUZ T 4376, and PIMUZ T 1895, caudal centra between the 6th position and the apical wedge-shaped centra still show small and rounded articular surfaces for the ribs, indicating they likely articulated with non-ossified elements (Fig. 7.5A and D). The presence of such articular surface, as well as neural spine inversion, has been used to infer the location of the tailbend in BES SC 999: the position of apical centra is 56–60 (Fig. 7.4F).

Neural arches– In PIMUZ T 4376, most of the presacral neural arches are exposed in right lateral view and preserved in articulation with each other. In BES SC 999, the neural arches are also well preserved, although they are sometimes partly covered by other bones, the specimen being exposed in ventral view. PIMUZ T 1895 shows a well-preserved articulated series of neural arches in the cranialmost portion of the trunk (Fig. 7.5B).
Among the studied specimen, only PIMUZ T 4376 shows a well preserved atlas-axis complex (Fig. 7.4A): the neural arches of the atlas and axis are fused; dorsally, a single craniocaudally expanded neural spine is visible, covering the same craniocaudal length as that of the two centra.
In cranial/caudal view the neural arches overall possess a triradiate outline; the contribution of the neural arch to the neural canal cavity is triangular in shape. The base of the neural arch is as long anteroposteriorly as the length of the centrum; its medial margin is straight, whereas the lateral margin shows a lateroventral

Fig. 7.5 - Selected elements of the axial skeleton of *Besanosaurus leptorhynchus*. (A, B) PIMUZ T 1895; (C) PIMUZ T 4847; (D) BES SC 999. *Abbreviations*: a, astragalus; c, centrum; cac, caudal centrum; car, caudal rib; chv, chevron; dia, diapophysis; Fi, fibula; Il, ilium; Is, ischium; na, neural arch; ns, neural spine; sc, sacral centrum; sr, sacral rib. Numbers indicate the position of the centra relatively to the section referred (ce, cervical; d, dorsal; ca, caudal). The apostrophe (‘) always indicates a left element. Scale bars represent 5 cm.

expansion that extends towards the diapophysis. This expansion is clearly visible up until the 38th/39th centrum, the last two centra where the facet for the neural arch of the centrum contacts the diapophysis (see description of dorsal centra). Prezygapophyses and postzygapophyses are of similar size in the cervical and anterior dorsal vertebrae; in the posterior dorsal and anterior caudal vertebrae, the prezygapophyses project cranially more than the postzygapophyses do caudally. The zygapophyses are paired, similar to the condition in *Shastasaurus* and *Cymbospondylus* (Merriam, 1908; Sander, 1989;), but unlike post-Triassic ichthyosaurs, in which the anterior neural arches show unpaired zygapophyses (e.g., McGowan & Motani, 2003; Moon & Kirton, 2016). The articular surfaces of the zygapophyses are almost horizontal (Fig. 7.4 and 7.5).
In lateral view, the dorsal neural spine of *Besanosaurus* is straight, slightly oriented caudally, and craniocaudally expanded, with a generally rounded dorsal margin, more rounded than what is visible in *Cymbospondylus buchseri* (Sander, 1989) and *Phantomosaurus neubigi* (Sander, 1997); this feature is more evident in the caudalmost dorsal vertebrae. The spines are inclined at an angle that varies along the column: cervical and dorsal spines are posteriorly inclined at an angle of about 25° (as also described for *Cymbospondylus buchseri*; Sander, 1989); near the inferred position of the sacrum the neural spines become more vertical and, more caudally, the anterior caudal neural spines are posteriorly inclined at an angle of about 15° (Fig. 7.5). The caudal neural spines, in the first half of the tail, are inclined posteriorly almost at an angle of 45°, but posterior to the tailbend, the spines become abruptly shorter and vertically oriented, whereas more caudally invert their inclination (Dal Sasso & Pinna, 1996: fig. 14). Taller neural spines, visible just before the wedge-shaped flexural centra, likely supported a short dorsal lobe of the tail fluke.

Haemal arches (chevrons) – In BES SC 999, chevrons are visible starting from the 5th or 6th caudal centrum. In cranial/caudal view, they are Y-shaped and the caudalmost are V-shaped. In lateral view, the chevrons are straight and the cranialmost one is dorsoventrally longer than the corresponding centrum. Approaching the tailbend, the dorsoventral height of the chevrons gradually decreases, whereas their lateral width remains constant (Fig. 7.2 and Fig. 7.4). Caudally to the tailbend, haemal arches keep decreasing in size, also showing a remarkable mediolateral width reduction. Both in BES SC 999 and PIMUZ T 4376, tiny haemal arches are visible almost until the very tip of the tail (Fig. 7.4G). This condition contrasts with parvipelvians and basal euichthyosaurians (e.g., *Californosaurus perrini*), in which the haemal arches are reduced in size and disappear more cranially than in Middle Triassic ichthyosaurs (e.g., Merriam, 1902; McGowan and Motani 2003; Moon & Kirton, 2016).

Ribs

In BES SC 999 and PIMUZ T 4376 the ribcage is complete and and most ribs are spaced as in vivo; in PIMUZ T 4847 and PIMUZ T 1895 it is partly incomplete (Fig. 7.2 and 7.3). At the level of the 55th presacral vertebra, the ribs suddenly become shorter and, as a result, the trunk tapers approaching the pelvic region. Post-scapular rib heads are exclusively holocephalous (Fig. 7.4 and Fig. 7.5), a condition similar to that in *Cymbospondylus buchseri* (Sander, 1989) and other Triassic non-euichthyosaurian ichthyosaurs (e.g., Merriam, 1902; Camp, 1980; Nicholls & Manabe, 2004; Shang & Li, 2009). In BES SC 999, the longest rib (articulating with the 29th presacral vertebra) is 46 cm long. In cross-section, the ribs are oval with a clear furrow running both on the cranial and caudal surface throughout their whole length.

Cervical ribs – Cervical ribs are typically dichocephalous (Fig. 7.4A and C). Capitulum and tuberculum are round and small, and separated by a small notch. The shafts of the cervical ribs are slightly recurved and the distal ends taper into pointed tips. The anterior and posterior furrows of the cervical ribs extending to the level of at least the 8th centrum are shallower than those in the dorsal ribs, resulting in a less constricted cross-

section of the midshaft. In PIMUZ T 4376, the rib articulating with the axis is the shortest among the preserved presacral ribs, being as long as the width of the adjacent centrum. Cervical ribs gradually increase in length, so that the last prescapular rib reaches one-third of the length of the longest dorsal rib.

Dorsal ribs – Dorsal (=postscapular) ribs are holocephalous (Fig. 7.4 and Fig. 7.5). They reach their greatest length posterior to the 15th centrum and maintain it almost up to the sacral region. Dorsal ribs are gently curved. The head region is slightly sigmoidal in craniocaudal view, similarly to what can be observed in *Cymbospondylus buchseri* (PIMUZ T 4351, MSNM V927). The proximal end is also dorsomedially expanded and the articular surface of the head matches the profile of the long and curved (cranially concave) diapophysis. Proximal and distal ends are equally broadened.

Sacral ribs – We distinguish two sacral ribs in BES SC 999 (Fig. 7.4E): they clearly show an expanded distal end that should have been connected to the ilium. Both proximal and distal ends are enlarged. In BES SC 999, the distal articular surface of the sacral ribs shows a degree of rugosity greater than in the adjacent ribs. Two further pairs represent potential sacral ribs: they are very short, straight, and possess a thickened midshaft if compared to the caudalmost dorsal ribs and to the rostralmost caudal ribs.

Caudal ribs – As mentioned above, likely the sixth caudal centrum articulates with the last ossified caudal rib, well visible in BES SC 999 (Fig. 7.4E). Between the 6th caudal centrum and the caudal peak, small and rounded articular surfaces for ribs are visible on the lateral side of the centra in BES SC 999, PIMUZ T 4376, and T 1895: the corresponding caudal ribs are not preserved in any of these three specimens, suggesting that these ribs were unossified, not present or lost early before fossilization. The ossified caudal ribs are short, straight, and rod-like, with dorsoventrally expanded proximal and distal ends. The last preserved caudal rib terminates in a pointed distal tip and shows an approximately compressed-conical morphology.

Gastralia

All specimens show gastralia, usually scattered and often broken, but PIMUZ T 1895 preserves some articulated elements (Fig. 7.2 and 7.3). Given their state of preservation, it is difficult to estimate the exact number of gastral ribs. Each gastral rib consists of five elements: one median unpaired element, and two lateral paired elements. The median element is boomerang-shaped with an angle of 135°–140° (145° in *C. buchseri*; Sander, 1989); it possesses a short median anterior process, which is relatively reduced in the smaller specimens (PIMUZ T 4376 and PIMUZ T 1895). The element that connects the median to the lateralmost gastralium is a thin recurved bone with pointed, slit-like articular facets on both ends. The lateralmost element shows a sigmoidal lateral (distal) half and a recurved medial half. As reported for the ribs, two shallow furrows are visible on the cranial and caudal surfaces of each gastral element. The gastral basket extended from the coracoids to the caudalmost region of the trunk.

7.4.2 Appendicular skeleton

Pectoral girdle

Scapula – The scapulae are well-preserved in BES SC 999 and PIMUZ T 4376 (Fig. 7.6A-C). In the holotype the right scapula is exposed in medial view, whereas the left one is exposed in lateral view; in PIMUZ T 4376, we observe the opposite condition. In PIMUZ T 1895 and PIMUZ T 4847, both scapulae are fragmentary and not well-preserved (Fig. 7.6D).

Overall, the scapula is flat with a relatively thicker, dorsoventrally expanded, proximal end of the shaft. The anterior flange of the scapula is large and prominent and makes the general profile of the scapula asymmetrically fan-shaped, a morphology shared among basal Merriamosauria. The longitudinal axis of the scapula is oriented at ~20° with respect to the glenoid facet. At the proximal end, in mediodorsal view, the coracoid facet results craniocaudally long and measures more than twice the length of the glenoid facet; on the other hand, the glenoid facet has a larger contribution in lateroventral view. The articular facet for the coracoid in the right scapula of BES SC 999shows a rugose surface indicating the presence of a considerable amount of cartilage. A neurovascular foramen is visible both on the lateroventral and the mediodorsal surfaces of the scapular shaft, at its mid-height. On the visible surfaces, radial striations extend from the ossification center to the margins of the bone.
The scapula of *Besanosaurus* closely resembles that of *Guizhouichthyosaurus tangae* (IVPP V 11853; Shang & Li, 2009), although the latter is slightly shorter proximodistally. It differs from the scapula of *Shonisaurus popularis* (Camp, 1980: fig. 40), *Shonisaurus sikanniensis* (Nicholls & Manabe, 2004: fig.12), *Callawayia neoscapularis* (McGowan, 1994: fig. 6), and parvipelvian ichthyosaurs in the presence of a convex and rounded craniodorsal margin, which on the other hand is more similar to that of *Californosaurus* (Merriam, 1908). Unlike *Shastasaurus pacificus*, *Besanosaurus* does not possess a notch on the cranial edge of the scapula, adjacent to the coracoid facet (Merriam, 1902: pl 10 and pl. 12).

Coracoid – BES SC 999 preserves a complete left coracoid exposed in ventral view; in PIMUZ T 4376 both coracoids are complete, but only the right one is clearly visible and exposed in dorsal view. PIMUZ T 4847 preserves both coracoids, although they are not well-preserved (Fig. 7.6).
The coracoids of *Besanosaurus* are platelike, axe-shaped elements, craniocaudally longer than mediolaterally broad, both in juveniles and adults. The proximal end is more prominent in BES SC 999 and PIMUZ T 4847 than in PIMUZ T 1895 and PIMUZ T 4376. On the lateral side of the proximal end, the scapular facet and the glenoid facet are in continuity with each other, although the glenoid contribution is almost two times dorsoventrally taller than the scapular facet. The cranial margin of the coracoid is characterized by the presence of an anterior notch that is much deeper in PIMUZ T 4847 than in PIMUZ T 4376, with an intermediate condition visible in BES SC 999. The caudal margin is slightly concave, a real posterior notch being absent. The medial margin, which forms the intercoracoid facet (with a possible craniomedial contact for the interclavicle), is long and rounded, contrary to *Callawayia neoscapularis* (McGowan, 1994) and *Shonisaurus popularis* (Camp, 1980), where this margin is straight.
CT images of the left coracoid of BES SC 999 reveal the presence of a slightly concave dorsal surface and a convex ventral surface. As in the scapula, radial striations extend from the ossification center to the margins of the bone.
As in other shastasaurids (e.g., *Guizhouichthyosaurus*, Shang & Li, 2009; *Shonisaurus*, Camp, 1980; Callaway & Massare, 1989; Nicholls & Manabe, 2004), in *Besanosaurus* both the cranial and caudal margin of the coracoid are concave. However, the coracoid of *Besanosaurus* results mediolaterally shorter than in the abovementioned taxa and the medial margin is not straight but rounded. The craniocaudal length of the coracoid peduncle is more than half the length of the coracoid itself, similarly to *Shastasaurus osmonti* (Merriam 1908), *Shonisaurus popularis* (Camp, 1980), and *Guizhouichthyosaurus tangae* (Shang & Li, 2009). The cranial extension of the coracoid in *Besanosaurus* is greater than the postglenoidal portion, as described for other shastasaur-grade ichthyosaurs (e.g., Maisch & Matzke, 2000); however, this latter portion in *Besanosaurus* is smaller than in '*Callawayia' wolonggangense*, *Guizhouichthyosaurus tangae* (Chen et al., 2007; Shang & Li, 2009)

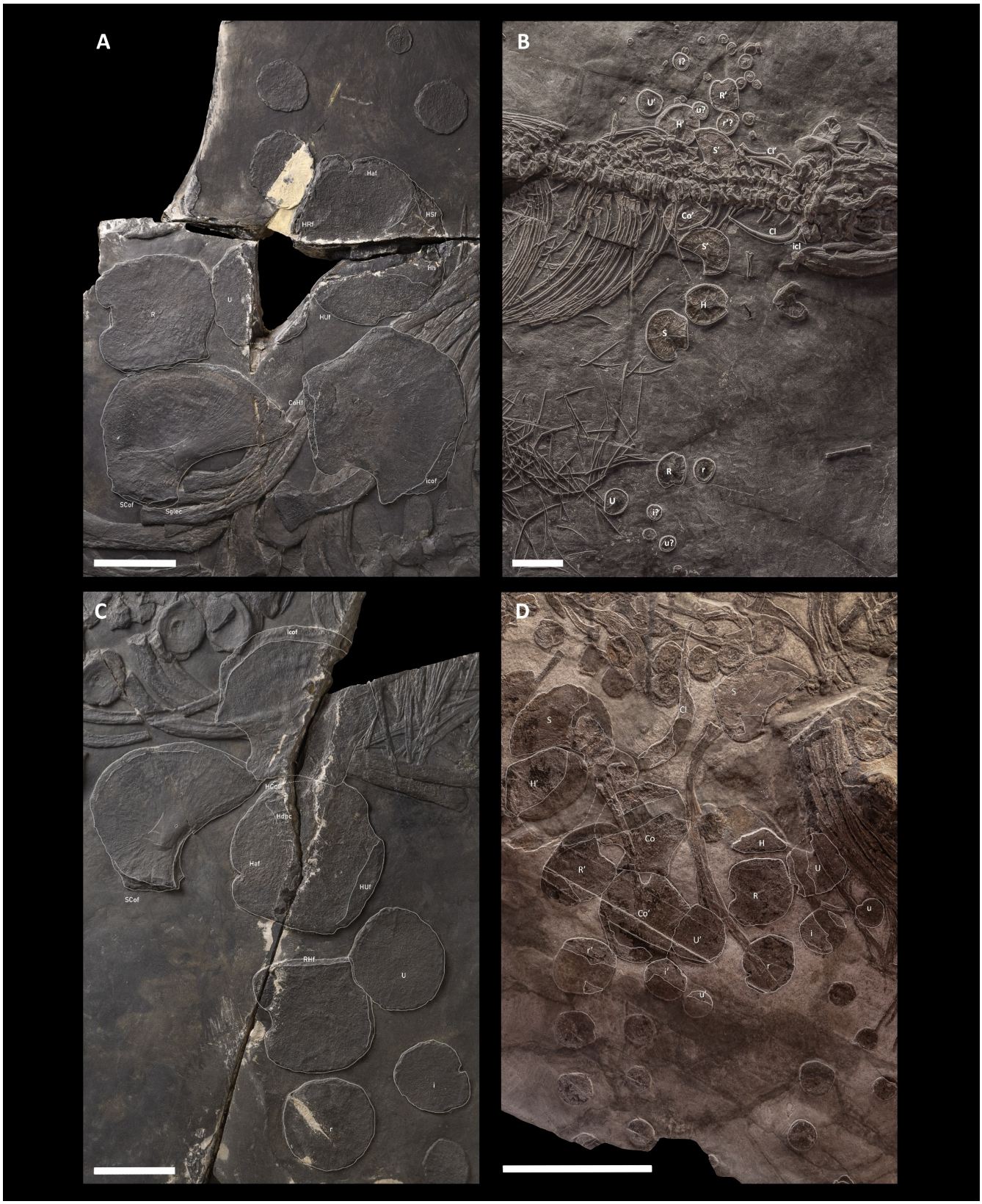

Fig. 7.6 - BES SC 999 left (A) and right (C) forefin and scapular girdle elements; (B) PIMUZ T 4376 and (D) PIMUZ T 4847 forefins and scapular girdle elements. *Abbreviations*: Cl, clavicle; Co, coracoid; CoHf, facet of the humerus for the coracoid; H, humerus; HSf, facet of the humerus for the scapula; Haf, anterior flange of the humerus; HCof, facet of the humerus for the coracoid; Hdpc, deltopectoral crest of the humerus; Hh, humerus head; HRF, facet of the humerus for the radius; HUf, facet of the humerus for the ulna; i, intermedium; icof, intercoracoidal facet; r, radiale; R, radius; RHf, facet of the radius for the humerus; S, scapula; Sglec, glenoid contribution of the scapula; SCof, facet of the scapula for the coracoid; U, ulna. The apostrophe (‘) always indicates a left element. In A, B, and C scale bars represent 5 cm; in D represents 25 cm.

Clavicle – Both clavicles are well-preserved in BES SC 999 and PIMUZ T 4376 (Fig. 7.2 and Fig. 7.6). In the latter, these bones are both exposed in dorsal view, whereas in the holotype the right clavicle is exposed in ventral view and the left one has rotated by 180° and is exposed in dorsal view.
The clavicles are long and slender, gently swollen at midshaft, and gently curved towards the glenoid region. The medial ends are feebly expanded whereas distally the clavicles taper to a pointed end The dorsal surfaces of the clavicles are convex, the ventral one is concave: in the distal half, this concavity consists of a deep groove that is shallower proximally. As reported in *Guizhouichthyosaurus* (Shang & Li, 2009), the medial margins articulate with the central interclavicle, so that the three elements form a continuous recurved cranial margin. The caudal tip of the clavicle contacts the scapula lateroventrally, which shows a specific dorsomedial articulation surface for the clavicle. The clavicles of *Besanosaurus* are similar to those of *Shastasaurus* (Meriam, 1902), *Guizhouichthyosaurus* (Shang & Li, 2009), and *Shonisaurus popularis* (Camp, 1980), although in this taxon they are proportionally much shorter.

Interclavicle – The only specimen where an interclavicle is visible is PIMUZ T 4376 (Fig. 7.6B). This bone is T-shaped, with long lateral processes contacting the clavicles cranially, and a thin triangular caudal process. A posterior ossified rod is apparently missing, but this could be due to the early ontogenetic stage of the specimen, or because it has gone lost during fossilization. It is unclear if the interclavicle prevented the two clavicles to contact each other or not. The interclavicle of *Besanosaurus* is similar to that of *'Callawayia' wolonggangense* (Chen et al.: fig. 3B). The preserved portion of the interclavicle is also similar to *Guizhouichthyosaurus tangae* (IVPP V 11853), except for the absence of the posterior rod. This feature recalls the interclavicle of *Mixosaurus cornalianus* BES SC 1000 (Renesto et al., 2020). Also, *Besanosaurus* and *Guizhouichthyosaurus* clearly differ from *Shonisaurus sikanniensis*, whose interclavicle shows a laterally expanded posterior rod and shortened lateral processes.

Forefin
None of the specimens show fully articulated and complete forelimbs; however, the left stylopodium and zeugopodium of BES SC 999 are preserved in articulation. The stylopodium, zeugopodium, and autopodium appear to be composed of plate-like elements. Each element of the forelimb is suboval to rounded in outline, except for the few bones that possess an anterior or posterior notch. The zeugopodium of *Besanosaurus* is ~66% the length of the stylopodium. The manus of *Besanosaurus* possesses four primary digits and one accessory digit. Thephalanges are well-separated, likely surrounded *in vivo* by a considerable amount of cartilage, in contrast to the hindlimbs, where the phalanges are tightly packed together and less rounded than in the forelimbs. The roundness of the forelimb elements is shared both by small and large (PIMUZ T 4376; BES SC 999, PIMUZ T 4847) *Besanosaurus* individuals; this character, which we suspect to be paedomorphic, is shared at least by *Guizhouichthyosaurus* (Shang & Li, 2009; Shang & Li, 2013) and *Guanlingsaurus* (Ji et al., 2013).

Humerus – PIMUZ T 4376 is the only specimen that preserves both humeri complete. In this specimen, the humeri are slightly craniocaudally broader than proximodistally long (Fig. 7.6). The same is true for the left humerus of BES SC 999, but not for the right one, which shows an opposite condition (Table 7.1). This difference is likely attributable to different stresses that during the process of fossilization acted on the holotype skeleton, which results largely taphonomically compressed. PIMUZ T 1895 and PIMUZ T 4847 possess incomplete and fragmentary humeri.

Table 7.1 – PIMUZ T 4376 and BES SC 999 humeri proportions.

Craniocaudal/proximodistal length ratio	Right humerus	Left humerus
PIMUZ T 4376	1.04	1.05
BES SC 999	0.98	1.09

Observing the bone in dorsal and ventral view, the distal width of the humerus is slightly larger than its proximal width. The anterior flange of the humerus is present but reduced and slightly tilted dorsally with respect to *Mixosaurus* and basal ichthyopterygians (Motani, 1999). It has a shallow notch in the middle in PIMUZ T 4376, and a deeper notch in BES SC 999. On the dorsal side of the humerus, the head is directed proximodorsally as in other shastasaurids and not proximally as in more basal ichthyopterygians (Motani, 1999). On the ventral side, the deltopectoral crest appears to be slightly raised, but this might be the result of taphonomical compression. For the same reason, the posterodistal tuberosity seems to be flat. A deltopectoral ridge runs distally from the deltopectoral crest toward the centre of the ventral surface.
In BES SC 999, on the dorsal side of the proximal end of the humerus, the facet for the scapula is visible. Symmetrically, on the ventral side, a small portion of the facet for the coracoid is visible. However, both these articular surfaces are not well preserved in the holotype, and in the other specimens these features are not clearly visible. The distal surface of the humerus hosts a relatively large, slightly concave, and anterodistally directed facet for the ulna; the facet for the radius is directed posterodistally. Judging from the CT images of BES SC 999, the radial facet appears ~1,5 times longer than the ulnar facet.
The humerus proportions in *Besanosaurus* resemble those in *Pessosaurus* (PMU 24585=PMU R176; Motani 1999: fig. 3; per. obs.) and *Guanlingsaurus* (GNG dq-50, Ji et al., 2013; YGMIR SPCV03107, Sander et al. 2011). An opposite condition is seen in *Pessopteryx* (Wiman, 1910) and *Guizhouichthyosaurus* (IVPP V 11853; Shang & Li, 2009), where the humerus is proximodistally longer than craniocaudally wide. On the other hand, the humerus of *Besanosaurus* is more rounded than in *Callawaya neoscapularis* (ROM 41993; McGowan, 1994) and *Shonisaurus popularis* (Camp, 1980).

Radius – The radius is the second largest bone in the forefin; it possesses a subsquared profile in dorsal/ventral view. Like the humeri, the radii are both complete and well-preserved in BES SC 999 and PIMUZ T 4376 (Fig. 7.6). The ?right radius is also preserved in PIMUZ T 4847.
The radius lies cranially to the ulna and contacts the humerus proximally: the facet for the latter is straight and long, visible in ventral view in BES SC 999, and is consistent with the presence of a radial facet directed anterodistally at the distal end of the humerus. The radius in BES SC 999 and PIMUZ T 4376 is slightly craniocaudally broader than proximodistally long. On the other hand, the ?right radius of PIMUZ T 4847 shows an opposite condition (Table 7.2). The different proportions of the radii in PIMUZ T 4847 and PIMUZ T 4376 are likely related to ontogeny. The anterior margin of the radius is characterized by a proximodistally wide notch in the adults; this notch is shorter and shallower in the juvenile. The caudal margin of the radius is characterized by a shallow concavity adjacent to the proximal end, which might have accommodated a small portion of the rounded proximocranial margin of the ulna. The radius of *Pessosaurus polaris* (PMU R176; Motani 1999: fig. 5) shares a similar morphology, despite being proximodistally much shorter than in *Besanosaurus.* The radius of *Besanosaurus* is also similar in shape to that of *Guizhouichthyosaurus* (IVPP 11853; Shang & Li, 2009), which however possesses a straighter caudal margin, making *Besanosaurus* somewhat intermediate between the two taxa. The radius of *Callawayia neoscapularis* (ROM 41993, McGowan, 1994) on the caudal margin has a similar depression on its caudal argin as that in *Besanosaurus*, however it possesses a concave distal margin and does not possess an anterior notch.

Table 7.2 – PIMUZ T 4376 and BES SC 999 radii proportions.

Craniocaudal/proximodistal length ratio	Right radius	Left radius
PIMUZ T 4376	1.12	1.11
BES SC 999	1.03	1.04
PIMUZ T 4847	0.98	-

Ulna – Both ulnae are preserved in PIMUZ T 4376 and BES SC 999 (Fig. 7.6). In the latter specimen, the ulnae are preserved close to their in vivo position, although the left one is incomplete, whereas in PIMUZ T 4376 they are disarticulated. An incomplete ulna is also preserved in PIMUZ T 4847. The ulna is always subcircular in outline and slightly smaller than the radius.
The ulnar roundness of *Besanosaurus* results similar to *Guanlingsaurus* (GMR 014; Yin et al, 2000: plate IX). The ulna of *Guizhouichthyosaurus* shows similarly rounded margins, but in contrast to *Besanosaurus*, it is markedly proximodistally longer than craniocaudally wide. In both ulnae of both PIMUZ T 4376 and BES SC 999, the roundness (defined by the International Organization for Standardization as the ratio between the inscribed and the circumscribed circles) equals ~0.8. For comparison, this ratio in *Guizhouichthyosaurus* (GMR 009; Shang & Li, 2009) is 0.67, in *Callawaya* (ROM 41993, McGowan, 1994) is 0.61.

Carpus – The proximal and distal carpals of *Besanosaurus* possess a generally subcircular profile (shafts are not retained as in other non-merriamosaurian ichthyosaurs [e.g., McGowan & Motani, 2003]). The radiale is the largest among the carpals, with the ulna being slightly smaller. All other carpal elements are smaller than the ulna. (Fig. 7.2, Fig. 7.6, and Fig. 7.7).
In BES SC 999, where these elements are preserved relatively close to their original position, three proximal carpals (radiale, intermedium, and ulnare) and four distal carpals can be identified. One small and rounded distal element, likely representing a pisiform, is also visible. It likely articulated caudally with the two carpal rows, similar to the condition in *Guizhouichthyosaurus* (Shang & Li, 2009). The radiale and ulnare are almost perfectly circular, whereas the intermedium seems to be slightly proximodistally longer than craniocaudally wide.
In BES SC 999 and PIMUZ T 4376, the radiale does not bear a notch; only the ?right radiale of PIMUZ T 4847 is notched on its anterior margin. Unusually, in BES SC 999 the ?posterior margin of the right intermedium is notched, whereas the left one is rounded like the other carpals. Therefore, we deem the presence of a notch on the cranial or caudal margin of the proximal carpals variable in *Besanosaurus*. Among shastasaurian grade ichthyosaurs, a non-notched radiale has also been reported in *Guizhouichthyosaurus tangae* (Shang & li, 2009), *Shonisaurus popularis* (Camp, 1980; Sander, 2000), and *Shastasaurus* (Meriam, 1902; 1908).

Metacarpus and manual phalanges – Metacarpals and manual phalanges are preserved in BES SC 999, PIMUZ T 4376, and PIMUZ T 4847 (Fig. 7.2). They are never in articulation with each other, although in the right forefin of BES SC 999 almost all phalanges are still present, scattered on the surface of the slabs. The metacarpals and the manual phalanges are all subcircular in outline. *Besanosaurus* had four primary digits (II, III, IV, V), with digit V possessing markedly smaller phalanges compared to the other three digits. Following this interpretation, *Besanosaurus* is the stratigraphically oldest ichthyosaur reported to date,

showing the loss of digit I. We estimate the presence of at least 20 phalanges on the longest digit (III). In *Besanosaurus* the autopodium (estimated to measure ~55 cm) is longer than the stylopodium+zeugopodium. Phalanges are not packed close to each other, but are well separated, likely surrounded in vivo by a considerable amount of cartilage. According to our reconstruction, a few tiny elements belonging to a postaxial accessory digit (VI) are also present; these phalanges and their arrangement are similar to those in *Guizhouichthyosaurus tangae*, although in the latter a higher number of phalanges of the postaxial accessory digit has been reported (Shang & Li, 2013). Rounded phalanges are also visible in *Shastasaurus osmonti*, *Californosaurus perrini* (Merriam, 1902), and *Shonisaurus popularis* (Camp 1980). The latter, on the other hand, possesses a notch on the cranial margin of each element of the autopodium, a character absent in *Besanosaurus.*

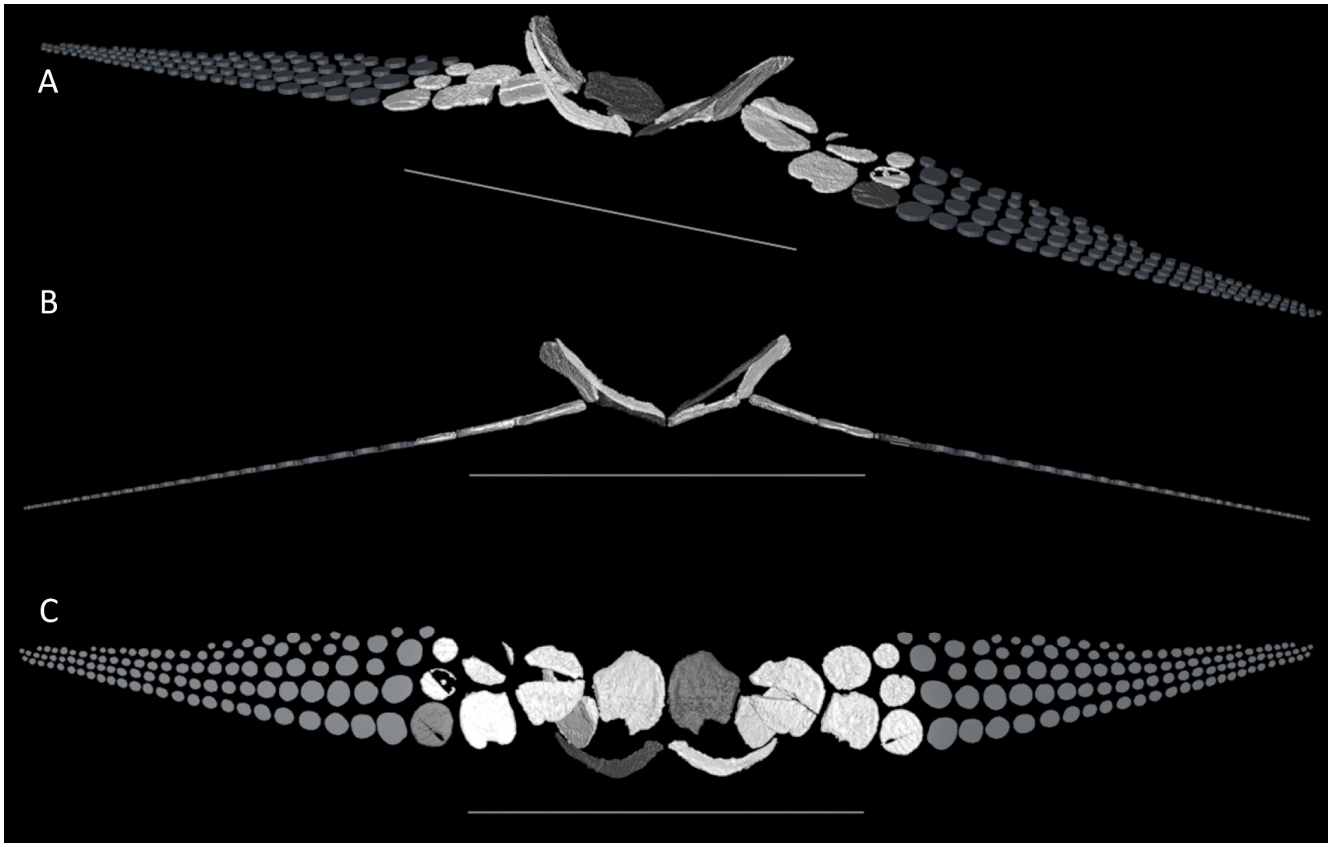

Fig. 7.7- 3D reconstruction of the scapular girdle and forefins of *Besanosaurus leptorhynchus* based on the CT scans of BES SC 999 in laterofrontal (A), ventral (B), and frontal (C) view. Original elements in white; elements deducted from the available material in grey. Scale bars represent 50 cm.

Pelvic girdle

The ilium of *Besanosaurus* is similar in size to the other pelvic bones, as in other shastasaurids (Merriam, 1908; Camp, 1980; Shang & Li, 2009; Ji et al., 2013) and *Callawayia neoscapularis* (Nicholls & Manabe, 2001), but differs from *Cymbospondylus* (Merriam 1908), *Mixosaurus* (Repossi, 1902) and *Californosaurus perrini* (Merriam 1902), in which the ilium is visibly smaller than the other pelvic bones.

The pubis and ischium of *Besanosaurus* are nearly equal in size, with the ischium being slightly smaller than the pubis, as is also the case in *Cymbospondylus* (Merriam, 1908), *Guizhouichthyosaurus tangae* (Shang & Li, 2009), and *Shonisaurus popularis* (Camp, 1980), but differs from *Shastasaurus alexandrae* (Merriam 1902), *Guanlingsaurus liangae* (Ji et al., 2013) and *Callawayia neoscapaularis* (Nicholls & Manabe, 2001),

in which the two bones are sub-equal in size, and *Californosaurus perrini* (Merriam, 1902), in which the ischium is slightly larger than the pubis.

Ilium – The ilia are well-preserved in BES SC 999 and PIMUZ T 4376. In PIMUZ T 4847, only an incomplete element resembling the ?left ilium is preserved (Fig. 7.8A, B, and D).
The ilium of *Besanosaurus* has a craniocaudally expanded proximal end that participated in the acetabulum and a craniocaudally expanded distal end that likely contacted the distal enlarged ends of two sacral ribs, as suggested for *Guizhouichthyosaurus tangae* (Shang & Li, 2009). The distal end of the ilium is craniocaudally wider than the proximal end, similar to *Mixosaurus* (Repossi, 1902), *Shastasaurus* (Merriam, 1902; 1908), and adult *Guanlingsaurus liangae* (Ji et al., 2013), but is different from the condition in *Cymbospondylus* (Merriam, 1908), *Guizhouichthyosaurus tangae* (Shang & Li, 2009), juvenile *Guanlingsaurus liangae* (Ji et al., 2013), *Callawayia neoscapularis* (Nicholls & Manabe, 2001) and *Californosaurus perrini* (Merriam, 1902), in which the proximal and distal ends of the ilium are of approximately equal width in lateral view. In BES SC 999, both the proximal and distal ends are also highly rugose, suggesting the presence of cartilage in vivo. The shaft of the ilium appears lateromedially flattened relative to the likely thickened proximal end (compare with Camp, 1980). The right ilium of BES SC 999 and the ?left ilium of PIMUZ T 4847 are preserved in approximately anterolateral/posterolateral view, although they have undergone severe compression. The ilia are slightly curved laterally, so the preserved concave margins in reality indicate the positions of the medial surfaces (compare with Camp, 1980: fig. 51). This is similar to *Shastasaurus* (Merriam, 1908: pl. 16, fig. 4) and recalls the basal morphology of *Utatsusaurus* (Motani, 1998). The curvature is also preserved in adult specimens of *Guanlingsaurus* (Ji et al., 2013: fig. 5) and *Callawayia neoscapularis* (Nicholls and Manabe 2001: fig. 11). Such curvature is less pronounced in *Californosaurus perrini*. In PIMUZ T 4376 this curvature is not visible, likely due to different preservation; in BES SC 999, the left ilium is preserved straight as well.

Pubis – Both pubes are well-preserved in BES SC 999 and PIMUZ T 4376 (Fig. 7.8); a poorly preserved element resembling a pubis is also visible in PIMUZ T 4847.
The pubis of *Besanosaurus* is plate-like. Its dorsal margin is concave, whereas the rest of the bone shows a sub-oval profile interrupted only by the aperture of the obturator foramen on its caudal margin. The proximal margin, bordering one-third of the cranioventral margin of the acetabulum, results dorsoventrally slightly thicker than the rest of the bone. The obturator foramen is sub-oval in outline, almost entirely enclosed within the pubis in the holotype BES SC 999, but slightly opens to the posterior margin of the pubis in the smallest specimen PIMUZ T 4376.Among basal Merriamosauria, *Guizhouichthyosaurus tangae* (Shang & Li, 2009) shares the most similar morphology with *Besanosaurus*. *Shastasaurus* (Merriam, 1902) also shows a similar morphology which, however, possesses a much more rounded ventral margin both in the pubis and the ischium. In dorsal and ventral view, *Besanosaurus* recalls the *Californosaurus perrini* pubis in outline, but the latter shows a wider aperture of the obturator foramen (Merriam, 1902); under this aspect, *Besanosaurus* resembles much more *Shastasurus osmonti* (Merriam, 1908: fig. 73; Dal Sasso & Pinna, 1996: fig. 21).

Ischium – Both ischia are well-preserved in BES SC 999 and PIMUZ T 4376 (Fig. 7.8); a possible ischium is also preserved in PIMUZ T 4847. The ischium is a plate-like bone similar in outline to the pubis, although the latter is slightly larger. In ventral and dorsal view, the bone forms a subcircular profile interrupted only by the concave dorsolateral and caudolateral margins. The proximal margin of this bone appears dorsoventrally slightly thicker than the rest of it and forms the caudoventral margin of the acetabulum.

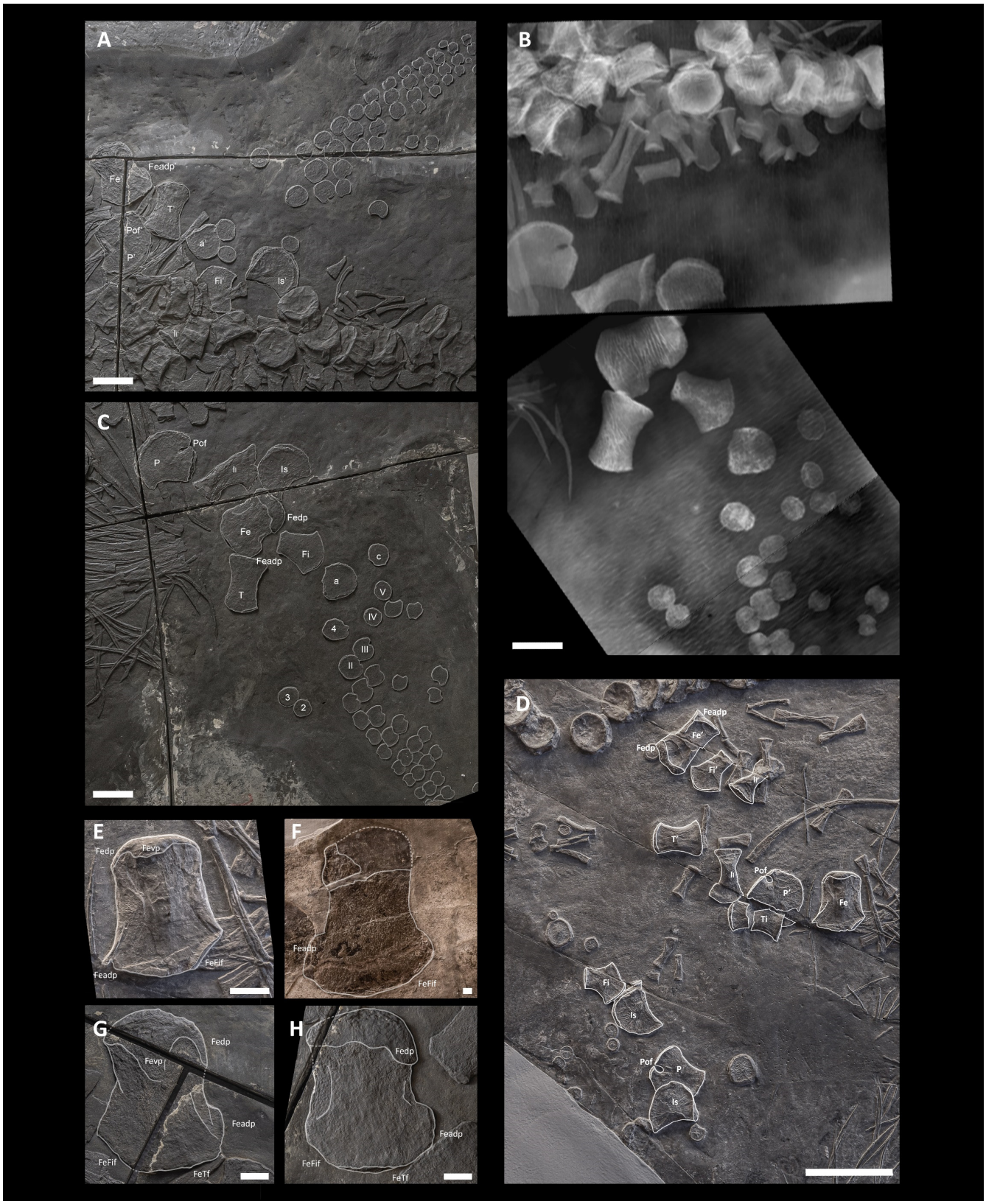

Fig. 7.8- BES SC 999 left (A) and rigth (C) hindfin and pelvic girdle elements; (B) BES SC 999, CT scan rendering of the right pelvic girdle and forefin elements; (D) PIMUZ T 4376 hindfin and pelvic girdle elements; (E) PIMUZ T 4376 right femur; (F) PIMUZ T 4847 femur; (G, H) left and right femora of BES SC 999. *Abbreviations*: a, astragalus; c, calcaneum; Fe, femur; Feadp, Femur anterodistal process; Fedp, dorsal process of the proximal epiphisis of the femur; FeFif, facet of the femur for the fibula; FeTf, facet of the femur for the tibia; Fevp, ventral process of the proximal epiphisis of the femur; Fi, Fibula; Il, Ilium; Is, Ischium; P, pubis; Pof, obturator foramen of the Pubis; T, Tibia; 2, 3, and 4, distal tarsals; II, III, IV, IV, and V metatarsals.The apostrophe (‘) always indicates a left element. Scale bars represent 5 cm in A-D, 1 cm in E-H.

Overall, the morphology of the ischium is similar to that of basal Merriamosauria where this bone is preserved [*Guizhouichthyosaurus tangae* (Shang & Li, 2009); *Shastasaurus pacificus* (Merriam, 1908); *Shonisaurus* popularis (Camp, 1980); *Californosarus perrini* (Merriam, 1902)]. In contrast to basal ichthyopterygians (Wiman, 1929; Motani et al. 1998; Motani et al., 2014), mixosaurids (e.g., Brinkmann, 2004), and *Toretocnemus* (Merriam, 1903), in *Besanosaurus* the medial symphysis between the pubes and ischia is not straight and well-defined, on the other end being well-developed in *Cymbospondylus*, shastasaurids, *Callawayia neoscapularis,* and *Californosaurus perrini* (Merriam, 1902; Merriam, 1908; Nicholls & Manabe, 2001).

Hindfin

Only BES SC 999 and PIMUZ T 4376 preserve both hindfins (Fig. 7.2). In the latter, most of the autopodia are missing, whereas in the holotype they are complete. In PIMUZ T 4847, only some proximal elements of the hindfins are preserved. Based on the preserved elements and our reconstruction, the hindlimb is about 70% shorter proximodistally than the forelimb. The fin possesses four digits representing primary digits II, III, IV, and V (Motani, 1999). Preaxial and postaxial accessory digits are absent. Moreover, in contrast to the forefin, the phalanges in the hindfin are more tightly packed together and constricted in the middle, showing a condition more similar to Mixosauridae (e.g., Repossi, 1902; Brinkman, 2004) than to *Guizhouichthyosaurus tangae* (Shang & Li, 2009) and *Shonisaurus popularis* (Camp, 1980), in which the phalanges are sub-oval to sub-circular in outline, and lack medial constrictions.

Femur – Femora are preserved in BES SC 999, PIMUZ T 4376, and PIMUZ T 4847, although in the latter specimen they are incomplete (Fig. 7.8F-H). In BES SC 999 the right femur is preserved in dorsal view, whereas the left femur is preserved in ventral view but, as a result of extreme compression, the preserved margins of the femora might not correspond to their actual cranial and caudal margins,. In PIMUZ T 4376 the right femur is preserved in ventral view, whereas the left femur is preserved in cranial view. In PIMUZ T 4847 the orientation of the femora is unclear.

In dorsal and ventral view, the femur shows concave cranial and caudal margins; despite this, the midshaft constriction is feeble. The craniocaudal length of the proximal end is shorter than that of the distal end. On the proximal end, well-developed dorsal and ventral processes are present. The dorsal process is positioned cranioproximally, whereas the ventral process is located more centrally (Maxwell et al., 2012). Both processes extend for approximately one-third of the femoral proximodistal length. Two distal facets for the tibia and fibula, in continuity with each other, can be distinguished at the distal end of the bone. The fibular facet is shorter, faces caudodistally, and is inclined at an angle >45° with respect to the proximodistal axis of the femur. The facet for the tibia is longer and faces entirely distally. Anterodistally, the femur also forms a distinct flange, as seen in *Pessopteryx* (Wiman, 1910).

In dorsal and ventral view, the *Besanosaurus* femur looks craniocaudally wider than the femora of *Guanlingsaurus liangae* (YGMIR SPCV03107; Sander et al., 2011) and *Shonisaurus popularis* (Camp, 1980). Also, in both of these taxa, the proximal end is craniocaudally shorter than in *Besanosaurus*. In comparison to *Besanosaurus*, *Californosaurus perrini* (Merriam, 1902) possesses a femur with a smaller proximal end, recalling the femoral shape of *Shonisaurus popularis*. Overall, the *Besanosaurus* femur is more similar to the femur type A (Shang & Li, 2013) of *Guizhouichthyosaurus tangae* (IVPP V 11853); than to any other taxa.

Tibia – Both tibiae are preserved in BES SC 999, PIMUZ T 4376, and PIMUZ T 4847 (Fig. 7.2, Fig. 7.3 and Fig. 7.8). In the holotype, the left one is still close to its in vivo position, whereas the right one is markedly

dislocated. In PIMUZ T 4376 and PIMUZ T 4847, the tibiae are disarticulated and betterpreserved in the former.
The proximal end of the tibia is straight in dorsal/ventral view and craniocaudally longer than the convex distal end. The caudalmost portion of the distal end likely contacted the astragalus, as in articulated hindfins of *Guizhouicthhyosaurus tangae* (Shang & Li, 2013). In dorsal and ventral view, the shaft is straight and long, with concave anterior and posterior margins; this is in contrast with the condition of *Guizhouichthyosaurus tangae* (Shang & Li, 2013), *Guanlingsaurus liangae* (Sander et al., 2011), *Shastasaurus osmonti* (Merriam, 1902), *Shonisaurus popularis* (Camp, 1980), and *Californosaurus perrini* (Merriam, 1902), where the tibial shaft is shorter and thicker, and the anterior margins are deeply concave.

Fibula – Both fibulae are preserved in BES SC 999, PIMUZ T 4376, and PIMUZ T 4847 4847 (Fig. 7.2, Fig. 7.3 and Fig. 7.8). Like the tibia, the left fibula is still close to its in vivo position in the holotype.
The proximal end is much smaller than the distal one. The facets for the calcaneum and the astragalus are wide, almost equal in size, and in continuity with each other. The separation between the two facets is not well-defined, although they are symmetrically inclined at an angle of ~45° with respect to the proximodistal axis of the fibula. In in-life position, the tibia and fibula were likely completely separated from each other as none of the two bones shows facets for mutual articulation.
Overall, the general shape of the *Besanosaurus* fibula is similar to that of *Cymbospondylus* (Merriam, 1908) and most other shastasaur-grade ichthyosaurs (e.g., Merriam, 1902; Sander et al., 2011; Shang & Li, 2013), with the exception of *Shonisaurus popularis*, in which the fibula produces a prominent distal flange (Camp, 1980).

Tarsus and metatarsus – BES SC 999 possesses two proximal tarsals: astragalus, and calcaneum; the presence of ossified tarsals is uncertain in PIMUZ T 4376 due to incomplete preservation of the hindfins. The astragalus is anteroposteriorly longer than proximodistally tall and much larger than the calcaneum, which is sub-circular in outline (Fig. 7.8 and Fig. 7.9). The general shape and proportions of the tarsal bones resemble those of *Guizhouichthyosaurus tangae* (Shang & Li, 2009; 2013) and *Guanlingsaurus liangae* (Yin et al., 2000; Ji et al., 2013), unlike *Shastasaurus alexandrae*, in which the astragalus is also larger than the calcaneum, but both tarsals are sub-circular in outline (Merriam, 1908).
In the *Besanosaurus* holotype, three elements are identified as distal tarsals (distal tarsals 2–4) and four elements are identified as metatarsals (metatarsals II–V). Distal tarsals 2 and 3 are sub-circular in outline and much smaller than the sub-oval distal carpal 3. Metatarsals II and III possess a rounded anterior margin and a shallow notch on the caudal margin. Metatarsals IV and V are sub-circular in outline and do not bear any notches. According to our reconstruction, metatarsal V contacted the distal portion of the calcaneum as in several Triassic ichthyosaurs (e.g., McGowan & Motani 2003). This differs from the condition reported by Shang & Li (2009, 2013) for *Guizhouichthyosaurus tangae*, in which distal tarsal 4 contacts the distal part of the calcaneum and metatarsal Vlies in the same row with the other metacarpals.
Pardo-Pérez et al. (2020: fig 1g, h) reported a case of ankylosis in the hindlimb metapodial elements II and III of BES SC 999. We confirm that a small portion of the caudal margin of metatarsal II is fused to the cranial margin of metatarsal III.

Pedal phalanges – In BES SC 999 the pedal phalanges retain rudimentary shafts,showing an anterior and/or a posterior shallow notch(Fig. 7.8A and 7.8C), whereas in PIMUZ T 4376 they are mostly rounded in outline, except for the largest proximal phalanges, which bear anterior notches (Fig. 7.3). These differences between the two specimens are here attributed to their different ontogenetic stages.

In BES SC 999, most of the pedal phalanges are preserved in in-life position, being in close contact or only slightly separated from each other. This provides evidence that in *Besanosaurus* the pedal phalanges were well-packed and the amount of interphalangeal cartilage was much lower in the hindfincontrary to the forefin (see above). As a result, the hindfins might have been stiffer than the forefins. This feature is in contrast with the condition seen in *Guizhouichthyosaurus* (Shang & Li, 2009), where manual and pedal phalanges show a similar degree of spacing, the pedal phalanges being not preserved in contact with each other. Furthermore, even in large (adult) specimens of *Guizhouichthyosaurus* (Shang & Li, 2009; 2013), all of the pedal phalanges appear to be rounded. Therefore, the pes of adult *Besanosaurus* appears to be more similar to *Mixosaurus*, in which the pedal phalanges retain constricted shafts and are tightly packed (e.g., Renesto et al., 2020).

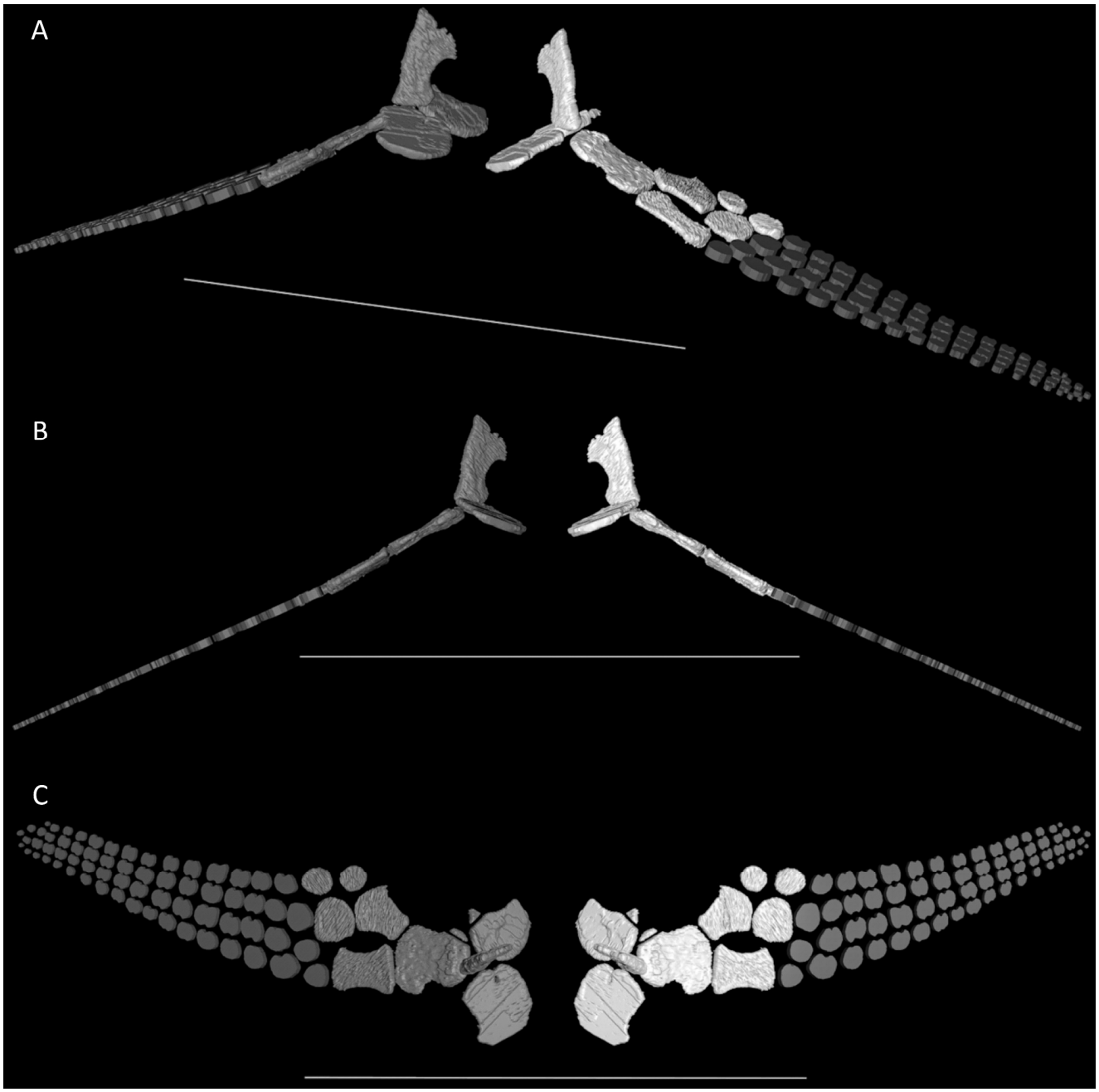

Fig. 7.9- 3D reconstruction of the pelvic girdle and hindfins of *Besanosaurus leptorhynchus* based on the CT scans of BES SC 999 in laterofrontal (A), dorsal (B), and frontal (C) view. Shang and li (2013: fig. 1) and McGowan & Motani (2003: fig. 70) used as references to reconstruct the hindfins. Original elements in white; element deducted from the available material in grey. Scale bars represent 50 cm.

7.5 Results: testing the swimming mode of *Besanosaurus*

To investigate the swimming mode of *Besanosaurus* we used Motani et al.'s (1996; see also Motani, 2005; Motani, 2008; Lindgren et al., 2013) method, expanded the dataset by adding some ichthyopterigian taxa to the original plot, and see how they distribute in comparison to some selected fishes. In this plot the x-axis is the "caudal fin H/L ratio" (fluke height divided by fluke length) and the y-axis is the "fineness ratio" (body height -excluding the dorsal fin- divided by prefluke length). Expanding the original dataset allows to have a broader representation of taxa in terms of phylogenetic diversity and swimming styles. The selected taxa of fishes have been chosen to represent the different categories of swim by lateral undulations [anguilliform, subcarangiform, carangiform, and thunniform, according to the portion of the body used to generate propulsion (McGowan, 1992; Motani et al., 1996). To do so, we provide silhouettes for both ichthyosaurs and fishes included in the analysis (Fig. 7.S1), as well as the measurements obtained from them and the reference used (Tab. 7.S1).

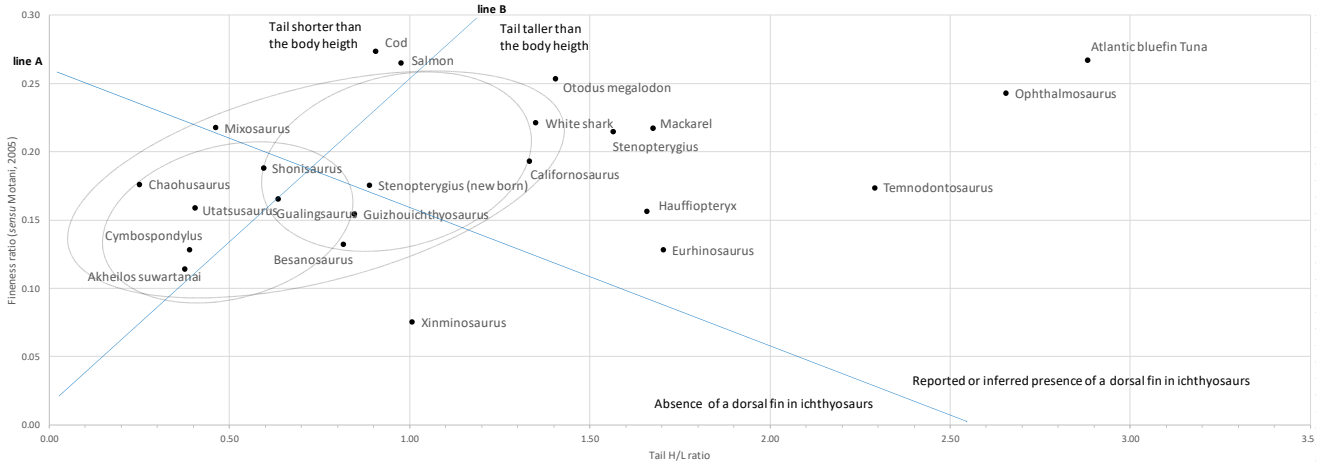

Fig. 7.10 - Graph showing the "caudal fin H/L ratio" (fluke height divided by fluke length; x-axis) *versus* the "fineness ratio" (body height -excluding the dorsal fin- divided by prefluke length; y-axis). The graph is built following Motani et al. (1996) method. Silhouettes for both ichthyosaurs and fishes, as well as the measurements obtained from them and the references used, are included in Fig. S1 and Tab. S1.

In the obtained plot (Fig. 7.10), for descriptive purposes we distinguish four areas divided by two lines "Line A" and "Line B". The ichthyosaurian taxa where a dorsal fin has been reported or inferred are plotted above line A. These include parvipelvians and *Mixosaurus*, but also all the examined fishes (except for *Akheilos*, a Scyliorhinidae). Below line A, basal Ichthyopterygia, Cymbospondylidae, and shastasaur-grade ichthyosaurs are plotting. Line B divides all those taxa that possess a caudal fluke (tail height *sensu* Motani et al., 1996) dorsoventrally taller than their body height (on the right), and taxa that have a tail dorsoventrally shorter than their body height (on the left). On the right of line B, parvipelvians and shastasaur-grade ichthyosaurs (except for *Shonisaurus*) are plotted, whereas on the left there are more basal ichthyopterygians.

Besanosaurus falls close to the shastasaur-grade ichthyosaurs included in this analysis, as well as close to *Cymbospondylus*. In fact, the fineness ratio of *Besanosaurus* is similar to the one obtained for *Cymbospondylus*, but the H/L ratio of the caudal fluke is more similar to that of *Guanlingsaurus.* Nonetheless, this ratio might be affected to a lesser extent by the lack of data regarding the presence and the height of a dorsal lobe of tail fluke. All non-parvipelvian ichthyosaurs fall inside the 95% confidence ellipse fitted to data for 94 species, belonging to 14 families of sharks (Motani et al. 1996: fig. 2a). Except for *Besanosaurus*, shastasaur-grade ichthyosaurs plot inside the carcharhinid ellipse. The very long tail of *Besanosaurus* causes it to fall in the scyliorhinid domain, close to *Cymbospondylus*. *Chaohusaurus* and

Utatsusaurus are also found in the scyliorhinid ellipse. Among Triassic ichthyosaurs, solely *Mixosaurus* falls outside the carcharhinid and the scyliorhinid ellipse, close to the fish species belonging to Odontaspidae and Sphyrenidae with the lowest fin H/L ratio reported by Motani et al. (1996).
In the plot of body fineness ratio, the anguilliform swimmers are grouped in the lower-left corner, whereas in the top right corner the thunniform swimmers are clustered (Motani et al. 1996). *Stenopterygius* clusters close to Lamniformes (*Carcharodon*, *Otodus*), i.e., the carangiform swimmers, whereas the rest of the parvipelvian ichthyosaurs are plotted closer to the thunniform corner, with *Ophthalmosaurus* clustering closer to the tuna than to any other ichthyosaur. On the other hand, Triassic ichthyosaurs appear to cluster among subcarangiform and anguilliform swimmers, with *Mixosaurus* being almost an outlier: this taxon possesses the highest fineness ratio among Triassic ichthyosaurs.

7.6 Discussion

7.6.1 Remarks on the swimming style of *Besanosaurus*, *Cymbospondylus*, and *Mixosaurus*

The fineness ratio of *Besanosaurus* results in between *Cymbospondylus*, which clusters among anguilliform swimmers, and the rest of the shastasaur-grade ichthyosaurs (*Shonisaurus, Guanlingsaurus, Ghouizhouichthyosaurus*); on the other hand, the tail H/L ratio is more similar to *Ghouizhouichthyosaurus* than to *Cymbospondylus*. This indicates that *Besanosaurus* has body proportions intermediate between the cited taxa. The consequent assumption that *Besanosaurus* might have swum in an intermediate way between *Cymbospondylus* and the rest of the shastasaur-grade ichthyosaurs is supported by the phylogenetic position inferred for these taxa (e.g., Maisch & Matzke, 2000; Sander et al., 2011; Moon, 2017; Moon & Stubbs, 2020; Ji et al., 2016; Motani et al., 2017; Bindellini et al., 2021) and by the morphology and position of the rib facets along the vertebral column. Slijper (1936) already reported the reduction of the rib count and the replacement of sternal and dichocephalous ribs by floating holocephalous ribs in the early evolution of whales, associating with this trend an increased thoracic flexibility needed by early whales to swim and dive. Furthermore, in Jurassic ichthyosaurs, ribs are dichocephalous cranially and holocephalous caudally and the transition point occurs after the 40th centrum (Buchholtz, 2001), whereas in Triassic ichthyosaurs dichocephalous ribs are present almost exclusively in the cervical region (e.g., Merriam, 1902; Camp, 1980; Sander, 1989; Fröbisch et al., 2006; Shang & Li, 2009). Buchholtz (2001) concludes that dichocephalous ribs have less freedom of movement than holocephalous ones and that the transition point marks the transition from a rigid to a more flexible body region. This hypothesis also supports the idea that Triassic ichthyosaurs were more anguilliform or subcarangiform swimmers, whereas parvipelvians were carangiform and thunniform swimmers.
Among the ichthyosaurs from the Besano Formation, the dimensions and position of the diapophyses in the dorsal vertebrae of *Cymbospondylus buchseri* most closely resemble the caudalmost-dorsal and cranialmost-caudals of *Besanosaurus leptorhynchus*. These centra are characterized by the presence of small and round diapophyses, that should have granted a greater range of movement to the ribcage. The fact that such morphology appears more cranially in *Cymbospondylus* than in *Besanosaurus* is consistent with a more anguilliform swimming style in *Cymbospondylus*. Uniquely in *Mixosaurus*, approaching the pelvis, a second facet for the articulation of dichocephalous ribs reappears on the sides of the centra (e.g., Brinkman, 2004). This condition, opposed to *Besanosaurus* and *Cymbospondylus*, should have granted more stiffness to the dorsum. In support of this assumption, we point out that *Mixosaurus*, among Triassic ichthyosaurs, is the only taxon of which a dorsal fin has been reported (Renesto et al., 2020). This taxon also shares a more

similar fineness ratio to that of *Carcharodon carcharias* and *Ophthalmosaurus*, than to that of *Cymbospondylus* and *Besanosaurus*. Moreover, this taxon possesses smaller hindfins in comparison to other Triassic taxa: in regard to the forefin/hindfin ratio, *Mixosaurus* falls closer to *Ophthalmosaurus* than to *Besanosaurus* and *Cymbospondylus*. Given the phylogenetic position of *Mixosaurus* (e.g., Motani, 1999; Jiang et al., 2006; Ji et al., 2016; Bindellini et al., 2021), we can assume that this taxon independently, and convergently to Jurassic taxa, evolved for the first time a combination of adaptations that would have appeared later in Parvipelvia. These should have granted a more efficient swim (in terms of net cost of locomotion) when compared to the swimming style of the coeval and sympatric larger taxa *Besanosaurus* and *Cymbospondylus*. The appearance of such adaptations might have been driven by the small size of *Mixosaurus*. This hypothesis is in accordance with Gutarra et al. (2019), who effectively demonstrated that large body sizes, as well as non-anguilliform swimming modes, markedly reduced the net cost of locomotion in ichthyosaurs. *Mixosaurus,* being small, not reaching the large sizes of Cymbospondylidae and shastasaur-grade ichthyosaurs, and occupying a niche distinct from the two large ichthyosaur taxa from the Besano Formation (Bindellini et al., 2021), could swim more efficiently. Also, in *Mixosaurus* a remarkable (unique among ichthyosaurs) increase in the heights of the vertebral centra in the middle portion of the tail has been suggested to be an adaptation for a high capability for acceleration (Motani, 1998).

None of the three ichthyosaurs known from the Besano Formation have been demonstrated to possess a lunate tail fluke. A heterocercal tail fluke should have granted greater maneuverability, but also would have resulted in a slower swimming speed (e.g., Thomson & Simanek, 1977; Motani, 2002; Croft et al., 2019). According to Gutarra et al. (2019), this was compensated in *Cymbospondylus* and *Besanosaurus* by large sizes, and in *Mixosaurus* by the abovementioned adaptations. In particular, in *Besanosaurus,* maneuverability could have been enhanced by a highly heterocercal tail and relatively long forefins (as suggested in sharks by e.g., Thomson & Simanek, 1977). Also, good maneuverability of the body supports the hunting strategy recently hypothesized for *Besanosaurus*, a longirostrine raptorial snap feeder catching preys by rapid and precise movements of the head and neck (Bindellini et al., 2021), making the animal even more suited to sudden body flexing movements along the sagittal plane.

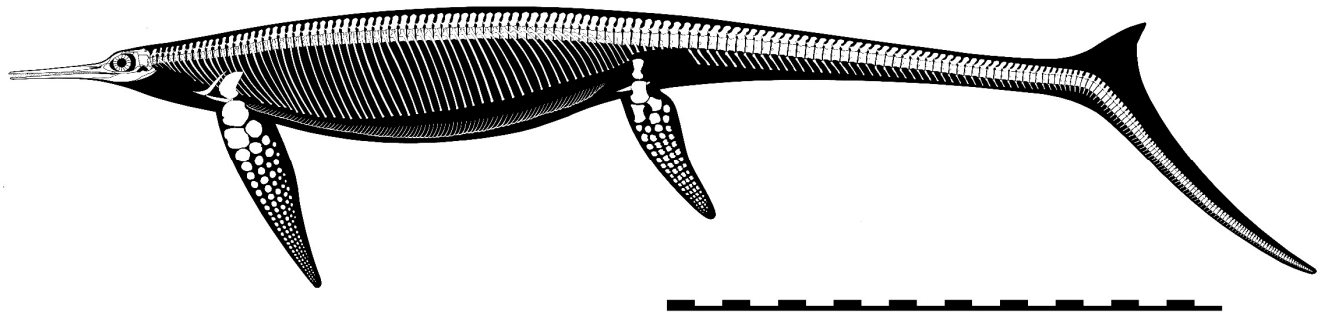

Fig. 7.11 - Full skeletal reconstruction of *Besanosaurus leptorhynchus*. Size and proportions are based on the holotype BES SC 999. The completeness of the specimens available for this study made the usage of other taxa to complete the drawing unnecessary. The skull is based on Bindellini et al. (2021). Scale bar represents 2 meters. Line drawing by Marco Auditore.

7.6.2 Remarks on forefins and hindfins

The pedal phalanges in *Besanosaurus* (BES SC 999) retain a rudimentary, but still distinctive, shaft (Fig. 7.2, Fig. 7.8A and 8C, and Fig. 7.11). This condition is remarkably similar to that seen in mixosaurids (e.g., Repossi, 1902; Brinkmann, 2004), but differs from all other shastasaur-grade ichthyosaurs, in which the pedal phalanges are circular in outline (e.g., Camp, 1980; Yin et al., 2000; Shang & Li, 2013).

Rounded phalanges surrounded by a significant amount of cartilage in the forefins of *Besanosaurus* would likely result in long and flexible appendages, useful for better maneuvering of the anterior half of the body.

On the other hand, hindfins with subrectangular and packed phalanges might have been stiffer and steadier. Similarly, long and robust hindfins have been suggested to enhance maneuverability in *Sveltonectes insolitus* (Fischer, 2011). Since the main purpose of the dorsal fin is to stabilize the animal against rolling and yawing (e.g., Lingham-Soliar, 2004; Sanden & Lauder, 2007), aside from enhancing maneuverability, long forefins and hindfins could compensate for the absence of a dorsal fin in large ichthyosaurs.

Xie et al. (2020) demonstrated that in some whale limbs, secondary ossification centers (SOCs) are reduced or absent, in an opposite condition to land mammals. The authors suggest that the return of cetaceans to an aquatic environment is associated with a gradual reduction in the size of SOCs in some lineages or even a complete loss in some species. In orcas (Xie et al., 2020: fig. 4), phalanges are short and round, separated from each other by a large amount of cartilage, as described and suggested here for the forefins of *Besanosaurus leptorhynchus*. Xie et al. (2020) also confirmed a complete lack of SOC in *Orcinus orca*. Given the similarities in the shape of the phalanges, the condition in *Besanosaurus* could have been similar to orcas, with a complete or almost complete loss of SOCs. On the contrary, we observe long phalanges in basal Ichthyopterygia, and therefore we can speculate that SOCs in these taxa were only reduced and not lost: starting from *Cymbospondylus* or *Besanosaurus* we might have a definitive loss of SOCs in the manual phalanges of the forefins, with cartilages instead of bony epiphyses. Later, in the evolution of Ichthyosauria, phalanges gradually get closer to each other until in Parvipelvia they become polygonal and tightly packed together in both the fore- and hindfins.

7.6.3 Comments on other relevant and diagnostic anatomical traits of *Besanosaurus*

PIMUZ T 1895 shows unambiguous evidence for the presence of a taibend in *Besanosaurus* (Fig. 7.5). The tailbend forms an angle of ~30°. The apical wedge-shaped centra show small and round articular facets for ribs, which are not preserved in the specimen, so they had either been lost prior to fossilization or were present as unossified elements. Similar articular facets are also present in BES SC 999 and are used to infer the location of the tailbend in this specimen. The position of the apical centra is estimated at around centrum 56–60. As a result, the tailbend in the holotype is inferred to be present 155 cm caudally to the sacrum. This would make the tail of *Besanosaurus* highly heterocercal in comparison to other known Triassic ichthyosaurs (Fig. 7.S1).

In the pubis, the obturator foramen opens to the caudal margin in all examined specimens. As reported in previous studies (Dal Sasso & Pinna, 1996; Motani, 1999; McGowan & Motani, 2003), the obturator foramen shows an elongated sub-oval outline, almost entirely enclosed within the pubis in the holotype BES SC 999, and slightly open in PIMUZ T 4376. The condition in PIMUZ T 4847, the largest specimen, is uncertain.

7.6.4 Affinities of *Besanosaurus* with *Pessopteryx* and *Pessosaurus*

Among Triassic ichthyosaurs, *Besanosaurus* shows some similarities with fossils attributed to *Pessopteryx* and *Pessosaurus,* from the Triassic of Svalbard (Wiman, 1910; Maisch & Matzke, 2000:85–86; McGowan & Motani, 2003:127–128, 135–136; Maxwell and Kear, 2013). The humeri referred to *Pessopteryx nisseri* are similar to *Besanosaurus*, although they do not show a notched anterior margin and they appear clearly proximodistally longer than craniocaudally wide (e.g., Wiman 1910: taf. VIII, fig. 1, 2; per obs. 2021.). An exception is PMU 24592b (Wiman 1910: taf. VIII, fig. 3; pers. obs. 2021), which shows a notched anterior margin and proportions more similar to those of BES SC 999.

The femora of *Besanosaurus* are also similar to those of *Pessopteryx nisseri*: the anterodistal process appears in both taxa but seems to be slightly less prominent in femora originally referred to *Pessopteryx* (e.g., PMU 24602, 24603; PMUR 1000–1007; pers. obs. 2021). The proportions of this process vary in other isolated femora from Svalbard, demonstrating a continuous range (e.g., PMU 24602, 24603; PMUR 1000–1007), and possibly indicating some intraspecific variation. PMU 24585 (Wiman, 1910: taf. VII, fig. 3), a femur attributed to *Pessosaurus polaris*, was described as being more similar to PIMUZ T 4376 than to BES SC 999; this is due to the fact that both in PIMUZ T 4376 and PMU 24585 an anterodistal process was considered to be missing (McGowan & Motani, 2003:128). Actually, in both specimens the anterodistal portion is broken and incomplete (pers. obs. 2021) and therefore the resemblance between the two specimens must be considered an artifact: in both cases the facet for the tibia is incomplete and the anterodistal process is almost completely missing; also, the fracture is partly filled by plaster in PIMUZ T 4376 (pers. obs. 2021).
PMU 24584 (PMUR 176 in Wiman, 1910: taf. VII, fig. 2), a specimen consisting of a coracoid, a radius, a humerus, and a podial element attributed to *Pessosaurus polaris*, was noticed as similar to PIMUZ T 4376 by Maisch and Matzke (2000), who considered the specimen as tentatively referable to *Mikadocephalus* cf. *gracilirostris*, a junior synonym of *Besanosaurus leptorhynchus* (Bindellini et al., 2021; McGowan & Motani,2003). The PMU 24584 radius is proximodistally relatively shorter than those of any other *Besanosaurus* specimens examined in this study (craniocaudal/proximodistal length ratio equals 1.6 in PMU 24584; see Table 7.2 for *Besanosaurus*), showing proportions more similar to those of *Shastasaurus osmonti* (Merriam, 1902: pl. 11). Furthermore, the humerus of PMU 24584 is also relatively shorter proximodistally than that of PIMUZ T 4376 and all other specimens of *Besanosaurus* examined (craniocaudal/proximodistal length ratio equals 1.13 in PMU 24584; see Table 7.1 for *Besanosaurus*) and is more similar in proportions to the humerus of *Guanlingsaurus* (Ji et al., 2013: fig. 3).
Another aspect worth of note is that, among the several phalanges attributed to *Pessopteryx* or *Pessosaurus* (e.g., Wiman 1910: taf. VIII; pers. obs. 2021), there were no phalanges with retained shafts. The absence of large phalanges with retained shafts in the Svalbard material indicates the possible absence of *Besanosaurus* from this ichthyosaur fauna.
In conclusion, although the presence of *Besanosaurus* and its possible synonymy with *Pessopteryx* and *Pessosaurus* was previously proposed, in light of the anatomical observations mentioned above, we do not consider *Besanosaurus* as present in the Triassic Svalbard ichthyosaur fauna and do not consider it a possible junior synonym of either of the two taxa (McGowan & Motani, 2003; Maisch & Matzke, 2000; Maisch, 2010).

7.7 Conclusions

In this work we described the postcranial anatomy of *Besanosaurus leptorhynchus* based on four specimens, which to date are the only known attributed to this taxon. Their remarkable completeness, especially of the holotype BES SC 999 and PIMUZ T 4376, allowed the study and description of the osteology of the whole skeleton. This, along with the recent publication of the skull material (Bindellini et al., 2021), fulfill the necessity of an extensive and complete revision of this taxon.
Besanosaurus leptorhynchus possesses a peculiar bauplan that in its proportions fits in between *Cymbospondylus* and shastasaur-grade ichthyosaurs. Vertebral count consists of 61 presacral centra, two sacral vertebrae, and at least 138 caudal vertebrae. The position and the anatomy of the facets for ribs articulation also shows characters in common both with *Cymbospondylus* and shasatasaur-grade ichthyosaurs. The caudal series represents 55% of the whole axial skeleton length. We also found clear

evidence for the presence of a tailbend that forms an angle of ~30° and give proof of the existence of a heterocercal tail, more similar to that of shastasaur-grade ichthyosaurs than to *Cymbospondylus* and mixosaurids. Remarkably, we found that pedal phalanges retain reduced shafts, absent in the rest of shastasaur-grade ichthyosaurs, but more similar to those of *Mixosaurus*. On the contrary forefin phalanges were round as in shastasaur-grade ichthyosaurs; we suggest that rounded phalanges surrounded by a significant amount of cartilage in *Besanosaurus* forefins would likely result in long and flexible fins, useful for better maneuvering of the anterior half of the body. Such adaptation is consistent with the niche and hunting strategy hypothesized for *Besanosaurus*. Furthermore, given the similarities in the morphology of the manual phalanges with some modern cetaceans (e.g., orcas, Xie et al., 2020), we suggest that *Besanosaurus* completely or almost completely lost SOCs in these bones. On the contrary, long phalanges observed in basal Ichthyopterygia suggest that SOCs in these taxa were only reduced and not lost: starting from *Cymbospondylus* or *Besanosaurus* we suspect a definitive loss of SOCs in the forefins manual phalanges, with cartilages instead of bony epiphyses.

To test the swimming capabilities of *Besanosausurus leptorhynchus* we expanded the dataset of Motani et al. (1996) by adding several ichthyosaurian and fish taxa to the original one: these allowed to have a broader representation of their phylogenetic diversity and swimming styles representing the different categories of swim by lateral undulations in which typically ichthyosaurs are subdivided. *Besanosaurus* plots in between anguilliform swimmers, such as *Cymbospondylus*, and shastasaur-grade ichthyosaurs. This result is supported by the anatomy reported in the description and by the phylogenetic position recovered in previous studies for *Besanosaurus.* On the other hand, *Mixosaurus* supposedly independently, and convergently to Jurassic taxa, evolved for the first time a combination of adaptations that would have appeared later in Parvipelvia, such as a more rigid trunk, smaller hindfins, and a dorsal fin. These adaptations should have granted a more efficient (in terms of net cost of locomotion) swim, when compared to the swimming style of the larger Triassic ichthyosaurs, and were likely driven by the peculiar small body sizes of this taxon. Different swimming styles for *Cymbospondylus, Mixosaurus,* and *Besanosaurus* are supported by the suggested niche partitioning of the three taxa dwelling in the Besano basin, as well as by their different anatomy, body proportions, and dimensions.

Eventually, we discuss the similarities of *Besanosaurus* with *Pessopteryx* and *Pessosaurus* concluding that, although the presence of *Besanosaurus* and its possible synonymy with the two taxa were suggested by other authors, in light of the anatomical difference highlighted in the discussion, we do not consider *Besanosaurus* a possible junior synonym of either of the two taxa.

In summary, this manuscript completes the revision of the taxon *Besanosaurus leptorhynchus*, being complimentary to the previous works regarding this ichthyosaur. This work also represents the base for future work focusing on the ontogenetic growth series represented in the six specimens housed in MSNM and PIMUZ and attributed to this taxon, as well as the study of the embryonic material preserved in the maternal cavity od BES SC 999.

7.8 Ackwnoledgements

We thank the volunteers of the former “Gruppo paleontologico di Besano”, who unearthed the holotype of *Besanosaurus leptorhynchus*, and many other exceptional fossils. We also thank D. Affer, F. Fogliazza and L Magnoni (MSNM), and C. Egli (PIMUZ) for preparation of the specimens; M. Auditore for anatomical drawings; L. Forzenigo, C. Bonelli, and G. Terribile (Fondazione IRCCS “Cà Granda” Ospedale Maggiore Policlinico di Milano) for CT analysis of the whole holotype of *B. leptorhynchus*; the Italian Ministry of

Culture and the "Soprintendenza Archeologia, Belle Arti e Paesaggio per le province di Como, Lecco, Monza e Brianza, Pavia, Sondrio e Varese" for permissions. For 3D-scanning the holotype of *Besanosaurus leptorhynchus*, we thank M. Merella and F. Nobile (UniPi). For access to key specimens in museum collections we thank C. Klug (PIMUZ), B. P. Kear (PMU), E. Maxwell (SMNS), R. B. Hauff (Urweltmuseum Hauff, Holzmaden), L. Cheng and X.-H. Chen (WGSC), C. Li and Q. Shang (IVPP), Pat Holroyd (UCMP), Kevin Seymour and Brian Iwama (ROM). We also thank M. Auditore, M. Balini, S. Maganuco, B. P. Kear, and G. Teruzzi, for helpful discussions. This paper is part of a Ph.D. project (G. Bindellini) focusing on the Besano Formation fossil fauna, led by the Università Statale di Milano (M. Balini) in agreement with the Museo di Storia Naturale di Milano (C. Dal Sasso).

7.9 References

Bindellini G, Balini M, Teruzzi G, Dal Sasso C. 2019. Ammonoid and *Daonella* zonation of the Sasso Caldo quarry (Besano Formation, Middle Triassic). In: *Strati 2019, 3rd International Congress on Stratigraphy—ST2.4 Ammonoids in stratigraphy*: Abstract book: 87.

Bindellini G, Wolniewicz AS, Miedema F, Scheyer TM, Dal Sasso C. 2021. Cranial anatomy of *Besanosaurus leptorhynchus* Dal Sasso & Pinna, 1996 (Reptilia: Ichthyosauria) from the Middle Triassic Besano Formation of Monte San Giorgio, Italy/Switzerland: taxonomic and palaeobiological implications. *PeerJ* 9:e11179

Brinkmann W. (2004). Mixosaurier (Reptilia, Ichthyosauria) mit Quetschzähnen aus der Grenzbitumenzone (Mitteltrias) des Monte San Giorgio (Schweiz, Kanton Tessin). *Kommission der Schweizerischen Paläontologischen Abhandlungen*:1-86

Buchholtz EA. 2001. Vertebral osteology and swimming style in living and fossil whales (Order: Cetacea). *Journal of Zoology*, 253(2):175-190.

Callaway JM, Massare JA. 1989. *Shastasaurus altispinus* (Ichthyosauria, Shastasauridae) from the Upper Triassic of the El Antimonio district, northwestern Sonora, Mexico. *Journal of Paleontology* 63(6):930–939.

Camp CL. 1980. Large ichthyosaurs from the Upper Triassic of Nevada. *Paleontographica* 170:139–200.

Chen XH, Cheng L, Sander P. 2007. A new species of *Callawayia* (Reptilia: Ichthyosauria) from the Late Triassic in Guanling, Guizhou. *Geology in China*, 34:974-982.

Crofts SB, Shehata R, Flammang B. 2019. Flexibility of heterocercal tails: what can the functional morphology of shark tails tell us about ichthyosaur swimming?. *Integrative Organismal Biology*, 1(1):obz002.

Dal Sasso C, Pinna G. 1996. *Besanosaurus leptorhynchus* n. gen. n. sp., a new shastasaurid ichthyosaur from the Middle Triassic of Besano (Lombardy, N. Italy). *Paleontologia Lombarda*, Nuova serie, 4:3-23.

Fröbisch NB, Sander PM, Rieppel O. 2006. A new species of *Cymbospondylus* (Diapsida, Ichthyosauria) from the Middle Triassic of Nevada and a re-evaluation of the skull osteology of the genus. *Zoological Journal of the Linnean Society*, 147:515-538.

Gutarra S, Moon BC, Rahman IA, Palmer C, Lautenschlager S, Brimacombe AJ, Benton MJ. 2019. Effects of body plan evolution on the hydrodynamic drag and energy requirements of swimming in ichthyosaurs. *Proceedings of the Royal Society B*, *286*(1898):20182786.

Ji C, Jiang DY, Motani R, Hao WC, Sun ZY, Cai T. 2013. A new juvenile specimen of *Guanlingsaurus* (Ichthyosauria, Shastasauridae) from the Upper Triassic of southwestern China. *Journal of Vertebrate Paleontology*, 33(2):340-348.

Ji C, Jiang DY, Motani R, Rieppel O, Hao WC, Sun ZY. 2016. Phylogeny of the Ichthyopterygia incorporating recent discoveries from South China. Journal of Vertebrate Paleontology, 36:e1025956.

Jiang DY, Schmitz L, Hao WC, Sun YL. 2006. A new mixosaurid ichthyosaur from the Middle Triassic of China. *Journal of Vertebrate Paleontology*, 26(1):60-69.

Lindgren J, Kaddumi HF, Polcyn MJ. 2013. Soft tissue preservation in a fossil marine lizard with a bilobed tail fin. *Nature Communications*, 4(1):1-8.

Lingham-Soliar T. 2005. Dorsal fin in the white shark, *Carcharodon carcharias*: a dynamic stabilizer for fast swimming. *Journal of Morphology*, 263(1): 1-11.

Maisch MW. 2010. Phylogeny, systematics, and origin of the Ichthyosauria. The state of the art. *Palaeodiversity*, 3:151-214.

Maisch MW, Matzke AT. 2000. The Ichthyosauria. *Stuttgarter Beiträge zur Naturkunde Serie B*, 298:1-159.

Maxwell EE, Zammit M, Druckenmiller PS. 2012. Morphology and orientation of the ichthyosaurian femur. *Journal of Vertebrate Paleontology*, 32(5): 1207-1211.

McGowan C. 1992. The ichthyosaurian tail: sharks do not provide an appropriate analogue. *Palaeontology*, 35(2): 555-570.

McGowan C. 1994. A new species of *Shastasaurus* (Reptilia: Ichthyosauria) from the Triassic of British Columbia: the most complete exemplar of the genus. *Journal of Vertebrate Paleontology*, 14:168-179.

McGowan C, Motani R. 2003. Part 8. Ichthyopterygia. In: Sues H-D, ed. *Handbook of Paleoherpetology.* Munchen: Verlag Dr. Friedrich Pfeil, 173 pp.

Merriam JC. 1902. Triassic Ichthyopterygia from California and Nevada. University of California Publications, Bulletin of the Department of Geology 3:63–108.

Merriam JC. 1903. New Ichthyosauria from the Upper Triassic of California. University of California Publications. *Bulletin of the Department of Geology*, 3:249–263.

Merriam JC. 1908. Triassic Ichthyosauria, with special reference to the American forms. *Memoirs of the University of California,* 1:1–196.

Moon BC. 2017. A new phylogeny of ichthyosaurs (Reptilia: Diapsida). *Journal of Systematic Palaeontology*, 17:129-155.

Moon BC, & Kirton AM. 2016. Ichthyosaurs of the British Middle and Upper Jurassic Part 1, Ophthalmosaurus. *Monographs of the Palaeontographical Society*, 170(647):1-84.

Moon BC, Stubbs TL. 2020. Early high rates and disparity in the evolution of ichthyosaurs. *Communications biology*, 3:1-8.

Motani R. 1999. Phylogeny of the Ichthyopterygia. *Journal of Vertebrate Paleontology*, 19:473-496.

Motani R. 2002. Scaling effects in caudal fin propulsion and the speed of ichthyosaurs. *Nature*, 415(6869):309-312.

Motani R. 2005. Evolution of fish-shaped reptiles (Reptilia: Ichthyopterygia) in their physical environments and constraints. *Annual Review of Earth and Planetary Sciences*, 33:395-420.

Motani R. 2008. Combining uniformitarian and historical data to interpret how Earth environment influenced the evolution of Ichthyopterygia. *The Paleontological Society Papers*, 14, 147-164.

Motani R, You H, McGowan C. 1996. Eel-like swimming in the earliest ichthyosaurs. *Nature*, *382*(6589), 347-348.

Motani R, Jiang DY, Tintori A, Rieppel O, Chen GB. 2014. Terrestrial origin of viviparity in Mesozoic marine reptiles indicated by Early Triassic embryonic fossils. *PloS one*, 9(2):e88640.

Motani R, Jiang DY, Tintori A, Ji C, Huang JD. 2017. Pre-versus post-mass extinction divergence of Mesozoic marine reptiles dictated by time-scale dependence of evolutionary rates. *Proceedings of the Royal Society B: Biological Sciences*, 284:20170241.

Motani R, Minoura N, Ando T. 1998. Ichthyosaurian relationships illuminated by new primitive skeletons from Japan. Nature, 393:255-257.

Nicholls EL, Manabe M. 2001. A new genus of ichthyosaur from the Late Triassic Pardonet Formation of British Columbia: bridging the Triassic Jurassic gap. *Canadian Journal of Earth Sciences*, 38(6): 983-1002.

Nicholls EL, Manabe M. 2004. Giant ichthyosaurs of the Triassic. A new species of *Shonisaurus* from the Pardonet Formation (Norian: Late Triassic) of British Columbia. *Journal of Vertebrate Paleontology*, 24:838-849.

Pardo-Pérez JM, Kear BP, Maxwell EE. 2020. Skeletal pathologies track body plan evolution in ichthyosaurs. *Scientific reports*, 10:1-7.

Repossi E. 1902. Il Mixosauro degli strati Triassici di Besano in Lombardia. *Atti della Società italiana di scienze naturali e del Museo civico di storia naturale di Milano*, 41: 361-372.

Renesto S, Dal Sasso C, Fogliazza F, Ragni C. 2020. New findings reveal that the Middle Triassic ichthyosaur *Mixosaurus cornalianus* is the oldest amniote with a dorsal fin. *Acta Paleontologica Polonica*, 65: 511-522.

Sander PM. 1989. The large ichthyosaur *Cymbospondylus buchseri*, sp. nov., from the Middle Triassic of Monte San Giorgio (Switzerland), with a survey of the genus in Europe. *Journal of Vertebrate Paleontology*, 9:163-173.

Sander PM. 1997. The paleobiogeography of *Shastasaurus*. In: Callaway JM, Nicholls EL, eds. *Ancient marine reptiles*. Academic Press, pp. 17-43.

Sander PM. 2000. Ichthyosauria: their diversity, distribution, and phylogeny. *Paläontologische Zeitschrift*, 74:1-35.

Standen EM, Lauder GV. 2007. Hydrodynamic function of dorsal and anal fins in brook trout (Salvelinus fontinalis). *Journal of Experimental Biology*, 210(2):325-339.

Sander PM, ChenX, Cheng L, Wang X. 2011. Short-snouted toothless ichthyosaur from China suggests Late Triassic diversification of suction feeding ichthyosaurs. *PLoS One*, 6:e19480.

Shang QH, Li C. 2009. On the occurrence of the ichthyosaur *Shastasaurus* in the Guanling biota (Late Triassic), Guizhou, China. *Vertebrata PalAsiatica*, 47:178-193.

Shang QH, Li C. 2013. The sexual dimorphism of *Shastasaurus tangae* (Reptilia: Ichthyosauria) from the Triassic Guanling Biota, China. *Vertebrata PalAsiatica*, 10: 253-264.

Slijper EJ. 1936. Die Cetaceen. Vergleichend-anatomisch und systematisch. *Capita zoologica*, 7.

Thomson KS, Simanek DE. 1977. Body form and locomotion in sharks. *American Zoologist*, 17(2):343-354.

Wiman C. 1910. Ichthyosaurier aus der Trias Spitzbergens. *Bulletin of the Geological Institution of the University of Upsala*, 10:124-148.

Wiman C. 1929. Eine neue Reptilien-Ordnung aus der Trias Spitzbergens. *Bulletin of the geological Institution of the University of Upsala*, 22: 183-196.

Xie M, Gol'din P, Herdina AN, Estefa J, Medvedeva EV, Li L, Newton PT, Kotova S, Shavkuta B, Saxena A, Shumate LT, Metscher BD, Großschmidt K, Nishimori S, Akovantseva A, Usanova AP, Kurenkova AD, Kumar A, Arregui IL, Tafforeau P, Fried K, Carlström M, Simon A, Gasser C, Kronenberg HM, Bastepe M, Cooper KL, Timashev P, Sanchez S, Adameyko I, Eriksson A, Chagin AS. 2020. Secondary ossification center induces and protects growth plate structure. *Elife*, 9:e55212.

Yin G, Zhou X, Cao Z, Yu Y, Luo Y. 2000. A preliminary study on the Early Late Triassic marine reptiles from Guanling, Guizhou, China. *Geology-Geochemistry*, 28(3): 1-23.

7.10 Supplementary materials

Table 7.S1 – Measurements of ichthyosaurs and fishes based on silhouettes of Fig. S1 and used to draw Fig. 7.10.

Ref	Taxon	Total length	Max body height	Tail heigth	Tail length	Fineness ratio	Tail H/L ratio
	Salmon	85	19	13.1	13.4	0.27	0.98
	Cod	129.4	29.6	19.2	21.2	0.27	0.91
	Mackerel	25	4.7	5.7	3.4	0.22	1.68
	Atlantic bluefin Tuna	231.5	55	73.5	25.5	0.27	2.88
	White shark	396.4	70	108	80	0.22	1.35
Cooper et al 2020	*Otodus megalodon*	1605	325	454	323	0.25	1.41
White et al 2019	*Akheilos suwartanai*	53.7	4.8	4.4	11.7	0.11	0.38
Motani et al 2014	*Chaohusaurus*	96.2	11.5	7.8	31	0.18	0.25
Motani et al 1998	*Utatsusaurus*	260	31	26.4	65.3	0.16	0.40
Jiang et al 2008, this paper	*Xinminosaurus*	225	15	27.2	27	0.08	1.01
McGowan and Motani 2003	*Cymbospondylus*	920	90	85	218	0.13	0.39
Renesto et al 2020	*Mixosaurus*	193.3	31.8	21.8	47.2	0.22	0.46
This paper	*Besanosaurus*	471	49	80	98	0.13	0.82
Motani 2008	*Gualingsaurus*	510	65	75	118	0.17	0.64
Shang & Li, 2009	*Guizhouichthyosaurus*	549.8	69.5	84.5	99.8	0.15	0.85
Camp 1980	*Shonisaurus*	1473	230	150	252	0.19	0.60
McGowan and Motani 2003	*Californosaurus*	251	41.5	48	36	0.19	1.33
McGowan and Motani 2003	*Temnodontosaurus*	676	105	165	72	0.17	2.29
McGowan and Motani 2003	*Eurhinosaurus*	556	60	150	88	0.13	1.70
Maxwell & Cortés	*Hauffiopteryx*	173.9	23.6	38.5	23.2	0.16	1.66
Motani et al 2014	*Stenopterygius*	230	42	54.3	34.7	0.22	1.56
Motani et al 2014	*Stenopterygius* (newborn)	63	9.5	8	9	0.18	0.89
McGowan and Motani 2003	*Ophthalmosaurus*	440.5	94	142.1	53.5	0.24	2.66

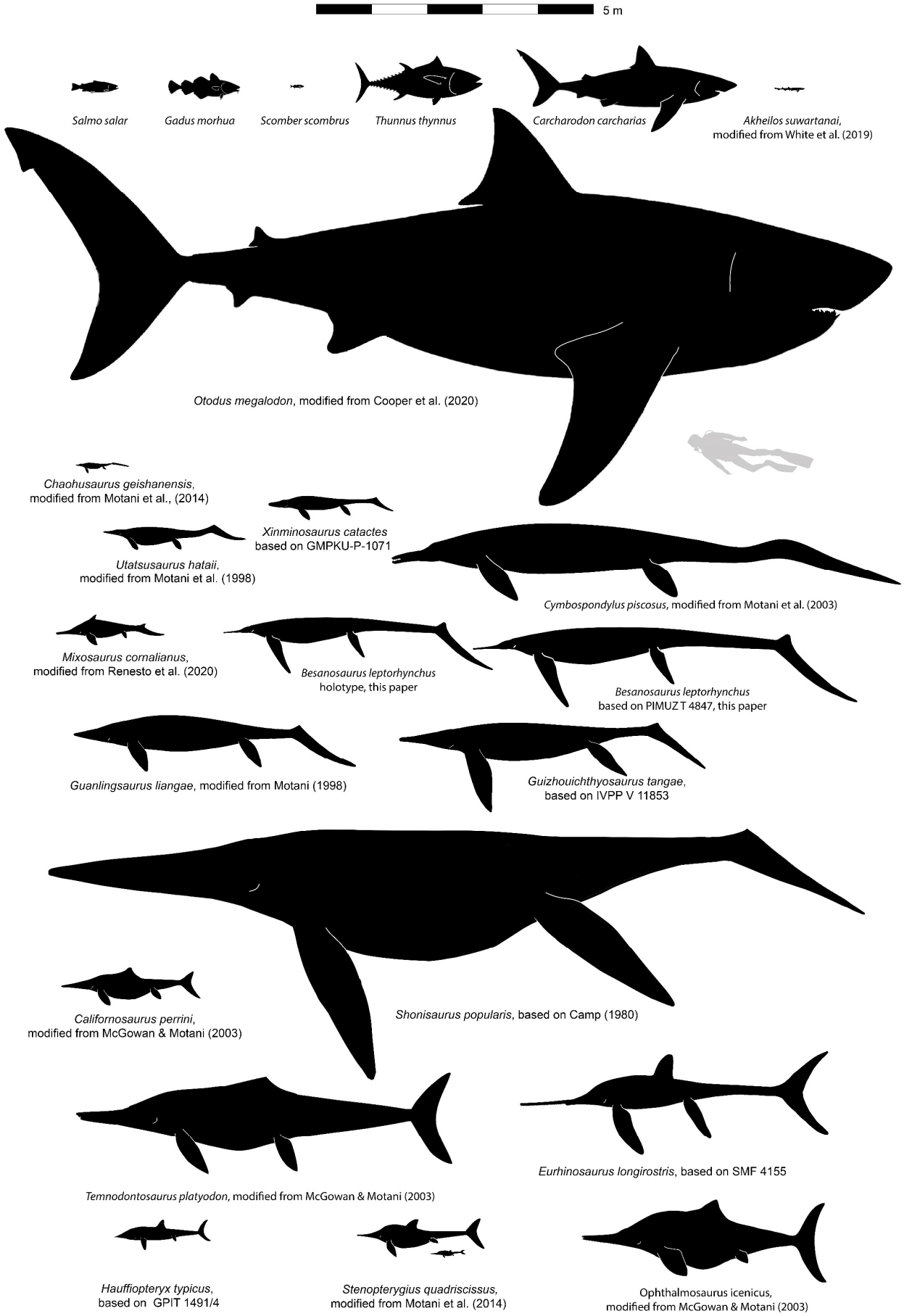

Figure 7.S1 - Ichthyosaurs and fishes silhouettes used to infer measurements in Fig. 7.10.

Chapter 8
Late-stage embryonic material in the holotype of *Besanosaurus leptorhynchus*

*Draft of a manuscript to be submittted to Frontiers in Earth Science
Feiko Miedema[1], Gabriele Bindellini[2], Andrzej S. Wolniewicz[3, 4], Erin E. Maxwell[1], Cristiano Dal Sasso[5]
[1] Staatliches Museum für Naturkunde Stuttgart, Stuttgart, Germany
[2] Dipartimento di Scienze della Terra "Ardito Desio", Università degli Studi di Milano, Milano, Italy
[3] School of Resources and Environmental Engineering, Hefei University of Technology, Anhui, China
[4] Institute of Paleobiology, Polish Academy of Sciences, Warsaw, Poland
[5] Sezione di Paleontologia dei Vertebrati, Museo di Storia Naturale di Milano, Milano, Italy
Switzerland

8.1 Abstract

In this work we report for the first time a detailed description and qualitative comparisons of the embryonic material preserved in the body cavity of the type specimen of *Besanosaurus leptorhynchus,* BES SC 999. Since that original publication of this taxon, the specimen has gone through further preparation and now the embryonic elements have been fully revealed, giving the chance to perform this study. The specimen has been observed making use of stereomicroscopy and computed tomography. The embryonic material is preserved inside the maternal body cavity, it results disarticulated, although relative *in vivo* positioning can be considered intact. The cranial material is preserved associated far anterior, close to the maternal pectoral girdle. The material in the body cavity of BES SC 999 has been unambiguously deemed embryonic on the basis of strong evidence: the embryo lays in an expected antero-posterior sequence; embryonic bone tissue is unaltered by any digestive processes; clear ossification differences between elements, consistent with other ichthyosaur embryos, have been observed; vertebral centra possess a small notochord pit. The material is also attributed to *Besanosaurus leptorhynchus* based on a combination of diagnostic characters, i.e., the presence of a triangular process of the quadrate, a large preglenoid process, a quadrangular femur. At the end of the manuscript assumptions are made about the placement of the uterus in *Besanosaurus*, parturition orientation preference, and developmental stage of *Besanosaurus leptorhynchus* embryo.

8.2 Introduction

Viviparity is the main reproductive mode for ichthyosauriforms. Viviparity is the main reproductive mode for ichthyosauriforms. This is evident by the many gravid females found in taxa across their phylogeny (Camp, 1980; Böttcher, 1990; Deeming et al., 1995; Brinkmann, 1996; Maxwell & Caldwell, 2003; Lomax & Massare, 2012; Kear & Zammit, 2013; Motani et al., 2014; Lomax & Sachs, 2017; Klein et al., 2020). *Besanosaurus leptorhynchus* is an early merriamosaurian ichthyosaur from the Middle Triassic of the Southern Alps (Dal

Sasso & Pinna, 1996). All specimens are from the Besano Formation, found in localities on both sides of the Swiss-Italian border (Bindellini et al., 2021). Recently, it was proposed that the monospecific genus *Mikadocephalus* should be considered a junior synonym of *Besanosaurus* on the basis of their similar cranial morphology (Maisch & Matzke, 1997; Bindellini et al., 2021). In the original description of the holotype of *Besanosaurus leptorhynchus* (BES SC 999) the authors noted clusters of embryonic elements on the basis of radiographs (Dal Sasso & Pinna, 1996: fig. 23). Since that original publication, the specimen has gone through further preparation and now the embryonic elements have been fully revealed (Miedema et al., 2021). Here we describe in detail and qualitatively compare the embryonic material with the maternal specimen. We further compare it to other known ichthyosaur prenatal development.

8.3 Material and Methods

We qualitatively studied the embryonic material preserved in the body cavity of the type specimen of *Besanosaurus leptorhynchus* BES SC 999. The fossil was unearthed in 1993 from the "Sasso Caldo" site near Besano (Varese, Italy), during systematic excavations led by the Museo di Storia Naturale di Milano (MSNM) in the Besano Formation (also known as Grenzbitumenzone). To observe any anatomical detail of the embryonic bones we used a Leica MZ9-5 stereomicroscope equipped with a plan 1.0x lens, 10/20x oculars, and a 0.63 to 6.0 zoom. A camera was mounted on top of the stereomicroscope for close-up photos.
X-ray computed tomography (CT) was performed on the whole skeleton of the holotype of *B. leptorhynchus* with a Siemens Somatom Definition Dual Source CT Scanner at the Radiology Department of the Fondazione IRCCS "Cà Granda" Ospedale Maggiore Policlinico di Milano. Detailed scans have been recorded for those slabs including the embryonic material. Analysis and post-processing were performed with RadiAnt, 3DimViewer, and Synedra View Personal. Multiplanar reconstructions (MPR) and volume rendering reconstructions (VR) allowed to inspect the bones hidden under other ones within the matrix, otherwise impossible to study without damaging the fossil.

8.4 Description

The embryonic material associated with BES SC 999 is mostly preserved inside the maternal body cavity on slab n. 30, with a few elements present on slabs n. 26 and 31 (see Dal Sasso & Pinna, 1996: fig. 5). All of the cranial material is preserved associated far anterior, close to the maternal pectoral girdle (Fig. 8.1). Embryonic pelvic girdle, posterior flipper, and haemal arches are visible associated more caudally (Fig. 8.1). Preflexural/precaudal vertebrae are scattered in between the maternal ribs and gastralia (Fig. 8.1).

8.4.1 Skull

Dermatocranium

Nasal. There is a clear ?right nasal bone situated between the angular and pterygoid anteriorly in the maternal body cavity (Fig. 8.1). The nasal is preserved in dorsomedial view, but is strongly folded along the midline, thereby obstructing any internal view (Fig. 8.2B). It is a slightly sigmoidally-shaped element, thickened in the midsection and heavily tapering rostrally and caudally. Dorsocaudally there is a ridged area, likely the developing frontal facet. The lateral flange differs from the medial flange in having a distinct ventral indentation (Fig. 8.2B'). This is the dorsal border and thereby represents the nasal contribution to the external naris. The nasal displays a medial depression on its lateral flange caudal to the external naris (Fig. 8.2B'). It is unclear if this depression has a function, but it is possibly homologous to the *excavatio internasalis* in Parvipelvia (Maisch & Matzke, 2000).

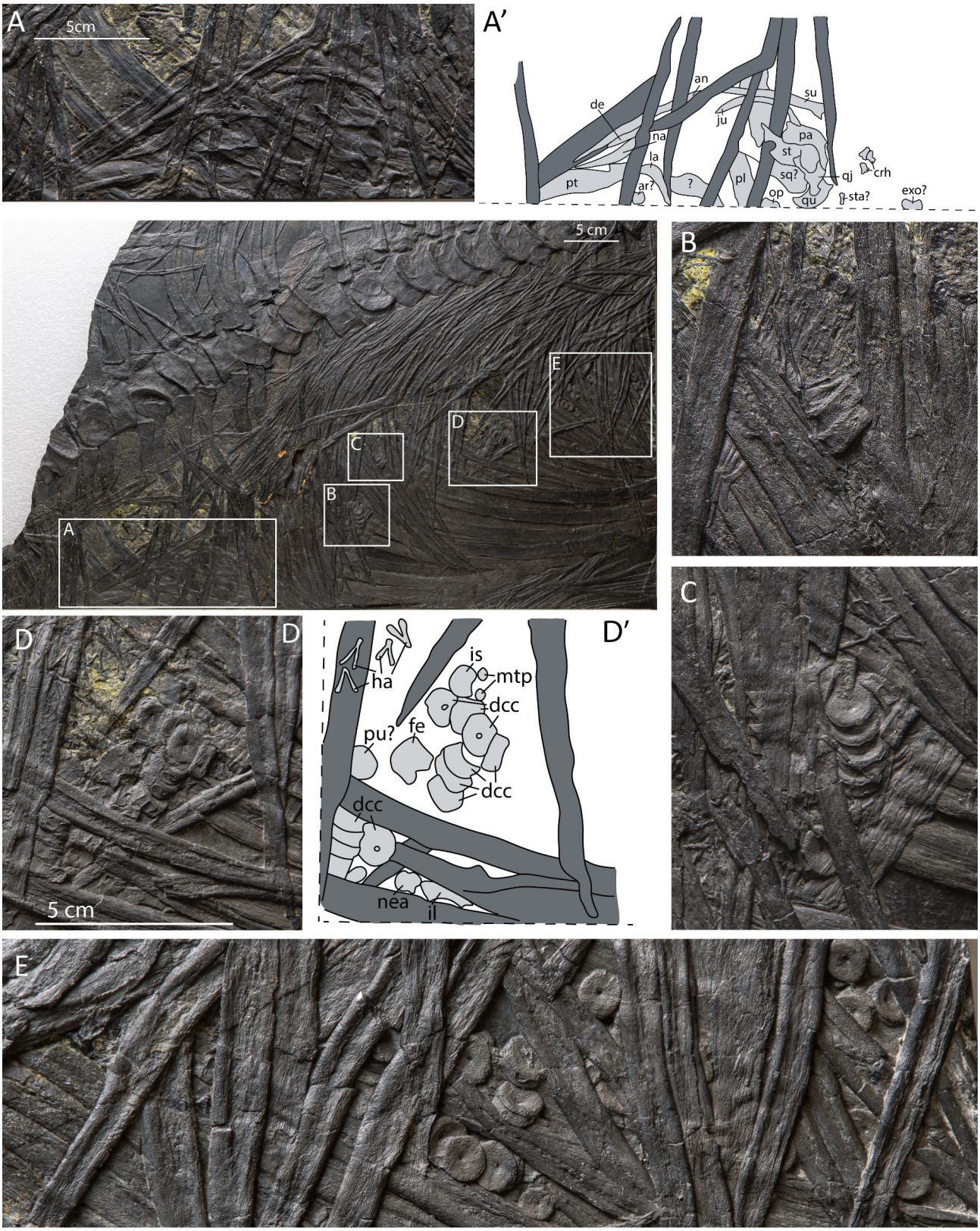

Fig. 8.1 - Overview and selected areas of the embryonic material in the body cavity of BES SC 999 *Besanosaurus leptorhynchus* preserved on slab 30. Zoomed-in areas correspond to the same letter in the overview photo, with their interpretation denoted by an apostrophe. A, cranium; B, cervical or anterior dorsal vertebrae; C, ?dorsal vertebrae; D, posterior dorsal or anterior caudal vertebrae, caudal ribs, podials; E, sacral area. Dark gray denotes maternal ribs or gastralia, light gray embryonic bones. Abbreviations: an, angular; ar, articular; crh, cervical rib-head; dcc, dorsal or caudal centrum; de, dentary; exo, exoccipital; fe, femur; ha, haemal arch; il, illium; is, ischium; ju, jugal; la, lacrimal; mtp, (meta)tarsal or phalanx; na, nasal; nea, neural arch; op, opisthotic; pa, parietal; pl, palatine; pt, pterygoid; pu, pubis; qj, quadratojugal; qu, quadrate; sq, squamosal; st, supratemporal; sta, stapes; su, surangular.

Lacrimal. In the area containing the nasal, articular, and pterygoid lies a left lacrimal in medial view (Fig. 8.1). The dorsal margin is covered by a maternal gastralium. The lacrimal is well ossified and its jugal facet already well-defined (Fig. 8.2D). The medial depression is divided medially. Ossification lines indicate that the origin of ossification lies centric in the medial depression.

Jugal. A left jugal is observed in between the parietal and surangular (Fig. 8.1). It is still covered by other material in the midsection, but the folding presents the outline of the bone (Fig. 8.2A). The element is preserved in lateral view. The jugal is L-shaped with a gentle curve, whereby the dorsal ramus gradually continues into the horizontal ramus. The dorsal ramus projects caudodorsally and already displays a distinct postorbital/quadratojugal facet. The horizontal ramus displays a distinct facet for the maxilla as seen by the heavily striated texture. The horizontal ramus does not seem to taper rostrally, although very likely the tip of the jugal is still hidden below a rib and/or slightly broken (Fig. 8.2A).

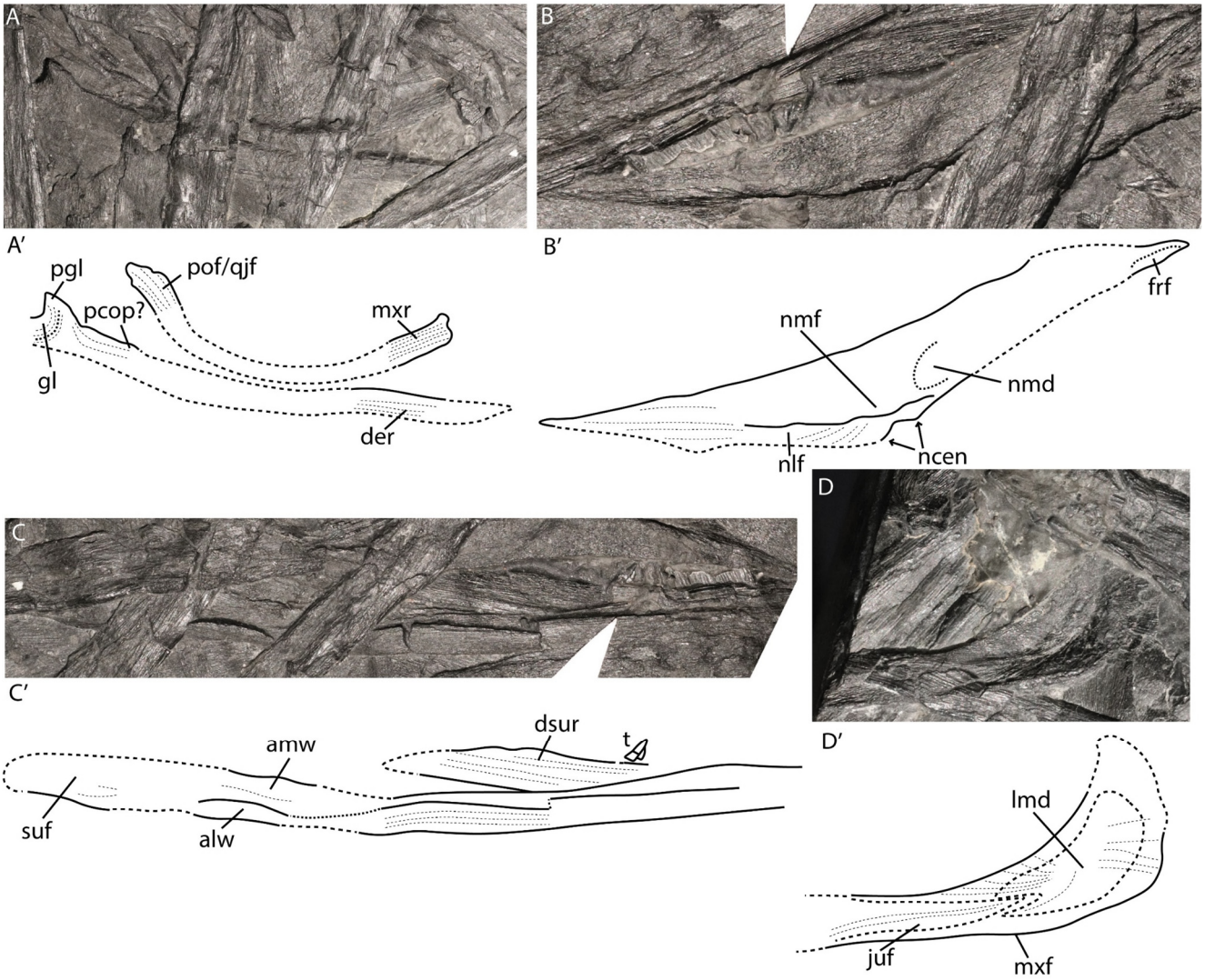

Fig. 8.2 - Identifiable embryonic dermatocranial elements of the rostrum and lower jaw. Interpretative drawings are denoted by an apostrophe with their corresponding letter. A, surangular and jugal; B, nasal; C, angular and dentary; D; lacrimal. Abbreviations: alw, angular lateral wall; amw, angular medial wall; der, dentary ramus; dsur, dentary surangular ramus; frf, frontal facet; gl, glenoid; juf, jugal facet; lmd, lacrimal medial depression; mxf, maxilla flange; mxr, maxilla ramus; ncen, nasal contribution to the external naris; nlf, nasal lateral flange; nmd, nasal mediodorsal depression; nmf, nasal medial flange; pcop, paracoronoid process; pgl, preglenoid process; pof/qjf, postorbital/quadratojugal facet; suf, surangular facet; t, tooth.

Pterygoid. A right pterygoid can be partially observed in dorsal view as the anterior-most embryonic cranial element (Fig. 8.1). The rostral end of the palatal ramus and the caudolateral end of the quadrate ramus are partially covered (Fig. 8.3A). The pterygoid is well-ossified. The palatal ramus contains a rostrocaudally oriented groove or furrow exposed dorsomedially. This may be the location of fusion of two earlier palatal prongs, as seen in *Stenopterygius* stage 3 (Miedema and Maxwell, 2022). Medially the pterygoid displays a surface demarcated by a thickening. This is possibly the parasphenoid facet. The quadrate ramus is fairly quadrangular. It is unsure if the caudoolaterally directed flange is developed.

Palatine. We tentatively identify a tooth-bearing left palatine in ventral view, situated caudally to the pterygoid in the maternal body cavity (Fig. 8.1). We think it is not a rostral or mandibular tooth-bearing element as the area would be too wide for one of those elements taphonomically flapped open in ventral view. Likewise, there is no indication of a groove or tooth row. The element is well-ossified (Fig. 8.3B). Striations indicate a central origin of ossification. It contains two teeth situated laterally on the ventral surface (Fig. 8.3B-B'). In between the two teeth there is a bulge, rostrally to the teeth lies a gap. This gap does not seem to be diagenetic and could therefore be a tooth-socket remnant. There is a small indentation laterally, which is likely the caudal edge of the internal naris.

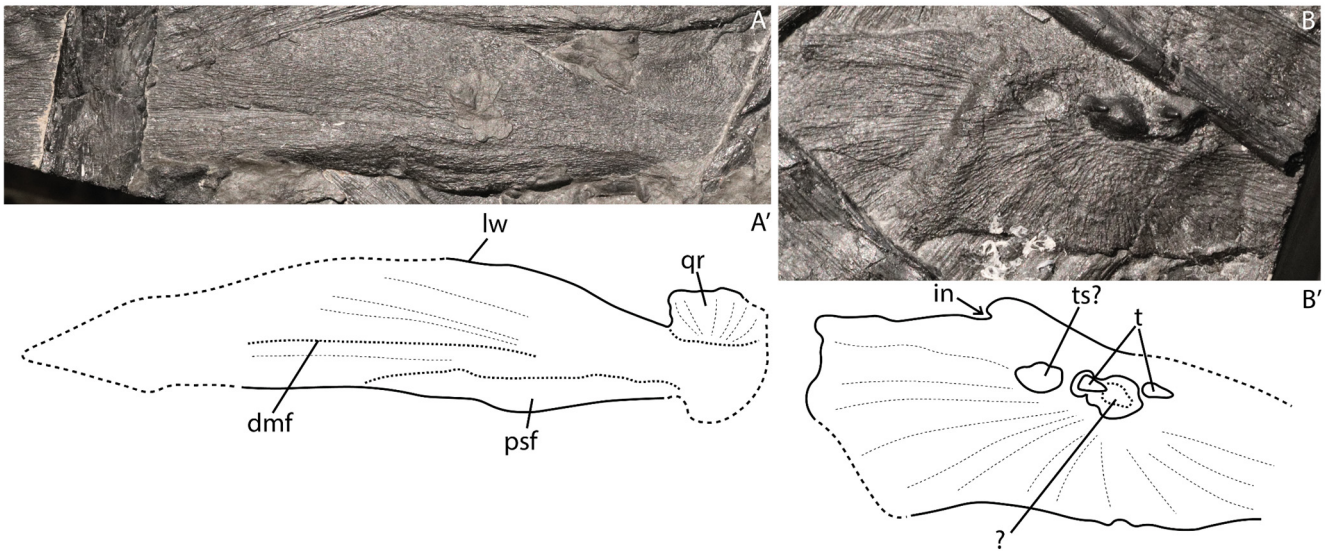

Fig. 8.3 - Identifiable embryonic dermatocranial elements of the palate. A, pterygoid; B, palatine. Interpretative drawings are denoted by an apostrophe with their corresponding letter. Abbreviations: dmf, dorsomedial furrow; in, internal naris; lw, lateral wing; psf, parasphenoid facet; qr, quadrate ramus; t, tooth; ts, tooth socket.

Quadratojugal. An embryonic ?right quadratojugal is present between the left quadrate and right supratemporal (Fig. 8.1). The quadratojugal is well-ossified and has well-defined medial and lateral edges (Fig. 8.4B-B'). The dorsal flange is partially covered by the overlying supratemporal. The bone process containing the quadrate facet is slightly offset caudally. Striations indicate an ossification center near the quadrate facet.

Supratemporal. A right supratemporal can be observed in between the embryonic quadratojugal and parietal (Fig. 8.1). The supratemporal is well-ossified. Striations indicate an ossification center centrally on the lateral flange (Fig. 8.4). The supratemporal is heavily mediolaterally compressed. The medial flange displays the quadrate fact and the anterolateral flange contains a well demarcated facet for the postfrontal.

Parietal. An embryonic right parietal is exposed in ventral view between the supratemporal and jugal (Fig. 8.1). The parietal is overall well-ossified, although the supratemporal ramus seems to be better defined than the area surrounding the parietal foramen. Likewise, the occipital ramus is present, but less well-ossified than the rest of the parietal body (Fig. 8.4C-C'). There is a clear medial depression where the dorsal part of the optic lobe is housed. The parietal foramen is caudally demarcated by a medially directed process and rostrally by the medially turning edge of the medial side of the parietal. The supratemporal ramus is quite long and contains a well-defined supratemporal facet. Striations indicate an ossification center directly caudolaterally to the optic lobe indentation.

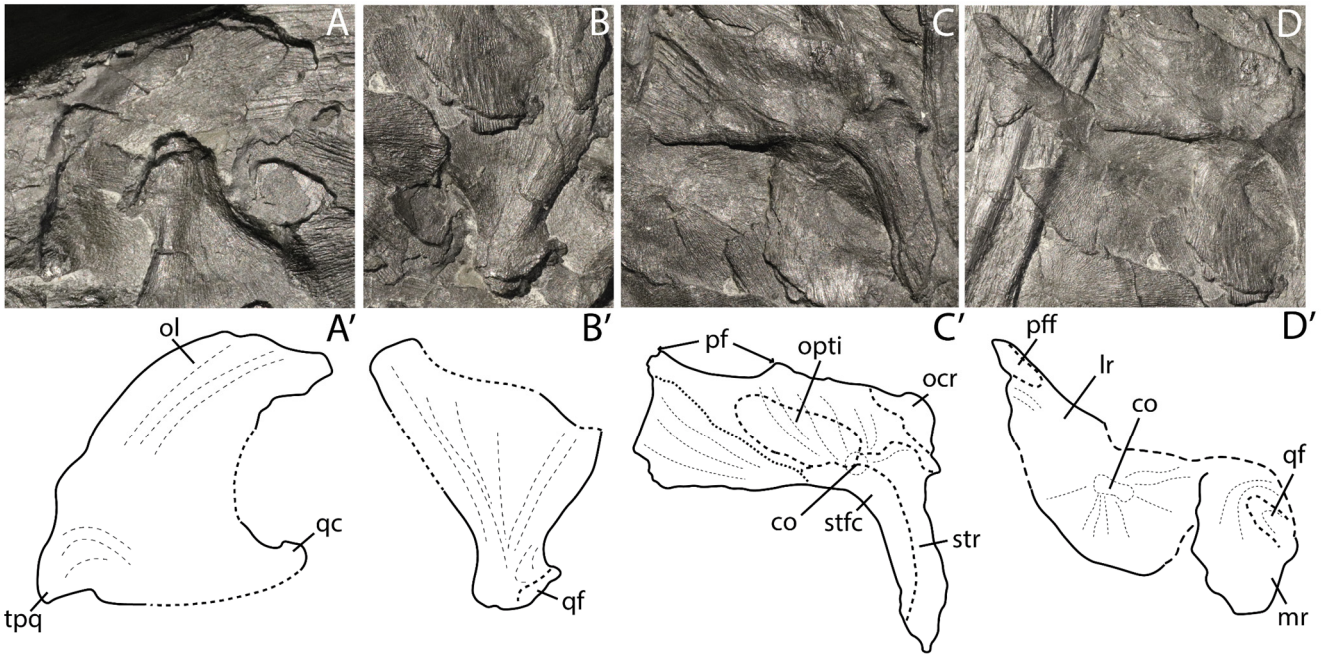

Fig. 8.4 - Identifiable embryonic dermatocranial elements of the cheek and skull roof, and the quadrate. A, quadrate; B, quadratojugal; C, parietal; D, supratemporal. Interpretative drawings are denoted by an apostrophe with their corresponding letter. Abbreviations: co, center of ossification; lr, lateral ramus; mr, medial ramus; ocr, occipital ramus; ol, occipital lamella; opti, optic lobe indentation; pf, parietal foramen; pff, postfrontal facet; qc, quadrate condyle; qf, quadrate facet; stfc, supratemporal facet; str, supratemporal ramus; tpq, triangular process of the quadrate.

Lower jaw. Exposed embryonic lower jaw elements are the right surangular, angular, and dentary. They lie in close association anterior on the block (Fig. 8.1). All dermatocranial lower jaw elements are well-ossified (Fig. 8.2C-C'). Striations on them indicate general growth in an rostrocaudal direction, but ossification centers are undiscernible. Only the caudal (surangular) ramus of the dentary is visible, as well as two disarticulated teeth. The angular displays well-formed lateral and medial walls which enclose a very elongated surangular facet The surangular is largely covered by other elements, but the glenoid area is exposed in medial view. The preglenoid process is already prominent. The paracoronoid process is still small or absent at this stage. The glenoid area is characterized by a more roughened, folded surface, indicating that the area is less ossified than the rest of the element. Centric striations indicate a differing ossification direction or center than the rest of the element (Fig. 8.2C).

Splanchnocranium

Quadrate. A left quadrate is preserved in medial view, partially overlapped by the embryonic quadratojugal (Fig. 8.1). The quadrate displays a degree of ossification similar to the other dermatocranial elements (Fig.

8.4A-A'). The occipital lamella curves caudally. The rostroventral triangular process is already well-developed and slightly offset from the rest of the occipital lamella. Ossification striations indicate dorsoventral growth for most of the occipital lamella except around the triangular process (Fig. 8.4). The condyle seems to be observable in this stage, although it is mostly hidden.

Stapes. A stapes is observed in close association to the quadrate and quadratojugal (Fig. 8.1). It is relatively well ossified, but the rugose surface texture indicates that it is less ossified than the dermatocranial elements or quadrate (Fig. 8.5D-D'). The stapes is very slender, only thickening medially at its head. The medial head, containing the basioccipital facet, is deflected in a ?ventral direction).

Articular. We tentatively identify a right articular situated near the lacrimal and pterygoid (Fig. 8.1). The roughened surface texture indicates that this element is likely a splanchno- or chondrocranial element (Fig. 8.5A-A'). The prearticular facet as well as a small retro-articular process seem to be well developed already. On the contrary, the rostral glenoid contribution has many indentations, indicating that portion is still developing and is less ossified than the caudal end).

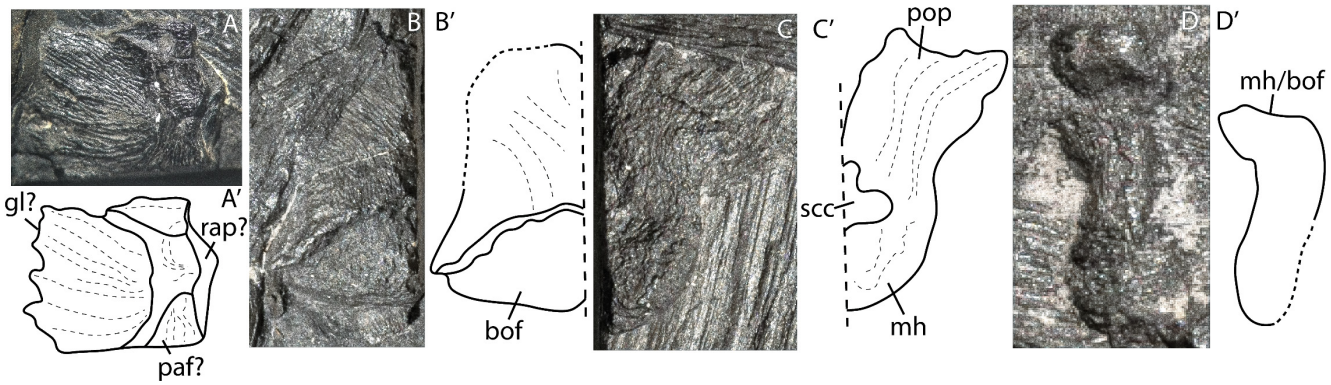

Fig. 8.5 - Tentatively identifiable embryonic chondrocranial and splanchnocranial elements. A, articular; B, exoccipital; C, opisthotic; D, stapes. Interpretative drawings denoted by an apostrophe with their corresponding letter. Abbreviations: bof, basioccipital facet; gl, glenoid; mh, medial head; paf, prearticular facet; pop, paroccipital process; rap, retro-articular process; scc, semicircular canal indentations.

Chondrocranium

Exoccipital. We identify an exoccipital, situated caudal to the other cranial elements, with a reasonable degree of confidence (Fig. 8.1). The rough folded surface texture indicates a splanchno- or chondrocranial affinity (Fig. 8.5B-B'). The exoccipital consists of a dorsoventrally projected column and a wide foot. The surface of the foot, containing the basioccipital facet, is better ossified than the surface of the column. Unfortunately, the lateral or medial side is lost. This could explain the absence of a hypoglossal foramen.

Opisthotic. An embryonic opisthotic is observed anterior to the cluster of embryonic elements pertaining to the cheek and skull roof area (Fig. 8.1). The opisthotic displays the same roughened, folded texture as the stapes and the exoccipital (Fig. 8.5C-C'). The paroccipital process is already apparent and it is deflected slightly dorsolaterally. The medial head is not well-defined, but small indentations for the semicircular canals are already visible.

8.4.2 Appendicular skeleton

Pectoral girdle

There is a quadrangular to round element preserved on block 31 which is mostly covered by maternal rib. This element is likely a coracoid or a scapula, given the shape and position in the maternal body cavity (ventral-posteroventral to the cranial area). The element is well ossified. Striations indicate a central ossification center (Fig. 8.6).

Pelvic girdle

The embryonic pelvic girdle is represented by at least an ilium and an ischium, and possibly a pubis. All the elements lie relatively close to each other posterior in the maternal body cavity (Fig. 8.1). The ischium is well ossified displaying a quadrangular to rounded shape with a concave lunate posterior margin (Fig. 8.6B-B'). The overall ossification is high except for the anterior (pubic) margin and the acetabulum contribution. The ilium is anteriorly partially hidden by a maternal rib. It is curved on the lateral and medial sides. Overall ossification is high, this is also the case for its acetabular contribution (Fig. 8.6A-A'). We tentatively identify a pubis in close proximity to the femur (Fig. 8.6C-C'). It is a round element and overall its ossification is similar to the ischium. The area which holds the obturator foramen is unfortunately hidden.

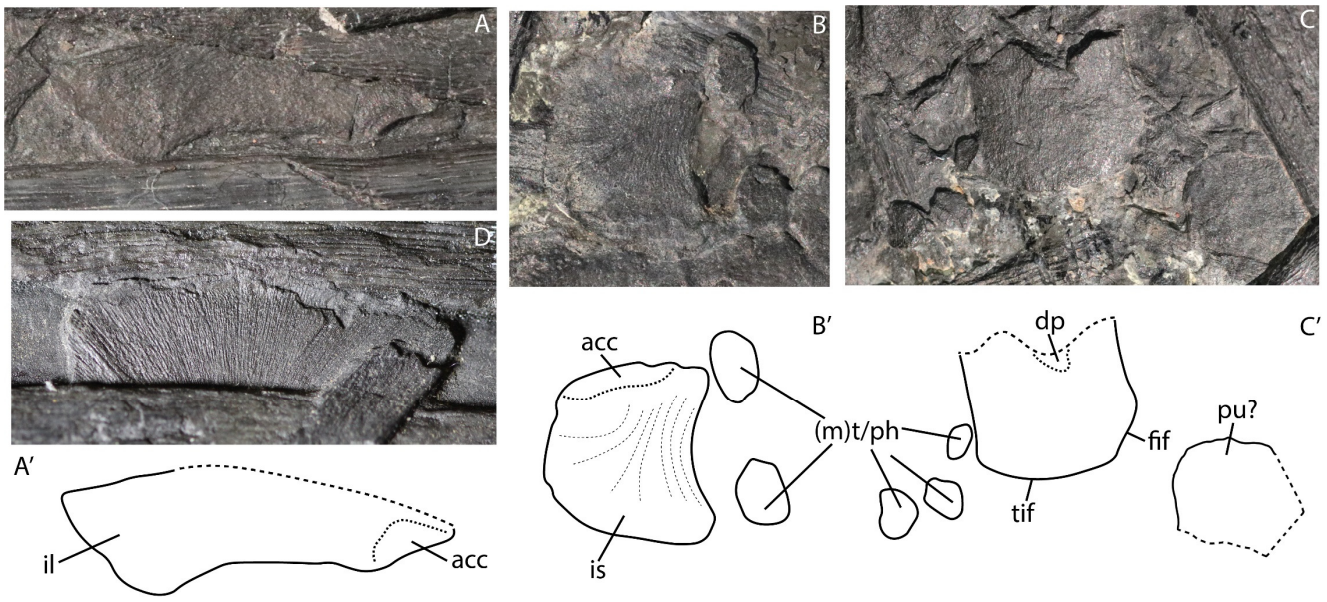

Fig. 8.6 - Identifiable embryonic postcranial appendicular elements. **A**, illium; **B**, ischium and podials; **C**, femur, ?pubis and podials; **D**, pectoral element, ?coracoid Interpretative drawings denoted by an apostrophe with their corresponding letter. **Abbreviations**: **acc**, acetabulum contribution; **dp**, dorsal process; **fif**, fibula facet; **il**, illium; **is**, ischium; **(m)t/ph**, (meta)tarsal or phalanx; **pu**, pubis; **tif**, tibia facet.

Femur and podials

A partial femur is positioned in close proximity to the pelvic girdle elements (Fig. 8.1). The element is quadrangular in shape and well-ossified. The dorsal margin of the femur is broken; the facets for tibia and fibula are already weakly apparent (Fig. 8.6C-C'). A small ?dorsal process is visible at the dorsal margin. Zeugo- and autopodial elements are present in the vicinity of the ischium and the femur. They are slightly less ossified than the femur and pelvic elements. None of these elements are identifiable to position in the flipper.

8.4.3 Axial skeleton

Vertebrae

The embryonic axial skeleton is mostly represented by many associated and some articulated vertebral centra, and neural arches. Most centra are preflexural, but posteriorly in the maternal body cavity posterior caudal vertebrae are also preserved (Fig. 8.1, Fig. 8.7). Most centra retain a small open notochord pit, which is relatively larger in the posterior caudal centra (Fig. 8.7D, F). Rib facets (diapophyses), ventral keels, and neural canals are already apparent on the preflexural centra (Fig. 8.7C, F). Neural arches are rare, but likewise present. Their surface texture indicates that they are less ossified than the centra. Nevertheless, most cervical (Fig. 8.7A), and one caudal neural arch (Fig. 8.7C-C') display pre- and postzygapohyses.

Ribs

Complete embryonic ribs are absent, but two groups of well ossified and packed rib shafts are present (Fig. 8.8). Also, several rib heads of cervical or anterior dorsal centra are apparent just posterior to the cranial area (Fig. 8.1). The rib heads display two distinct bulges containing facets, the capitulum and tuberculum. The capitulum and tuberculum are connected by a sheet of bone (Fig. 8.7A-A').

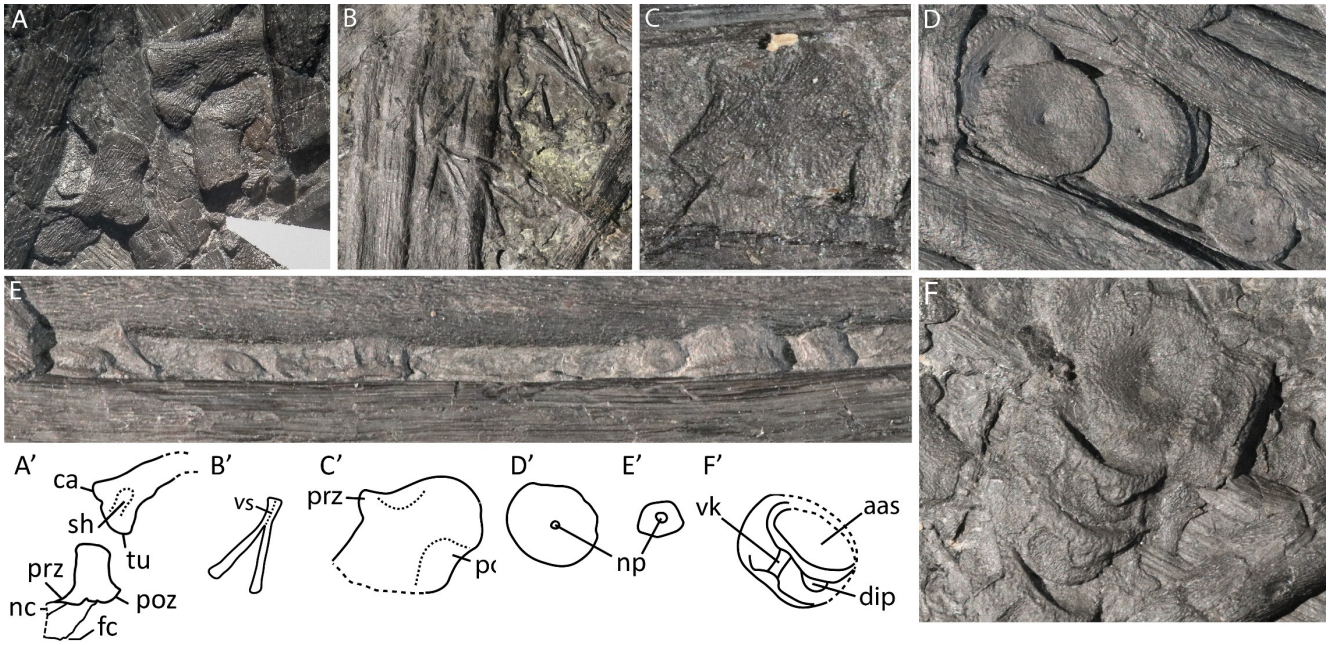

Fig. 8.7 - Identifiable embryonic postcranial axial elements . **A**, cervical rib head and neural spine; **B**, haemal arches; **C**, caudal neural arch; **D**, dorsal vertebral centra; **E**, posterior caudal centra; **F**; posterior dorsal or anterior caudal centra. Interpretative drawings denoted by an apostrophe with their corresponding letter. **Abbreviations**: **aas**, anterior articular surface; **ca**, capitulum; **dip**, diapophysis; **fc**, facet for centrum; **nc**, neural canal; **np**, notochord pit; **poz**, postzygapophysis; **prz**, prezygapophysis; **sh**, sheet of bone; **tu**, tuberculum; **vk**, ventral keel; **vs**, ventral suture.

Haemal arches

Haemal arches are likewise already ossified. They appear to have two ossification centers and fuse ventrally. This is seen by the suture line in some of the arches (Fig. 8.7 B-B').

Gastralia

Few, thin but well ossified gastralia cluster along with the two groups of packed rib shafts (Fig. 8.8). Medial and lateral gastralia can be recognized. Their surface is striated as the rib cranial/caudal surfaces are, as well as the maternal corresponding elements. Some of the gastralia show a pointed midline process.

8.5 Discussion

Notes on taxonomy and predation vs reproduction hypotheses

With the discovery of a macropredatory (*sensu* Jiang et al., 2020) incident performed by a *Guizhouichthyosaurus tangae* individual, it was suggested that macropredatory behavior was possible in *Besanosaurus leptorhynchus*, and that the small vertebrae originally discovered in the maternal body cavity were possibly mixosaurid centra (Jiang et al., 2020). We deem the material in the body cavity of BES SC 999 unambiguously embryonic on the basis of the following evidence: the material is associated and lies in an expected antero-posterior sequence; the material is pristine and clearly unaltered by digestive processes; there are clear ossification differences between elements, especially in the cranium, consistent with other ichthyosaur embryos (discussed below); vertebral centra contain a small notochord pit.

The material is different from the maternal specimen in some capacity on the basis of ontogeny (discussed below), but is clearly attributable to *Besanosaurus leptorhynchus* on the basis of the following characters: triangular process of the quadrate; large preglenoid process; quadrangular femur. Lastly, macropredatory behavior in *Besanosaurus* is deemed unlikely in a recent analysis (Bindellini et al., 2021).

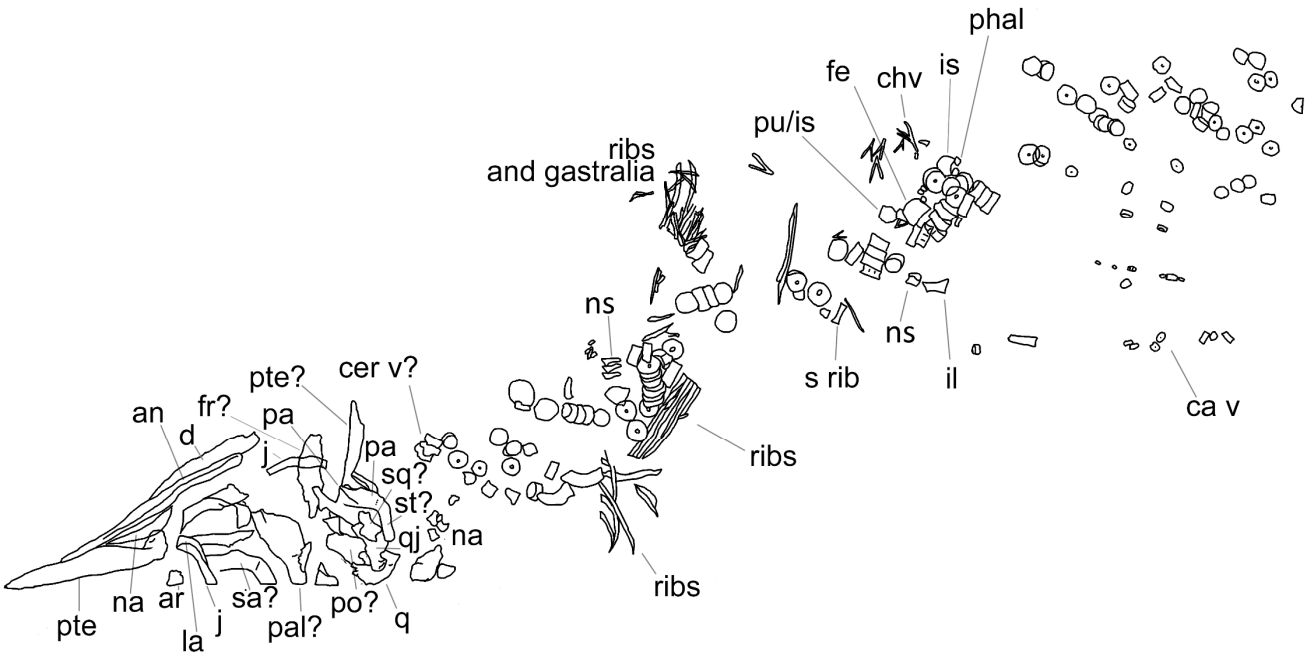

Fig. 8.8 – Map of the embryonic material in the maternal body cavity of BES SC 999, *Besanosaurus leptorhynchus* holotype. Abbreviations: an, angular; ar, articular; ca v, cauda vertebra; cer v, cervical vertebra; chv, chevron; d, dentary; fe, femur; fr, frontal; il, ilium; is, ischium; j, jugal; la, lacrimal; na, nasal; ns, neural spine; pa, parietal; pal, palatine; phal, phalange; po, postorbital; pte, pterygoids; pu, pubis; q, quadrate; qj, quadratojugal; s rib, sacral rib; sa, surangular; sq, squamosal; st, supratemporal.

Litter size, uterine position, and parturition orientation

The embryonic material is disarticulated, but relative *in vivo* positioning is largely still intact (Fig. 8.8). All cranial material is positioned far anteriorly, directly posterior to the maternal pectoral girdle. The vertebrae are scattered to a degree and may seem evenly distributed, but in our opinion, there is a clear linear anterior-posterior gradient whereby caudal vertebrae are only found clustered more posteriorly in the maternal body cavity. This is also apparent from the embryo CT (Fig. 8.9). Pelvic girdle and femur are found closely associated more posterior than the cranium. There are no obvious duplicates in terms of cranial or appendicular elements. This leads us to the most parsimonious conclusion that all the material represents a

single embryo. The far anterior placement of the cranium suggests the embryo was still in utero and had not yet started moving posteriorly for parturition. The anterior placement of the uterus is possibly synapomorphic for all euichthyosaurs, as it is now recorded in *Besanosaurus*, *Stenopterygius,* and *Cymbospondylus* (Böttcher, 1990; Klein et al., 2020). The anterior orientation of the embryonic cranium suggests future caudal presentation at birth (tail-first). Caudal presentation is the most common form of parturition in *Stenopterygius*, albeit not exclusive (Böttcher, 1990). Single gravid specimens of *Chaohusaurus* and *Cymbospondylus* show cranial presentation at birth or in utero (head-first), hinting at the possibility that parturition orientation preference may have shifted over ichthyosaur phylogeny (Motani et al., 2014; Klein et al., 2020).

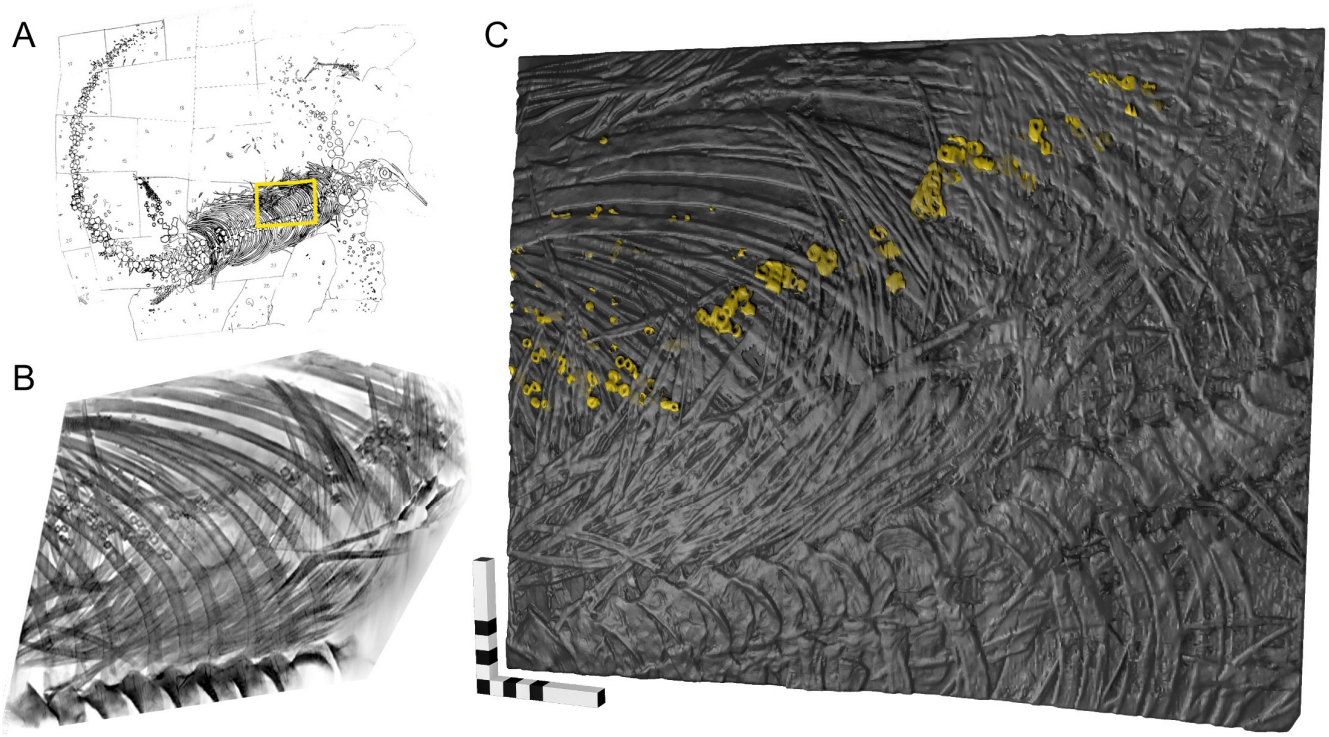

Fig. 8.9 - Rendering of the slab n° 30 of the specimen BES SC 999, the holotype of *Besanosaurus leptorhynchus*. (A) A drawing of the specimen (from Dal Sasso & Pinna, 1996) with the rendered portion highlighted in yellow; (B) bidimensional rendering of the maternal rib cage; (C) 3D rendering of the same anatomical portion: in yellow are highlighted the small vertebrae of the embryo. Scale bar equals 10x10 cm.

Relative stage and ontogenetic variation

Staging of fossil embryos is difficult as the material is often incomplete and represents only a snapshot in prenatal development. Recently, relative stages were proposed in the ichthyosaur *Stenopterygius quadriscissus* on the basis of relative cranial ossification (Miedema and Maxwell, 2022). Both the dermatocranial and chondro-splanchnocranial elements of the cranium of the *Besanosaurus* embryo are in advanced stages of ossification. All dermatocranial elements are well-ossified and all in a similar fashion. The dermatocranium is better ossified than the chondrocranial and splanchnocranial elements except for the quadrate, which has a degree of ossification similar to the dermatocranium. Delayed chondro-splanchocranial ossification in comparison to dermatocranium is well-observable in *Stenopterygius* and is common throughout Diapsida (Miedema and Maxwell, 2022). It is noteworthy that the parietal and pterygoid do not lag the other dermatocranial elements in ossification. The parietal is well-ossified with a distinct offset supratemporal ramus, defined optic lobe indentation and occipital flange. The pterygoid displays a dorsomedial furrow along its palatal ramus. It is possible that the palatal ramus was split at an earlier stage

of development, similar to stage 3 *Stenopterygius* (Miedema and Maxwell, 2022). The overall well-ossified cranium and the absence of delay of ossification in the parietal and pterygoid compared to other dermatocranial elements suggest that the developmental stage of the *Besanosaurus* embryo is comparable to stage 4 *Stenopterygius* (Miedema and Maxwell, 2022). This means that the embryo was in the later stages of prenatal osteological development prior to birth.

Ontogenetic differences

Overall the embryo resembles the adult morphology quite well, although there are distinct differences. The paracoronoid process on the surangular is underdeveloped compared to postnatal stages (Bindellini et al., 2021). This process is present is similar between stage 4 embryos and sexually mature specimens in *Stenopterygius*, but undergoes strong postnatal ontogenetic changes in that taxon (Miedema and Maxwell, 2022). The embryonic jugal is more lunate in shape whereas in the postnatal stages it is more quadrangular (Bindellini et al., 2021). This ontogenetic variation is very similar to *Stenopterygius* (Miedema and Maxwell, 2022). The medial side of the pterygoid is less concave than postnatally. The dorsal part of the paroccipital process of the opisthotic is not as wide as postnatally and the basioccipital facet is possibly not developed yet (although this facet could also have been lost in excavation) (Bindellini et al., 2021). A large difference in paroccipital process development between a perinatal and postnatal specimens was also observed in *Platypterygius australis* (Kear & Zammit, 2013). It is difficult to say whether there is a large difference in the shape of the semi-circular canal indentations on the opisthotic due to the state of development. However, it seems that the angle between the horizontal- and vertical semicircular canal indentations is similar pre- and postnatally. The indentations are relatively wider postnatally (Bindellini et al., 2021). A large difference in angle between the canal indentations was observed in *Stenopterygius* (Miedema & Maxwell, 2019). Strikingly, the triangular process on the quadrate seems relatively larger than some postnatal specimens (Bindellini et al., 2021). The curvature of the occipital lamella seems relatively constant over ontogeny, which is likewise similar to the ontogenetic trajectory of *Stenopterygius* and *Platypterygius australis* (Kear & Zammit, 2013; Miedema & Maxwell, 2019).

Possibility of palatal teeth

Palatal teeth are absent in most known ichthyosaurs. Teeth are supposedly present on the pterygoid of some individuals of the basal ichthyosauriform *Utatsusaurus hataii* (Motani, 1999). More widely known is the presence of teeth on the interpreted palatine of *Wimanius odontopalatus*, also one of the defining features of the taxon (Maisch & Matzke, 1998). More recently it was shown that the basal ichthyosauriform *Chaohusaurus brevifemoralis* has a single tooth row on the posterior part of the palatine (Yin, Ji & Zhou, 2021). We therefore think that the presence of palatal dentition in the embryo of *Besanosaurus* is a distinct possibility. In the embryo the teeth are also arranged in a single row, as in *Wimanius* and *Chaohusaurus* (Maisch & Matzke, 1998; Yin, Ji & Zhou, 2021). Unfortunately, we do not have a distinctly fully-exposed palatine in any of the other specimens of *Besanosaurus leptorhynchus*, so it is not possible to compare this morphology in a different ontogenetic stage. It is therefore also uncertain whether the palatal teeth persisted throughout ontogeny.

8.6 Conclusions

Here is reported a detailed description and qualitative comparisons of the embryonic material preserved in the body cavity of the type specimen of *Besanosaurus leptorhynchusI,* BES SC 999. The embryonic material is mostly preserved inside the maternal body cavity. It results disarticulated, although relative *in vivo*

positioning is largely still intact. The cranial material is preserved associated far anterior, close to the maternal pectoral girdle. The embryonic pelvic girdle, posterior flipper, and haemal arches are visible associated more caudally in the maternal body cavity. Preflexural/precaudal vertebrae are scattered in between the maternal ribs and gastralia

We deem the material in the body cavity of BES SC 999 unambiguously embryonic on the basis of the following evidence: it lays in an expected antero-posterior sequence; embryonic bone tissue results unaltered by digestive processes; existence of clear ossification differences between elements, consistent with other ichthyosaur embryos; vertebral centra shows a small notochord pit.

The material is attributable to *Besanosaurus leptorhynchus* on the basis of the presence of the following diagnostic combination of characters: presence of a triangular process of the quadrate; large preglenoid process; quadrangular femur. Moreover, overall the embryo resembles the adult morphology quite well, although some distinct differences have been pinpointed in the discussion.

We deem the anterior placement of the uterus possibly synapomorphic for all euichthyosaurs, since to date has been recorded in *Besanosaurus*, *Stenopterygius,* and *Cymbospondylus*. Furthermore, the anterior orientation of the embryonic cranium suggests future caudal presentation at birth (tail-first). Since *Chaohusaurus* shows cranial presentation at birth or in utero, we suggest that parturition orientation preference may have shifted over ichthyosaur phylogeny. The overall well-ossified cranium suggests that the developmental stage of *Besanosaurus leptorhynchus* embryo was in the later stages of prenatal osteological development prior to birth.

8.7 References

Bindellini G, Wolniewicz AS, Miedema F, Scheyer TM, Dal Sasso C. 2021. Cranial anatomy of *Besanosaurus leptorhynchus* Dal Sasso & Pinna , 1996 (Reptilia: Ichthyosauria) from the Middle Triassic Besano Formation of Monte San Giorgio , Italy / Switzerland : taxonomic and palaeobiological implications. *PeerJ* 9:e11179. DOI: 10.7717/peerj.11179.

Böttcher R. 1990. Neue Erkenntnisse über die Fortpflanzungs- biologie der Ichthyosaurier (Reptilia). *Stuttgarter Beiträge zur Naturkunde* B.

Brinkmann W. 1996. Ein Mixosaurier (Reptilia, Ichthyosauria) mit Embryonen aus der Grenzbitumenzone (Mitteltrias) des Monte San Giorgio (Schweiz, Kanton Tessin). *Eclogae Geologicae Helvetiae* 89:1321–1344.

Camp CL. 1980. Large Ichthyosaurs from the Upper Triassic of Nevada. *Paleontographica, Abteilung A* 170:139–200.

Dal Sasso C, Pinna G. 1996. *Besanosaurus leptorhynchus* n. gen. n. sp., a new shastasaurid ichthyosaur from the Middle Triassic of Besano (Lombardy, N. Italy). *Paleontologia Lombarda, New Series* 4:1–22.

Deeming DC, Halstaed LB, Manabe M, Unwin DM. 1995. An ichthyosaur embryo from the Lower Lias (Jurassic: Hettangian) of Somerset, England, with comments on the reproductive bioology of ichthyosaurs. In: Sarjeant WAS ed. *Vertebrate fossils and the evolution of scientific concepts*. 423–442.

Jiang D, Motani R, Tintori A, Rieppel O, Ji C, Zhou M, Wang X, Lu H, Li Z. 2020. Evidence Supporting Predation of 4-m Marine Reptile by Triassic Megapredator. *ISCIENCE*. DOI: 10.1016/j.isci.2020.101347.

Kear BP, Zammit M. 2013. In utero foetal remains of the Cretaceous ichthyosaurian *Platypterygius*: Ontogenetic implications for character state efficacy. *Geological Magazine* 151:71–86. DOI: 10.1017/S0016756813000113.

Klein N, Schmitz L, Wintrich T, Sander PM. 2020. A new cymbospondylid ichthyosaur (Ichthyosauria) from the Middle Triassic (Anisian) of the Augusta Mountains, Nevada, USA. *Journal of Systematic Palaeontology* 0:1–25. DOI: 10.1080/14772019.2020.1748132.

Lomax DR, Massare JA. 2012. The first reported *Leptonectes* (Reptilia: Ichthyosauria) with associated embryos, from Somerset, England. *Paludicola* 8:263–276.

Lomax DR, Sachs S. 2017. On the largest Ichthyosaurus: A new specimen of Ichthyosaurus somersetensis containing an embryo. *1. Acta Palaeontologica Polonica* 62:575–584.

Maisch MW, Matzke AT. 1997. *Mikadocephalus gracilirostris* n. gen., n. sp., a new ichthyosaur from the Grenzbitumenzone (Anisian-Ladinian) of Monte San Giorgio (Switzerland). *Paläontologische Zeitschrift* 71:267–289. DOI: 10.1007/BF02988496.

Maisch MW, Matzke AT. 1998. Observations on Triassic ichthyosaurs. Part II: A new ichthyosaur with palatal teeth from Monte San Giorgio. *Neues Jahrbuch fur Geologie und Palaontologie - Monatshefte* 1:26–41.

Maisch MW, Matzke AT. 2000. The Ichthyosauria. *Stuttgarter Beiträge zur Naturkunde, Geologie* Serie B:1–159.

Maxwell EE, Caldwell MW. 2003. First record of live birth in Cretaceous ichthyosaurs: closing an 80 million year gap. *Proceedings of the Royal Society B: Biological Sciences* 270:S104–S107. DOI: 10.1098/rsbl.2003.0029.

Miedema F, Maxwell EE. 2019. Ontogeny of the braincase in *Stenopterygius* (Reptilia, Ichthyosauria) from the Lower Jurassic of Germany. *Journal of Vertebrate Paleontology* 39. DOI: 10.1080/02724634.2019.1675164.

Miedema F., Bindellini G., Dal Sasso C., Scheyer T.M., Maxwell E.E. (2021). Conserved cranial development and early ontogeny in Triassic and Jurassic Ichthyosaurs. In: Belvedere M., Díez Díaz V., Mecozzi B., Sardella R (eds.). Abstract book of the XVIII annual conference of the European Association of Vertebrate Palaeontologists, online, 5 th - 9 th July 2021. Palaeovertebrata, 44: 116.

Miedema F., Maxwell E.E. (2022). Ontogenetic variation in the skull of *Stenopterygius quadriscissus* with an emphasis on prenatal development. *Scientific Reports,* 12: 1707.

Motani R. 1999. Phylogeny of the Ichthyopterygia. *Journal of Vertebrate Paleontology* 19:473–496. DOI: 10.1080/02724634.1999.10011160.

Motani R, Jiang DY, Tintori A, Rieppel O, Chen GB. 2014. Terrestrial origin of viviparity in Mesozoic marine reptiles indicated by Early Triassic embryonic fossils. *PLoS ONE* 9. DOI: 10.1371/journal.pone.0088640.

Yin Y, Ji C, Zhou M. 2021. The anatomy of the palate in Early Triassic *Chaohusaurus brevifemoralis* (Reptilia: Ichthyosauriformes) based on digital reconstruction. *PeerJ*:1–19. DOI: 10.7717/peerj.11727.

Chapter 9
Conclusions

Several topics have been addressed in this thesis and the results are briefly summarized in this final chapter. All the available ammonoids and bivalves from the Sasso Caldo site (Besano Formation), housed in the collections of the Museo di Storia Naturale di Milano, have been examined and determined. The systematic study led to the recognition of 15 ammonoid taxa belonging to 10 genera, and five species belonging to the bivalve genus *Daonella*. Ammonoids recovered at Sasso Caldo are *Repossia*, *Stoppaniceras*, *Nevadites*, *Serpianites*, *Lecanites*, *Longobardites*, *Celtites*, *Gymnites*, *Monophyllites*, and *Flexoptychites*. *Daonella* is represented by the species *D. vaceki*, *D. pseudomoussoni*, *D. airaghii*, *D. fascicostata*, and *D. luganensis*.

The study of bed-by-bed collected specimens allowed the biochronostratigraphic classification of the Sasso Caldo section and the time-calibration of invertebrate and vertebrate bioevents. The biochronostratigraphic study of the Sasso Caldo succession allowed a precise correlation with the known Swiss fossil localities of Monte San Giorgio where the Besano Formation outcrops. The study of the invertebrate fauna led to the conclusion that the lowermost bed of the Besano Formation outcropping at Sasso Caldo is laterally equivalent to bed 61 of the Punkt 902/Mirigioli section in Switzerland. The 25 uppemost beds at Sasso Caldo are here referred to the San Giorgio Formation. At Sasso Caldo the Anisian/Ladinian boundary is also preserved. These results evidence that at Sasso Caldo crops out almost all the middle Besano Formation, as well as the entire upper Besano Formation. Following Brack et al. (2005), all the above-mentioned taxa occur in the *N. secedensis* Zone, whereas the upper limit of the *R. reitzi* Zone should be located below bed 61.

According to Röhl et al. (2001), the deposition of the middle Besano Formation reflects the establishment of an intraplatform basin with a discontinuous open-marine influence, whereas the deposition of the lower and upper Besano Formation corresponds to a shallower subtidal restricted platform environment. This trend is also observed in the distribution of the specimens housed in the collection of the MSNM: sauropterygians and components of the terrestrial biota of a purported landmass very close to the basin characterize the upper Besano Formation at Sasso Caldo, whereas ammonoids, the bivalve *Daonella,* and large marine vertebrates, especially ichthyosaurs, are typical of the middle Besano Formation and absent in the upper part of the section. Aside from ammonoids and *Daonella*, the most important specimens, chosen for their preservation, completeness, and rarity have been studied for this Ph.D. thesis also to test the hypothesis of variations in the influence of open sea on the Besano basin.

Among the terrestrial taxa recovered at Sasso Caldo from the upper Besano Formation, a remarkably well-preserved fossil scorpion (BES SC 1973) is described in this work. This finding corroborates the hypothesized existence of a near shoreline during the deposition of the upper Besano Formation. The preservation of the specimen is exceptional: structures such as trichobothria and median eyes are still clearly visible. BES SC 1973 is assigned to a new taxon gen. et sp. nov., included in the family Protobuthidae. This taxon is characterized by the presence of a strongly carinate carapace, including three main carinae, and a straight shaft of the fixed finger of the chela. This finding represents the first

arachnid recorded from the Besano Formation, and the second genus attributed to the family Protobuthidae. This specimen is also the first reported Italian Mesozoic fossil scorpion. Furthermore, the description of this new genus and species increases the Triassic diversity of scorpions, given the extreme rarity of this clade.

Shifting our focus onto vertebrates, MSNM V927 and 928, a portion of the axial skeleton of a large diapsid, is here attributed to *Helveticosaurus zollingeri.* This animal has been recovered in association with the ammonoid *Ticinites*, at the base of the *N. secedensis* Zone, in coincidence with the establishment of the intraplatform basin that characterizes the middle Besano Formation. In spite of its fragmentary condition, this fossil represents an important addition to the occurrence of *Helveticosaurus*, a rare diapsid known only from the Besano Formation. Besides being the first record of skeletal remains and the second specimen assigned to the taxon in Italy, this specimen sheds light on the anatomy of its sacral region, not preserved in the known specimens of *Helveticosaurus*. Along with MSNM V927 and 928, an isolated tooth from the Middle Salvatore Dolomite (ST166120) is redescribed, with the help of a digital model. The tooth helped to better understand the morphology of the dentition in *Helveticosaurus* and better define the niche occupied by this animal in the Middle Triassic coastal ecosystems. Given its stratigraphical occurrence and anatomy, *Helveticosaurus* might have been a dweller of the carbonate platform, with an amphibious lifestyle strictly associated with the shoreline environments and a carnivorous generalistic diet. The swimming style of *Helveticosaurus* here partly revised, is suggested to be intermediate between the otariid and the otter model.

Among vertebrates with a pelagic lifestyle, ichthyosaurs represent an important component of the fauna from the middle Besano Formation. In this thesis are described MSNM V926, a portion of a ribcage, and SMNS 50010, an isolated partial forefin of a large ichthyosaur. Both are attributed to *Cymbospondylus buchseri*. Although the presence of *Cymbospondylus* was reported in the past from some Italian localities and its presence is known on the Swiss side of Monte San Giorgio, MSNM V926 represents the first specimen attributed to *C. buchseri* recovered on the Italian side of the mountain. The rediscovery of these specimens in the historical collections of museums suggests the necessity of an in-depth reevaluation of the fossil material from the Besano Formation housed and scattered in collections across Europe.

A great part of this thesis is dedicated to the revision of *Besanosaurus leptorhynchus*. The specimens studied and attributed to *Besanosaurus leptorhynchus* preserve a remarkably complete cranial and postcranial anatomy so that this taxon can be now accounted among the best-understood Middle Triassic Ichthyosaur taxa. The revision of the skull morphology of this taxon clarified long-standing controversies regarding its cranial anatomy and the taxonomy of shastasaurids from Monte San Giorgio. The six specimens here described represent a potential ontogenetic series composed of an embryo, likely two subadults, and four adults. They can be ordered by increasing size as follows: embryonic material of BES SC 999, PIMUZ T 4376, PIMUZ T 1895, BES SC 999, BES SC 1016, GPIT 1793/1, PIMUZ T 4847. Also, *Besanosaurus* resulted the largest Middle Triassic ichthyosaur taxon of the Western Tethys to date, since a full adult size is confidently estimated to be almost 8 m in PIMUZ T 4847.
Besanosaurus is characterized by a long, slender, and gracile snout, representing an ecological specialization never seen before the Anisian in a large-sized diapsid. In this work a snap-feeder-like hunting strategy is hypothesized, with a specific preference for small and elusive prey (such as coleoids and/or small fishes). The specialization represented by a longirostrine skull morphology might have been driven by prey preference and the methods of prey capture. This should have granted an increased feeding efficiency, which in turn might have led to a more efficient way of consuming metabolic

resources, triggering the possibility to acquire bigger body sizes without shifting to a higher metabolic level. On the other hand, bigger sizes might also have helped the animal hunting preys, according to the hypothesized hunting strategy for *Besanosurus* and as observed in other extinct and extant large vertebrates, activating a positive feedback between gigantism and longirostry.

The study of the postcranial anatomy of *Besanosaurus leptorhynchus* is based on four specimens: PIMUZ T 4376, PIMUZ T 1895, BES SC 999, PIMUZ T 4847. The results suggest that this taxon possesses a peculiar bauplan, which in its proportions fits in between *Cymbospondylus* and the shastasaur-grade ichthyosaurs. The caudal series represents 55% of the whole axial skeleton length. In the reported analysis, clear evidence is found for the presence of a tailbend that forms an angle of ~30° and gives proof of the existence of a heterocercal tail, more similar to that of shastasaur-grade ichthyosaurs than to *Cymbospondylus* and mixosaurids. Remarkably, pedal phalanges are found to retain reduced shafts, absent in the rest of shastasaur-grade ichthyosaurs, but more similar to those of *Mixosaurus*. On the contrary, hindfin phalanges were round as in shastasaur-grade ichthyosaurs: is therefore suggested that *Besanosaurus* completely or almost completely lost secondary ossification centers in these bones.

Swimming capabilities of *Besanosaurus leptorhynchus* have been tested following Motani et al. (1996): the animal results intermediate between anguilliform swimmers, such as *Cymbospondylus*, and shastasaur-grade ichthyosaurs. On the other hand, in *Mixosaurus* for the first time is observed a combination of adaptations that would have appeared only later and convergently in Parvipelvia.

Among the ichthyosaurs from the Besano-Monte San Giorgio fauna (*Cymbopondylus,* mixosaurids, and *Besanosaurus*), different hunting strategies, demonstrated by different morphologies and dimensions of the rostra, as well as different body proportions and swimming styles, should have led to the maintenance of low interspecific competition (i.e., niche partitioning).

Lastly, the key phylogenetic position occupied by *Besanosausurus leptorhynchus* in the ichthyosaurian phylogeny has been investigated: the analysis, performed with a matrix that includes around 90% of unambiguous updated scores for *B. leptorhynchus* and revised scores for other Triassic taxa, shows that this taxon represents the basalmost member of shastasaur-grade ichthyosaurs, recovered to be a paraphyletic group.